THE UNIVERSITY *of* EDINBURGH

Reactivation of developmental genes to promote neovascularisation and cardiac regeneration after myocardial infarction

Michelle Nga Huen Tang

Doctor of Philosophy

The University of Edinburgh

2025

For my grandparents, who sowed the seeds of curiosity and guided my earliest steps with love and care.

This work is their harvest, nurtured by their wisdom and devotion.

Declaration

I hereby declare that the work presented in this thesis has been composed by myself at the University of Edinburgh, and the work is my own, unless stated otherwise.

This thesis has not been submitted for any other degree or professional qualification.

Michelle Nag Huen Tang

10th October 2025

Publications

- Li Z, Solomonidis EG, Berkeley B, **Tang MNH**, Stewart KR, Perez-Vicencio D, McCracken IR, Spiroski AM, Gray GA, Barton AK, Sellers SL, Riley PR, Baker AH, Brittan M. **Multi-species meta-analysis identifies transcriptional signatures associated with cardiac endothelial responses in the ischaemic heart**. Cardiovasc Res. 2023 Mar 17;119(1):136-154. https://doi.org/10.1093/cvr/cvac151

- **Tang, M.N.H***., Berkeley, B*. and Brittan, M. (2023), **Mechanisms regulating vascular and lymphatic regeneration in the heart after myocardial infarction**. J. Pathol., 260: 666-678. https://doi.org/10.1002/path.6093

Abstract

Myocardial infarction (MI) remains a leading cause of heart failure (HF), compounded by the limited regenerative capacity of the adult heart. Despite advances in MI treatments, HF remains common, highlighting the urgent need for novel strategies to prevent HF progression and promote cardiac regeneration. Effective cardiac repair requires rapid reconstruction of a functional vascular network, yet the mechanisms driving neovascularisation remain poorly understood. Increasing evidence suggests that genes deployed during embryonic development can be reactivated in the adult heart to support regeneration pathways. Owing to its exceptional regenerative ability, the zebrafish represents a powerful model to investigate myocardial-vascular regeneration pathways. I hypothesised that reactivation of foetal genes in adult coronary endothelial cells (ECs) promotes neovascularisation and cardiac repair post-MI.

Multimodal omics analyses identified Annexin A2 *(ANXA2*) and Poly(A) binding protein cytoplasmic 1 *(PABPC1*) as endothelial genes expressed during development and reactivated in the adult coronary vasculature post-MI. Protein level upregulation of both targets was confirmed in cardiac ECs from MI patients versus healthy controls (n = 7; %ANXA2^{+}CD31^{+} ECs = 77.1± 12.1 versus. 56.9 ± 9.2, P = 0.002; %PABPC1^{+}CD31^{+} ECs = 68.0 ± 15.6 *versus*. 37.9 ± 18.6, P = 0.013). The ANXA2 fibrinolytic co-regulator, Serpin Family E Member 1 (SERPINE1), was also significantly increased in MI (%SERPINE1^{+}CD31^{+} ECs = 32.7 ± 11.7 *versus*. 16.1 ± 7.3, P = 0.001). These findings suggest that a balanced interplay between ANXA2 and SERPINE1 may influence coronary neovasculogenic responses post-MI, in addition to their known roles in fibrinolysis.

ANXA2 was prioritised as a lead candidate for functional analysis. CRISPR/Cas9-mediated knockdown of orthologues *anxa2a/b* was generated in Tg(*fli1:eGFP*)^{y1tg} / Tg(*myl7:DsRed2-NLS*)^{f2}) zebrafish to investigate the role of *ANXA2* in cardiovascular development and regeneration. At 3 days post-fertilisation (dpf), crispants (CRISPR-Cas9 engineered animals) exhibited developmental abnormalities, including smaller eyes (n = 45 – 80; eye diameter in mm = 0.68 ± 0.16 *versus*. 0.91 ± 0.07, P < 0.0001), shorter body length (body length in mm = 9.75 ± 0.99 *versus*. 10.82 ± 0.41, P < 0.0001), and disrupted intersegmental vessels (n = 25-48; number of complete intersegmental vessels = 23.31 ± 3.05 *versus*. 27.83 ± 1.36, P < 0.0001). By 5 dpf, 45.3% of crispants displayed mild phenotypes, and 45.0% showed moderate or severe developmental defects, such as curled tails, pericardial oedema, failure to hatch, and full body malformations.

I developed and optimised a cardiac laser injury and regeneration model in <5 dpf larvae. Laser injury significantly reduced heart rate, EC number, and ventricular volume at 2 hours post-injury (hpi) (n = 20-38; heart rate in bpm = 142.63 ± 67.44 *versus*. 200.74 ± 66.15, P = 0.0012; GFP^{+} EC counts = 62.00 ± 28.27 *versus*. 107.09 ± 29.46, P=0.0018; diastolic endocardial volume of ventricle (μm^3) = $3.02e^6$ ± $2.37e^6$ *versus*. $7.29e^6$ ± $5.22e^6$, P = 0.0014), all of which had shown complete recovery by 48 hpi in wild type (WT) siblings. Compared with injured WT siblings, mild *anxa2ab* crispants showed partial regeneration at 48 hpi, characterised by reduced EC

repopulation (n = 24; GFP^+ EC counts = 61.70 ± 21.25 vs 89.00 ± 20.11, P < 0.0001), diminished cardiomyocytes numbers ($mCherry^+$ cardiomyocyte counts = 56.61 ± 17.03 vs 83.25 ± 14.06, P < 0.0001), and smaller ventricular volume (diastolic endocardial volume of ventricle (μm^3) = $6.19e^6$ ± $2.00e^6$ vs $1.03e^7$ ± $2.62e^6$; P < 0.0001). Moderate *anxa2ab* crispants exhibited severely impaired regeneration, with persistently low EC and cardiomyocyte counts, reduced ventricular volume, and distorted ventricular morphology (n = 21; GFP+ EC counts = 34.71 ± 19.21 vs 76.79 ± 13.01; mCherry+ cardiomyocyte count = 25.29 ± 17.01 vs 72.47 ± 13.34; diastolic endocardial volume of ventricle (μm^3) = $4.14e^6$ ± $2.49e^6$ vs $8.88e^6$ ± $2.00e^6$; P < 0.0001).

Quantitative reverse transcription polymerase chain reaction (qRT-PCR) at 48 hpi revealed transcriptional alterations in targets associated with *ANXA2* function in crispants, including S100 calcium binding protein A10ab *(s100a10ab*), vascular endothelial growth factor Ab *(vegfab*), C-X-C motif chemokine ligand 12b *(cxcl12b*), Notch receptor 1a/3 *(notch1a/3*), and *pabpc1ab*, but not *serpine1*. This suggests *ANXA2* may act upstream of a network of endothelial and regenerative signalling genes, and that its loss compromises repair responses.

Overall, this study identifies *PABPC1* and *ANXA2* as developmental genes reactivated upon cardiac injury, with *ANXA2* deficiency leading to impaired cardiac regeneration. The phenotypic defects observed in *anxa2ab* knockdown zebrafish highlight the essential role of *ANXA2* in embryonic development, neovascularisation, and cardiac repair. ANXA2 and SERPINE1 act antagonistically to regulate plasmin generation and fibrin turnover; an imbalance between ANXA2 and SERPINE1 may contribute to the impaired neovascularisation, pathological cardiac remodelling and fibrosis that drives the progression of heart failure. Therefore, elucidating *ANXA2/SERPINE1*-mediated pathways may provide strategies to enhance neovascularisation and heart regeneration. Future work should focus on understanding the mechanisms by which *ANXA2, PABPC1 or other related genes* regulate endothelial responses to injury, to inform the development of novel regenerative therapies for cardiovascular disease and the prevention of heart failure, for which there is currently no cure.

Lay summary

A heart attack (also known as a myocardial infarction) is one of the leading causes of heart failure worldwide. Heart failure often results after a heart attack because, unlike some species, the adult human heart has very limited ability to repair itself. After a heart attack, rebuilding a healthy blood vessel network to restore blood supply to the damaged heart muscle is vital for recovery. However, the biological processes that drive the growth of new blood vessels (called neovascularisation) remain poorly understood.

Recent research has suggested that, after injury, the adult heart may "switch back on" certain genes that were active during embryonic development. These genes could provide important instructions for repair. I hypothesised that reactivation of foetal genes in blood vessel cells in the adult heart (endothelial cells) promotes neovascularisation and cardiac repair following a heart attack.

This study investigated the roles of two developmental genes – Annexin A2 *(ANXA2*) and Poly(A) Binding Protein Cytoplasmic 1 *(PABPC1*) – in repairing blood vessels in the heart after injury. Analysis of heart tissue from patients who had suffered a heart attack, compared with healthy control human hearts, revealed that ANXA2 and PABPC1 were reactivated in blood vessel cells of the damaged heart. Another gene, Serpin Family E Member 1 (*SERPINE1)*, which interacts with *ANXA2* in controlling blood clot breakdown, was also increased, suggesting that these molecules may work together to influence repair.

The role of *ANXA2* was further explored using zebrafish, a small freshwater fish with an exceptional ability to regenerate its heart after injury. Using gene-editing technology (CRISPR-Cas9), the zebrafish versions of *ANXA2 (anxa2a* and *anxa2b*) were silenced. Zebrafish lacking this gene developed abnormally, showing smaller eyes, shorter body length, and disorganised blood vessels. A new zebrafish model of heart injury was also established using a precise laser. Normal zebrafish rapidly restored heart structure and function following injury, but those lacking *ANXA2* showed much poorer recovery. They had fewer blood vessel cells, fewer heart muscle cells, and smaller heart chambers, with some fish showing severe structural defects. Loss of *ANXA2* also disrupted the activity of several other developmental and regenerative genes, including *VEGF*, *CXCL12*, *NOTCH*, and *PABPC1*.

Overall, my findings demonstrate that *ANXA2* is essential for both healthy development and heart regeneration. Understanding how *ANXA2, PABPC1* and related genes control blood vessel growth and repair after injury may help uncover new treatments to improve recovery after heart attacks in humans and prevent the progression to heart failure, for which there is no current cure.

Acknowledgements

This thesis marks the end of a long and memorable four-year journey, one that would not have been possible without the many people who have supported me throughout my PhD.

First and foremost, I would like to express my gratitude to my supervisors, Prof Mairi Brittan and Prof Andy Baker, for their time, supervision, and guidance throughout my PhD journey. Thank you for consistently challenging me to improve, and for giving me the freedom to explore ideas and steer my project independently. This experience has shaped me into a more confident and capable researcher. My project began with much uncertainty and constant change, but through your expertise, encouragement, and support, it has evolved into something truly exciting and unique.

Mairi, I'm especially grateful to you for introducing the zebrafish study into my project (which has now become one of its main highlights) and for connecting me with the wonderful collaborators in the zebrafish field who have offered me invaluable advice and support throughout. Reflecting on the past, I want to thank you for your patience and understanding during the difficult and stressful times. I deeply appreciate your thorough and timely feedback on my thesis drafts, and I will always remember your kind words in calling me a "good scientist".

Andy, I am truly thankful for your willingness to make time for me and provide constructive feedback on my project despite your busy schedule. Your practical advice and encouragement have been greatly appreciated, and your final reminder regarding the thesis submission deadline helped me stay on track.

Many thanks to my funders, the Medical Research Scotland and N2 Pharmaceuticals, for supporting my PhD.

I would also like to thank all members of the Brittan and Baker labs, past and present, for being supportive in the lab. I especially want to acknowledge Dr Ziwen (Cass) Li for mentoring me during the first two years of my PhD. Thank you for teaching me many lab techniques, for your help troubleshooting experiments, and for being there to offer advice and encouragement whenever I needed it. I also want to acknowledge Dr Mukesh Lalwani, who was incredibly kind and helpful in teaching me the fundamental techniques of zebrafish crispants during the latter half of my PhD. I feel deeply grateful for everything I have learnt from both of you.

I wish to express my sincere appreciation to Prof Martin Denvir, who acted as an unofficial third supervisor, for always showing genuine interest in my project, and taking the time to meet with me in person to discuss results. Thank you for your kindness, encouragement, and insightful advice. I would also like to thank Dr Emma Kals for her help in the lab during the final months of my PhD.

I am deeply grateful to Dr Jonathan Taylor (University of Glasgow), who has been extremely influential in my zebrafish project. Without his expertise and guidance in

teaching me to operate and troubleshoot the SPIM microscope, imaging zebrafish hearts would not have been possible. I would also like to thank his PhD student, Karlin Ross, for his help with SPIM imaging.

My sincere thanks to Dr James Minchin and Dr Panna Tandon for their generosity in sharing insights and suggestions on zebrafish genetics, and for providing invaluable feedback to help me improve my zebrafish crispants study.

A huge thank you to Prof Paddy Hadoke for taking the time to listen and support me through the challenges of my PhD project and my mental health, as well as offering helpful feedback and advice on my project.

I would like to thank my thesis committee chair, Dr Andrea Caporali, and committee members, Dr Gianfranco Matrone, Nikolay Solovyev (N2), and Natalia Romanova-Mossig (N2) for their time, encouragement and feedback during our annual review meetings. I am particularly thankful to Andrea for his support in teaching me how to perform the Matrigel tube formation and ECIS permeability assays, and to Gianfranco for his advice on optimising the cardiac laser injury method in zebrafish larvae.

Thank you to Dr Carl Tucker, Paul Strachan, and the rest of the aquatic staffs for taking care of my zebrafish and maintaining the world-class aquatic facilities that made my research possible. I wish to express my appreciation to Carl for providing inductions in zebrafish husbandry techniques and for his continued assistance with zebrafish-related aspects of my project.

Thank you to Mike Millar and Dr Rolly Wiegand and Hazel Stewart for providing inductions on operating various imaging microscopes and for their technical support with tissue imaging.

To all my friends, thank you for filling these years with friendship, laughter, and warmth. Thank you for being there for me, for your emotional support through every phase of this journey, and for adding fun and lightness along the way.

To my Fur Baby – Toby, thank you for being my emotional support animal and for bringing comfort through countless sleepless nights of writing by faithfully warming my lap. Thank you for being the best writing companion and for always bringing your toys to me as the perfect distraction. Your presence made the long writing hours lighter and more enjoyable. 

A special thank you to Sheldon, for always being there through my lowest and highest moments. I deeply appreciate your unconditional support and encouragement, and for making the difficult days more bearable. Thank you for being the safe space I could always turn to during my toughest challenges, for helping proofread my thesis, and for providing bioinformatics advice. Above all, thank you for constantly reassuring me of my capability as a scientist. My PhD journey would not have been the same without you.

At last, I am indebted to my mum – for giving me life, unwavering love, strength, and wisdom. Thank you for always pushing me to strive for excellence and for sacrificing so much to give me the future I have today. I want to thank you for the safe and loving home you provided, where I could dream and nurture my ambitions. Thank you for taking such good care of me and cooking delicious meals during the stressful final weeks of thesis writing. Although you may still have no clue what exactly I research, I know I have made you proud.

I would like to thank my grandparents, 李天骄 and 朱长江, who shaped who I am long before I ever became a scientist. My grandmother nurtured me with curiosity, wisdom, and kindness, and my grandfather inspired my love of animals and science, teaching perseverance and the courage to never give up. Though memories fade and distance separates us, your love and guidance remain deeply rooted in me. Your influence on my life is immeasurable, and I hope I have made you both very proud.

Writing this thesis has brought back countless memories of the days and nights spent in the lab. Looking back, it was a time filled with challenges, fulfilment, and a unique kind of fun that I will always treasure. I feel truly fortunate to have had the opportunity to dedicate four years of my life to working on something I enjoy, and to contribute (even in the smallest way) to the field of science and research. Throughout this journey, I have not only grown into a more mature scientist but have also experienced immense personal growth. I am incredibly proud of how far I have come and all that I have achieved. Little did the younger Michelle know that she would one day become the first in her family to earn a PhD! I want to thank myself for being brave, for the endurance, discipline, persistence, and resilience to stay grounded through uncertainty and keep moving forward. Most importantly, I have recognised my own strength and capability. This PhD journey has shown me that I can trust my own judgment, believe in my abilities, and take on whatever comes my way.

Though this chapter closes, I leave it with deep gratitude and look forward with hope and excitement to the next chapter of my life.

Table of Contents

DECLARATION 3

PUBLICATIONS 4

ABSTRACT 5

LAY SUMMARY 7

ACKNOWLEDGEMENTS 8

TABLE OF CONTENTS 11

LIST OF FIGURES 17

LIST OF TABLES 19

LIST OF ABBREVIATIONS 20

CHAPTER 1: INTRODUCTION 25

1.1. MYOCARDIAL INFARCTION, CURRENT TREATMENTS, AND NOVEL THERAPEUTIC APPROACHES 25

1.2. MECHANISMS AND MOLECULAR REGULATION OF NEOVASCULARISATION IN POST-MYOCARDIAL INFARCTION REPAIR 28

1.3. COMPARATIVE INSIGHTS INTO CARDIAC REGENERATION: CONSERVED MECHANISMS AND LOST POTENTIAL FROM ZEBRAFISH TO HUMANS 34

1.3.1 REGENERATIVE CAPACITY OF THE HEART ACROSS SPECIES AND DEVELOPMENTAL STAGES 34

1.3.2 ZEBRAFISH AS A MODEL FOR COMPLETE CARDIAC REGENERATION 35

1.3.3 CARDIAC REGENERATION IN HUMANS 36

1.4. REACTIVATION OF DEVELOPMENTAL GENE PROGRAMMES AS A THERAPEUTIC APPROACH IN ADULT CARDIOVASCULAR DISEASE 37

1.5. MULTI-OMICS APPROACHES TO INFORM OUR UNDERSTANDING OF CARDIOVASCULAR DISEASE RESEARCH AND ADVANCED TECHNOLOGIES 40

1.6. CURRENT CLINICAL TRIALS TO PROMOTE NEOVASCULARISATION POST-MI IN THE HEART 43

1.7. CRISPR/CAS9 SYSTEM 45

1.8. COLLABORATION WITH N2 PHARMACEUTICALS (EXTERNAL PARTNER ORGANISATION) 46

1.9. HYPOTHESES AND AIMS 49

1.9.1 HYPOTHESES: 49
1.9.2 AIMS: 49

CHAPTER 2: MATERIALS & METHODS 50

2.1 BIOINFORMATIC ANALYSIS OF MULTIMODAL OMICS DATASETS 50

2.1.1 ANALYSIS OF CRESCENDO CORONARY ENDOTHELIAL CELL ATLAS 50
2.1.2. ANALYSIS OF SINGLE NUCLEI RNA-SEQUENCING DATA FROM HUMAN ACUTE MYOCARDIAL INFARCTION 52
2.1.3 ANALYSIS OF SINGLE CELL RNA-SEQUENCING DATA FROM REGENERATING ZEBRAFISH HEARTS 55

2.2 SPATIAL TRANSCRIPTOMICS 56

2.3 CRISPR/CAS9-MEDIATED GENOME MUTAGENESIS 58

2.3.1 ALT-R CRISPR/CAS9-MEDIATED GENOME MUTAGENESIS 58
2.3.1 DETERMINING DGRNA EFFICIENCY 60

2.4 ZEBRAFISH HUSBANDRY AND GENERAL TECHNIQUES 62

2.4.1 ZEBRAFISH MAINTENANCE 62
2.4.2 PHENYLTHIOUREA TREATMENT 63
2.4.3 ANAESTHESIA 63

2.5 LARVAL ZEBRAFISH IMAGING AND QUANTIFICATION 64

2.5.1 QUANTIFICATION OF LARVAE EMBRYONIC DEVELOPMENT 64
2.5.2 QUANTIFICATION OF LARVAE VASCULAR DEVELOPMENT 64
2.5.3 ZEBRAFISH CARDIAC IMAGING USING HEARTBEAT-SYNCHRONISED SELECTIVE PLANE LIGHT SHEET ILLUMINATION MICROSCOPE 64

2.6 LARVAL VENTRICULAR LASER ABLATION 66

2.7 QUANTIFICATION OF RELATIVE MRNA EXPRESSION OF TARGET GENES IN ZEBRAFISH LARVAE 66

2.7.1 RNA EXTRACTION 66
2.7.2 REVERSE TRANSCRIPTION FOR CDNA SYNTHESIS 67
2.7.3 REAL TIME-QUANTITATIVE PCR 67

2.8 TREATMENT OF LARVAL ZEBRAFISH WITH N2-01 DRUG 69

2.9 HUMAN CARDIAC TISSUE STAINING 69

2.9.1 HUMAN CARDIAC SAMPLES 69
2.9.2 MASSON'S TRICHROME 71
2.9.3 IMMUNOFLUORESCENCE STAINING OF HUMAN CARDIAC TISSUE 72
2.9.4 CONFOCAL FLUORESCENCE IMAGING AND QUANTIFICATION 72

2.10 CELL CULTURE TECHNIQUES 73

2.10.1 EDU CELL PROLIFERATION ASSAY 73
2.10.2 MATRIGEL TUBE FORMATION ASSAY 74

2.11 ASSEMBLY OF GRAPHS AND STATISTICAL ANALYSIS 74

CHAPTER 3: RESULTS – IDENTIFICATION OF TARGET GENES USING A MULTI-OMICS APPROACH 76

3.1 INTRODUCTION 76

3.2 RESULTS: *ANXA2* IDENTIFIED AS A REACTIVATED FOETAL GENE, WITH *SERPINE1* AS A POTENTIAL CO-REGULATOR OF NEOVASCULARISATION AFTER MI 78

3.3 BIOLOGICAL FUNCTIONS AND MECHANISMS OF ANXA2 AND ITS POTENTIAL IMPLICATIONS IN CARDIOVASCULAR DISEASE RESEARCH 86

3.4 BIOLOGICAL FUNCTIONS AND MECHANISMS OF SERPINE1 AND ITS POTENTIAL IMPLICATIONS IN CARDIOVASCULAR DISEASE RESEARCH 90

3.5 DISCUSSION 92

CHAPTER 4: RESULTS – REDUCED REGENERATIVE CAPACITY OF *ANXA2A/B* ZEBRAFISH CRISPANTS AFTER CARDIAC LASER INJURY 95

4.1 INTRODUCTION 95

4.2 CRISPR/CAS9-MEDIATED GENOME EDITING OF *ANXA2A/B* IN ZEBRAFISH 98

4.3 *ANXA2A/B* KNOCKDOWN IMPAIRED EMBRYONIC AND CARDIOVASCULAR DEVELOPMENT 106

4.4 A LARVAL ZEBRAFISH CARDIAC LASER INJURY AND REGENERATION MODEL 113

4.5 *ANXA2A/B* KNOCKDOWN IMPAIRED REGENERATION FOLLOWING CARDIAC LASER INJURY 116

4.6 TRANSCRIPTIONAL ALTERATIONS IN FIBRINOLYTIC, ANGIOGENIC, AND REGENERATION-ASSOCIATED GENES IN *ANXA2A/B* CRISPANTS PRIOR TO CARDIAC INJURY 119

4.7 TRANSCRIPTIONAL ALTERATIONS IN FIBRINOLYTIC, ANGIOGENIC, AND REGENERATION-ASSOCIATED GENES IN *ANXA2A/B* CRISPANTS FOLLOWING CARDIAC INJURY 123

4.8 DISCUSSION 126

CHAPTER 5: RESULTS – ANXA2 AND SERPINE1 ARE INDUCED DURING ENDOGENOUS NEOVASCULOGENIC RESPONSES IN HUMAN HEART 135

5.1 INTRODUCTION 135

5.2 CO-LOCALISATION OF ANXA2 AND SERPINE1 WITH CD31+ CELLS IN THE INFARCT BORDER ZONE OF MI 136

5.3 CO-LOCALISATION OF ANXA2 WITH VIMENTIN+ CELLS IN THE INFARCT BORDER ZONE OF MI 141

5.4 *ANXA2* GENE EXPRESSION ACROSS CARDIAC CELL TYPES IN CONTROL, ISCHAEMIC, AND FIBROTIC ZONES. 143

5.5 *SERPINE1* GENE EXPRESSION ACROSS CARDIAC CELL TYPES IN CONTROL, ISCHAEMIC, AND FIBROTIC ZONES. 145

5.6 DISCUSSION 147

CHAPTER 6: RESULTS – REACTIVATION OF THE FOETAL ENDOTHELIAL GENE *PABPC1* IN MYOCARDIAL INFARCTION: IMPLICATIONS FOR CARDIAC REPAIR 151

6.1 INTRODUCTION 151

6.2 *PABPC1* AS A NOVEL CANDIDATE FROM CRESCENDO AND COMPARATIVE GENE EXPRESSION ANALYSIS ACROSS MULTI-OMICS DATASETS 157

6.3 BIOLOGICAL FUNCTIONS AND MECHANISMS OF PABPC1 AND ITS POTENTIAL IMPLICATIONS IN CARDIOVASCULAR DISEASE RESEARCH 162

6.4 PABPC1 EXPRESSION IS INDUCED DURING ENDOGENOUS NEOVASCULOGENIC RESPONSES IN HUMAN HEART 165

6.5 *PABPC1* GENE EXPRESSION ACROSS CARDIAC CELL TYPES IN CONTROL, ISCHAEMIC, AND FIBROTIC ZONES. 167

6.6 *PABPC1* PARALOGUES EXPRESSION IN *ANXA2A/B* CRISPANTS BEFORE AND AFTER CARDIAC LASER INJURY 170

6.7 DISCUSSION 172

CHAPTER 7: INVESTIGATION OF THE CARDIOPROTECTIVE PROPERTIES OF BLUE MUSSEL-DERIVED DRUG N2-01 IN COLLABORATION WITH N2 PHARMACEUTICALS (EXTERNAL PARTNER ORGANISATION) 177

7.1 INTRODUCTION 177

7.2 N2-01 DRUG MODULATES ENDOTHELIAL BEHAVIOUR BY SUPPRESSING CELL PROLIFERATION WHILE ENHANCING ANGIOGENIC NETWORK FORMATION 179

7.3 N2-01 TREATMENT RESULTED IN DELAYED DEVELOPMENT AND EARLY EMBRYONIC LETHALITY IN ZEBRAFISH 183

7.4 DISCUSSION 185

CHAPTER 8: GENERAL DISCUSSION 189

8.1 SUMMARY OF FINDINGS 189

8.2 CLINICAL IMPLICATIONS 191

8.3 CONCLUSION 194

REFERENCES 196

List of Figures

Figure 1. Schematic illustration of the temporal dynamics of cardiac regeneration in mice after myocardial infarction. 28
Figure 2. Graphical illustration outlining the strategy for meta-analysis of integrated single cell and single nucleus RNA-sequencing studies of coronary endothelial cells in mice and humans, spanning developmental and adult stages as well as healthy and diseased states...... 42
Figure 3. **Schematic of ventricular laser ablation and imaging in 3 dpf zebrafish larvae.**. 65
Figure 4. Multi-omics identification of ANXA2 as a reactivated foetal endothelial gene following myocardial injury. 81
Figure 5. In-house spatial transcriptomic data showing sections of adult human heart tissue from an uninjured, healthy control (UI), patients presenting with acute MI (aMI) and chronic MI (cMI). 82
Figure 6. Multi-omics identification of SERPINE1 as a top differentially expressed gene following acute MI...... 84
Figure 7. Expressions of ANXA2 paralogues (anxa2a and anxa2b) and serpine1 from endothelial cell-specific adult zebrafish heart regeneration single cell transcriptomics data (Ma et al., 2021).. 85
Figure 8. Generation of anxa2a/b knockdown in zebrafish using Alt-R CRISPR-Cas9 method...... 102
Figure 9. anxa2a/b crispants showed impaired embryonic development at 3 and 5 days post-fertilisation (dpf)...... 108
Figure 10. anxa2a/b crispants showed impaired trunk vascular development at 3 days post-fertilisation (dpf). 111
Figure 11. anxa2a/b crispants showed impaired cardiovascular development at 5 days post-fertilisation (at 48 hours timepoint).. 113
Figure 12. A larval zebrafish model of cardiac injury and regeneration.. 115
Figure 13. anxa2a/b knockdown impaired cardiac regeneration within the 48-hour regenerative window in larval zebrafish.. 119
Figure 14. Relative mRNA expression of fibrinolytic, angiogenic, and regenerative genes in uninjured 5 dpf anxa2a/b crispants...... 122
Figure 15. Relative mRNA expression of fibrinolytic, angiogenic, and regenerative genes in anxa2a/b crispants following 48 hours post-injury (hpi). 126
Figure 16. ANXA2 expression is upregulated in human cardiac tissues from myocardial infarction (MI) patients.. 138
Figure 17. SERPINE1 expression is upregulated in human cardiac tissues from MI patients.. 140
Figure 18. Co-expression of ANXA2 with Vimentin^{+} cells in human myocardial infarction (MI)...... 142

Figure 19. Single-cell transcriptomic profiling of ANXA2 across cardiac cell types in human control and myocardial infarction (MI)...... 144
Figure 20. Single-cell transcriptomic profiling of SERPINE1 across cardiac cell types in human control and myocardial infarction (MI)...... 146
Figure 21. Dot plot generated from our coronary endothelial cell meta-atlas, CrescENDO, illustrating the common upregulated DEGs (n=17) in foetal and dHF/cHF adult heart ECs compared to the uninjured adult heart...... 156
Figure 22. PABPC1, a foetal endothelial gene identified from CrescENDO, is reactivated in endothelial cells after myocardial injury across species and multi-omics datasets...... 159
Figure 23. In-house spatial transcriptomic data showing sections of adult human heart tissue from an uninjured (UI), healthy control, patients presenting with acute MI (aMI) and chronic MI (cMI). 160
Figure 24. Expression of PABPC1 paralogues (pabpc1a and pabpc1b) from endothelial cell-specific adult zebrafish heart regeneration single cell transcriptomics data..... 161
Figure 25. PABPC1 protein expression is induced in endothelial cells of the human heart following myocardial infarction (MI)...... 166
Figure 26. Cell type–specific expression of PABPC1 in control, ischaemic (IZ), and fibrotic (FZ) myocardial zones. 169
Figure 27. PABPC1 paralogues (pabpc1a/b) expression in anxa2a/b crispants before and after laser cardiac injury.. 171
Figure 28. Higher concentration of N2-01 appears to inhibit coronary endothelial cell proliferation following 24 hours of treatment. 181
Figure 29. N2-01 promoted endothelial tubule network formation at 5 hours post-treatment. 182
Figure 30. N2-01 treatment delays zebrafish embryonic development and reduces survival.. 184

List of Tables

Table 1. **Datasets included in the CrescENDO database**.. 51
Table 2. Clinical data for all samples used in from publicly available, processed single-nuclei RNA sequencing (snRNA-seq) dataset. 53
Table 3. Details of patients used for spatial transcriptomics.. 57
Table 4. CRISPR/Cas9 target sites. 59
Table 5. AltR CRISPR-Cas9 Injection mixture prepared for anxa2a/b knockdown 59
Table 6. Sequences of left and right primers for each target and PCR amplicon size are shown. 61
Table 7. PCR reaction components 61
Table 8. Thermocycling conditions for a routine PCR 61
Table 9. Denature/reanneal thermal cycler conditions. 62
Table 10. Zebrafish lines used in this project. 63
Table 11. Reverse Transcription reaction mix 67
Table 12. Pre-designed KiCqStart® SYBR® green primers for zebrafish genes 68
Table 13. RT-qPCR reaction mix 69
Table 14. Details of patients used for study by Masson's Trichrome and immunofluorescence staining (adapted from Li et al., 2022b). 70
Table 15. Top differentially expressed genes and their predicted functions of each of the 10 heterogeneous cardiac endothelial cell clusters/states in the adult mouse heart under healthy condition or following myocardial infarction (MI). 78
Table 16. Classification criteria for analysis of the gross developmental phenotype in anxa2a/b zebrafish crispants. 100
Table 17. The proportion of zebrafish larvae in each phenotypic category (normal, mild, moderate, severe, and dead) at 3 and 5 days post-fertilisation (dpf). 101
Table 18. Summary of one-way ANOVA with multiple comparisons for anxa2a qPCR validation data (related to Figure 8). 103
Table 19. Summary of one-way ANOVA with multiple comparisons for anxa2b qPCR validation data (related to Figure 8). 104
Table 20. Summary of one-way ANOVA with multiple comparisons for body length quantitative data (related to Figure 9). 109
Table 21. Summary of one-way ANOVA with multiple comparisons for eye diameter quantitative data (related to Figure 9). 110
Table 22. Common upregulated DEGs in foetal and dHF adult heart endothelial cells compared to the uninjured adult heart.. 152

List of Abbreviations

AKT serine/threonine kinase 1 (Akt1)

Aldehyde dehydrogenase 1 family, member A2 (raldh2)

Angiopoietin-1 (Ang-1)

Annexin A2 (ANXA2)

Atrioventricular (AV)

Average expression (avg.exp)

Beta-2 microglobulin (b2m)

Border zone (BZ)

Bone morphogenetic protein (BMP)

BRG1-assoicated factor 180 (BAF180),

Cadherin (Cdh5)

Cardiopulmonary bypass (CPB)

Cell death inducing p53 target 1 (Cdip1)

Circular RNA (circRNA)

CRISPR RNA (crRNA)

C-X-C motif chemokine ligand 12 (Cxcl12)

C-X-C motif chemokine receptor 4 (Cxcr4)

Cyclic adenosine monophosphate/protein kinase A (cAMP/PKA)

Days post-fertilisation (dpf)

Days post-injury (dpi)

Differentially expressed genes (DEGs)

Dilated cardiomyopathy-induced heart failure (dHF)

Disintegrin and metalloproteinase 8 (ADAM8)

Double-strand breaks (DSBs)

Duplex-guide RNA (dgRNA)

Duplex-guide RNA-Cas9 ribonucleoprotein complex (dgRNP)

Endoplasmic reticulum (ER)

Endothelial adhesion molecule (VCAM-1)

Endothelial cells (EC)

Endothelial-to-Mesenchymal transition (EndoMT)

Endothelial nitric oxide synthase (eNOS)

Epithelial-to-mesenchymal transition (EMT)

ETS Variant Transcription Factor 2 (ETV2)

Eukaryotic translation initiation factor 4G (eIF4G)

Extracellular matrix (ECM)

Fibroblast growth factor (FGF)

Fibrotic zone (FZ)

Fibulin-1 (Fbln1)

First-generation (F0)

Food and Drug Administration (FDA)

FOG family member 2 (ZFPM2/FOG-2)

Frizzled receptor-2 (Fzd2)

GATA Binding Protein 4 (Gata4)

Gene ontology (GO)

Heart failure (HF)

Heme oxygenase-1 (HO-1)

Hepatocyte growth factor (HGF)

Homeodomain Interacting Protein Kinase 3 (Hipk3)

Homologous recombination (HR)

Hours post-fertilisation (hpf)

Human cardiac microvascular endothelial cells (HCMECs)

Human Leukocyte Antigen (HLA)

Hydrogen peroxide (H_2O_2)

Hypoxia-inducible factor-1 (HIF-1)

Inflammatory-dilated cardiomyopathy (DCMi)

Intersegmental vessels (ISVs)

Interferon-related developmental regulator 1 (ifrd1)

Ischaemic cardiomyopathy-induced heart failure (cHF)

Ischaemic zone (IZ,

limb-bud and heart (Lbh)

lipopolysaccharide (LPS)

low-density lipoprotein (LDL)

low-density lipoprotein receptor-related protein 5 (lrp5)

Mammalian target of rapamycin (mTOR)

Matrix metalloproteinases (MMPs)

Mesenchymal-endothelial transition (MEndoT)

Mesenchymal stem cells (MSCs)

Methyltransferase 7 (PRMT7)

Myocardial infraction (MI)

NADPH oxidases (NOX)

Nitric oxide (NO)

NK2 homeobox 5 (Nkx2.5)

Non-homologous end joining (NHEJ)

Nuclear factor erythroid 2-related factor 2 /Nrf2)

Nuclear factor-kappa B (NF- κB)

Optimal Cutting Temperature (OCT)

Oxidative modification of low-density lipoprotein (ox-LDL)

Parachordal vessels (PAVs)

Percentage of expressing cells (pct.exp)

Phenylthiourea (PTU)

Photo Activated Laser Microdissection (PALM)

Placenta growth factor (PIGF),

Plasmalemma vesicle-associated protein (Plvap)

Plasminogen activator inhibitor type-1 (PAI-1)

Platelet-derived growth factor (PDGF)

Platelet-derived growth factor receptor alpha (PDGFRα)

Poly(A) binding protein cytoplasmic 1 (PABPC1)

Polyadenylate-binding protein 1 (PABP1)

Protein C receptor (PROCR)

(Pro)renin receptor (atp6ap2)

Quantitative polymerase chain reaction (RT-qPCR)

Reactive oxygen species (ROS)

Regions of interests (ROIs)

Relative quantification (RQ)

Remote zone (RZ)

Ribonucleoproteins (RNPs)

Ribosomal protein L7 (rpl7)

S100 calcium-binding protein A10 (S100A10)

Selective plane illumination microscope (SPIM)

Serpin peptidase inhibitor clade E member 1 (SERPINE1)

Single cell/nuclei RNA-sequencing (sc(n)RNA-seq)

Single-cell chromatin accessibility sequencing (snATAC-seq)

Sp3 transcription factor (SP3)

Standard deviation (SD)

T7 Endonuclease I (T7E1)

T-box factor 18 (tbx18)

T-box transcription factor 5 (Tbx5)

T-cell factor-4 (TCF4)

Tenascin C (Tnc)

Thrombomodulin (THBD)

Tissue plasminogen activator (tPA)

Trans-activating crRNA (tracrRNA)

Transcription activator-like effector nucleases (TALENs)

Transcription factor 21 (Tcf21)

Transcription factor EB (TFEB)

Transforming growth factor beta (TGF-β)

Traumatic brain injury (TBI)

urokinase-type plasminogen activator (uPA)

Vascular endothelial growth factor (VEGF)

VEGF receptors (VEGFR)

Wild type (WT)

Wilms tumour 1 (WT1)

Zinc-finger nucleases (ZFNs)

α-smooth muscle actin (α-SMA)

Chapter 1: Introduction

1.1. Myocardial Infarction, current treatments, and novel therapeutic approaches

Myocardial infarction (MI), colloquially known as a “heart attack”, is the most common contributor to heart failure (HF) worldwide (Jenča et al., 2021). Heart failure affects approximately 55.5 million patients globally according to the data from the Global Burden of Disease Study 2021, while recent estimates suggest the global prevalence of over 64 million, affecting 1% - 3% of the adult population; with numbers continuing to rise (Chen et al., 2025, Savarese et al., 2023). Almost 1 in 4 MI patients without a history of HF were reported to develop incident HF within 3 months of discharge (Butler et al., 2025). Development of HF after MI is often associated with adverse events, impaired quality of life, and lower survival (Jenča et al., 2021). Most incidences of MI result from underlying coronary heart disease, primarily precipitated by coronary occlusion (Ojha et al., 2022). Typically, the occlusion is thrombotic and occurs from the rupture of atherosclerotic plaques. This leads to a reduced or complete cessation of blood flow to the myocardium, subsequently resulting in hypoxia-induced myocardial apoptosis and necrosis (Ojha and Dhamoon, 2023). The loss of cardiomyocytes recruits activated fibroblasts to deposit extracellular matrix (ECM) proteins and form permanent scar in the infarcted area, which may cause irreversible functional deterioration, resulting in chronic heart failure and death (Stockdale et al., 2018).

Current treatments focus on delaying or preventing the progression to heart failure, but cannot ultimately halt or reverse cardiac remodelling, hence are non-curative (Cahill et al., 2017). Percutaneous coronary intervention (PCI), commonly achieved by ballooning the narrowed segment of the arterial wall, or implanting a stent to maintain patency, is the prevailing clinical procedure for alleviating coronary occlusion and restoring cardiac blood perfusion after MI (Ahmad et al., 2022). Despite continuous improvements of PCI procedures on survival from MI, the “no reflow” phenomenon (myocardial hypoperfusion despite the relief of coronary obstruction) can impact the effectiveness of revascularisation and has a strong negative impact on clinical outcome (Porto et al., 2006). And the incidence of coronary no reflow after receiving primary PCI is widely reported in between 5% and 32% of patients (Ndrepepa, 2023). Patients experiencing no-reflow during PCI face a higher risk of early post-infarction complications, adverse left ventricular remodelling, repeat hospitalisations for heart failure, and higher mortality (Derntl and Weidinger, 2012, Porto et al., 2006). While therapeutic advances have reduced cardiovascular mortality, non-cardiovascular deaths, particularly cancer and infection, remain common in patients with cardiovascular diseases. The contribution of each cause varies with different types of cardiovascular diseases and the level of multimorbidity (Drozd et al., 2021). Thus, a

holistic and personalised care approach that addresses the patient's overall health profile is important to improving long-term outcomes and survival.

Furthermore, pharmacologic drugs (i.e., beta-blockers, inhibitors of the renin angiotensin aldosterone system, and mineralocorticoid receptor antagonists) (De Luca, 2020), and device therapies (i.e. implantable cardioverter defibrillators and cardiac resynchronisation therapy) have multiple limitations (Breitenstein and Steffel, 2019, Dickstein et al., 2010). A comparative study of HF patients from two different eras (1993-1995 *versus*. 2006-2009) showed that medical advances, particularly increased beta-blocker use, significantly improved survival, reduced sudden death rates, and improved reverse cardiac remodelling and symptom relief, although progressive HF and non-cardiac complications remain challenges (Cubbon et al., 2011). Medications are only palliative, and mechanical assist devices are associated with complications related to infection, thrombosis, and power supply (Gerbin and Murry, 2015). Organ replacement by heart transplantation is an effective treatment, however it is only available to selected patients with end-stage cardiac disease due to donor shortage and human leukocyte antigen (HLA) matching. In addition, heart transplantation is accompanied with surgical risk and complications such as graft rejection, immunosuppression and post-transplant infection (Tu et al., 2020). Yet strategies to promote myocardial repair have failed to translate into clinical settings.

Novel approaches to repair the infarcted heart include cell therapy, gene therapy, stimulating endogenous pathways, direct cellular reprogramming, cardiac tissue engineering, and biomaterial delivery (Duelen and Sampaolesi, 2017, Melly et al., 2012, Collins et al., 2015, White and Chong, 2020, Cahill et al., 2017, Yu et al., 2021, Venugopal et al., 2012). Exogenous cell transplantation aims to deliver cells that could replace the lost cardiomyocytes by contributing to production of new myocardial tissue, as well as stimulating repair mechanisms via paracrine effects (Gerbin and Murry, 2015). Though cell-based cardiac regeneration has demonstrated good potential in pre-clinical animal studies, there are major challenges for clinical translation (Collins et al., 2015). For example, cell therapy approaches may show limited success by focusing on only a single cell type, typically of bone marrow origin (Duelen and Sampaolesi, 2017). In addition, cells were observed to have poor cell engraftment, viability and aggregation, as well as minimal integration into the host tissue (Kir et al., 2021). To optimise successful engraftment and cell survival, further investigation should aim to determine the appropriate cell types and delivery methods to be utilised. It was subsequently shown that the reparative potential of cell therapy may rely largely on paracrine signalling and secreted factors (White and Chong, 2020). Therefore, utilising paracrine factors to provide a pro-regenerative microenvironment becomes an attractive prospect (Ryan et al., 2020). Furthermore, the combination of stem cell biology with novel bioengineering and bio-delivery approaches could improve the efficacy of cell transplantation (Mitrousis et al., 2018). The ideal cardiovascular therapeutics would stimulate cardiac regeneration and replace the damaged myocardium. Future treatments should consider reciprocal and independent actions

of the key mechanisms of cardiac regeneration: remuscularisation, electromechanical stability, angiogenesis and arteriogenesis, resolution of fibrosis, and immunological balance (Bertero and Murry, 2018). However, the underpinning mechanisms remain poorly understood, and, with regeneration in mammalian models restricted to early developmental stages, the adult mammalian heart shows limited regenerative capabilities. It is not clear whether targeting endogenous mechanisms alone i.e. without an exogenous intervention, will suffice to induce regeneration in the adult mammalian heart (Price et al., 2019, Frangogiannis, 2015).

Efficient cardio-protection, modulated early inflammation, sustained neovascularisation, and myocardial renewal, are all essential to support cardiac repair and to counteract pathological remodelling (Balbi et al., 2019). Heart regeneration requires a concerted effort by several cell types within the heart, including epicardial cells, endothelial cells (ECs), nerves, fibroblasts and lymphatic cells (Ryan et al., 2020). We will need to stimulate such a coordinated response in human MI patients, utilising combined therapies to elicit a substantial improvement in regeneration (Price et al., 2019). The success of complete cardiac regeneration and clinical translation relies on the comprehensive understanding of the intrinsic mechanisms driving tissue repair and the scarring response. A major challenge in defining the molecular mechanisms for regeneration has been the lack of tools for conditionally manipulating specific genes in a tissue-specific manner in adult organisms. Recently, new tools such as CRISPR enable genome editing of regeneration pathways in model organisms (Goldman and Poss, 2020). Single-cell RNA sequencing is also a useful technology for identifying gene expression changes during cardiac regeneration (Wang et al., 2020b, Skelly et al., 2018, Farbehi et al., 2019). Improved knowledge in the molecular pathways specific for cardiac repair and regeneration might lead to new therapeutics, where reactivation of targeted genes may help to treat cardiovascular injuries.

1.2. Mechanisms and molecular regulation of neovascularisation in post-myocardial infarction repair

Following the onset of ischaemia, cardiac muscle undergoes a dynamic series of molecular, cellular, and extracellular responses that determine the remodelling and functional recovery of the myocardium. Post-MI healing generally occurs in three overlapping phases: 1) necrosis and apoptosis, 2) inflammation and extracellular matrix degradation, 3) remodelling and regeneration: ECM deposition, myocyte hypertrophy/renewal and revascularisation (Silvestre et al., 2013) (**Figure 1**). However, most of the processes governing the activation of vessel growth and vascular remodelling, are often compromised by the deleterious post-infarct microenvironment, characterised by fibrosis, inflammation, and reduced perfusion, which collectively suppress angiogenic and regenerative responses (Tzahor and Poss, 2017). Thus, restoring vascular homeostasis (through modulation of hypoxia pathways, immune activity, and haemodynamic forces) and stimulating neovascularisation may represent promising therapeutic strategy to re-establish vascular function and improve cardiac repair in the ischaemic heart (Silvestre et al., 2013, Tzahor and Poss, 2017).

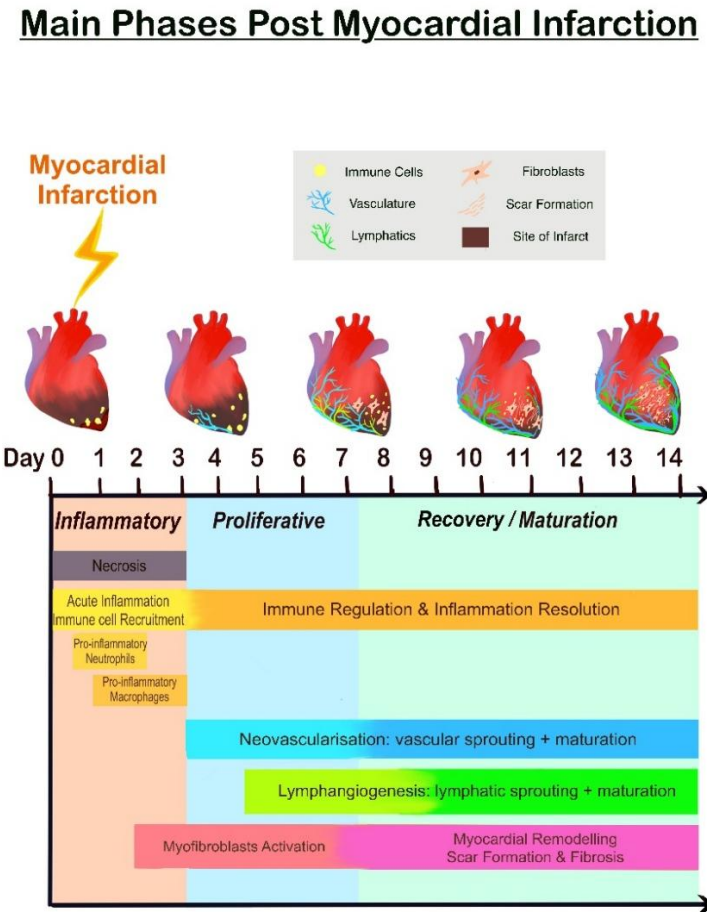

Figure 1. Schematic illustration of the temporal dynamics of cardiac regeneration in mice after myocardial infarction. *The top panel indicates the key for the schematic and graphical representation of the injured/repairing mouse heart. Following a myocardial infarction, ischaemic injury and cardiomyocyte necrosis trigger*

an extensive inflammatory response. During this inflammatory phase, monocytes and macrophages migrate into the infarcted region, where they clear necrotic cells and degrade extracellular matrix components. As inflammation subsides, the heart transitions into a proliferative or reparative phase, characterised by the activation of neovascularisation pathways and the initiation of myocardial remodelling through (myo)fibroblast proliferation. In the final recovery/maturation phase, activated fibroblasts and myofibroblasts continue to mediate scar formation and the development of fibrosis. (Figure created by me for the review in Berkeley et al., 2023)

Restoring perfusion to the injured myocardium remains a central challenge in post- MI therapy. New therapeutic strategies are urgently required to enhance myocardial perfusion, limit infarct expansion, and promote cardiac regeneration following MI (Berkeley et al., 2023). While much of the focus in heart repair has historically centred on cardiomyocyte proliferation and remuscularisation (Salerno et al., 2022), effective regeneration also depends critically on rapid and coordinated neovascularisation – the formation of new blood vessels. This process ensures sufficient oxygen and nutrient delivery to the regenerating myocardium, supporting cardiomyocyte survival, tissue repair, and long-term functional recovery (Uygur and Lee, 2016). Early and effective neovascularisation can rescue ischaemic myocardium, limit infarct expansion, and prevent the progression to HF by modulating cardiomyocyte hypertrophy and contractility (Cochain et al., 2013). Yet, despite considerable research, no effective treatment currently exists that can reliably induce coronary neovascularisation.

Neovascularisation refers to the formation of new microvascular networks either *de novo* or from pre-existing blood vessels. Although primarily observed during embryonic development, neovascularisation can also occur postnatally, particularly in response to ischaemia, inflammation, hypoxia or altered shear stress (Cai et al., 2022, Arellano Mendoza et al., 2007). This complex process comprises several biological processes: vasculogenesis, angiogenesis, arteriogenesis, and lymphangiogenesis, each contributing uniquely to vascular growth and adaptation (Hutchings et al., 2021, Rizzi et al., 2017).

Vasculogenesis is the *de novo* formation of blood vessels from endothelial progenitor cells derived from the bone marrow or circulation, which migrate to sites of injury/neovascularisation and differentiate into mature ECs (Isner and Asahara, 1999). During embryogenesis, vasculogenesis involves the differentiation of endothelial precursors (angioblasts) into ECs, followed by the assembly of a primitive vascular network (Carmeliet, 2000). However, this initial network is immature and functionally limited, requiring further maturation through angiogenesis, which therefore represents the primary therapeutic target for vascular regeneration (Carmeliet, 2000).

Angiogenesis describes the sprouting of new capillaries from pre-existing, mature blood vessels through EC proliferation, migration, and basement membrane remodelling (Zhu et al., 2021). Under physiological conditions, it is vital for embryonic vascular development, reproduction, and wound healing; it is tightly regulated by a fine

balance between pro- and anti-angiogenic factors (Cai et al., 2022). Angiogenesis proceeds through sequential key steps: activation of quiescent ECs by angiogenic stimuli, directed migration and proliferation to form sprouts, recruitment of pericytes to stabilise nascent vessels, and basement membrane reconstruction to generate a mature, functional microvasculature. In response to adult tissue injury, angiogenesis can be reactivated, allowing ECs and pericytes to coordinate vessel elongation, anastomosis, and remodelling until vascular homeostasis is restored (Zhu et al., 2021).

Arteriogenesis, in contrast, is the enlargement and maturation of pre-existing collateral arterioles into functional arteries, driven by increased shear stress within the vessel wall (López-Camarillo et al., 2020, Caporali et al., 2018, van Royen et al., 2001). It involves endothelial activation, monocytes recruitment, and smooth muscle cells proliferation, resulting in the formation of new arterial conduits that restore perfusion to ischaemic regions (Arellano Mendoza et al., 2007). Lymphangiogenesis follows shortly after vascular network establishment, arising from venous endothelial sprouts to form the lymphatic system, which supports tissue fluid balance, immune cell trafficking, and inflammation resolution during cardiac repair (Hutchings et al., 2021).

Neovascularisation during heart regeneration might recapitulate key processes of embryonic coronary vessel development (Kim et al., 2010). Coronary vasculature formation progresses through sequential, tightly regulated stages, beginning with proepicardium formation, which is dependent on NK2 homeobox 5 (Nkx2.5) and GATA Binding Protein 4 (Gata4), followed by migration of proepicardial cells to envelop the myocardium and form the epicardium. This migration is regulated by retinoic acid, angiopoietin-1 (Ang-1), t-box transcription factor 5 (Tbx5), Sp3 transcription factor (SP3), and Wilms tumour 1 (WT1). Within the epicardium, epicardial-derived cells arise via epithelial-to-mesenchymal transition (EMT), a process driven by myocardial fibroblast growth factor (FGF) and transforming growth factor beta (TGF-β) signalling and further modulated by transcriptional regulators friend of zinc finger protein/FOG family member 2 (ZFPM2/FOG-2) and BRG1-assoicated factor 180 (BAF180), as well as subepicardial matrix components such as podoplanin. Thymosin β4 secreted by the cardiomyocytes promotes epicardial-derived cell migration into the myocardium, where they respond to angiogenic factors (vascular endothelial growth factor (VEGF), FGF-2) and arteriogenic factors (platelet-derived growth factor (PDGF), TGF-β) to form the coronary vessel network (Smart et al., 2009). Similar molecular pathways are reactivated during adult zebrafish heart regeneration, where PDGF signalling plays a central role in epicardial function and reactivation of developmental neovasculogenic pathways (Kim et al., 2010).

The main stimuli for neovascularisation are hypoxia and inflammation. Hypoxia stabilises hypoxia-inducible factor-1 (HIF-1), which binds to over 40 hypoxia-sensitive genes, is involved in inducing angiogenesis and protective metabolic adaptation (de Muinck and Simons, 2004). Inflammatory macrophages and T-lymphocytes infiltrate the infarct zone and secrete angiogenic and arteriogenic factors such as VEGF, bFGF/FGF-2, and TGF-β (Corliss et al., 2016, Silvestre et al., 2013, Simões and Riley,

2022). Reactive oxygen species (ROS) also play a central role in neovascularisation. While excessive ROS contributes to oxidative stress and exacerbates cardiovascular disease, physiological levels act as essential second messengers that regulate endothelial proliferation, migration, and differentiation (Cholan et al., 2017, Hutchings et al., 2021). Hypoxia and reoxygenation promote the generation of ROS, which can stimulate angiogenesis directly or indirectly via active oxidation products, such as peroxidized lipids that are elevated in atherosclerosis (Kim and Byzova, 2014). This links oxidative stress to pathological angiogenesis, primarily via HIF-dependent upregulation of VEGF signalling (Kim and Byzova, 2014). In blood vessels, NADPH oxidases (NOX) are a major source of ROS, catalysing their production at the endothelial cell membrane. NOX-derived ROS initiate angiogenesis and support newly formed vessels at sites of injury by promoting migration of ECs, tubule formation, and the proliferation of vascular smooth muscle cells, thereby stabilising the neovasculature (Cholan et al., 2017, Hutchings et al., 2021). Maintenance of an optimal ROS level is therefore critical, as both insufficient or excessive ROS can impair cellular signalling and compromise regenerative processes. Study found impaired outgrowth ECs-mediated vascular repair in South Asian men is causally linked to decreased expression of AKT serine/threonine kinase 1 (Akt1) and endothelial nitric oxide synthase (eNOS), which are crucial for vascular health. The findings suggest that targeting the Akt1/eNOS pathway could be a strategy for treating cardiovascular disease in this population (Cubbon et al., 2014). Insulin resistance has also been reported to impair the function of circulating angiogenic progenitor cells and delay endothelial repair after arterial injury, indicating that metabolic dysfunction alone is sufficient to compromise endogenous vascular regeneration (Kahn et al., 2011).

Multiple growth factor families coordinate neovascularisation; with VEGF serving as the primary regulator. Secreted by hypoxic or proliferating tissues, VEGF-A activates ECs via VEGF receptors (VEGFR), initiating a Dll/Notch cascade that coordinates tip and stalk cell behaviour during sprouting (Pitulescu et al., 2017). FGFs similarly stimulate endothelial proliferation, migration and differentiation through receptor tyrosine kinase activation and downstream signalling cascades (Pontes-Quero et al., 2019, Cross and Claesson-Welsh, 2001). The angiopoietin-Tie axis further contributes to vascular maturation and stability. Angiopoietin-1 (Ang-1) binds to Tie2 receptors on ECs to enhance barrier integrity, survival, migration, and sprouting (Gaonac'h-Lovejoy et al., 2020), whereas Angiopoietin-2 (Ang-2) acts as a functional antagonist, inhibiting Ang-1/Tie2 signalling to restrain excessive vessel growth and branching *in vivo* (Hu and Cheng, 2009). A study found that treatment with recombinant connective tissue growth factor (CTGF) prevented microvascular rarefaction in human blood vessel organoids following glycolysis inhibition-induced damage, suggesting a reparative role for CTGF in restoring microvessel structure, and identifying CTGF as a critical paracrine regulator of microvascular integrity (Romeo et al., 2023).

Therapeutic strategies to enhance intrinsic angiogenesis may involve either supplementing paracrine factors exogenously (such as growth factors, microRNAs, or

exosomes) or upregulating endogenous pro-angiogenic pathways (Lupu et al., 2020). To date, several growth factors, including VEGF, placenta growth factor (PlGF), FGF, and hepatocyte growth factor (HGF), have demonstrated potent angiogenic potential (Cahill and Kharbanda, 2017). Delivery of these factors via naked DNA plasmids, viral vectors, or recombinant proteins improves cardiac function and myocardial angiogenesis in animal studies (Lee et al., 2019). For instance, intramyocardial injection of synthetic modified mRNA encoding human VEGF-A in murine MI models stimulated expansion of epicardial cardiac progenitor cells and directed their differentiation towards endothelial lineage, which resulted in enhanced myocardial perfusion and improved survival of recipients (Zangi et al., 2013). Subsequent study in a porcine model of MI has shown that administration of biocompatible, purified VGEF-A mRNA one week after MI, significantly improved left ventricular ejection fraction, inotropy, and ventricular compliance. This also led to increased arteriolar and capillary density, and reduced myocardial fibrosis at two months post-treatment (Carlsson et al., 2018).Similarly, lentiviral ETS Variant Transcription Factor 2 (ETV2) delivery into murine infarcted heart has shown to significantly upregulate genes linked to angiogenesis, anti-fibrosis, and anti-inflammatory responses (Lee et al., 2019).

Finally, the microRNA-15 family negatively controls cardiomyocyte proliferation and postnatal cardiac regenerative capacity. Inhibition of microRNA-15 from birth to adulthood was shown to enhance myocyte proliferation and improves cardiac function following adult MI (Porrello et al., 2013). Similarly, study using adeno-associated viral vector to deliver human microRNA-199 into infarcted pig hearts has resulted in enhanced cardiomyocyte proliferation and cardiac repair, with marked improvements in cardiac function, increased muscle mass, and reduced scar size (Eulalio et al., 2012, Gabisonia et al., 2019). However, most treated pigs developed fatal arrhythmias 7–8 weeks post-treatment due to uncontrolled, persistent microRNA expression. While the microRNA therapy holds exciting potential for cardiac regeneration, future applications must ensure precise dosing and controlled delivery to avoid adverse effects. In a porcine model of MI, the delivery of microRNA-21 via nanocarriers encapsulated within an injectable hydrogel matrix and administered into infarct regiones, significantly reduced inflammation by inhibiting the MI macrophage polarisation. This treatment also promoted local neovascularisation through the upregulation of VEGF-A and PDGF-BB in ECs, and rescued at-risk cardiomyocytes (Li et al., 2021b). Overexpression of the circular RNA (circRNA) of Homeodomain Interacting Protein Kinase 3 (Hipk3) via adeno-associated virus 9 in adult mice promoted cardiomyocyte proliferation, reduced apoptosis in cardiomyocyte, and increased vessel density in the infarcted region at 14 days post-MI, while also improving cardiac function and reducing fibrotic area (Si et al., 2020).

Beyond their structural role in vascular formation, ECs play a key role in paracrine and autocrine regulation of the cardiac myocytes. Endothelial-derived angiocrine factors such as neuregulin-1, endothelin-1, and nitric oxide directly regulate cardiomyocyte contractility, metabolism, and survival (Rafii et al., 2016). Neuregulin is expressed and

released by ECs in response to hypoxia-induced myocyte death, and co-culture experiments have shown that endothelial-derived neuregulin protects adult murine cardiomyocytes from hypoxic/ischaemic injury (Hedhli et al., 2011). Moreover, neuregulin gene deletion or silencing resulted in impaired post-ischaemic myocyte repair and loss of cardioprotection (Hedhli et al., 2011).

Following MI, local ischaemia initiates a cascade of vascular and inflammatory events, including endothelial disruption, increased capillary permeability, and loss of cardiomyocytes, activating local cytokine and growth factor release. These signals recruit endothelial progenitor cells and stimulate EC proliferation, migration, and vessel formation, particularly in the peri-infarct region, where vascular density progressively expands into the infarct core (Cai et al., 2022, Hutchings et al., 2021, Isner and Asahara, 1999). Enhancing endothelial survival and inhibiting apoptosis appear key to sustaining angiogenesis. A novel population of cardiac interstitial cells named telocytes has been shown to facilitate cardiac angiogenesis and regeneration after MI. Cardiac telocyte-derived exosomes suppress apoptosis in microvascular ECs by silencing the pro-apoptotic gene, cell death inducing p53 target 1 (*Cdip1*), and reducing caspase-3 activation, thereby promoting endothelial survival and sustained angiogenesis (Liao et al., 2021).

In conclusion, post-MI neovascularisation is a tightly regulated interplay between hypoxia, inflammation, ROS signalling, growth factor activation, and progenitor cell mobilisation. By re-establishing perfusion and supporting myocardial survival, these mechanisms are fundamental to cardiac repair. However, their precise regulation remains incompletely understood. These likely involve a precise balance between pro- and anti-angiogenic regulators and effectors. Therapeutic strategies that modulate these mechanisms to enhance angiogenesis, arteriogenesis, and vasculogenesis hold significant promise for improving outcomes in ischemic heart disease.

1.3. Comparative insights into cardiac regeneration: conserved mechanisms and lost potential from zebrafish to humans

1.3.1 Regenerative capacity of the heart across species and developmental stages

Cardiac regeneration after injury was first reported in the 1970s and was long considered to be restricted to lower vertebrates such as amphibians and fish (Poss et al., 2002, Becker et al., 1974, Oberpriller and Oberpriller, 1974). For decades, this phenomenon was believed to be absent in mammals, as adult mammalian hearts typically respond to injury with fibrotic scar formation rather than regeneration (Iismaa et al., 2018). Despite this, subsequent discoveries showing that neonatal mammals retain a short window of regenerative potential have transformed our understanding of heart cell plasticity. Neonatal murine and porcine hearts can completely restore structure and function after injury, but this capacity declines rapidly after birth (Haubner et al., 2012, Ye et al., 2018, Porrello et al., 2011).

The hearts of one-day-old neonatal mice can fully regenerate and restore normal anatomy and function after surgical resection of the left ventricular myocardium; however this regenerative capacity is lost by postnatal day seven (P7) (Porrello et al., 2011). Similarly, complete functional mammalian cardiac regeneration was first observed in a neonatal mouse model of myocardial infarction within seven days after birth. This regenerative window is linked to the capacity of neonatal cardiomyocytes to maintain proliferation, which is supported by sustained expression of cell cycle regulators (Haubner et al., 2012). However this regenerative potential is lost beyond the first week after birth due to cardiomyocyte binucleation and cell-cycle exit (Naqvi et al., 2014).

In addition to neonatal cardiomyocyte proliferation, neovascularisation is a crucial component of neonatal heart repair. Endothelial cell activation, migration, and sprouting was shown to precede cardiomyocyte ingrowth, highlighting an interdependence between vascular and myocardial regeneration (Ingason et al., 2018). Extensive sprouting of collateral arteries was observed to develop from arterial ECs in the neonatal mouse heart 4 days post after MI via C-X-C motif chemokine receptor 4/ C-X-C motif chemokine ligand 12 (Cxcr4/Cxcl12) signalling (Das et al., 2019). These collateral arteries act as bridges between non-injured and obstructed arteries, creating bypass routes to enhance blood vessel perfusion and facilitate neonatal heart regeneration (Das et al., 2019). A similar window for myocardial regeneration has been observed in neonatal pigs, where 2-day-old hearts demonstrated early functional regenerative capacity after MI, characterised by cardiomyocyte proliferation and absence of scarring. However, this capacity is quickly lost when cardiomyocytes exit the cell cycle after birth, and by postnatal day 3–14 infarcted hearts did not

demonstrate the same level of regeneration and developed myocardial scarring without functional recovery (Zhu et al., 2018, Ye et al., 2018).

1.3.2 Zebrafish as a model for complete cardiac regeneration

Among vertebrates, the zebrafish (*Danio rerio*) exhibits one of the most remarkable examples of natural cardiac regeneration. Although structurally simpler – possessing only a single atrium and ventricle – the zebrafish heart shares key histological and cellular similarities with higher vertebrates, making it an ideal comparative model to understand the limiting factors impeding mammalian regeneration (Ryan et al., 2020). Following cardiac damage, zebrafish initiate inflammatory (the recruitment of immune cells and the clearance of cellular debris) and reparative responses (deposition of collagen and other extracellular matrix (ECM) components) similar to those in mammals (Ryan et al., 2020). However, humans exhibit scar formation and poor renewal of cardiomyocytes, whereas zebrafish exhibit resolution of collagen-rich scar and complete myocardial renewal (Ryan et al., 2020). Adult zebrafish can fully regenerate their hearts within 60 days following ventricular amputation, without permanent fibrotic scarring (Poss et al., 2002, Poss et al., 2003). Regenerative responses have also been confirmed in zebrafish embryos at 24 hours post-fertilisation (hpf) following cardiac amputation (Raya et al., 2003). Studies of multiple zebrafish heart injury models such as cryoinjury, genetic ablation, hypoxia, and laser-induced injury have provided evidence showcasing the exceptional regenerative ability of the larval and adult zebrafish heart (González-Rosa et al., 2017, Ross Stewart et al., 2021, Matrone et al., 2013).

Around three to four days post-injury, adult zebrafish heart regeneration is initiated by expansion of myocardial progenitor cells localised at the apical edge of existing myocardium (Lepilina et al., 2006). By seven days, epicardial cells begin to invade the wound, induce developmental markers, and rapidly proliferate. A subpopulation of these epicardial cells then undergo epithelial-to-mesenchymal transition (EMT) to contribute to neovascularisation and vascularise the regenerating muscle (Lepilina et al., 2006). Other studies have reported another origin of regenerated myocardium in the zebrafish after ventricular resection. They found zebrafish myocardium regeneration occurs primarily through activation and proliferation of pre-existing dedifferentiated cardiomyocytes (Kikuchi et al., 2010, Jopling et al., 2010).

Efficient zebrafish heart regeneration depends on the rapid and coordinated formation of new blood vessels alongside myocardial replenishment. Without timely endothelial invasion and revascularisation of the injured area, cardiomyocyte proliferation fails, leading to fibrotic scar formation rather than regeneration (Marín-Juez et al., 2016). Following injury, coronary vessel growth is orchestrated by reciprocal signalling between the epicardium and endocardium (the epicardium directs vascular patterning through Cxcl12/Cxcr4 signalling, while the endocardium promotes angiogenesis via Vegfa pathways). (Marín-Juez et al., 2019). The resulting neovasculature not only

restores perfusion but also provides structural scaffolds and paracrine cues that support cardiomyocyte proliferation and tissue remodelling. In addition, both tissues produce retinoic acid (a crucial signalling molecule for embryonic cardiac growth) which further stimulates cardiomyocyte proliferation and myocardial regeneration (Kikuchi et al., 2011a). Recapitulation of timely and injury-spanning neovascularisation presents the initial and crucial phase in the process of cardiac regeneration, extending beyond its classical role as a transport system of oxygen and nutrient (Marín-Juez et al., 2019).

1.3.3 Cardiac regeneration in humans

The adult human heart was long regarded a post-mitotic organ, lacking regenerative capacity. However, radiocarbon dating studies by Bergmann and colleagues challenged this paradigm, revealing evidence of low-level cardiomyocyte turnover (<1% per year) throughout the adult human lifespan (Bergmann et al., 2009). Carbon-14 concentrations were measured in cardiomyocyte DNA from individuals born before and after the atmospheric spike caused by nuclear bomb testing during the Cold War (Bergmann et al., 2009). Carbon-14 was used as a "birth date" marker for cells as it was incorporated into newly synthesised DNA during cell division. And elevated levels of Carbon-14 in individuals post-testing indicated continual cardiomyocyte renewal throughout life. Although the number of cardiomyocytes is established perinatally and remains stable during the human lifespan, adult cardiac ECs exhibit higher proliferation rates (>15% per year) compared to cardiomyocytes and mesenchymal cells (<4% per year), suggesting ongoing vascular plasticity even in adulthood (Bergmann et al., 2015). However the validity of studies have been debated due to concerns surrounding their methodology, data interpretation, and appropriateness of patient samples, and the findings are yet to be replicated (Kajstura et al., 2012).

A compelling clinical observation further supports the existence of regenerative potential in humans. A newborn patient who suffered a severe MI due to coronary artery occlusion achieved complete structural and functional recovery within 12 months. Follow-up imaging and clinical assessment revealed that the patient's heart was indistinguishable in function and morphology from those of age-matched healthy patients (Haubner et al., 2016).

This single case indicates that, akin to zebrafish and some neonatal mammals, newborn humans may possess an endogenous capacity to repair myocardial damage and restore cardiac function following MI. In contrast, the adult human heart remains largely incapable of physiological regeneration after ischaemic injury. As observed in other mammalian species, the regenerative potential in humans appears to be confined to early developmental stages, implying that intrinsic regenerative programmes may persist transiently after birth but are subsequently silenced or repressed as maturation proceeds.

Taken together, these findings highlight a conserved but developmentally restricted regenerative capacity across vertebrates. Understanding how organisms such as zebrafish coordinate vascular and myocardial regeneration and elucidating the molecular mechanisms underlying the loss of these processes in adult mammals, will be pivotal for designing therapeutic strategies to reactivate regenerative pathways in the human heart.

1.4. Reactivation of developmental gene programmes as a therapeutic approach in adult cardiovascular disease

Tissue regeneration and embryonic development share many molecular and cellular hallmarks. It is increasingly recognised that genes essential for embryogenesis are often reactivated following injury, initiating regenerative processes that promote cell proliferation, migration, and morphogenesis (Goldman and Poss, 2020). Certain fish and amphibians demonstrated a remarkable capacity for cardiac regeneration throughout life (Poss et al., 2003). The activation of embryogenesis genes was previously described during retinal (Fausett and Goldman, 2006) and cardiac (Lepilina et al., 2006) regeneration in zebrafish. In post-injury zebrafish models, re-expression of embryonic cardiogenesis genes contributed to cardiac regeneration through activation and proliferation of cardiomyocyte subpopulations (Kikuchi et al., 2010).

In adult zebrafish, injury triggered re-expression of embryonic epicardial genes, including aldehyde dehydrogenase 1 family, member A2 *(raldh2)* and T-box factor 18 *(tbx18)*, which promoted cardiomyocyte proliferation and myocardial regeneration (Kikuchi et al., 2011b, Lepilina et al., 2006, Wang et al., 2015). These developmentally activated epicardial-derived cells facilitated regeneration by invading and vascularising the new myocardium via Fgf signalling (Lepilina et al., 2006). In the adult murine heart, injury reactivated the normally quiescent epicardium and endocardium, leading to the re-expression of embryonic genes and the initiation of reparative and revascularisation programmes. Together, these activated tissues provided guidance cues and Vegfa-mediated signalling to induce coronary revascularisation, forming structural scaffolds that supported cardiomyocyte replenishment and tissue repair (Marín-Juez et al., 2016, Marín-Juez et al., 2019). Together, these findings suggested that reactivation of developmental programmes was a conserved mechanism underlying heart regeneration in zebrafish.

The discovery that the neonatal mammalian heart retains transient regenerative capacity has stimulated extensive research to determine whether reactivation of developmental programmes could enhance repair in adult hearts. Although early studies of foetal gene reactivation has primarily been focused on cardiomyocytes (Gidh-Jain et al., 1998), it is also evident that similar mechanisms occur in other cardiac cell types, such as endothelial and epicardial cells (Mehdiabadi et al., 2022). In adult mammals, including mice, the normally quiescent epicardium was shown to

be reactivated following injury to re-express embryonic developmental genes such as *Wt1*, *Tbx18*, Transcription factor 21 *(Tcf21)*, and *Raldh2*, thereby promoting cell proliferation, neovascularisation, and ischaemic heart repair (Smart et al., 2011, Vieira et al., 2017, Zhou et al., 2011, van Wijk et al., 2012). Similarly, *Wt1*, a key regulator of embryonic heart development, was re-activated in the coronary vasculature following cardiac damage in adult zebrafish (González-Rosa et al., 2011) and rats (Wagner et al., 2002).

Following cardiac injury, reactivation of foetal gene programmes in the epicardium and endocardium plays a vital role in coordinating coronary revascularisation. The injured-activated epicardium guided regenerating coronary vessels through Cxcl12/Cxcr4 signalling, while the endocardium contributed via Vegfa-mediated pathways, together directing coronary vessel growth and organisation (Marín-Juez et al., 2019). These regenerating coronaries not only restored perfusion but also provided structural scaffolds and paracrine cues essential for cardiomyocyte replenishment. In parallel, both activated tissues re-express developmental regulators such as retinoic acid, a key embryonic cardiac morphogen, to stimulate cardiomyocyte proliferation and regeneration (Kikuchi et al., 2011a). This coordinated reactivation of developmental angiogenic and developmental pathways highlights the pivotal role of blood vessels beyond their transport function, positioning timely, injury-induced neovascularisation as an initiating and crucial phase of cardiac regeneration.

Upon reactivation after ischaemic injury, the quiescent adult mouse epicardium recapitulated foetal-like characteristics, promoting the proliferation of epicardium-derived cells between three days and two weeks post-MI. These cells subsequently differentiated into mesenchymal cells, which modulated myocardial injury and supported angiogenesis by secreting paracrine factors that promoted neovascularisation and myocardial healing (Zhou et al., 2011). In *PdgfbCreERT2* mice, quiescent endocardium and coronary sinus cells responded to ischaemic injury by recapitulating developmental programmes such as thymosin β4, thereby facilitating the formation of new capillary networks within the infarcted myocardium (Dubé et al., 2017). Although direct epicardial contribution to new vessel formation was minimal, the epicardium provided essential directional cues for neovascular outgrowth toward the infarcted myocardial tissue (Dubé et al., 2017). Likewise, endocardial angiogenesis contributed to restored perfusion in the hypoxic region and rescued reversibly injured cardiomyocytes via VEGFR2 signalling in a murine MI model (Kobayashi et al., 2017). These findings emphasise the therapeutic potential of reactivating foetal gene programmes in adult hearts to stimulate neovascularisation and promote myocardial healing following MI.

The role of mesenchymal-endothelial plasticity in this process remains debated. Mesenchymal-endothelial transition (MEndoT) was previously reported to contribute to substantial numbers of coronary ECs after MI (Ubil et al., 2014). However, another study reported that pre-existing ECs were the main contributors to neovascularisation, with no evidence of fibroblast contribution, suggesting no contribution of MEndoT to

neovascularisation (He et al., 2017). Interestingly, a partial induction of Endothelial-to-Mesenchymal transition (EndoMT) appeared to contribute to clonal expansion and new vessel growth under ischaemia, although functionally active blood vessels not formed (Manavski et al., 2018). In contrast, advanced lineage tracing study in a mouse MI model reported no significant contribution from EndoMT post-MI, but the adult cardiac endothelium was maintained primarily through resident ECs clonal proliferation (Li et al., 2019c).

Conversely, aberrant expression of foetal genes has been linked to (mal-)adaptive changes in cardiac function in the adult failing heart. The ventricular re-expression of some foetal genes, including atrial and brain natriuretic peptide, foetal isoforms of contractile proteins, foetal type cardiac ion channels and some smooth muscle genes, has been associated with cardiac remodelling in response to pathological stress (Kuwahara et al., 2012). Indeed, foetal gene programmes are frequently used as biomarkers of cardiac hypertrophy and HF in pre-clinical models (Dirkx et al., 2013). In addition, several foetal genes such as limb-bud and heart (*Lbh*), *frizzled receptor-2* (*Fzd2*), fibulin-1 (*Fbln1*), and tenascin C (*Tnc*), have also been found to be reactivated in cardiac ECs during myocardial remodelling or HF (Vermeulen et al., 2019).

It is possible that the re-activation of foetal gene programmes initially serves a reparative or adaptive purpose following cardiac injury, promoting survival of myocardium. However, when this re-expression is sustained or becomes dysregulated or chronic, this foetal-like reprogramming may not be sufficient to support cardiac healing, which progress to maladaptive changes that ultimately lead to cardiac dysfunction and HF (Dirkx et al., 2013). Interestingly, the reparative process in adult hearts was correlated with a high and robust expression of inflammatory and fibrotic genes, whereas the foetal heart demonstrated diminished inflammatory and fibrotic response leading to complete cardiac regeneration (Zgheib et al., 2014).

Understanding the mechanisms behind the differential gene expression between foetal and adult diseased hearts could reveal new therapeutic targets to promote cardiac repair. Future research should therefore focus on elucidating how reactivated embryonic genes influence endothelial and myocardial regeneration, and how temporal regulation of these pathways could be harnessed to enhance repair while preventing maladaptive remodelling (Berkeley et al., 2023). Ultimately, these insights highlight the importance of targeted strategies to reactivate developmental angiogenic programmes to improve neovascularisation in the adult human heart after MI.

1.5. Multi-omics approaches to inform our understanding of cardiovascular disease research and advanced technologies

Recent advances in high-throughput single cell/nuclei and spatial omics technologies have transformed our understanding of complex diseases, particularly in cardiovascular diseases e.g. MI and HF (Berkeley et al., 2023). Traditional bulk omics approaches measure the average molecular signals from entire tissue samples, which can mask the heterogeneity and distinct behaviours of individual cell types (Lim et al., 2024). In contrast, single-cell/nuclei and spatial omics enable researchers to reveal expression profiles of thousands of individual cells and allow detailed dissection of transcriptional diversity and cellular states in both health and diseased hearts (Abplanalp et al., 2022).

A typical single-cell RNA sequencing (scRNA-seq) workflow includes single-cell capture, reverse transcription, amplification, library preparation, sequencing and data analysis (Chen et al., 2021). Single-nucleus RNA sequencing (snRNA-seq) offers technical advantages when analysing adult cardiomyocytes and minimises stress-induced aberrant gene expression during cell isolation (Chen et al., 2021). New techniques have advanced beyond single-cell transcriptomics to profile multiple omics layers, such as the genome, proteome, epigenome, and metabolome, which can reveal gene regulatory mechanisms in the heart (Tan et al., 2023). Emerging techniques like single-cell chromatin accessibility sequencing (scATAC-seq), proteomics and DNA methylomics are increasingly integrated with transcriptomic and spatial data to provide a comprehensive, multi-dimensional view of gene expression and cellular interactions within native cardiac tissue architecture (Chen et al., 2021). This spatial multi-omics approach overcomes limitations of traditional methods, improving our understanding of cellular heterogeneity and complex interactions relevant to cardiovascular diseases, including MI (Kiessling and Kuppe, 2024).

Yet spatial transcriptomics faces several technical and methodological limitations that can affect data interpretation and reproducibility. Spatial transcriptomics methods vary widely in resolution, capture efficiency, and transcriptome coverage, requiring careful method selection and tissue-specific optimisation by the investigator. Most platforms are optimised for fresh frozen tissue rather than paraffin-embedded sample, and additional tissue-specific optimisation is often required. Widespread adoption is further limited by high cost, technical complexity, the need for specialised equipment, and a complex analytical landscape (Piñeiro et al., 2022). In particular, spot-based spatial transcriptomics lacks true single-cell resolution; for example, each 10x Visium spot (55 µm diameter) captures transcripts from approximately 1 to 30 cells, resulting in mixed transcriptomics signals that obscure individual cell types (Zhu et al., 2024, Thuilliez et al., 2024). Compared to scRNA-seq, spatial transcriptomics has lower detection sensitivity and higher dropout rates, capturing fewer transcripts overall and making it challenging to detect rare or weakly expressed genes, which may be crucial for

identifying specific cell states or early developmental signals (Maden et al., 2023, Molla Desta and Birhanu, 2025).

To overcome these limitations, computational deconvolution using scRNA-seq references is often applied to estimate cell-type contributions within mixed-cell spots. However, accuracy is limited by reference bias, batch effects, low-resolution spots, oversimplified assumptions, and difficulties in detecting rare cell types (Zhou et al., 2023, Gaspard-Boulinc et al., 2025). Additional limitations include restriction to thin 2D tissue slices (5-20 μm), profiling of small regions that may not capture tissue heterogeneity, and the high cost and labour intensity that often limit studies to few biological replicates, reducing statistical power of the findings (Sui et al., 2024, Jeon et al., 2023). Together, these challenges highlight the need for advanced experimental and computational strategies to improve the resolution, sensitivity, and interpretability of spatial transcriptomics data.

Despite these challenges, single-cell and spatial multi-omics approaches have been successfully applied to map cardiac cellular composition and reveal important functional roles for non-myocyte cell types, including cardiomyocytes, endothelial cells (ECs), fibroblasts, and immune cells, in both murine and human hearts (Skelly et al., 2018, Tucker et al., 2020, Litviňuková et al., 2020, Jones et al., 2022, Consortium, 2018). The single-cell atlases generated from healthy cardiac tissues now serve as the baseline for comparison to identify cell type-specific and chamber-specific transcriptional changes during cardiac injury/disease (Tan et al., 2023). Notably, an atlas of over 32,000 single-EC transcriptomes from 11 healthy mouse tissues identified 78 distinct EC subclusters, highlighting the extensive heterogeneity and specialisation of ECs, which are highly influenced by their tissue of origin (Kalucka et al., 2020). This atlas provided a list of genetic markers for organ-specific ECs; for instance, brain ECs expressed genes for neurotransmitter transport, while heart ECs expressed genes related to fatty acid metabolism. Significant differences in EC metabolic gene signatures further indicates that ECs adapt their metabolism to suit the specific needs of their surrounding tissue (Kalucka et al., 2020). ScRNA-seq of *Pdgfb*-lineage mouse cardiac ECs mapped their transcriptome and heterogeneity in healthy and infarcted hearts, revealing ten transcriptionally distinct EC profiles, associated with proliferation, cardiac and ECM remodelling. This study identified plasmalemma vesicle-associated protein (*Plvap*) to be highest in clusters predominantly comprised of ECs from the MI group, and as a novel endothelial-specific marker with a functional role in cardiac neovascularisation after ischaemic injury in both mice and humans (Li et al., 2019b). A later multi-species meta-analysis of coronary EC data from scRNA-seq studies in the healthy and injured mouse and human hearts, generated the EC meta-atlas CrescENDO, showing temporal transcriptome shifts during the inflammatory, angiogenic, and vascular maturation phases following injury/disease (Li et al., 2022b) (**Figure 2**).

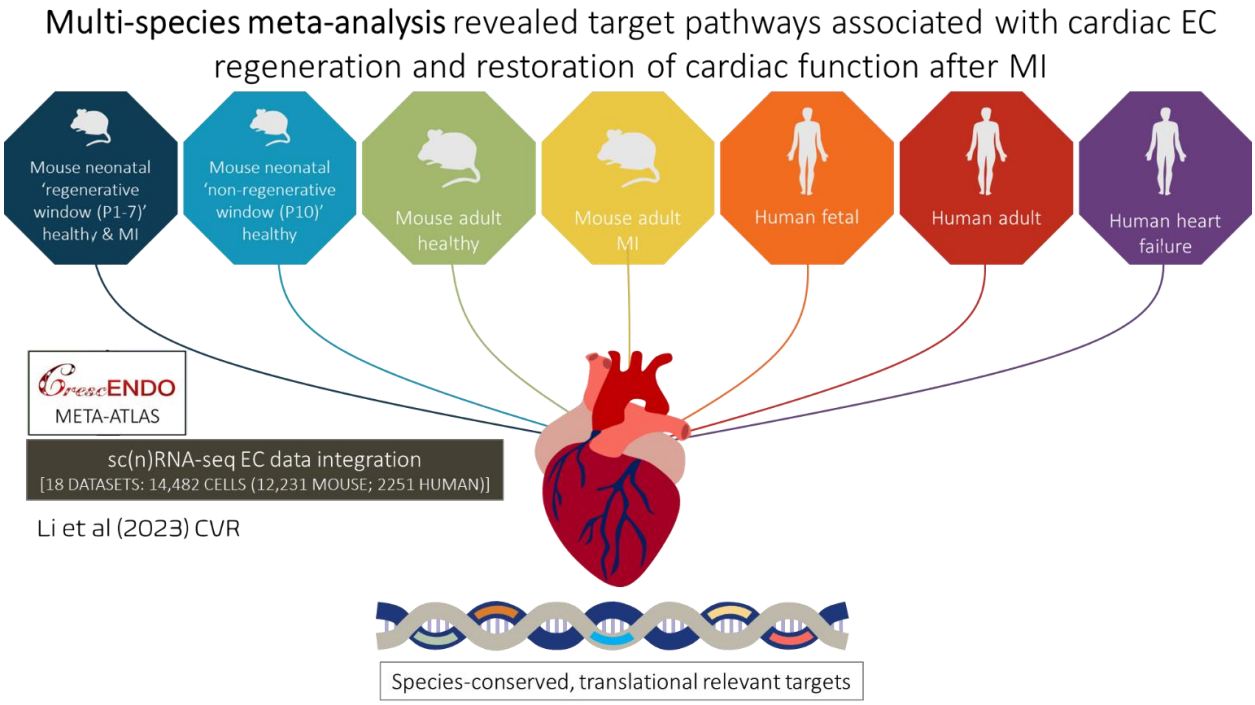

Figure 2. Graphical illustration outlining the strategy for meta-analysis of integrated single cell and single nucleus RNA-sequencing studies of coronary endothelial cells in mice and humans, spanning developmental and adult stages as well as healthy and diseased states. *This comprehensive analysis generated an extensive resource of candidate targets with potential roles in coronary vascular regeneration, which can be accessed through the CrescENDO meta-atlas (adapted from Li et al., 2022b).*

While mammalian studies have shed light on the limited regenerative responses of the adult heart, zebrafish single-cell and spatial transcriptomic provide a complementary model to uncover mechanisms that underlie complete cardiac regeneration. Using single cell transcriptomics, researchers mapped over 61,000 non-cardiomyocyte cell populations during zebrafish heart regeneration following ventricular apex amputation (Ma et al., 2021). This study showed that effective cardiac regeneration relies on the cooperative, functional coordination of various non-myocyte cell types, particularly macrophages, rather than solely the proliferation of cardiomyocytes. Disrupting macrophage function compromised intercellular interactions among non-cardiomyocytes, resulting in defective cardiac repair (Ma et al., 2021). Spatially resolved RNA sequencing (tomo-seq) was used to generate a high-resolution genome-wide atlas of gene activity in the regenerating zebrafish heart following cryoinjury (Wu et al., 2016). This study identified two wound border zones with distinct expression profiles, including the re-expression of embryonic cardiac genes and targets of bone morphogenetic protein (BMP) signalling. They found that upregulating BMP signalling is crucial for cardiomyocyte dedifferentiation and proliferation, and its inhibition impairs regeneration (Wu et al., 2016). Single nucleus RNA-sequencing (snRNA-seq) of the injured zebrafish heart revealed distinct cardiomyocyte

populations with diverse functions related to stress response, myofibril assembly, proliferation and contraction (Forman-Rubinsky et al., 2025). A comprehensive 3D and 4D spatiotemporal transcriptomic and cellular atlas of the uninjured and regenerating zebrafish heart was generated using integrated spatial transcriptomics (Stereo-seq) and scRNA-seq across eight stages of regeneration. This work characterised cardiomyocyte dynamics during regeneration, identified novel regenerative genes such as interferon-related developmental regulator 1 *(ifrd1)* and (pro)renin receptor (*atp6ap2)*, and characterised non-cardiomyocyte contributions, particularly macrophages, in coordinating the repair process (Li et al., 2025).

By integrating single-cell and spatial omics, it was made possible to map the hearts' cellular landscape at an unprecedented resolution, gaining new insights into the temporal and localised transcriptomic responses to myocardial injury. This allows for the deconvolution of complex processes like inflammation, remodelling, fibrosis, and repair or failure following MI (Abplanalp et al., 2022). By uncovering disrupted or rewired cell-cell communication networks post-MI, these approaches provide mechanistic insights into the roles of vascular, immune, and fibroblast during repair, offering novel molecular targets to enhance cardiac regeneration and improve clinical outcomes.

1.6. Current clinical trials to promote neovascularisation post-MI in the heart

There is a number of different approaches that are in development or have been used in clinical trials to treat patients with cardiovascular diseases, such as administration of stem and progenitor cells, stromal cells, extracellular vesicles and exosomes, growth factors, non-coding RNAs, episomes, gene therapies, biomaterials, and tissue engineering products (Fernández-Avilés et al., 2017). To date, most clinical trials have focused on inflammation, infarct size, and ventricular remodelling. Although these studies are safe in humans, but they have shown inconsistent efficacy, and significant prolonged clinical improvements were rare (Berkeley et al., 2023, Seropian et al., 2014). These inconsistent conflicting results can likely be attributed to variations in study design and evaluated endpoints (Rogozińska et al., 2020).

Clinical trials were attempted to induce therapeutic neovascularisation in patients. Catheter-based intracoronary VEGF gene transfer for coronary heart disease, was proven to be feasible and well-tolerated, however no differences in clinical restenosis rate or minimal lumen diameter were present after the 6-month follow-up, while a significant increase was detected in myocardial perfusion (Hedman et al., 2003). Percutaneous intramyocardial transfer of VEGF/FGF in patients with refractory heart ischaemia did not show significant improvement in myocardial perfusion, while the treatment was considered safe throughout the follow-up period of 1 year (Kukuła et al., 2011). VEGF-A has emerged as a promising angiogenic intervention strategy.

Intradermal injection of modified mRNA encoding VEGF-A in mice with diabetic wounds resulted in sustained microvascular response and accelerated diabetic wound healing by improving vascularisation and oxygenation without adverse effects (Sun et al., 2018). Purified modified mRNA encoding human VEGF-A was validated as a safe and effective treatment for ischaemic heart disease, as it significantly improved neovascularisation, heart function, and tissue recovery without triggering an innate immune response when administered two months after MI in mini-pigs (Carlsson et al., 2018). The ongoing EPICCURE (Phase 2a) trial, which aimed to evaluate the efficacy of VEGF-A mRNA therapy for cardiac angiogenesis in patients undergoing coronary artery bypass grafting surgery, was prematurely terminated due to slow patient recruitment (Collén et al., 2022). However, the study successfully met its primary endpoint of safety.

Plasmid-mediated gene therapy has been a popular delivery method for treating cardiovascular disease. A Phase 1/2 trial evaluated the safety of percutaneous catheter-based gene transfer of naked plasmid DNA encoding for phVEGF2 to left ventricular myocardium in inoperable patients with class III or IV angina. This trial reported significant reduction in anginal class (Losordo et al., 2002). The preliminary safety data and the observed positive trends in efficacy supported the need for further investigation in a larger Phase 2/3 trial. However, a subsequent larger scale NORTHERN trial investigating gene therapy with 2,000 µg of VEGF plasmid DNA delivered via the endocardial route using an electroanatomical NOGA guidance catheter, reported disappointing results, with no benefit over placebo for patients with severe angina. (Stewart et al., 2009). The AGENT-3 and AGENT-4 trials, evaluating Ad5FGF-4 gene therapy for angina, were halted early after an interim analysis indicated the primary end point of improved exercise tolerance would not reach significance(Henry et al., 2007). However a gender-specific benefit was observed in women (Henry et al., 2007). Therefore, the challenges of effect gene delivery and therapeutic angiogenesis in human trials remain significant.

Adult cardiac progenitor cells have shown promise for treating various cardiac conditions, such as MI and HF, primarily through paracrine release of factors e.g. cytokines, chemokines, growth factors, and exosomes. Preclinical studies showed that exosomes derived from cardiac progenitor cells can mimic effects of cell transplantation in damaged heart (Bryl et al., 2024). Numerous early-phase trials of myocardial ischemia provided proof of concept that cardiac progenitor cells or mesenchymal stem cells (MSCs) could enhance vascularity in ischemic regions and improve cardiac function. However, these benefits were often short-lived and difficult to reproduce in larger, diverse patient populations due to poor cell engraftment, unclear mechanisms, inconsistent efficacy, and potential pro-inflammatory adverse effects (Sabra et al., 2021). The CHART-1 large-scale trial evaluated the efficacy and safety of cardiopoietic stem cells (MSCs) in larger heart failure cohort, although safety was demonstrated, no primary efficacy endpoint was met (Bartunek et al., 2017).

A study using adeno-associated viral vector to deliver human microRNA-199 into infarcted pig hearts has resulted in enhanced cardiomyocyte proliferation and cardiac repair, with marked improvements in cardiac function, increased muscle mass, and reduced scar size (Eulalio et al., 2012, Gabisonia et al., 2019). However, most treated pigs developed fatal arrhythmias 7–8 weeks post-treatment due to uncontrolled, persistent microRNA expression. MicroRNA therapy holds great potential for cardiac regeneration; however, despite significant preclinical advances, the field is still in its initial stages. A limited number of candidates have entered clinical development, none have progressed to phase III clinical trials or received the US Food and Drug Administration (FDA) approval, and some have been terminated due to toxicity concerns. This highlights key challenges that must be addressed for broader clinical use: ensuring microRNA sensitivity, specificity, and selectivity towards their intended targets, reducing immunogenic and off-target effects, improving targeted delivery strategies, and determining the optimal dosing for therapeutic efficacy while minimising side effects (Seyhan, 2024).

1.7. CRISPR/Cas9 system

Gene-editing technologies have been developed to enable precise manipulation of genomic sequences across a range of model organisms, including mice, *drosophila*, and zebrafish (Ma and Liu, 2015). More traditional genome-editing tools, such as zinc-finger nucleases (ZFNs) and transcription activator-like effector nucleases (TALENs), relied on engineered DNA-binding protein arrays fused to a nuclease domain to induce double-strand breaks (DSBs) at specific genomic loci (Amacher, 2008, Bedell et al., 2012).

The advent of the clustered regularly interspaced short palindromic repeats (CRISPR)/Cas9 system revolutionised genome editing by introducing a simpler, RNA-guided approach for generating site-specific DSBs (Ran et al., 2013). Originally discovered as part of the microbial adaptive immune defence, the CRISPR-Cas9 system employs a duplex-guide RNA (dgRNA) complex to direct Cas9 to its genomic target. The dgRNA is formed by annealing a CRISPR RNA (crRNA), a 20-nucleotide sequence complementary to the target DNA site, with a trans-activating crRNA (tracrRNA), a scaffold RNA molecule that binds to the crRNA and facilitates Cas9 recognition (Jacobi et al., 2017, Hoshijima et al., 2019). The dgRNA (Integrated DNA Technologies) guides the Cas9 nuclease to the target DNA sequence adjacent to a protospacer adjacent motif (PAM; typically, NGG).

Upon binding of the dgRNA-Cas9 complex to the target DNA, Cas9 undergoes a conformational change and cleaves both DNA strands approximately three base pairs upstream of the PAM site, thereby inducing DSBs. Following DSB induction, the cell activates endogenous DNA repair mechanisms, primarily non-homologous end joining (NHEJ) or homologous recombination (HR) (Ran et al., 2013).

NHEJ directly ligates the broken DNA ends but is highly error-prone, frequently introducing insertions or deletions (indels) that can cause frameshift mutations and premature stop codons in the targeted gene, resulting in functional gene knockouts (Wang et al., 2016). In contrast, HR uses a homologous DNA template from another chromosome as a reference for precise DNA repair, ensuring high-fidelity restoration of the damaged site (Jasin and Rothstein, 2013). To generate specific mutations or targeted insertions, an exogenous donor oligonucleotide containing the desired sequence can be introduced, which is then incorporated into the genome via the HR pathway.

1.8. Collaboration with N2 Pharmaceuticals (External Partner Organisation)

This PhD project included an industrial collaboration with N2 Pharmaceuticals, a company based at the Roslin Innovation Centre in Edinburgh. The company relocated there following the award of a SMART Scotland grant to support the development of N2-01, a bioactive compound extracted from *Mytilus edulis* (blue mussel). N2-01 was originally developed by Mr. Nikolay Solovyev, in collaboration with scientists from the Institute of Experimental Medicine and the State Academy of Veterinary Medicine, St. Petersburg, Russia. N2 Pharmaceuticals has since patented a proprietary extraction method to produce N2-01, a mixture of short peptides and amino acids derived from blue mussel meat through enzyme-acid hydrolysis (https://www.n2pharma.co.uk).

Blue mussels are a sustainable marine resource rich in bioactive peptides with proven antioxidant, anti-inflammatory, antithrombotic, and cardioprotective properties. Hydrolysates derived from *Mytilus edulis* have demonstrated multiple bioactivities, including inhibition of metabolic enzymes such as pancreatic cholesterol esterase, pancreatic lipase, and α-glucosidase (Lu et al., 2025, Wang et al., 2013a). These activities indicate that *Mytilus edulis* hydrolysates can modulate lipid and glucose metabolism while reducing oxidative stress, highlighting their potential as natural therapeutic agents for managing metabolic and cardiovascular disorders such as hyperlipidaemia, obesity, and type 2 diabetes.

Furthermore, *Mytilus edulis* hydrolysates have shown the capacity to improve endothelial function across multiple disease models, including sepsis, preeclampsia, cancer, and kidney failure. They demonstrated anti-inflammatory activity by suppressing pro-inflammatory cytokine production such as nuclear factor-kappa B (NF- κB) (Kim et al., 2016). Similarly, mussel water extracts containing taurine also demonstrated protective effects against cell death stimulated by lipopolysaccharide (LPS)-induced inflammation in zebrafish, with the ability to attenuate inflammation through the inhibition of reactive oxygen species and nitric oxide (NO) (Cheong et al., 2017). It is also reported that pre-treatment with blue mussel hydrolysates exerted a cytoprotective effect against oxidative stress-mediated endothelial dysfunction and

injury by suppressing intracellular reactive oxygen species generation and apoptotic stimuli endothelial protection (Suryaningtyas et al., 2021). Additional evidence showed that *Mytilus edulis* derivatives had antithrombotic and antioxidant functions, protecting ECs from hydrogen peroxide (H_2O_2)- mediated oxidative injury through inhibition of caspase-3 activation and apoptosis (Oh et al., 2019, Qiao et al., 2018), Hence, these studies suggest *Mytilus edulis* hydrolysates may be effective in protecting oxidative stress-mediated endothelial dysfunction or related cardiovascular disease such as atherosclerosis.

Enzyme-assisted hydrolysates of blue mussel have demonstrated their potential to attenuate muscle atrophy in both *in vitro* and *in vivo* zebrafish models (Amarasiri et al., 2023). Treatment with alcalase-assisted *Mytilus edulis* hydrolysate enhanced C2C12 myoblast proliferation, increased nuclear number, myotube coverage and diameter, and reduced levels of proteins responsible for muscle atrophy, including E3 ubiquitin ligases, as well as increasing levels of proteins associated with muscle hypertrophy including myogenin and myosin heavy chain (Amarasiri et al., 2023). Correspondingly, alcalase-assisted *Mytilus edulis* hydrolysate administration in zebrafish improved locomotor performance and increased body weight, demonstrating its efficacy in promoting muscle maintenance and growth *in vivo* (Amarasiri et al., 2023). Certain mussel-derived peptides exhibit antioxidant and anti-inflammatory properties that may slow progression of atherosclerosis by preventing oxidative modification of low-density lipoprotein (ox-LDL) cholesterol and reducing arterial wall inflammation. Blue mussel alcalase hydrolysate specifically inhibits ox-LDL-induced foam cell formation in macrophages by modulating cholesterol influx and efflux pathways, while mitigating inflammation and oxidative stress via NF-κB inhibition and heme oxygenase-1/nuclear factor erythroid 2-related factor 2 (HO-1/Nrf2) activation (Marasinghe et al., 2023).

Dietary consumption of blue mussels is believed to be associated with cardiovascular benefits, including blood pressure reduction, in Southeast and East Asian populations (Je et al., 2005). *In vivo*, angiotensin I-converting enzyme inhibitory peptides derived from fermented blue mussel sauce significantly lowered blood pressure in spontaneously hypertensive rats, supporting potential antihypertensive effects (Je et al., 2005, DAI et al., 2012). Moreover, continuous subcutaneous administration of small doses (1.0 µl/hour) of N2-01 efficiently protected mice against Lipopolysaccharide-D-Galactosamine-induced acute liver injury, with 100% survival rate, attributed to suppression of pro-inflammatory cytokines, regulation of NO, and reduced endothelial adhesion molecule (VCAM-1) expression and vascular permeability (Starikova et al., 2021).

N2-01 is currently registered in Russia as a veterinary medicine, with over 25,000 animals treated successfully for pathologies linked to endothelial dysfunction (https://www.n2pharma.co.uk). This preclinical success suggests potential translation for cardiovascular diseases related to endothelial dysfunction, including hypertension, heart failure, and coronary artery disease. The vascular endothelium is central to cardiovascular homeostasis, regulating vascular tone, permeability, and angiogenesis

(Galley and Webster, 2004, Sun et al., 2020). Endothelial dysfunction, characterised by NO dysregulation, oxidative stress, inflammation, and apoptosis, contributes to the progression of atherogenesis and hypertension, and heart failure (Premer et al., 2019). Following MI, ischaemic injury triggers endothelial dysfunction, impeding neovascularisation and cardiac recovery. This process is exacerbated by endoplasmic reticulum (ER) stress, which promotes apoptosis and disrupts angiogenic signalling. Recent findings identified endothelial protein arginine methyltransferase 7 (PRMT7) as a key regulator of ER stress and apoptosis, essential for vascular homeostasis, EC survival and cardiac recovery post-MI (Tran et al., 2025). Given its multifunctional bioactivity and endothelial-protective properties, N2-01 represents a promising candidate for cardiovascular regeneration. However, the cellular and molecular mechanisms underlying its protective effects remain poorly understood.

1.9. Hypotheses and Aims

1.9.1 Hypotheses:

1. Reactivation of developmental genes (*ANXA2* and *PABPC1*) in the adult coronary endothelium promotes neovascularisation and cardiac regeneration following myocardial infarction.

2. An imbalance in the co-regulation of fibrinolytic pathway genes *ANXA2* and *SERPINE1* disrupts fibrinolysis, impairs plasmin-dependent neovascularisation, and promotes pathological cardiac remodelling after myocardial infarction.

3. The N2-01 medicine exerts cardioprotective effects by modulating inflammatory responses, regulating oxidative stress, and preserving endothelial cell function, thereby supporting cardiovascular repair.

1.9.2 Aims:

1. To identify developmental genes reactivated in the adult coronary vasculature after myocardial injury using multimodal omics analyses, and to validate and compare the gene and protein expression of candidates (ANXA2, SERPINE1 and PABPC1) in human cardiac tissue from uninjured adult hearts and patients with MI.

2. To investigate the role of lead candidate gene *ANXA2* in embryonic and cardiovascular development using CRISPR/Cas9 mutagenesis in transgenic zebrafish.

3. To determine whether CRISPR/Cas9-induced knockdown of *ANXA2* impairs embryonic development and cardiac regeneration following cardiac laser injury in larval zebrafish.

4. To evaluate the effects of N2-01 on endothelial function and cardiac regeneration by assessing endothelial proliferation, angiogenic tube formation, and its ability to rescue developmental and regenerative defects in anxa2a/b crispant zebrafish embryos.

Chapter 2: Materials & Methods

2.1 Bioinformatic analysis of multimodal omics datasets

2.1.1 Analysis of CrescENDO coronary endothelial cell atlas

Previously published single cell/nuclei RNA-sequencing (sc(n)RNA-seq) data of human and mouse coronary vascular ECs (Li et al., 2022b) was accessed through the web-based Shiny application CrescENDO (www.crescendo.science), developed by Cass Ziwen Li. This coronary EC atlas was generated by integrating multiple sc/snRNA-seq datasets spanning foetal, adult and diseased human and mouse hearts (***Table 1***).

Expression of genes of interest (*ANXA2, SERPINE1*, and *PABPC1*) was queried individually using the CrescENDO interface. Gene expression was visualised as dot plots, where dot size indicated the percentage of expressing ECs, and colour intensity represented the average expression level.

***Table 1. Datasets included in the CrescENDO database**. Multi-species meta-analysis of integrated single cell and nuclei RNA-sequencing datasets from developing and adult mouse and human hearts in healthy and diseased states, adapted from (Li et al., 2022b).*

Species	Repository accession number	Injury/Disease status	Age	Number of ECs post-filtering	References
Mouse	GSE117893	21 days post-MI	Neonatal (P2)	270	Li et al., Development 2018
	GSE118545	Healthy	Neonatal (P6)	1510	Hu et al., Genes & Development 2018
			Neonatal (P10)	1211	
	E-MTAB-7376	3 days post-MI	Adult	519	Farbehi et al., eLife 2019
	GSE132880	Healthy	Adult	2747	Li et al., EHJ 2019
		7 days post-MI		5168	
	GSE136088	14 days post-MI	Adult	285	DePasquale et al., Nuclei acids research 2019
	E-MTAB-9816	1 day post-MI	Adult	59	Tombor et al., Nature Communications 2021
		3 days post-MI		116	
		14 days post-MI		169	
		28 days post-MI		177	
Human	GSE106118	Healthy	Foetal 5 - 25 weeks	240	Cui et al., Cell reports 2019
	GSE134355	Healthy	Foetal 11-12 weeks	532	Han et al., Nature 2020
			Adult	165	
	SRP234812	Healthy	Foetal 19 - 22 weeks	532	Suryawanshi et al., Cardiovascular research 2020
	GSE109816	Healthy	Adult	386	Wang et al., Nature cell biology 2020
	GSE121893	cHF	Adult	132	
		dHF		264	

2.1.2. Analysis of single nuclei RNA-sequencing data from human acute myocardial infarction

Publicly available, processed single-nuclei RNA sequencing (snRNA-seq) data from human myocardial tissues were accessed via CellxGene (Kuppe et al., 2022). The dataset comprised myocardial samples from healthy donors and patients with acute MI (**Table 2**). The cardiac samples used in the Kuppe dataset included: four control donors (range of ages was 44-61 years; median age 51 years; 75% male, 25% female), six patients for FZ (range of ages was 58-74 years; median age 63 years; 83.3% male, 16.7% female), twelve patients for IZ (range of ages was 29-66 year; median age 48.5 years; 66.7% male, 33.3% female), six patients for RZ (range of ages was 44-60 year; median age 49.5 years; 66.7% male, 33.3% female), and three patients for BZ (range of ages was 40-57 year; median age 44 years; 100% male).

All primary data processing steps, including quality control, dimensional reduction, clustering, and cell-type annotation, were performed by the original authors. The processed dataset was downloaded and imported into R Studio for secondary analysis. Using the Seurat package, the predefined cell clusters were explored, and endothelial cell populations were extracted for focused analysis.

Pseudobulk differential expression analysis was subsequently performed using the limma package to identify differentially expressed genes (DEGs) between myocardial zones (control, ischaemic, border, fibrotic, and remote). The results were visualised using dot plots, showing endothelial-specific transcriptional changes associated with angiogenesis and cardiac regeneration.

For cell type-specific expression analysis, annotated cell clusters (e.g. ECs, fibroblasts, smooth muscle cells, pericytes, macrophages, and cardiomyocytes) were compared to assess the relative expression of genes of interest, including ANXA2, SERPINE1, and PABPC1. Dot plots were generated using Seurat's DotPlot function to visualise both the average expression (avg.exp; scaled/normalised) and percentage of expressing cells (pct.exp) across major cardiac cell types and myocardial zones (control, ischemic, border, fibrotic, and remote).

To enable quantitative comparison and graphical presentation, the numerical values of avg.exp and pct.exp were extracted from the Seurat dot plot data frames and exported to GraphPad Prism. Bar graphs were created to compare expression patterns of target genes across multiple cardiac cell types and myocardial zones, providing a clearer visualisation of cell type-specific and spatial transcriptional patterns following acute MI.

Table 2. Clinical data for all samples used in from publicly available, processed single-nuclei RNA sequencing (snRNA-seq) dataset; *from healthy donors and patients with myocardial infarction (MI) and adapted from Kuppe et al (2022).*

Patient	Myocardial Zone	Age	Gender	Infarction location	Days after MI	Pathologists' description
P1	CTRL	44	m	n.a.	control	Normal myocardium
P17	CTRL	61	m	n.a.	control	Normal myocardium
P7	CTRL	55	f	n.a.	control	Normal myocardium
P8	CTRL	44	m	n.a.	control	Normal myocardium
P14	FZ	59	m	anterior LV	62	Young scar with fibroblasts and some collagen
P18	FZ	64	f	anterior LV	153	Scar with fibroblasts and collagen
P20	FZ	63	m	anterior LV	166	Scar with fibroblasts and collagen
P19	FZ	58	m	infer posterolateral	40	Granulation tissue transforming into young scar; no necrotic cardiomyocytes; most macrophages already cleared, not yet much collagen
P4	FZ	74	m	anterior LV	88	Central part granulation tissue: dead cardiomyocytes cleared; fibroblasts and macrophages; not yet much collagen. At borders maybe also some necrotic cardiomyocytes with neutrophils (blue area)
P5	FZ	63	m	n.a.	101	Young scar; dead cardiomyocytes cleared; fibroblasts; not yet much collagen
P13	IZ	51	m	complete LV (left main occlusion perioperatively)	45	Granulation tissue; most cardiomyocytes cleared; macrophages and maybe fibroblasts, no collagen yet
P15	IZ	43	f	anterior LV	11	Ischemic tissue, granulation tissue and borderzone
P9	IZ	52	f	subacute inferolateral myocardial infarction	2	Normal myocardium and granulation tissue; only few necrotic cardiomyocytes (most cleared); fibroblasts

						and macrophages; no collagen yet
P9	IZ	52	f	subacute inferolateral myocardial infarction	2	Granulation tissue most necrotic cardiomyocytes cleared; macrophages and fibroblasts; no collagen yet
P10	IZ	38	m	anterior LV and septal acute myocardial infarction	6	Ischemic necrotic cardiomyocytes, macrophages, and neutrophils
P15	IZ	43	f	anterior LV	11	Ischemic, necrotic cardiomyocytes with in between inflammatory cells
P16	IZ	66	m	anterior LV	4	Ischemic necrotic cardiomyocytes with neutrophils, also smaller area with granulation tissue
P3	IZ	57	m	anterior LV	2	Ischemic necrotic cardiomyocytes, oedema, neutrophils (also some adipocytes of epicardial area)
P2	IZ	44	m	anterior LV due to occlusion of the left coronary artery	5	Ischemic left side slide normal border zone; necrotic cardiomyocytes, oedema, neutrophils
P21	IZ	61	m	anterior LV	12	Could not locate
P22	IZ	46	m	anterior LV	7	Could not locate
P23	IZ	29	m	anterior LV	10	Myocardium with myocyte hypertrophy, fibrosis, and patchy vacuoles
P11	RZ	60	f	posterolateral acute myocardial infarction	31	Normal myocardium, maybe in capillaries slightly increased inflammatory cells
P3	RZ	57	m	anterior LV	2	normal remote myocardium
P6	RZ	47	m	anterior LV	3	normal remote myocardium
P6	RZ	47	m	anterior LV acute myocardial infarction	3	Normal remote myocardium
P9	RZ	52	f	subacute inferolateral myocardial infarction	2	Normal remote myocardium with some waviness of fibres
P2	RZ	44	m	anterior LV due to occlusion of the left coronary artery	5	Normal myocardium and granulation tissue; only few necrotic cardiomyocytes (most cleared); fibroblasts

						and macrophages; not yet much collagen
P12	BZ	40	m	anterior LV acute myocardial infarction	31	Normal remote myocardium with maybe waviness of fibres
P2	BZ	44	m	anterior LV due to occlusion of the left coronary artery	5	Border zone/remote myocardium; normal myocardium within capillaries (between cardiom) some inflammatory cells
P3	BZ	57	m	anterior LV	2	Border zone/remote myocardium, more or less normal myocardium

2.1.3 Analysis of single cell RNA-sequencing data from regenerating zebrafish hearts

Publicly available, processed single-cell RNA sequencing (scRNA-seq) data of non-cardiomyocytes from regenerating adult zebrafish hearts following ventricular resection were downloaded from the NCBI Gene Expression Omnibus (GEO; accession number GSE145980) (Ma et al., 2021).

The files were uploaded to Trailmaker™ (Parse Biosciences; https://app.trailmaker.parsebiosciences.com), a cloud-based platform designed for scRNA-seq data analysis and visualisation. Trailmaker™ applies an integrated preprocessing pipeline, including quality control, normalization, dimensionality reduction, and unsupervised clustering, to prepare the dataset for downstream analyses within its *Insights* module.

EC clusters were identified based on established marker gene expression and subsequently subset for focused analysis of candidate gene expression dynamics across regeneration time points. Gene expression patterns were visualised using dot plots generated within Trailmaker™, which utilize the Seurat framework in R for calculation and display. In these plots, the dot size represents the percentage of cells within a cluster expressing a given gene, while the dot colour intensity corresponds to the average scaled expression level. Scaled expression values were computed from normalized data, standardized to have a mean of 0 and standard deviation of one, enabling cross-cluster comparison of gene expression profiles.

2.2 Spatial transcriptomics

The laboratory protocols for 10X Visium Spatial transcriptomic were previously conducted by Dr. Cass Ziwen Li and Dr. Emmanouil Solomonides (former members of the Brittan Laboratory).

Human myocardial tissue samples, including healthy controls, acute and chronic MI specimens, were provided by Dr. Stephanie Sellers (University of British Columbia) (**Table 3**). The tissues were cryopreserved or embedded in Optimal Cutting Temperature (OCT) compound, then sectioned by the University of Edinburgh Histology Research Service. Tissue sections were mounted directly onto Visium Spatial Gene Expression Slides (10x Genomics) containing oligo-barcoded capture areas. Spatial transcriptomic library preparation was performed using the Visium Spatial Gene Expression Reagent Kit (10x Genomics, PN-1000186) according to the manufacturer's instructions. Following sequencing, spatially resolved gene expression patterns were analysed and visualised using the 10x Genomics Loupe Browser software.

Table 3. Details of patients used for spatial transcriptomics. *Adapted from Li et al., 2022b).*

	Tissue bank		**Age**	**Sex**	**Cause of death**
Healthy subjects (n = 2)	University of British Columbia		52	Male	1a Chest injuries, 1b Road traffic collision (cyclist)
	University of British Columbia		53	Male	1a - Suspension by ligature
		Time post-MI			**Diagnosis/histology**
Acute MI Patients (n = 1)	University of British Columbia	<30 days	52	Male	Severe complicated atherosclerosis of major epicardial coronary arteries, ischemic heart disease, degenerative valvular disease of aortic valve, mitral annular calcification
Chronic MI Patients (n = 3)	University of British Columbia	>12m	n/a	n/a	Coronary atherosclerosis, haemorrhagic infarction involving posterior, posterolateral and poster septal LV myocardium
	University of British Columbia	>12m	57	Female	Anterior MI in 2005. CAD with 90% stenosis of proximal left anterior descending artery
	University of British Columbia	>12m	n/a	n/a	Anterior MI in May 2016. LVAD in November 2016. Transplanted in August 2018. Gross and histologic features consistent with chronic ischemia/remote myocardial infarctions.

2.3 CRISPR/Cas9-mediated genome mutagenesis

2.3.1 Alt-R CRISPR/Cas9-mediated genome mutagenesis

Sequence information for target genes was obtained from the Ensembl zebrafish genome browser (Danio rerio genome assembly GRCz11; www.ensemble.org), focusing on the protein-coding sequences. All known transcripts, alternatively spliced variants, and isoforms were reviewed to ensure that the custom-designed dgRNAs accounted for all functional variants of the protein coding gene.

The whole cDNA sequence of anxa2a and anxa2b were screened for potential target sites using CHOPCHOP (http://chopchop.cbu.uib.no/) and IDT CRISPR-Cas9 guide RNA design checker (https://eu.idtdna.com/site/order/designtool/index/CRISPR_SEQUENCE). The experimental workflow for generating mutagenised F0 larvae (crispants) was based on work published by (Hoshijima et al., 2019).

In this system, RNA duplexes of chemically synthesised crRNAs and tracrRNAs were complexed with Cas9 ribonucleoproteins (RNPs) to form the dgRNA-Cas9 ribonucleoprotein (dgRNP) complex. These dgRNPs are highly effective at inducing DSB-repair-mediated mutations in zebrafish, even at target sites that appear resistant to the activity of dgRNPs. Hoshijima et al. (2019) demonstrated that using pairs of dgRNPs to target adjacent sites on the same chromosome can efficiently generate deletion mutations through simultaneous DSB induction.

For each gene, two target sequences were designed to span two separate coding exons. Alt-R CRISPR-Cas9 crRNA with specific target sequences (**Table 4**) were ordered from Integrated DNA Technologies (https://eu.idtdna.com/pages/products/crispr-genome-editing/alt-r-crispr-cas9-system). Alt-R crRNAs (100uM stock) and tracrRNA (100uM stock) were mixed in equal volumes to make 50uM crRNA:tracrRNA duplexes (95°C, 5 min, cool to room temperature for 5-10 minutes, rapidly cool to 4°C).

The AltR CRISPR-Cas9 injection mix was assembled as described in **Table 5** and heated to 37 °C for 10 min and cooled to room temperature for 5 min before microinjection in the morning. Approximately 1 nl of the AltR CRISPR-Cas9 injection mixture was injected into zebrafish embryos at the one-cell stage using a PicoPump (World Precision Instruments). Successful injections were confirmed at 3-6 hpf by visualising phenol red dye in the eggs.

Table 4. CRISPR/Cas9 target sites.

crRNA	Gene	Exon	Target Sequence + [PAM]	Strand
anxa2a_Dr Cas9 AL_KO1	*anxa2a*	3	CTACCCTACTGTTGTTCCAG [AGG]	+
anxa2a_Dr Cas9 AP_KO2	*anxa2a*	6	TGGAGATCAAGAAAGTCTAC [AGG]	+
anxa2b_Dr Cas9 AP_KO1	*anxa2b*	2	TCATAAGCTGCCACCACTGT [AGG]	+
anxa2b_Dr Cas9 AJ_KO2	*anxa2b*	5	GGTGTGTTCTCGCAATAAAG [AGG]	-

Table 5. AltR CRISPR-Cas9 Injection mixture prepared for anxa2a/b knockdown

Mutation	Reagents	Volume
anxa2a* + *anxa2b	25uM crRNA+tracrRNA deplux mix – anxa2a_**Dr Cas9 AL_**KO1	0.3 µl
	25uM crRNA+tracrRNA deplux mix – anxa2a_**Dr Cas9 AP_**KO2	0.3 µl
	25uM crRNA+tracrRNA deplux mix – anxa2b_**Dr Cas9 AP_**KO1	0.3 µl
	25uM crRNA+tracrRNA deplux mix – anxa2b_**Dr Cas9 AJ_**KO**2**	0.3 µl
	25uM Cas9 stock	1 µl
	Phenol Red	2 µl
	ddH_2O	1 µl
		Total 5.2 µl

2.3.1 Determining dgRNA efficiency

Primer pairs flanking each CRISPR target site were designed using Primer3 Plus (https://www.primer3plus.com/) and CHOPCHOP (http://chopchop.cbu.uib.no/). Primers were designed to ideally be 20-22 nucleotides long, with a G/C content close to 50%, and to produce amplicons between 100 and 400 base pair (bp). Primer specificity was further validated using Ensembl BLAST to ensure unique genomic targeting. All primer sequences are listed in **Table 6**.

Genomic DNA was extracted from individual embryos at 1, 2, or 4 dpf. Each embryo was lysed in 50ul of 50nM NaOH, and incubated at 95°C for 20-30 minutes, followed by cooling to 4°C for 10 minutes. Samples were neutralised by adding 5µl of 1M Tris-HCl (pH 8.0), vortexed briefly to ensure tissue disruption, and centrifuged at 3000 rpm (1500 x g) for 10 minutes at room temperature. The clean supernatant containing genome DNA (gDNA) was transferred to a fresh Eppendorf tube or 96-well plate and stored on ice or at -20°C until use.

PCR amplification was performed using 1 µl of extracted gDNA (**Table 7**) as template under programmed thermal cycle under conditions described in **Table 8**. Following amplification, 2µl of the PCR product was run on a 2% agarose gel electrophoresed at 100V for 1 hour to ensure a single, clean band of product.

The remaining of PCR product was denatured and reannealed, forming hybrid DNA duplexes, in the thermal cycler under the condition described in **Table 9**. To assess CRISPR/Cas9 cutting efficiency, the annealed PCR product was treated with T7 Endonuclease I (T7E1) to cleave mismatched sites. The T7E1 digestion reaction contained: which contained: 10X Buffer 2 (1 µl), T7E1 enzyme (0.25 µl), ddH_2O (0.75 µl), and annealed PCR product (8 µl), and was incubated at 37 °C for 30 minutes.

The T7EI reaction product was run for 1 hour on a 2% agarose gel at 100V to resolve smaller fragments. T7E1 surveyor cuts DNA strands when a mismatch greater than one base is present, which results in the formation of smaller fragments. Afterwards, the gel was imaged under ultraviolet light to visualise cleavage patterns and assess dgRNA efficiency.

Table 6. Sequences of left and right primers for each target and PCR amplicon size are shown.

Mutation	**Left (forward) primer**	**Right (reverse) primer**	**Product size**
***anxa2a* exon 3**	TGTTTGGCTGTAGGGAGAGC	GCAGAATGAAGGGCAGGACT	326 bp
***anxa2a* exon 6**	TGCAATAGAACTGGTGCTTACTAGT	CCCCTGAAGTATCTCCAGCC	405 bp
***anxa2b* exon 2**	TGTAGTATCAACACAAATGCAACA	ACTGCGAAATCAAGCATGTGT	276 bp
***anxa2b* exon 5**	TGGCTATACAAGTTGGCACTGT	CCTGTGCAAGGGCCAGTAG	313 bp

Table 7. PCR reaction components

Components	**11 µl reaction**
Q5® High-Fidelity 2X Master Mix (New England BioLabs)	5 µl
gDNA	2 µl
Nuclease free H_2O	2 µl
FW left primer	1 µl
RV right primer	1 µl

Table 8. Thermocycling conditions for a routine PCR

Step	**Temp**	**Time**
Initial Denaturation	98°C	30 secs
Denaturation	98°C	10 secs
Annealing	57°C	30 secs
Extension	72°C	30 secs
Repeat 35 cycles		
Final Extension	72°C	2 min
Hold	10°C	∞

Table 9. Denature/reanneal thermal cycler conditions.

Step	Temp	Time
Initial Denaturation	95°C	5 min
Annealing	95-85°C	2°C /sec gradient
	85-25°C	0.1°C /sec gradient
Hold	10°C	∞

2.4 Zebrafish husbandry and general techniques

2.4.1 Zebrafish maintenance

Adult zebrafish (*Danio rerio*) were maintained in the Bioresearch & Veterinary Services (BVS) Aquatics Facility at the University of Edinburgh, managed by Dr. Carl Tucker. Fish were reared under standard laboratory conditions on a 14-hour light/10-hour dark cycle at 28.5 °C and 22% humidity.

For embryo collection, pairwise breeding was set up in the late afternoon using either small mating tanks (one male and one female separated by a divider) or 40 litre group tanks equipped with marble-filled spawning trays. Fish were allowed to acclimatise overnight, and at the onset of the light cycle the following morning, dividers were removed to initiate spawning. Eggs were collected from 10:00 am using a fine mesh strainer, examined for viability under a stereomicroscope, and transferred into 50 mm Petri dishes containing conditioned aquarium water supplemented with 0.1% methylene blue to prevent fungal growth. Embryos were incubated at 28.5 °C and monitored daily for normal development and morphology according to established staging criteria (Kimmel et al., 1995). Water was refreshed daily.

A double transgenic zebrafish line, Tg(*fli1:eGFP*)^{y1tg} / Tg(*myl7:DsRed2-NLS*)^{f2}, was used in the experiments (**Table 10**). This line enables fluorescent visualisation of ECs (GFP-labelled) and cardiomyocyte nuclei (DsRed-labelled), facilitating imaging of cardiac tissue architecture and regeneration dynamics.

All experiments were conducted in compliance with the Animals (Scientific Procedures) Act, 1986 and approved by the University of Edinburgh Animal Welfare and Ethical Review Board under a UK Home Office licence. All experimental procedures were performed on staged larvae aged 3-5 dpf at room temperature (23 °C), with embryos and larvae housed at 28.5 °C throughout.

Table 10. Zebrafish lines used in this project.

Strain	Reporter	Reference
Tg(*fli1:eGFP*)^{y1}	Green endothelial cells	(Lawson and Weinstein, 2002)
Tg(*myl7:DsRed2-NLS*)^{f2}	Red cardiomyocytes	(Rottbauer et al., 2002)

2.4.2 Phenylthiourea treatment

To inhibit pigment formation and improve optical transparency for imaging, zebrafish embryos were treated with 0.003% phenylthiourea (PTU) (Fisher Scientific) dissolved in conditioned aquarium water supplemented with 0.1% methylene blue. Treatment commenced at 24 hpf and continued throughout larval development until the end of imaging experiment. This approach allowed improved visualisation of cardiac and vascular structures in live larvae (Karlsson et al., 2001).

2.4.3 Anaesthesia

Prior to imaging or experimental procedure, zebrafish larvae were anaesthetised by immersion in 40 µg/mL tricaine methanesulfonate (MS-222; Sigma-Aldrich) dissolved in conditioned aquarium water. Anaesthetised larvae were maintained in the tricaine solution for the minimal duration required to complete the procedure. Following the experiment, larvae were promptly transferred to fresh conditioned aquarium water to allow full recovery.

2.5 Larval zebrafish imaging and quantification

2.5.1 Quantification of larvae embryonic development

For general imaging of whole larvae in both brightfield and fluorescence, the Leica M205 FA stereomicroscope (Leica, Wetzlar, Germany) was used with GFP, mCherry, and BFP filter sets, and images were acquired using the 2.5X objective.

At 3 dpf, zebrafish larvae were anaesthetised and positioned laterally for brightfield imaging. Morphological assessments were performed to compare developmental growth among *anxa2a/b* crispants, uninjected controls, and Cas9-only controls. Key parameters, including total body length and eye diameter, were measured using Fiji (ImageJ). Measurements were performed by first calibrating the scale using a known-distance scale bar, then drawing a line between the points of interest. The length was read from the status bar, and measurements were recorded using Analyse → Measure.

2.5.2 Quantification of larvae vascular development

At 3 dpf, zebrafish larvae were anaesthetised and positioned laterally for imaging. The vasculature was visualised using a Leica M205 FA fluorescence stereomicroscope (Leica, Wetzlar, Germany) equipped with a 2.5X objective. Endothelial and endocardial cells labelled with green fluorescence protein (GFP) were imaged using the standard GFP filter set.

High-resolution images of the larval trunk were captured to assess vascular development. The total number of complete intersegmental vessels (ISVs) and parachordal vessels (PAVs) were quantified using the Cell Counter plugin in Fiji (ImageJ).

2.5.3 Zebrafish cardiac imaging using heartbeat-synchronised selective plane light sheet illumination microscope

Zebrafish hearts were imaged using a heartbeat-synchronised selective plane illumination microscope (SPIM) developed by Dr. Jonathan Taylor (Taylor et al., 2011, Taylor et al., 2019a). Larvae were imaged at 3 dpf (0 hour), 4 dpf (24 hours), and 5 dpf (48 hours) to monitor cardiovascular development and compare uninjected controls with *anxa2a/b* crispants.

To determine whether *anxa2a/b* knockdown impairs cardiac regenerative capacity, longitudinal cardiac imaging was performed using SPIM at 0, 2, 24, and 48 hours post-injury (hpi) (***Figure 3***). Imaging was performed on double-transgenic Tg(*fli1:eGFP*)^{y1tg} / Tg(*myl7:DsRed2-NLS*)^{f2}) larvae, in which endothelial and endocardial cells are labelled with green fluorescence protein (GFP) and cardiomyocyte nuclei with red fluorescence protein (mCherry), allowing simultaneous visualisation of vascular and myocardial structures. For imaging, larvae were drawn up into fluorinated ethylene

propylene tubes containing tricaine solution at standard concentration and sealed with a small ball of Blu-Tack.

High frame rate brightfield videos (80 fps) were processed using a heartbeat-synchronisation algorithm integrated into custom 'SPIM GUI' software. This algorithm predicts the precise millisecond when the heart will reach a pre-selected phase of the cardiac cycle. A timer box gates the triggering of camera exposure and laser pulse, ensuring that each plane of the z-stack is illuminated only once per timepoint. This enables acquisition of 1 µm-spaced z-stacks of the beating heart, which appear as though the heart is arrested at a single phase; in this study, maximal diastole was selected for all larvae. The heartbeat-synchronisation algorithm is adaptive, continuously updating reference brightfield frames to compensate for heart drift in the mounting media or morphological changes during development, maintaining consistent phase alignment throughout imaging.

SPIM z-stacks of the ventricles were processed using Imaris (Bitplane) to generate 3D surface renderings for quantitative analysis of cardiac development and regeneration. Maximum intensity projections were produced, and ventricular ECs and cardiomyocytes were surface rendered for further analysis.

Cell quantification was performed using Imaris functions: "Spots" was used to render cardiomyocyte and endothelial nuclei from GFP or mCherry signals, with thresholds manually adjusted to accurately identify nuclei. Ventricular surfaces were rendered from GFP+ endothelial signals using the "Surface" function, and the volume (µm³) of these surfaces was measured to determine diastolic endocardial volume of ventricle. Heart rate was quantified manually.

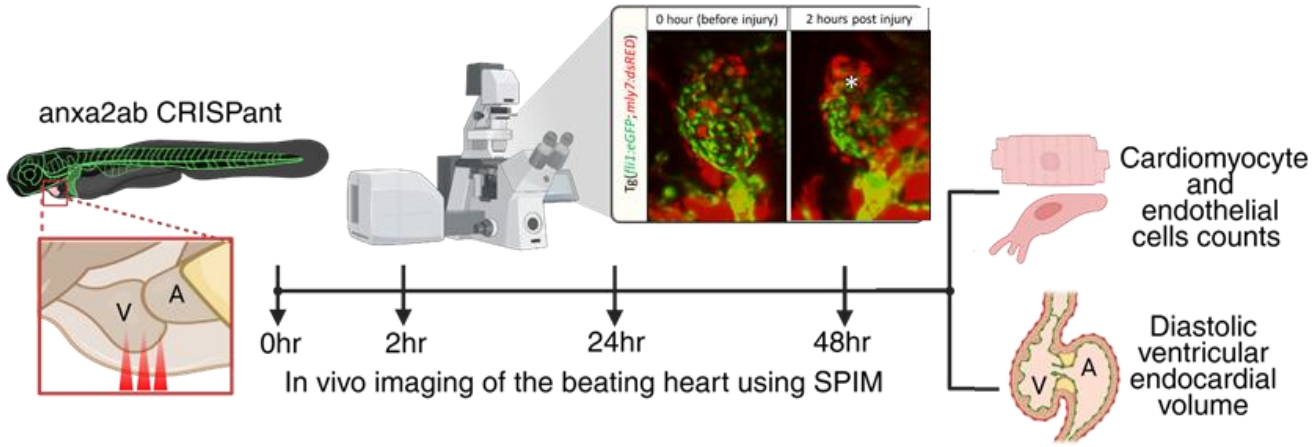

Figure 3. Schematic of ventricular laser ablation and imaging in 3 dpf zebrafish larvae. *Photoactivated localisation microscopy (PALM) was used to induce laser injury to the ventricles of Tg(fli1:eGFP)^{y1tg} / Tg(myl7:DsRed2-NLS)^{f2}) anxa2a/b crispant zebrafish at 3 days post-fertilisation. Heartbeat-synchronised selective plane light sheet illumination microscope (SPIM) was used to image zebrafish heart at 0, 2, 24, 48 hours post-injury. The role of anxa2a/b in cardiac regeneration was assessed by*

quantifying heart rate, cardiomyocyte and endothelial cell counts, and ventricular surface volume.

2.6 Larval ventricular laser ablation

A Zeiss Photo Activated Laser Microdissection (PALM) laser system (Zeiss, Oberkochen, Germany) was used to precisely generate a laser injury to the ventricular apex of 72 hpf larvae, as described in (Kaveh et al., 2020, Taylor et al., 2019a, Matrone et al., 2013). Larvae were anaesthetised and mounted laterally on a glass slide in 20 µl of the same tricaine-conditioned aquatic water. Larvae were oriented with the head pointing leftward, positioning the ventricle as the uppermost chamber to facilitate precise laser targeting.

The ventricle was visualised under a 20X objective on the PALM system. Laser ablation was applied in a stepwise protocol to minimise rupture risk: three low power pulses (38 AU) were first delivered across the apex to transiently arrest contraction. This was followed by a single medium-power pulse (40 AU) directed at the centre of the apex. If rupture did not occur, up to three high-power pulses (42 AU) were applied.

Injuries were assessed and deemed successful once ventricular contractility decreased, and the myocardial wall had swollen without causing cardiac rupture and bleeding. A successful cardiac injury should result in the ventricular apex losing fluorescent endothelial signal. Uninjured larvae were treated identically up to the point of laser injury and kept in the same environmental conditions as injured fish thereafter.

2.7 Quantification of relative mRNA expression of target genes in zebrafish larvae

2.7.1 RNA extraction

To measure mRNA levels of target genes in larval zebrafish, pools of 20–30 anaesthetised 5 dpf larvae were collected and frozen at −20 °C until processing. On the day of extraction, RLT buffer (Qiagen) was supplemented with 10 µl of β-mercaptoethanol per 1 ml to inactivate RNases. Frozen larvae were homogenised in RLT buffer using a fine needle and syringe.

Total RNA was extracted using the RNeasy Micro Plus Kit (Qiagen, Manchester, UK) according to the manufacturer's instructions. RNA was eluted in 14 µl of RNase-free water, and 1 µl of each sample was analysed using a NanoDrop™ One spectrophotometer (Thermo Fisher Scientific) to assess RNA concentration (ng/µl) and purity. RNA quality was verified by A260/A280 ratios between 1.8–2.0 and A260/A230 ratios between 2.0–2.1.

2.7.2 Reverse Transcription for cDNA synthesis

Complementary DNA (cDNA) was synthesised using the SuperScript™ IV First-Strand Synthesis System (Life Technologies) according to the manufacturer's protocol. Briefly, 11 µl of total RNA (250–500 ng) in RNase-free water was mixed with 1 µl of 50 µM Oligo(dT) $_{20}$ primers and 1 µl of 10 mM dNTPs**,** then incubated at 65 °C for 5 minutes to denature secondary RNA structures (**Table 11**). The mixture was subsequently placed on ice for 1 minute.

A reverse transcription master mix containing 4 µl of 5× SuperScript IV buffer**,** 1 µl of 100 mM DTT**,** 1 µl of 40 U/µl RNasin® Plus RNase inhibitor, and 1 µl of 200 U/µl SuperScript IV reverse transcriptase was then added to each reaction. The reaction mix was briefly vortexed, centrifuged, and incubated at 55 °C for 10 minutes for cDNA synthesis, followed by 80 °C for 10 minutes to inactivate the enzyme (**Table 11**). Synthesised cDNA was stored at -20 °C until further use.

Table 11. Reverse Transcription reaction mix

Components	***Volume***
50uM Oligo(dT)$_{20}$ primers	1 µl
10mM dNTPs	1 µl
Sample mRNA (250/500ng) in ddH2O	11.5 µl
	Incubate for 5 min at 65°C
5x Superscript IV buffer	4 µl
100mM DTT	1 µl
RNasin Plus (ribonuclease inhibitor)	1 µl
SSIV Reverse transcriptase	1ul
	Vortex and centrifuge before transferring to Thermocycler (55°C for 10min, 80°C for 10min, 4°C forever); store cDNA at -20°C

2.7.3 Real time-quantitative PCR

All real-time quantitative polymerase chain reaction (RT-qPCR) procedures were performed on ice to minimise RNA degradation. Each sample was run in technical triplicate for every primer pair using pre-designed KiCqStart™ SYBR Green Primers specific to zebrafish (Merck, 100 µM stock) (**Table 12**

). Reactions were set up in a final volume of 10 µl per well in 384-well plates.

Each reaction mixture contained 5 µl of Luna Universal qPCR SYBR Green Master Mix (New England Biolabs), 0.25 µM of each forward and reverse primer, and 25–50 ng/µl of cDNA template, adjusted to volume with RNase-free water (**Table 13**). The reaction plates were sealed with optical adhesive film, briefly centrifuged at 2,000–2,500 rpm for 1 minute to remove air bubbles and collect liquid at the bottom of the wells, and subsequently loaded into a QuantStudio Real-Time PCR System (Applied Biosystems). A no-template control (NTC), in which cDNA was replaced with RNase-free water, was included to verify the absence of contamination or non-specific amplification from the reagents. Two reference (housekeeping) genes, beta-2 microglobulin *(b2m)* and ribosomal protein L7 *(rpl7)*, were used for normalisation (Rassier et al., 2020, McCurley and Callard, 2008).

Relative quantification (RQ) values were calculated using the $2^{-\Delta\Delta Ct}$ method and normalised to the geometric mean of the housekeeping genes. The resulting RQ values were $\log_2$-transformed to facilitate interpretation and statistical analysis (Taylor et al., 2019b). Log_2 transformation provides a balanced, symmetrical scale around zero, with positive values indicating upregulation and negative values indicating downregulation of gene expression. This approach both simplifies visualisation and ensures data are more suitable for parametric statistical tests that assume normal distribution. On this $\log_2$ scale, each unit represents a twofold change in gene expression, allowing intuitive comparison between samples.

Table 12. Pre-designed KiCqStart® SYBR® green primers for zebrafish genes

Gene	Forward Primer Sequence (5'-3')	Reverse Primer Sequence (5'-3')
b2m	TTGGCTCTCTCGAATAAAAC	CTTTCGGAGTGGAGACTTTC
rpl7	TCGTAAGGCTGGAAACTATT	ACACCATTGATACCTCTGAT
anxa2a	ACAGGGAATTGTTCAAGAAG	AAAGTCCCCTGAAGTATCTC
anxa2b	AAAAGCATCAATGAAGGGTC	ACCATCTCAATCAGACTCTC
plat	GGAAACTTCCATCAATCACC	CACACACACCTTGATTGTTA
plg	CTACAACTCCAACACAGTCT	TTCTGAAGGAGCAGATTGAT
tie1	TAAAATGCTCAAGGAGTTCG	CTTCCAATTCTCCAGCAAAG
vegfaa	TTTTCAGCTGAGTTTCACAG	CTTGGCTTTTCACATCTTTC
vegfab	AACGACAAGAGAGAAATCCA	CATGCGTACTTTTAGTCCAT
serpine1	GTCTATTCCAAGGTTCTCCAT	CTGAAAATGTCTCCAAGACC
notch1a	TGCATCGACAAAATCAACTC	AACTCCCAGAAAACCCTTTA
notch2	AGATGAATGTCTATCCAGCC	GCTTTACACTTGCAGTCATA
notch3	GAAATCGGAAAGTCAGCATT	AAGGCAATAGTAGCTTCAAC
tgfb1a	GACGTGAAACAGACAATGAT	CTCCAAGGTTTCTTCATCTTC
tgfb2	GAGCTTTACCAGGTTTTAGG	TGTTGATGTATCGCTGTGTA
s100a10a	CCGAATACTAATGGAGAACG	TCCTTCTGAGACTTAAGGAAC
s100a10b	CCTTTATCAGCACATTCACA	TTTAAGCTCTCTTCGACTCA
runx1	AGCAGACACTTATGCTCTAA	CTTCAGCGATGTTTACCTTT
cxcr4a	ATGGCTTATTACGGACACAT	AGAAAGATCCTCTGGAAGTC
cxcl12b	ATCCTGCAATACTAATGCTC	GTGATGTTTTGGTAAGCAGT

pabpc1a	AGGTTATGCCTATGTCAACT	CCTTGATCACGTCAAAGTTC
pabpc1b	CAAAGAGTTTACCAACGTCTAC	GCTCATGGCATTACCATATT

Table 13. RT-qPCR reaction mix

Component	**10ul reaction for 384 well**
Luna Universal qPCR	5 µl
Forward primer (10µM)	0.25ul (0.25µM)
Reverse primer (10uM)	0.25ul (0.25µM)
Water (to total 20ul incl. cDNA)	0.1 µl cDNA 4.5 µl RNase-free H2O

2.8 Treatment of larval zebrafish with N2-01 drug

To assess the effects of N2-01 treatment on zebrafish development and evaluate its potential to rescue developmental defects in *anxa2a/b* crispants, zebrafish embryos were exposed to N2-01 immediately following CRISPR dgRNPs microinjection at the one-cell stage. As no specific concentration of N2-01 was provided, treatment was performed using dilutions as instructed. Embryos (n = 15 per group) were treated with 1/3 and 1/6 dilutions of N2-01: 3.33 ml N2-01 diluted in 6.67 ml 0.1% methylene blue fish medium (1/3 dilution) and 1.67 ml N2-01 diluted in 8.33 ml 0.1% methylene blue fish medium (1/6 dilution). Embryos were maintained under standard larval zebrafish maintenance conditions. Uninjected embryos, with or without N2-01 treatment, were used as controls. Embryonic morphology, developmental progression, and viability were monitored daily from 1-3 dpf using brightfield stereomicroscopy. Developmental stages were determined according to Kimmel et al. (1995).

2.9 Human cardiac tissue staining

2.9.1 Human cardiac samples

Cardiac tissue samples from healthy controls and MI patients were obtained from the University of British Columbia and the Edinburgh Brain Bank. The mean age of control subjects was 42.4 years (range 19-63, n = 7, 100% male), and the mean age of MI patients was 58.7 years (range 40-72, n = 7, 100% male) (**Table 14**). However, information regarding the timepoint post-MI for the human MI samples (Edinburgh Brain Bank) used in the immunostaining and histology study were not available.

Table 14. Details of patients used for study by Masson's Trichrome and immunofluorescence staining (adapted from Li et al., 2022b).

	Tissue bank	Age	Sex	Cause of death
Healthy subjects (n = 7)	University of British Columbia	52	Male	1a Chest injuries, 1b Road traffic collision (cyclist)
	University of British Columbia	53	Male	1a - Suspension by ligature
	Edinburgh Brain Bank	39	Male	No significant pathology.
	Edinburgh Brain Bank	42	Male	no significant abnormalities.
	Edinburgh Brain Bank	29	Male	no significant pathology.
	Edinburgh Brain Bank	19	Male	1a – Unascertained
	Edinburgh Brain Bank	63	Male	n/a
				Diagnosis/histology
MI Patients (n = 7)	University of British Columbia	70	Male	Atherosclerotic coronary artery disease, myocardial infarction-remote, left lateral, with aneurysm, myocardial infarction-acute, circumferential
	University of British Columbia	52	Male	Severe complicated atherosclerosis of major epicardial coronary arteries, ischemic heart disease, degenerative valvular disease of aortic valve, mitral annular calcification
	University of British Columbia	55	Male	Coronary atherosclerosis, haemorrhagic infarction involving posterior, posterolateral and posteroseptal LV myocardium
	Edinburgh Brain Bank	72	Male	Early neutrophilic infiltrate with contraction band necrosis; areas of established scarring
	Edinburgh Brain Bank	40	Male	Enlarged heart (580 g) with hyperaemia anterolateral LV,

				pallor posterolateral LV; severe coronary atherosclerosis; aortic fatty streaks
	Edinburgh Brain Bank	71	Male	Acute myocardial damage with haemorrhage and neutrophilic infiltration; some established ischemic damage
	Edinburgh Brain Bank	51	Male	Perivascular and confluent myocardial fibrosis; occasional contraction band necrosis

2.9.2 Masson's Trichrome

Masson's Trichrome staining was performed on human myocardial tissue sections (10 µm of cryosections) to visualise collagen fibres (blue), allowing clear distinction between scarred and healthy regions (red) (Sridharan et al., 2022). Most MT staining on tissues provided by Dr. Stephanie Sellers (University of British Columbia) was previously carried out by Dr. Cass Li and Bronwyn Berkeley (former members of the Brittan lab). I performed MT staining on additional control and MI tissue sections obtained from the Edinburgh Brain Bank using the Trichrome Stain Kit (ab150686; Abcam, UK). Human formalin-fixed, paraffin-embedded sections were processed by SuRF Histology. Slides were deparaffinised in xylene (2 x 5 minutes) and rehydrated through a graded ethanol series (100%, 90%, 80%, 70%; 20 seconds each). Sections were incubated in Bouin's solution at room temperature overnight to enhance staining, then rinsed thoroughly in tap water. Nuclei were stained with Weigert's iron haematoxylin and rinsed in deionised water. Cytoplasm was stained with Biebrich scarlet/acid fuchsin solution for 10 minutes, followed by differentiation in phosphotungstic/phosphomolybdic acid solution for 25 minutes. Collagen was then counterstained with Aniline Blue for 20 minutes, followed by treatment with 0.2% acetic acid. Finally, sections were dehydrated through ascending ethanol concentrations (95% then 100%), cleared in xylene (3 x 5 minutes), and mounted using Pertex mounting medium (CellPath, UK).

Slides were imaged using an Axioscan.Z1 slide scanner (Zeiss, Germany) using Zen2.6 software at 20x magnification. Regions of interest (ROI) and image annotations were generated using Zen2.6 software. Infarct border zones were defined based on the Masson's Trichrome staining, which clearly distinguishes fibrotic scar tissue (purple/blue) from healthy myocardium (red). ROIs were selected to include both the fibrotic area and the immediately adjacent non-fibrotic myocardium, representing the infarct border zones for subsequent analysis.

2.9.3 Immunofluorescence staining of human cardiac tissue

Serial paraffin sections were deparaffinised and rehydrated in xylene and various concentrations of ethanol (100%, 95%, 80% and 70%). Paraffine sections were washed in 10mM sodium citrate buffer (2.94g citric acid in 1L dH20, pH 6.0) for 15 minutes at room temperature. Then slides were microwaved in sodium citrate buffer (4 x 4 minutes) and subsequently left to cool to room temperature on ice. Paraffin sections were washed in PBS for 5 minutes, permeabilised in 0.5% Triton X-100/PBS for 30 minutes, and blocked in 10% normal goat serum (NGS, Thermo Fisher Scientific) plus 3% BSA in 0.5% Triton X-100/PBS for 1 hour at room temperature.

Paraffin sections were incubated in primary antibodies (rabbit recombinant anti-ANXA2 at 1:100, invitrogen # MA5-32689; rabbit anti-PABP/PABPC1 at 1:250, Niki Gray Lab; rabbit anti-PAI1 at 1:100, abcam #66705; mouse anti-CD31 at 1:800, cell signalling #3528; Alexa Fluor 647-conjugated monoclonal mouse anti-Vimentin at 1:200 BioLegend #677807) diluted in the blocking solution overnight at 4 ºC.

After further washes in 0.5% Triton X-100/PBS (2 x 10 minutes), paraffin sections were incubated in fluorescence-conjugated secondary antibodies (goat anti-rabbit Alexa Fluor 488 at 1:200 5, invitrogen A11008; goat anti-mouse Alexa Fluor 647 at 1:200, invitrogen A21235) diluted in blocking solution for 1 hour at room temperature, and washed in 0.5% Triton X-100/PBS. Paraffin sections were counterstained with DAPI (1:500) in PBS for 15 minutes. Slides were then immersed in Sudan Black or TrueBlack (Cambridge bioscience 23007-BT) for 5 minutes, then washed in PBS (3 x 5 minutes). Paraffin sections were mounted in Fluoromount-GTM without DAPI (Invitrogen).

2.9.4 Confocal fluorescence imaging and quantification

High-resolution imaging was performed using a Zeiss LSM 780 confocal laser scanning microscope equipped with GASP detectors, which enable low-intensity laser illumination to minimise phototoxicity in samples. Images were acquired in 8-bit format using the Zeiss ZEN software suite.

For paraffin-embedded tissue sections, the following laser lines and detectors were used: DAPI (405 nm, 417-508 nm), Alexa Fluor 488 (488 nm, 498-579 nm), and Alexa Fluor 647 (633 nm, 641-758 nm). For each healthy and MI tissue section, five regions of interest (ROIs) (850.19 µm × 850.19 µm) were acquired using a 20× Plan Apo VC, NA 0.8 objective, with a 3 µm Z-step spanning a total thickness of 12 µm and 2 × 2 tile scans, focused on the infarct border region identified from Masson's Trichrome staining. Images were processed and analysed using Fiji v2.0 (ImageJ, Derby, UK). Cell counting was performed with the Cell Counter plugin, and the total cell number was determined by counting DAPI-positive nuclei.

To quantify target expression in ECs, the percentage of CD31+ cells co-expressing ANXA2, SERPINE1, or PABPC1 was calculated as follows:

$\%ANXA2^+$ CD31+ = $N_{ANXA2+CD31+}$ /N_{CD31+} * 100%

$\%SERPINE1^+$ CD31+ = $N_{SERPINE1+CD31+}$ /N_{CD31+} * 100%

$\%PABPC1^+$ $CD31^+$ = $N_{PABC1+CD31+}$ /N_{CD31+} * 100%

Similarly, ANXA2 expression in Vimentin+ cells was quantified by calculating the percentage of Vimentin+ cells that were also positive for ANXA2.

2.10 Cell culture techniques

2.10.1 EdU cell proliferation assay

Human cardiac microvascular endothelial cells (HCMECs; #C-12285 PromoCell) were seeded at 1-2 x 10^4 cells per well onto collagen-coated coverslips in 24-well plates (Collagen Type I solution from rat tail, Sigma-Aldrich #C3867-1VL) in Endothelial Cell Basal Medium MV2 (#C-22221, PromoCell) supplemented with the Endothelial Cell Growth Medium MV2 Supplement Pack (#C-39221, PromoCell). Cells were serum-starved overnight in 0.2% foetal bovine serum (FBS, HyClone). The following day, cells were treated with N2-01 drug in either complete growth medium or 5% FBS in basal medium for 24-48 hours. 10 ng/ml VEGF-165 was used as a positive control for cell proliferation.

For the EdU assay, 10 µM EdU (5-ethynyl-2´-deoxyuridine, Click-iT™ EdU Alexa Fluor™ 647 Imaging Kit, ThermoFisher #C10340, reconstituted in DMSO) was added to the culture medium containing 10% FBS (HyClone) and incubated for 6 hours at 37 °C. Following EdU incorporation, cells were stained with 5 µM Calcein AM for 30 minutes at 37 °C to assess viability. Cells grown on coverslips were then fixed in 4% paraformaldehyde (PFA) in PBS for 15 minutes at room temperature, permeabilised using 0.5% Triton X-100 in PBS for 20 minutes at room temperature and incubated in Click-iT™ reaction cocktail (prepared according to the manufacturer's instructions) for 30 minutes at room temperature, protected from light. The coverslips were then washed twice in 3% BSA in PBS (KPL 10% BSA Diluent/Blocking Solution Kit, Seracare) and mounted on slides using Fluoromount-GTM Mounting Medium with DAPI (ThermoFisher Scientific).

Images were acquired on a Zeiss LSM 780 confocal microscope using a 20X Plan-Apochromat 0.8 NA objective. Laser lines and detectors were: DAPI (405 nm, 417-508 nm), Alexa Fluor 488 (488 nm, 498-579 nm), and Alexa Fluor 647 (633 nm, 641-744 nm). For each treatment group (cell only control, 10 ng/ml VEGF-165, 1/3 N2-01, 1/6 N2-01, 1/12 N2-01), three ROIs (708.49 µm x 708.49 µm) were acquired per cell line. Cell proliferation was analysed by measuring $DAPI^+$ EdU^+ cell count, and cell viability

was measured as $DAPI^+$ Calcein AM^+ cells via the Cell Counter plug-in in Fiji v2.0 (ImageJ).

To normalise the data, the percentage of EdU^+ cells in each treated group was divided by the average percentage of EdU^+ cells in the untreated control group. This set the control's average fold change to 1, allowing for a direct comparison of relative proliferation across conditions.

2.10.2 Matrigel tube formation assay

Human cardiac microvascular endothelial cells (HCMECs, passage 3-5) were cultured in collagen-coated flasks using Endothelial Cell Growth Medium MV2 until reaching 80-90% confluency. To assess the ability of ECs to generate tube-like structures (equivalent to angiogenic potential) under various experimental conditions, Matrigel Matrix, Growth Factor Reduced (BD Biosciences; aliquots from Caporali Lab) was used. Matrigel was thawed on ice and 50 µl was added to each well of a 96-well plate, then allowed to solidify at 37 °C for 30 minutes. Cells were washed with DPBS, detached using 1X Trypsin-EDTA, collected in 10% FBS, and centrifuged at 300 g (1,000 rpm) for 3 minutes. The resulting cell pellet was resuspended in complete growth medium, and 1.5×10^4 HCMECs per well (passage 6) were seeded in 50 µl onto the solidified Matrigel according to their treatment groups, with technical triplicates for each condition. Plates were incubated at 37 °C to allow tube formation.

Network formation was initially assessed at 5 hours using a light microscope, with three images captured per well at 4X objective. Cells were incubated overnight to obtain a second imaging time point (~22 hours). Quantitative analysis of tube-like structures was performed in ImageJ (Fiji) using the Cell Counter plugin to count the number of tubules (enclosed structures).

2.11 Assembly of graphs and statistical analysis

Graphs were generated using GraphPad Prism 8.0, which was also used for all statistical analyses. Data are presented as mean ± standard deviation (SD). Outliers were identified using the "Identify Outliers" built-in analysis function in GraphPad Prism, applying the ROUT method with a Q value of 1%. Samples flagged as outliers were excluded from subsequent analyses, and the final sample size after outlier removal is reported for each figure.

Data distribution was evaluated prior to the application of parametric statistical tests. Normality was assessed using the built-in "Normality and Lognormality Tests" function in GraphPad Prism, which automatically applies multiple Gaussian distribution tests,

including Anderson-Darling, D'Agostino & Pearson, Shapiro-Wilk and Kolmogorov-Smirnov tests, using a significance level (alpha) of 0.05.

Comparisons between groups were performed using the appropriate statistical tests: unpaired t-test with Welch's correction for two-group comparisons, ordinary one-way ANOVA with multiple comparisons for single-factor multi-group analyses, or two-way ANOVA with multiple comparisons for experiments with two independent variables. Statistical significance is indicated as: $p < 0.05$ (*), $p < 0.01$ (**), $p < 0.001$ (***), $p < 0.0001$ (****).

Chapter 3: Results – Identification of target genes using a multi-omics approach

3.1 Introduction

The development and widespread application of single-cell RNA-sequencing (scRNA-seq) technology has revolutionised cardiovascular research, enabling high-resolution and unbiased characterisation of cell state, lineage, heterogeneity, and function. This approach has provided molecular insight into coronary vessel development and vascular responses following ischaemic injury (Marín-Sedeño et al., 2021).

Previously, genetic-lineage tracing studies showed that all new coronary vessels forming in the injured mouse heart are derived from pre-existing resident ECs, not from other cell sources (He et al., 2017). Supporting this, vascular endothelial cadherin (*Cdh5*)- specific lineage tracing 'Confetti' mouse model reported that clonal expansion of pre-existing *Cdh5*-expressing ECs contributed to vessel growth after acute MI (Manavski et al., 2018). Similarly, the Brittan Lab employed an endothelial cell-Confetti lineage-tracing mouse model (*Pdgfb-iCreERT2-R26R-Brainbow2.1*) to demonstrate that the structural integrity of adult cardiac endothelium was maintained via neovasculogenesis by clonal expansion of resident ECs, rather than bone marrow derived cells, within the infarct border region at 7 days post-MI (Li et al., 2019b). Building on these findings, our group applied single-cell RNA sequencing (scRNA-seq) to characterise ten transcriptionally distinct EC states and the molecular pathways likely involved in neovasculogenesis after MI. This work identified and validated plasmalemma vesicle-associated protein (*Plvap*) as a novel endothelial-specific marker with a functional role in cardiac neovascularisation following ischaemic injury in both mice and humans (Li et al., 2019b). Nevertheless, scRNA-seq captures only a static snapshot of gene expression and therefore cannot fully resolve dynamic processes. Moreover, findings from non-human datasets may not always translate directly to clinical settings.

To address these limitations, the Brittan group conducted a meta-analysis of integrated single cell and nuclei RNA-sequencing datasets (sc(n)RNA-seq) from developing and adult mouse and human hearts in healthy and diseased states (Li et al., 2022b) (**Table 1**). Unlike conventional statistical meta-analyses, this approach involved systematic curation, integration, and re-analysis of coronary EC datasets across multiple studies. This work resulted in the construction of a human and mouse coronary EC meta-atlas, CrescENDO (www.crescendo.science), which maps the endothelial transcriptome during development and in response to cardiac injury, revealing conserved molecular mechanisms underpinning coronary vascular regeneration (Li et al., 2022b).

More recently, a multimodal omics approach combining single-nucleus RNA sequencing (snRNA-seq), single-cell chromatin accessibility sequencing (snATAC-seq), and spatial transcriptomics was applied to generate a spatially resolved multi-

omic map of the human heart following acute MI (Kuppe et al., 2022). This approach enabled high-resolution characterisation of cardiac cell type composition and transcriptional signatures within distinct anatomical zones: the ischaemic zone (IZ, necrotic myocardium), border zone (BZ, surrounding viable myocardium), remote zone (RZ, unaffected myocardium), and fibrotic zone (FZ, late-stage post-MI scar) (**Table 2**). Informatic analyses of datasets from this study, referred herein as the 'Kuppe dataset' enabled us to identify EC-specific transcriptional signatures driving human injury response and tissue remodelling in different myocardial tissue regions (Kuppe et al., 2022).

In parallel, the Brittan group used the 10X Genomics Visium approach for spatial transcriptomics to investigate gene expression patterns in human control, acute, and chronic MI samples provided by Dr. Stefanie Sellers at the University of British Columbia. Anatomically resolved gene expression patterns were observed using the 10X Genomics Cell Loupe Browser. Analysing earlier timepoints, such as acute MI samples, provides valuable insight into the transcriptional patterns activated during the initial phases of endogenous neovascularisation in the human heart (Cochain et al., 2013).

To complement mammalian datasets and gain an evolutionary perspective, I also analysed publicly available scRNA-seq data from regenerating adult zebrafish hearts. Zebrafish possess a remarkable capacity for heart regeneration, making them a powerful model to identify fundamental mechanisms of heart regeneration including pro-regenerative endothelial responses, which may inform strategies to reactivate similar pathways in mammals (Gemberling et al., 2013). The dataset used in this chapter (Ma et al., 2021) profiles non-cardiomyocyte populations at multiple time points following ventricular apex amputation, capturing the molecular features, cellular functions, and intercellular interactions of non-cardiomyocytes (including macrophages, fibroblasts, and ECs) during the process of cardiac regeneration. Informatic analysis of this zebrafish dataset enabled us to examine the temporal dynamics of selected candidate genes, compare their expression profiles between zebrafish and mammalian systems, and determine their potential role during different stages of tissue repair.

Through informatic analyses of these publicly available and in-house datasets, I aimed to identify and prioritise novel endothelial candidate genes that align with my central hypothesis that reactivation of developmental pathways may promote adult cardiovascular regeneration. Candidate genes identified through this approach were subsequently selected for experimental validation to investigate their function in angiogenesis and cardiac repair.

3.2 Results: *ANXA2* identified as a reactivated foetal gene, with *SERPINE1* as a potential co-regulator of neovascularisation after MI

The EC-specific scRNA-seq dataset from Li et al., (2019) revealed ten heterogeneous EC states in the healthy and post-ischaemic adult mouse heart at 7 days post-MI. Among these, the Brittan group first identified annexin A2 (*Anxa2)* as one of the top differentially expressed genes within an MI-specific mouse endothelial cluster (cluster 8), a population of coronary ECs present at 7 days post-MI but absent in the healthy adult heart (Li et al., 2019b). Gene ontology (GO) term analysis of this cluster predicted roles in endothelial extracellular matrix proteins and cardiac remodelling after MI, implicating *anxa2* as a relevant target to further investigation (**Table 15**). This dataset was subsequently incorporated into the coronary endothelial meta-atlas CrescENDO, enabling integration with other single-cell datasets. Using CrescENDO (**Table 1**), I examined both annexin A2 expression levels and the proportion of ECs expressing the gene across species and developmental stages, providing a broader, comparative context for its relevance in cardiac endothelial injury response.

Table 15. Top differentially expressed genes and their predicted functions of each of the 10 heterogeneous cardiac endothelial cell clusters/states in the adult mouse heart under healthy condition or following myocardial infarction (MI) *(adapted from Li et al., 2019b).*

Cluster number	Enrichment in EC from healthy or MI groups	Top differentially expressed genes	Specific to cluster	Predicted function in Pdgfb-EC
1	NA (P = 0.34)	*Arhgap18, Adm, Hspb1, CD36*	No	Cellular homeostasis
2	MI (P = 0.02)	*Ifit1, Ifit2, Ifit3, Ifit3b, Usp18, Cxcl10*	Yes	Interferon signalling
3	MI (P = 0.0006)	*Myl2, Mb, Myl3, Tnnt2, Tnni3, Actc1*	Yes	Ventricular cardiac muscle remodelling
4	NA (P = 0.07)	*Klra3, Klra9, Klra10*	Yes	Killer cell lectin-like receptor signalling
5	NA (P = 0.51)	*Dll4, Notch1, Hey1, Jag1, Gja4*	Yes (Hey1, Jag1, Gja4)	Endothelial cell regulation via Notch signalling
6	MI (P = 0.006)	*Plvap, Lrg1, Pbp1, Bgn, vWF*	No	Ventricular remodelling [via retinoic acid (RA) signalling]

7	MI (100%)	*Ackr1, Ehd4, Tmem176a, Tmem252, Tmem176b, Selp*	Yes (Ackr1, Tmem252, Selp)	Stalk cell markers. Tip and stalk cell-mediated neovasculogenesis
8	**MI (P = 0.07)**	*Fbln2,* ***Anxa2****, Col5a2, Emilin1, Hmcn1, Bgn, Mgp*	Yes (Col5a2, Mgp)	**Endothelial ECM proteins, Cardiac remodelling post-MI**
9	NA (P = 0.69)	*Serpina1b, Serpina1d, Serpina1e*	Yes	Serine protease inhibitor alpha-1 antitrypsin (AAT) signalling
10	MI (P = 0.02)	*Mki67, Top2a, Cenpf, Cks2, Birc5, Cenpa, Ube2c, Cdc20*	Yes	Proliferation and cell cycle regulation

ANXA2 subsequently emerged as a key gene of interest due to its distinctive expression pattern across development and disease. It is highly expressed in embryonic coronary ECs, expressed at very low levels in healthy adult ECs, and re-expressed following cardiac injury. Using the coronary endothelial meta-atlas CrescENDO (**Table 1**), I examined both *ANXA2* expression levels and the percentage of ECs expressing the gene across species and developmental stages.

In human healthy foetal hearts, over 80% of cECs exhibited high levels of *ANXA2*, whereas expression was very low in uninjured adult human hearts. Similarly, in postnatal mouse hearts, *Anxa2* was detected in about 25% of ECs at uninjured postnatal day 6 (P6) (within the 7 day regenerative window after birth (Porrello et al., 2011, Haubner et al., 2012, Wang et al., 2019)) but became undetectable by day 10 (P10) (**Figure 4**). While *ANXA2* expression remained low in patients with heart failure caused by ischaemic cardiomyopathy (cHF) and heart failure caused by dilated cardiomyopathy (dHF), it was consistently upregulated in 60-80% of ECs at multiple timepoints (1, 3, 7, 14, and 28 days) post-MI in mice (**Figure 4**).

To further investigate target expression in human acute MI, I analysed processed snRNA-seq data from Kuppe *et al.* (2022), accessed via CellxGene (https://cellxgene.cziscience.com/collections/8191c283-0816-424b-9b61-c3e1d6258a77) (**Table 2**). Endothelial clusters were isolated for differential expression analysis in R Studio, which revealed *ANXA2* upregulation in acute MI, with the highest expression in approximately 30% of ECs within the fibrotic zone (FZ) (**Figure 4**).

Spatial Transcriptomics analysis was then performed to determine the anatomical localisation of *ANXA2* within the heart. By aligning spatial gene expression data with H&E-stained tissue sections, *ANXA2* expression was found to be low in uninjured controls but increased in both acute and chronic MI samples (one to three subjects per group; **Table 3**), localising mainly to the infarct border zone, a region known for active neovascularisation (Gu et al., 2006, Ma et al., 2025) (**Figure 5**). Although the small sample size prevented robust quantitation, the results were consistent across samples and therefore were used qualitatively to validate and complement findings from sc(n)RNA-seq analyses.

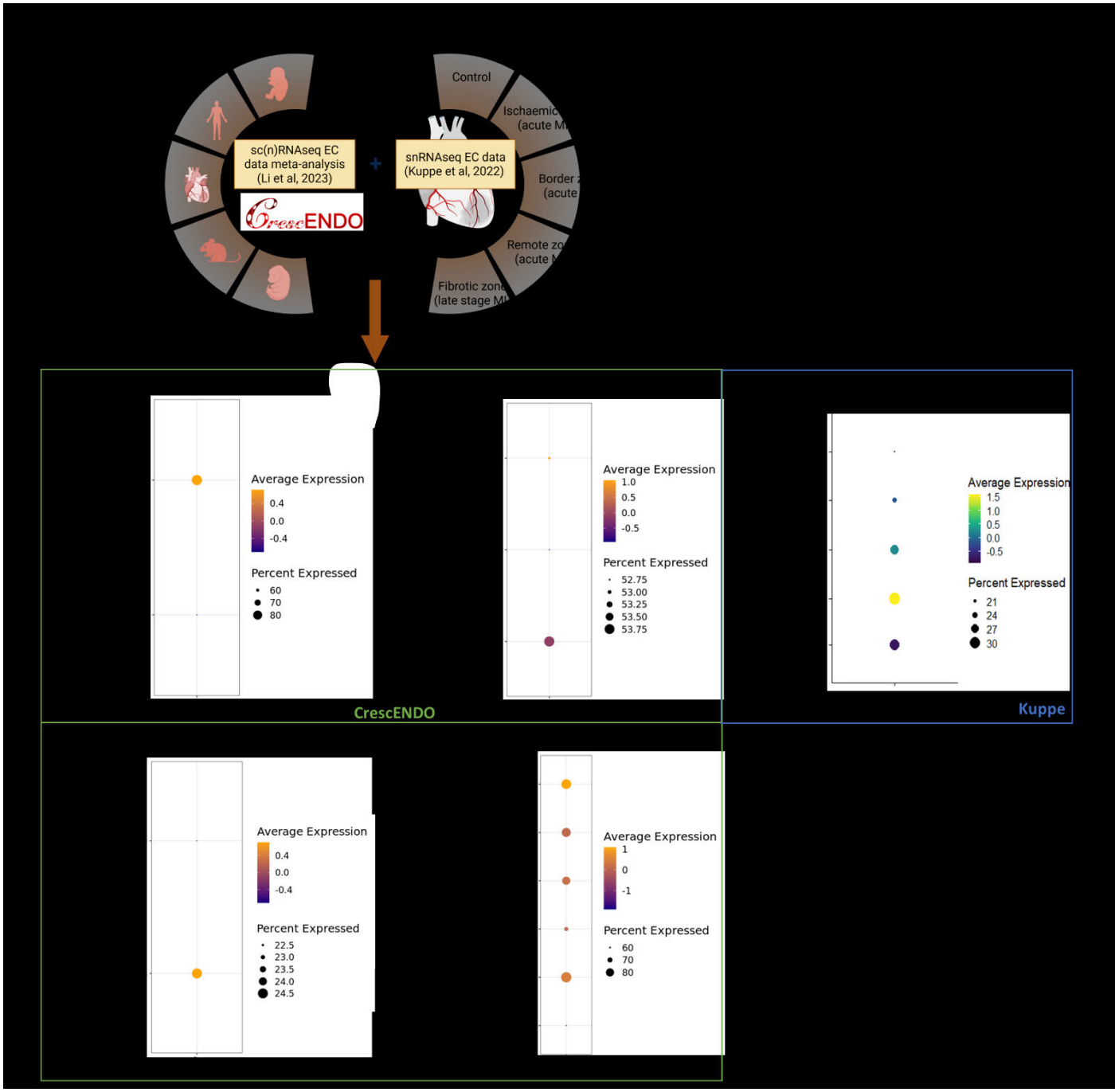

Figure 4. Multi-omics identification of ANXA2 as a reactivated foetal endothelial gene following myocardial injury. *Informatic analyses of in-house and public endothelial- sc(n)RNAseq datasets identified ANXA2 as a developmentally regulated endothelial gene that is re-expressed in the heart after injury (**Table 1**). (A) Schematic overview of datasets analysed, including the coronary EC meta-atlas CrescENDO (Li et al., 2022) and the multi-omics map of human hearts after acute MI (Kuppe et al., 2022), covering foetal, adult healthy and diseased hearts. (B) Dot plots showing ANXA2 endothelial expression across (i) human foetal, adult, and heart failure (cHF, heart failure caused by ischaemic cardiomyopathy; dHF, heart failure caused by dilated cardiomyopathy), (ii) different myocardial zones post-MI (control, ischaemic zone, border zone, , remote zone, and fibrotic zone) (iii) neonatal mouse at P6 and P10, and (iv) adult mouse ECs at multiple time points post-MI. Dot size represents the*

percentage of ECs expressing ANXA2; colour indicates scaled average expression level (z-score).

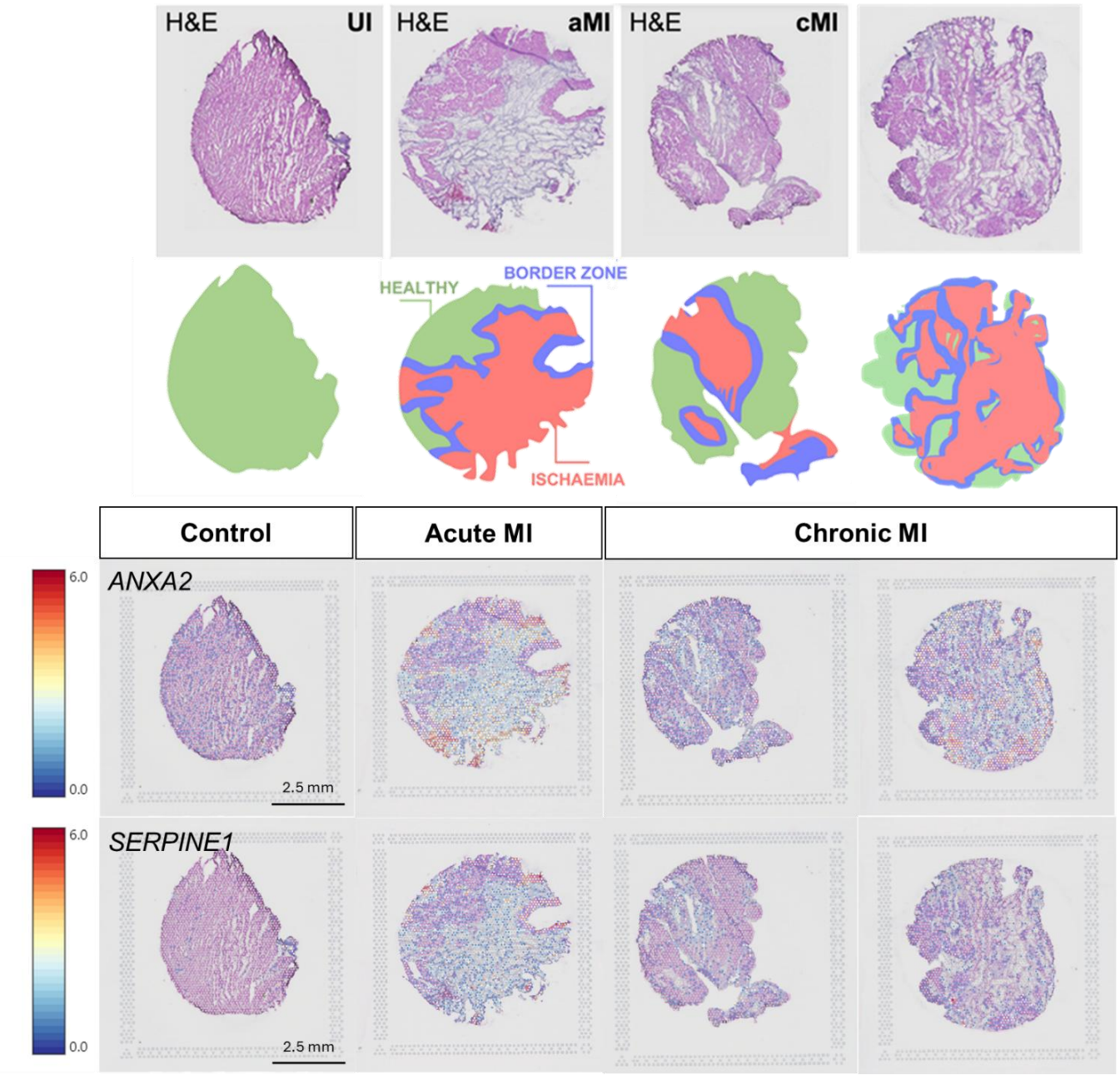

Figure 5. In-house spatial transcriptomic data showing sections of adult human heart tissue from an uninjured, healthy control (UI), patients presenting with acute MI (aMI) and chronic MI (cMI). *Panel 1 shows H&E staining of the tissue samples, and panel 2 highlights areas of healthy tissue (green), areas of ischaemic damage (red), and the ischaemia border zones (blue). For each gene (ANXA2 and SERPINE1), expression levels (as measured by the summed log-normalised counts from 0-6) are shown. Although the study included a limited number of replicates (one to three subjects per group), which prevented robust quantification, the results were consistent and comparable across individuals in each group.*

The ANXA2 heterotetramer is an important endothelial cell-surface co-receptor for plasminogen and tissue plasminogen activator (tPA), where it promotes tPA-dependent conversion of plasminogen to plasmin (Liu and Hajjar, 2016a). Plasmin facilitates fibrinolysis by degrading fibrin, maintaining blood fluidity, preventing clot formation, and supporting angiogenesis (Dassah et al., 2009, Liu and Hajjar, 2016a). In contrast, serpin peptidase inhibitor clade E member 1 (SERPINE1) acts as a major negative regulator of fibrinolysis by inhibiting tPA and urokinase-type plasminogen activator (uPA), thereby preventing plasmin-mediated fibrin degradation (Sillen and Declerck, 2020). Given these opposing functions, I next examined *SERPINE1* expression in the CrescENDO and ST datasets to investigate its potential co-regulation with *ANXA2* in the context of coronary development, neovascularisation, and cardiac regeneration.

Pseudobulk differential expression analysis of endothelial clusters from the Kuppe dataset revealed *SERPINE1* as one of the top upregulated genes in ECs (and all other cardiac cell types) in the ischaemic zone (IZ) post-MI compared with control hearts (**Figure 6**). Interestingly, *SERPINE1* was not expressed during heart development and was minimally expressed in cHF and dHF patients in CrescENDO (**Figure 6**). Our in-house spatial transcriptomic data further demonstrated mild *SERPINE1* upregulation in the acute MI infarct border zone, where endogenous neovascularisation is active, and its expression declined in chronic MI samples, where regenerative activity is minimal (**Figure 5**).

To extend these findings to a regenerative model, I analysed publicly available scRNA-seq data from regenerating adult zebrafish hearts after ventricular resection (GEO: GSE145980; (Ma et al., 2021)). The dataset included samples at 0 (uninjured), 2, 7, and 14 days post-injury (dpi). Data were processed using Trailmaker™, a cloud-based platform for scRNA-seq data analysis. Focusing on endothelial clusters, I found that zebrafish *anxa2a* showed strong upregulation at 2 and 14 dpi, with ~80% of ECs expressing the gene compared with uninjured controls, peaking at 14 dpi. In contrast, *anxa2b* expression remained low (<1% of ECs) at all time points. Similarly, *serpine1* expression increased significantly after injury, with ~40% of ECs expressing it at 2 and 7 dpi, reaching a peak at 7 dpi (**Figure 7**).

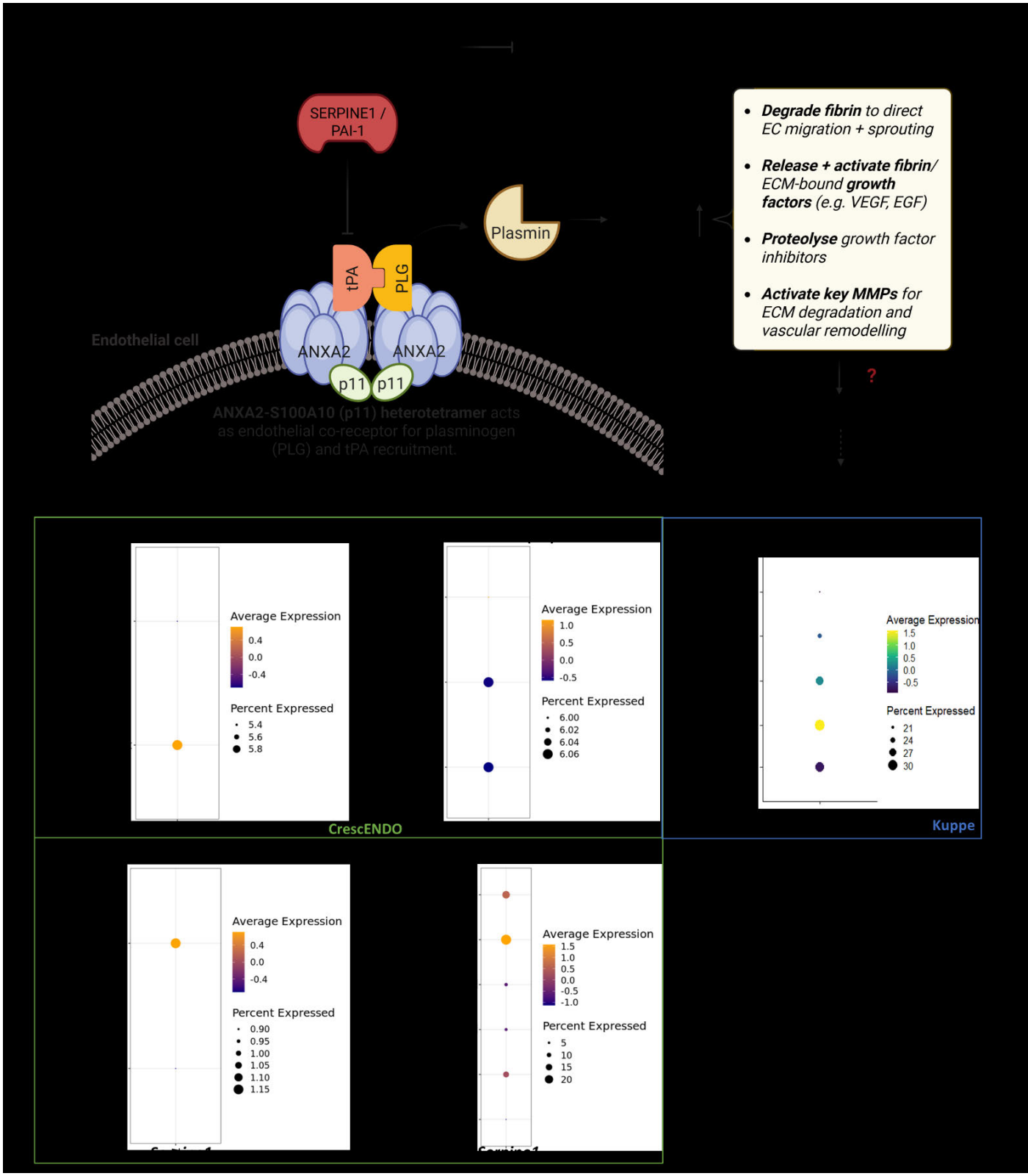

Figure 6. Multi-omics identification of SERPINE1 as a top differentially expressed gene following acute MI. *(A) Schematic representation of the fibrinolytic pathway regulated by ANXA2 and SERPINE1, illustrating their co-regulation of plasmin production and potential downstream effects on angiogenesis and cardiac regeneration. The ANXA2–S100A10 (p11) heterotetramer on the endothelial cell membrane acts as a co-receptor for tissue plasminogen activator (tPA) and*

plasminogen (PLG) recruitment to catalyse plasmin generation. Plasmin degrades fibrin to facilitate endothelial cell migration and sprouting, releases and activates extracellular matrix (ECM)-bound growth factors (e.g., VEGF, EGF), proteolyses growth factor inhibitors, and activates key matrix metalloproteinases (MMPs) to promote ECM degradation and remodelling. SERPINE1/PAI-1 inhibits this pathway by blocking tPA activity, thereby regulating plasmin production and fibrinolysis. (B) Dot plots showing SERPINE1 expression in endothelial cells across (i) human foetal, adult, and heart failure (cHF, heart failure caused by ischaemic cardiomyopathy; dHF, heart failure caused by dilated cardiomyopathy), (ii) different myocardial zones post-MI (control, ischaemic zone, border zone, , remote zone, and fibrotic zone) , (iii) neonatal mouse at P6 and P10, and (iv) adult mouse ECs at multiple time points post-MI. Dot size represents the percentage of ECs expressing SERPINE1; colour indicates scaled average expression level (z-score).

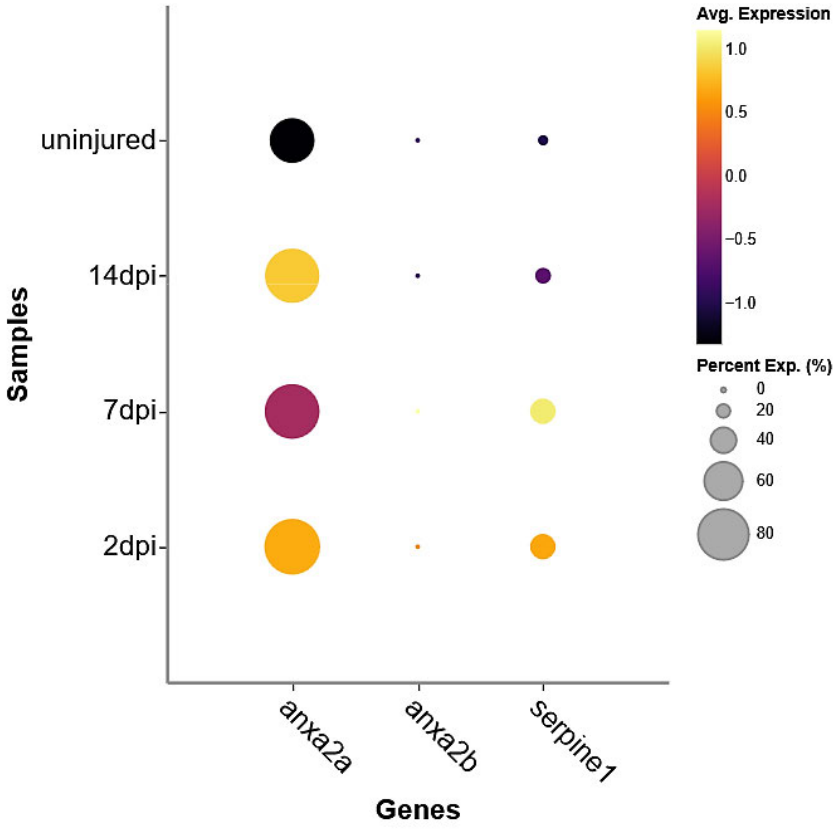

Figure 7. Expressions of ANXA2 paralogues (anxa2a and anxa2b) and serpine1 from endothelial cell-specific adult zebrafish heart regeneration single cell transcriptomics data (Ma et al., 2021). *Dot plot showing the percentage of expressing cells and average expression level of anxa2a, anxa2b, and serpine1 in zebrafish hearts at 2, 7, and 14 days post-injury (dpi) compared to uninjured controls. Dot size represents the percentage of ECs expressing target gene; colour indicates scaled average expression level (z-score).*

3.3 Biological functions and mechanisms of ANXA2 and its potential implications in cardiovascular disease research

Annexin A2 (ANXA2) is a calcium(Ca^{2+})-dependent, phospholipid- and membrane-binding protein that can either exist as a monomer or as a heterotetramer complex with the plasminogen receptor protein, S100A10 (P11) (Gerke et al., 2005, Madureira et al., 2011). ANXA2 is primarily localised in the cytoplasm and plasma membrane with a small population in the nucleus. It is expressed by various cell types, including endothelial, trophoblast, epithelial, tumour, and immune cells such as macrophages, monocytes, and dendritic cells (Dallacasagrande and Hajjar, 2020).

The biological roles of ANXA2 depend on its localisation and structural form. Intracellularly, the soluble monomeric form plays crucial roles in many cellular processes such as exocytosis, endocytosis, membrane organisation, signal transduction, cytoskeletal movement, cell proliferation, apoptosis, and neovascularisation (Yang et al., 2018, Bharadwaj et al., 2013, Dallacasagrande and Hajjar, 2020). It also contributes to microdomain formation, membrane repair, and trafficking along endo- and exocytic pathways and RNA export from the nucleus (Bharadwaj et al., 2013).

Extracellularly, ANXA2 forms a heterotetrameric complex comprising two ANXA2 molecules bound to an S100 calcium-binding protein A10 (S100A10) dimer. ANXA2 anchors S100A10 to the cell surface, where S100A10 binds plasminogen via its C-terminal domain, forming a co-receptor complex for tPA and plasminogen (Madureira et al., 2011). The ANXA2 heterotetramer acts as an endothelial-surface co-receptor for plasminogen and tPA, which facilitates tPA-dependent conversion of plasminogen to plasmin, thereby promoting fibrinolysis, maintaining blood fluidity, preventing intravascular thrombosis, and supporting angiogenesis (Dassah et al., 2009, Liu and Hajjar, 2016a, Kumar et al., 2022). The complex also protects tPA and plasmin from inactivation by their physiologic inhibitors, PAI-1 and α2-antiplasmin, respectively (Madureira et al., 2011). The depletion of cellular ANXA2 often results in both reduced levels of S100A10 and diminished plasmin generation (Bharadwaj et al., 2013). In short, ANXA2 serves as a molecular bridge between membrane dynamics and fibrinolytic regulation, linking cytoskeletal organisation to vascular homeostasis.

ANXA2 expression is developmentally regulated. During embryogenesis, it is highly localised in the amniotic epithelial cells, mesenchymal cells of the amnion and chorion (foetal membranes), and ECs surrounding the blood vessels in the decidua (maternal uterine tissue) (Sun et al., 1996). The plasmin generated from the interaction of tPA, ANXA2 and plasminogen is important for the activation of matrix-degrading MMPs and subsequently the normal turnover of the ECM of foetal membranes (Bogic et al., 1999). ANXA2 is also highly expressed in the foetal brain during radial glia proliferation, but is absent in normal adult brain (Reeves et al., 1992). In the developing chick heart,

ANXA2 is expressed in the endocardium during atrioventricular (AV) cushion formation, and ANXA2-mediated plasmin activity was shown to play a role in the release of active TGF-β3 during chick AV canal epithelial-mesenchymal transformation, where endocardial cells are converted into a mesenchymal phenotype (Krishnan et al., 2004). Together, these findings highlight ANXA2 as a key regulator of developmental morphogenesis, ECM remodelling, and early vascular formation.

ANXA2 is a critical mediator of angiogenesis. Migrating ECs utilise the ANXA2/tPA/plasminogen complex to degrade ECM during sprouting angiogenesis (Lim and Hajjar, 2021). tPA may enhance angiogenesis indirectly by activating adenosine A2A receptors, which decrease release of SERPINE1 (PAI-1) and increase ANXA2 surface expression (Valls et al., 2021). ANXA2 is highly expressed in vascular ECs, where it promotes retinal neovascularisation through PI3K/AKT signalling (Li et al., 2022a, Zhao et al., 2009). Its interaction with the ANXA2 receptor activates AKT/ERK pathways, enhancing endothelial proliferation and migration following cerebral ischaemia or oxygen-glucose deprivation injury (Lin et al., 2023). Recombinant ANXA2 administration reduces early blood-brain barrier disruption, increases angiogenesis, and improves vessel density after traumatic brain injury (Cheng et al., 2021). These studies establish ANXA2 as a multifunctional regulator of endothelial survival, migration, and angiogenic remodelling in both physiological and injury contexts.

In myocardium, ANXA2 is localised in intramyocardial capillaries, coronary ECs, and ECM but is absent from cardiomyocytes (Camors et al., 2005). Immunolabelling of ANXA2 showed robust staining in the interstitium between cardiomyocytes and around coronary arteries in failing hearts. ANXA2 is known for its membrane trafficking and collagen binding properties, which are implicated in fibrosis development and ECM organisation. Notably, the absence of ANXA2 in cardiomyocytes from both non-failing and failing hearts indicates that it likely doesn't have a significant role in regulating $Ca2^{+}$ handling in the heart (Camors et al., 2005). ANXA2 was later identified to be one of the plasma biomarkers of HF in mouse and human (Chugh et al., 2013).

ANXA2 also functions as a receptor for tenascin-C, an ECM glycoprotein involved in atherosclerosis and MI progression, facilitating macrophage migration and pro-angiogenic phenotype angiogenesis via its interaction with ANXA2 – the expression of which is regulated by hypoxia-inducible factor-1α (Wang et al., 2018). Furthermore, ANXA2 binds and inhibits proprotein convertase subtilisin/Kexin type 9 (PCSK9)-mediated low-density lipoprotein (LDL) receptor degradation. This interaction helps lowering LDL cholesterol and reducing the risk of atherosclerosis and coronary heart disease (Seidah et al., 2012, Fairoozy et al., 2017).

One study showed the lack of ANXA2 can results in poor myofibre repair and progressive decline in muscle function. Hence ANXA2 could be a regulator of myofibre repair and injury-triggered muscle inflammation (Defour et al., 2017). Recent study demonstrated that adeno-associated virus-mediated ANXA2 overexpression post-MI

improved left ventricular function, increased microvessel density, and reduced infarct size (Zhang et al., 2023b). Mechanistically, ANXA2 promoted M1-to-M2 macrophage polarisation via YAP inhibition and enhanced endothelial proliferation and migration via integrin β3 activation (Zhang et al., 2023b). Finally, studies in zebrafish have linked ANXA2 to regenerative capacity. Loss of *runx1*, a transcription factor upregulated during cardiac injury, resulted in increased expression of *anxa2a* and *s100a10b*, reduced *serpine1*, and elevated plasminogen levels, collectively increasing myocardial survival and proliferation, diminishing myofibroblast formation and fibrin deposition, and promoting overall heart regeneration (Koth et al., 2020, Lowe et al., 2021). Overall, ANXA2 appears to promote cardiac repair by coordinating endothelial, macrophage, and ECM-mediated regenerative responses.

Despite its protective functions, ANXA2 can exert detrimental effects under certain pathological conditions. Overexpression of circRNA ANXA2 promoted cardiomyocyte apoptosis in myocardial ischaemic-reperfusion injury by inhibiting expression of microRNA-133 and aggravates myocardial ischemia-reperfusion injury (Zong and Wang, 2020). While phosphorylation of ANXA2 by ADAM8 (disintegrin and metalloproteinase 8), elevated in plasma of acute MI patients, suppressed autophagy and angiogenesis, promoted inflammation, and ultimately worsened cardiac dysfunction (Ji et al., 2024).

ANXA2 dysregulation has also been observed in pre-eclampsia, where its decreased expression coincides with elevated tPA and SERPINE1 levels, potentially the imbalance between these fibrinolytic components might contribute impaired fibrinolysis and disease pathogenesis (Ruikar et al., 2023). Circulating ANXA2 concentrations were found higher in diabetic cardiomyopathy patients and were negatively correlated with cardiac systolic and diastolic functions, which suggested it might be a predictor of disease and a potential therapeutic target for diabetic cardiomyopathy (He et al., 2023). A recent study found that Prostaglandin E2 activates the EP4 receptor, which promotes ANXA2 translation and phosphorylation at Thr208 via the cyclic adenosine monophosphate/protein kinase A (cAMP/PKA) pathway, which in turn increases the proliferation and migration of vascular smooth muscle cells in pulmonary arterial hypertension (Xu et al., 2025). Pharmacological inhibition or genetic deletion of ANXA2 in this context protected against pulmonary arterial hypertension progression in rodent models, suggesting its pathogenic role in the development of pulmonary arterial hypertension (Xu et al., 2025). These findings suggest that function of ANXA2 is highly context-dependent, protective in some regenerative and vascular settings, yet pathogenic when dysregulated or excessively activated, and this may be modulated by post-translational modifications and interacting partners.

Notably, ectopic expression of ANXA2 has been shown to protect against renal tubular cell apoptosis and kidney injury by promoting lysosomal functions and autophagy (Shen et al., 2022). Mechanistically, ANXA2 induces β-catenin activation, which further triggers T-cell factor-4 (TCF4)-induced transcription factor EB (TFEB),

stabilising lysosomal function and supporting autophagy (Shen et al., 2022). During acute inflammation, ANXA2 primarily plays an anti-inflammatory role by maintaining vascular integrity and limiting vascular permeability. This action modulates the recruitment of leukocytes, preventing inflammasome activation and mitigating the release of inflammatory mediators (Dallacasagrande and Hajjar, 2020). In the later stages of acute inflammation, ANXA2 contributes to the initiation of angiogenesis and wound healing by promoting cell surface fibrinolytic activity. However, in chronic inflammation or when ANXA2 becomes dysregulated, ANXA2 can adopt pro-inflammatory actions and cause tissue damage through excessive angiogenesis, as seen in diabetic retina or malignancies (Dallacasagrande and Hajjar, 2020). Plasmin generated via the ANXA2 complex also activates macrophages at sites of inflammation such as atherosclerotic lesions, this could trigger signalling cascade (e.g. Janus kinase JAK1/TYK2 signalling, Akt-dependent NF- κB, ERK1/2, and p38 MAPK) that results in the induction of proinflammatory gene expression and promotes inflammatory cell recruitment (Li et al., 2007). These show ANXA2 functions as both a regulator of vascular homeostasis and an immune modulator, balancing fibrinolysis, inflammation, and repair processes depending on its activation context.

Cardiopulmonary bypass (CPB) frequently results in post-operative organ complications, particularly acute lung injury, driven by systemic inflammation and consequent endothelial dysfunction. ANXA2 plays a protective role in maintaining pulmonary microvascular integrity in the hypoxic murine lung by preventing phosphorylation of vascular endothelial cadherin at the endothelial-endothelial adherence junction. Following CPB, degradation of ANXA2 correlates with more severe respiratory dysfunction in children under two years, suggesting that maintaining ANXA2 stability could reduce postoperative lung injury associated with cardiopulmonary bypass in paediatric patients (Hsing et al., 2023).

Taken together, ANXA2 is a multifunctional and context-dependent regulator of fibrinolysis, ECM turnover, angiogenesis, inflammation, and tissue repair. Its developmental expression and reactivation following injury suggest a potential role in coordinating tissue remodelling and cardiovascular repair. While its fibrinolytic function is well established, its precise molecular mechanisms in neovascularisation and cardiac regeneration remain largely unexplored, representing a promising area for future research in MI therapy. Future studies should focus on delineating the temporal, dose-dependent, and post-translational regulation of ANXA2 to identify therapeutic windows that harness its regenerative potential while minimising pathological outcomes.

3.4 Biological functions and mechanisms of SERPINE1 and its potential implications in cardiovascular disease research

Fibrinolysis serves a dual purpose: in the bloodstream, it is responsible for breaking down fibrin to maintain vessel patency; while in tissues, it regulates ECM degradation, governs cell adhesion and migration, and thus is essential for tissue remodelling. The primary regulator of fibrinolysis is Serpin peptidase inhibitor clade E member 1 (SERPINE1), also known as plasminogen activator inhibitor type-1 (PAI-1) (Morange et al., 2007). SERPINE1 is primarily produced by hepatocytes and secreted into the circulation by the liver. To a lesser extent, PAI-1 is also synthesised and secreted by kidney, spleen, heart, lung, and adipose tissues. Its expression and release are modulated by growth factors, inflammatory cytokines, hormones, glucose, and endotoxins (Yaron et al., 2021).

SERPINE1 circulates in two pools: a low-level, predominantly active plasma pool (5–50 ng/mL) and a larger platelet-associated pool (up to 300 ng/mL) that retains only 2–5% functional activity upon platelet lysis (Sillen and Declerck, 2021). Circulating platelets continuously synthesise SERPINE1, which is released upon platelet activation, contributing to clot stability by limiting fibrinolysis (Yaron et al., 2021).

Homeostasis is an important physiological process for maintaining vascular integrity and securing a sufficient blood flow throughout the circulatory system. Therefore, it requires a dynamic interplay between the vascular system, blood platelets, the coagulation system, and the fibrinolytic system (Sillen and Declerck, 2020). Through inhibition of tPA and uPA, SERPINE1 suppresses plasmin generation, shifting the haemostatic balance toward a hypofibrinolytic, prothrombotic state (Sillen and Declerck, 2020). Persistent overexpression of SERPINE1 is implicated in the pathogenesis of thromboinflammation, cardiovascular disease, tissue fibrosis, cancer, and age-related diseases (Sillen and Declerck, 2020).

Additionally, impaired fibrinolytic potential as evidenced by elevated levels of SERPINE1 and tPA antigen, has also been identified as a predictor of cardiovascular disease events and an increased risk of coronary heart disease (Tofler et al., 2016, Song et al., 2017). In humans, elevated plasma SERPINE1 levels are linked to atherothrombosis, and single nucleotide polymorphisms within the *SERPINE1* gene are associated with the risk of MI (Morange et al., 2007). Studies in transgenic mice overexpressing wild-type or a stabilized active mutant of human SERPINE1, demonstrated that these mice developed either transient venous thrombosis or age-dependent coronary arterial thrombosis and myocardial infarction, respectively (Erickson et al., 1990, Eren et al., 2002). Beyond thrombosis, SERPINE1 has been identified as a marker of cellular senescence and a major contributor to organismal aging and age-related morbidities like thrombosis, arteriosclerosis, obesity, diabetes, organ fibrogenesis, and emphysema (Vaughan et al., 2017). Pharmacological

inhibition of SERPINE1 has shown protective effects against vascular aging, extended murine life span, and reduced cellular oxidative stress (Vaughan et al., 2017). Additionally, inhibiting SERPINE1 has reduced atherosclerosis in mice with obesity and metabolic syndrome, while decreasing macrophage accumulation and cell senescence in atherosclerotic plaques, as well as obesity-relating metabolic dysfunction (Khoukaz et al., 2020).

There is also a relationship between elevated SERPINE1 and thromboinflammation, which leads to cardiovascular complications. Proinflammatory cytokines, such as IL-6 and TNF-a, released during proinflammatory state (e.g., acute tissue injury and sepsis), directly contribute to increased SERPINE1 synthesis (Morrow et al., 2021). In this context, the role of SERPINE1 is primarily seen as a protective mechanism to limit pathogen spread and support tissue repair. However aberrant/excessive activation can lead to hypofibrinolysis and thrombosis, highlighting the potential of SERPINE1 as a viable target for the treatment of various diseases, including MI (Morrow et al., 2021).

Experimental studies supported a context-dependent role for SERPINE1 in cardiac remodelling. Increased expression of SERPINE1 was initially observed in the cardiomyocytes near the infarct border and fibrous lesions, and SERPINE1 deficiency reduces development of fibrosis in mice post-MI (Takeshita et al., 2004). Contradictorily, a recent study found a complete loss of SERPINE1 leads to severe cardiac fibrosis in mice. This fibrosis is linked with reduced inflammation, lower levels of TGF-B and proteases associated with tissue remodelling. Furthermore, the absence of SEPRINE1's direct target, uPA, or its downstream product, plasmin, was found to alleviate the severity of cardiac fibrosis in SERPINE1 knockout mice. Hence SEPRINE1 protects mice against cardiac fibrosis by inactivating uPA and ultimately limiting plasmin generation (Gupta et al., 2017).

While the role of SERPINE1 in cardiovascular disease is well-documented, its regenerative function remains debated. In zebrafish, *serpine1* acts as an early endocardial injury-response gene regulating endocardial and myocardial proliferation. Pharmacological inhibition of *serpine1* (Tiplaxtinin) enhanced endocardial proliferation without altering fibrosis or endocardial activation after cryoinjury (Münch et al., 2017). During juvenile zebrafish heart development and regeneration, *serpine1* expressed by *hapln1a*+ epicardial cells organised hyaluronic acid into linear structures along and preceding coronary structure, serving as a guide for coronary vessel formation (Sun et al., 2023). Similarly, increased hyaluronic acid synthesis in murine hearts facilitated post-infarct healing by supporting macrophage survival and myofibroblast activation (Petz et al., 2019).

Together, these studies suggest that SERPINE1 exerts complex, context-specific effects on fibrinolysis, thrombosis, fibrosis, and regeneration. Importantly, SERPINE1 and ANXA2 act in opposition to regulate plasmin generation and fibrin turnover. Excess SERPINE1 suppresses angiogenesis by inhibiting plasmin-mediated matrix

remodelling, whereas ANXA2 promotes plasmin production and endothelial sprouting. The balance between these two regulators appears critical for vascular repair after MI, but the angiogenic mechanisms of the ANXA2-SERPINE1 axis remain poorly defined. Further investigation could reveal therapeutic opportunities to modulate this balance and enhance cardiac regeneration.

3.5 Discussion

Using a multi-omics approach integrating human, mouse, and zebrafish datasets, I identified *ANXA2* as a developmentally regulated endothelial gene that is silenced in adulthood and re-expressed following acute myocardial injury. Analysis of the coronary endothelial meta-atlas, CrescENDO, revealed that A*nxa2* is highly expressed in >80% of foetal coronary ECs and in ~25% of ECs in uninjured P6 mouse hearts but becomes almost absent in the adult heart (**Figure 4**). This downregulation coincides with the transition from a pro-angiogenic developmental state to a mature, quiescent vasculature, suggesting that ANXA2 is closely linked to the highly angiogenic environment of the growing heart. Importantly, *Anxa2* expression was robustly reactivated post-MI in mice, with 65-80% of ECs expressing high levels of this gene across multiple time points up to 28 days post-MI in mice, compared to 50% of ECs expressing low levels in the uninjured adult mouse heart.

In human MI hearts (Kuppe dataset), ~30% of ECs in the FZ expressed high levels of *ANXA2*, whereas in control hearts *ANXA2* expression was largely downregulated in ECs (**Figure 4**). Spatial Transcriptomics analyses provided further insight into the localisation of *ANXA2* expression, indicating a high expression in the infarct border zone in acute MI, compared to the ischaemic zone and the remote zones. This fits with my postulation that *ANXA2* may play a role in neovascularisation by coronary ECs post-MI, since the infarct border region is a known critical site for neovascularisation and perfusion recovery (**Figure 5**) (Li et al., 2019b, Kocher et al., 2001). These findings suggest *ANXA2* acts as an injury-responsive gene, reawakening a foetal-like, pro-angiogenic state in ECs to support repair.

As part of the ANXA2/S100A10 heterotetramer, ANXA2 serves as a co-receptor for plasminogen and tPA, promoting the conversion of plasminogen to plasmin (Liu and Hajjar, 2016a). Plasmin subsequently degrades fibrin and activates matrix metalloproteinases (MMPs), promoting ECM degradation/remodelling, facilitating endothelial migration, fibrin clearance, and vessel sprouting (Dassah et al., 2009). The injury-induced re-expression of *ANXA2* in ECs may therefore support both proteolytic clearance of fibrin deposits and vascular sprouting, ultimately facilitating reperfusion and cardiac repair.

In parallel, I investigated *SERPINE1* in the same datasets due to the known co-regulatory role with *ANXA2* in fibrinolysis. SERPINE1, a major inhibitor of fibrinolysis, suppresses tPA- and uPA-mediated plasmin generation, shifting towards a

hypofibrinolytic, pro-thrombotic state (Sillen and Declerck, 2020). In my analysis of the Kuppe dataset, *SERPINE1* was among the most highly upregulated gene across all cell types in the ischaemic zone of acute MI, with pronounced expression in ECs (**Figure 6**). Its absence during heart development and very low levels in chronic and dilated heart failure (CrescENDO) suggest that *SERPINE1* is not a housekeeping gene with continuous expression, but an acute injury-inducible regulator. Spatial Transcriptomics revealed a mild upregulation of *SERPINE1* at the infarct border zone in acute MI, followed by its reduction in chronic MI (**Figure 5**), suggesting *SERPINE1* may be transiently induced during the early phase of injury, potentially acting to maintain blood clots, limit excessive fibrinolysis, prevent uncontrolled matrix degradation and promote scar stabilisation in the injury area (Morange et al., 2007, Sillen and Declerck, 2021, Yaron et al., 2021). The control of *SERPINE1* expression/activity is critical to repair outcomes and must be temporally regulated. As deficient or elevated levels of SERPINE1 could result in healing anomalies including excessive bleeding, thrombosis, fibrosis and impaired wound resolution (Simone et al., 2014).

The findings from the zebrafish dataset (Ma et al., 2021) closely mirrored my results obtained from CrescENDO and the Kuppe human acute MI sc(n)RNA-seq datasets, which provided additional evidence for the evolutionary conservation of my target genes. In regenerating zebrafish hearts, *anxa2a* (the ANXA2 paralogue) was strongly induced in ECs at 2 dpi and peaked at 14 dpi (**Figure 7**), suggesting it may be a late response gene that became upregulated during the window of peak vascular sprouting and maturation (Ross Stewart et al., 2021). By contrast, *anxa2b* remained minimally expressed across all time points, indicating *anxa2a* as the main paralogue engaged in vascular repair during zebrafish heart regeneration (**Figure 7**).

Similarly, *serpine1* expression was markedly upregulated at 2 dpi and peaked at 7 dpi, presenting itself as an early injury-response gene (**Figure 7**). This aligns with previous zebrafish studies showing *serpine1* was absent in the uninjured adult heart but strongly upregulated in the wound endocardium shortly after injury, with expression declining at later stages (Münch et al., 2017). Functionally, *SERPINE1* has been reported to stabilise ECM during the early regenerative phase and serve as a critical regulator for organising coronary growth (Sun et al., 2023). The temporal enrichment of *anxa2a* and *serpine1* in ECs during the peak regenerative phase in zebrafish reinforce their relevance as candidate genes for promoting vascular regeneration.

A key strength of this work includes the multi-omics approach combining sc(n)RNA-seq and spatial transcriptomics across human, mouse, and zebrafish datasets. This approach enabled high-resolution mapping of candidate gene expression, spatial localisation within the heart, and evolutionary validation of conserved injury responses. Such cross-validation strengthens confidence that *ANXA2* and *SERPINE1* are biologically relevant endothelial regulators rather than dataset-specific artefacts.

However, several limitations should be acknowledged. The zebrafish dataset included only seven samples, with two biological replicates per time point and a single heart at 14 dpi, which may reduce statistical power and limit generalisability. Additionally, the discrete time points examined in zebrafish (2, 7, and 14 dpi) and mouse (1, 3, 7 and 28 days post-MI) provide only snapshots of gene expression and cellular activity. This may miss transient or short-lived injury-response genes, potentially underestimating their contribution to repair or endothelial modulation. Higher temporal resolution, combined with live imaging or single-cell transcriptomics at shorter intervals, would better capture the kinetics of injury-induced gene expression.

While sc(n)RNA-seq and spatial transcriptomics reveal transcript-level changes, they do not directly confirm protein expression, localisation, or functional relevance. Post-transcriptional regulation, translation efficiency, and post-translational modifications may influence *ANXA2*, *SERPINE1*, and other candidate genes. Complementary proteomics, immunostaining, and functional assays are therefore necessary to validate whether transcript changes translate into biological effects.

Finally, although transcriptomic correlations strongly implicate *ANXA2* and *SERPINE1* in endothelial injury responses, causality has not been established. Future studies using CRISPR/Cas9-mediated *anxa2a/b* knockout or pharmacological inhibition of *SERPINE1* will be required to define their functional roles in neovascularisation and cardiac regeneration in zebrafish and mammalian models. Mechanistic studies examining downstream signalling pathways, ECM interactions, and crosstalk with inflammatory and fibroblast populations, as well as combinatorial interventions targeting both *ANXA2* and *SERPINE1*, may help optimise the balance between angiogenesis, proteolytic activity, and scar stabilisation.

Taken together, my findings suggest that *ANXA2* and *SERPINE1* may form a regulatory axis that coordinates fibrinolysis, ECM turnover, fibrin clearance, and angiogenesis after MI. *ANXA2* promotes a proteolytic, pro-angiogenic environment, while *SERPINE1* acts as a counter-regulator to prevent excessive matrix degradation and ensure scar stability. Tight temporal and spatial control of this axis is likely essential for coordinating the extent and duration of neovascularisation and ensuring balanced tissue repair after MI. Disruption of this balance may impair vascular regeneration or lead to pathological fibrosis, highlighting both *ANXA2* and *SERPINE1* as promising therapeutic targets for improving cardiac regeneration while minimising adverse fibrosis.

My informatic transcriptomic analyses identified *ANXA2* as a developmentally expressed gene that is reactivated in the adult heart after injury, suggesting it may play a pivotal role in establishing an angiogenic, regenerative environment for the adult injured mammalian heart. Based on the findings reported in this chapter, *ANXA2* was therefore prioritised for site-directed mutagenesis and functional analysis in zebrafish to investigate its role in angiogenesis and cardiac regeneration.

Chapter 4: Results – Reduced regenerative capacity of *anxa2a/b* zebrafish crispants after cardiac laser injury

4.1 Introduction

The Zebrafish (*Danio rerio*) was first introduced as a genetic model organism in the 1980s (Streisinger et al., 1981), and has since become a powerful and versatile model system used to study cardiac development, disease, and drug discovery. Zebrafish has several unique advantageous features over other mammalian models, including strong genetic and physiological conservation with humans (~70% of human genes have at least one zebrafish orthologue, compared to ~80% shared with mice), high reproductive output, external fertilisation, optical transparency during early development, and ease of genetic manipulation. These characteristics make zebrafish an efficient model for forward and reverse large-scale genetic studies, pharmacological and toxicological screening, and mechanistic investigation of cardiovascular function (Angom and Nakka, 2024, González-Rosa, 2022).

While mice remain the standard mammalian model for cardiovascular research, they have several limitations in their applications. Their basal heart rate and electrophysiological characteristics differ from those of humans, and *in vivo* studies often require invasive imaging or experimental procedures that need animal sacrifice. In addition, generating and maintaining transgenic mouse lines is both time consuming and expensive. Zebrafish, by contrast, offer a cost-effective, high-throughput, and non-invasive alternative for assessing cardiac development and function *in vivo* (Angom and Nakka, 2024).

Structurally, the zebrafish heart shares key components with vertebrate: two chambers (an atrium and a ventricle) operating within a single circulatory loop, with a vascular network of arteries, veins and capillaries, and a lymphatic system. The zebrafish heart is the first organ to develop during embryogenesis. By 24 hours post-fertilisation (hpf), a linear cardiac tube, composed of an inner endocardial and an outer myocardial layer, already shows cardiac contractions (González-Rosa, 2022). The main cell types of this early heart tube are atrial and ventricular cardiomyocytes, and endocardial cells (González-Rosa, 2022). The endocardial cells are a specific type of ECs, and the endocardial cells lining the early heart tube bud from the same *kdrl*$^{+}$*/fli1*$^{+}$ endothelial progenitor cells that give rise to other ECs (Brown et al., 2016, Lawson and Weinstein, 2002, Capon et al., 2022, Gurung et al., 2024).

And by 3-5 days post fertilisation (dpf), the zebrafish heart becomes fully developed, with an inflow tract, atrium, trabeculated ventricle, valves, an outflow tract ending in the bulbus arteriosus, and epicardial covering has formed (Kemmler et al., 2021, Brown et al., 2016). The coronary vessels form several weeks after fertilisation,

originating from endocardial cells at the atrioventricular canal that sprout and grow over the ventricular surface (Harrison et al., 2015). And the cardiac lymphatic vessels develop subsequently during the juvenile and early adulthood stages, using pre-existing coronary arteries as a scaffold to guide their expansion down the ventricle (Harrison et al., 2019, Gancz et al., 2019).

Zebrafish have exceptional cardiac regenerative capacity. Even following surgical removal of up to 20% of the ventricle, zebrafish can achieve complete structural and functional regeneration within 30-60 days post-injury (Poss et al., 2002, Ross Stewart et al., 2021). This regenerative response involves a coordinated interplay between cardiomyocyte proliferation, neovascularisation, and extracellular matrix remodelling, rather than forming permanent scar tissue like mammals. Therefore zebrafish is a valuable model to uncover molecular and cellular mechanisms that could be harnessed to therapeutically improve cardiac repair in humans post-MI (Asnani and Peterson, 2014). Importantly, zebrafish embryos can survive without a functional circulatory system for up to seven days through passive oxygen diffusion. This feature makes zebrafish embryos an ideal model to study severe cardiovascular defects/injury that would otherwise be lethal in other organisms (Bakkers, 2011, González-Rosa, 2022).

Various methods of zebrafish cardiac injury have been developed, including ventricular resection, cryoinjury, genetic ablation, hypoxia/reoxygenation, explant culture, and laser injury (Ross Stewart et al., 2021). Among these, laser ablation in 3-5 dpf zebrafish larvae (after hatching but before reaching the free-feeding stage) has unique advantages over other cardiac injury system. Regeneration in zebrafish embryos can be completed within 2 days post-injury (Matrone et al., 2013, Matrone et al., 2014, Kaveh et al., 2020). Also, laser ablation is a technically precise method to induce controlled cardiac damage, as well as avoiding additional ethical and regulatory burdens under UK Home Office guidelines. When combined with advanced live *in vivo* imaging approaches such as selective plane illumination microscopy (SPIM) (Taylor et al., 2019a), this system enables quantitative tracking of cardiac morphogenesis, cardiac cell dynamics, and reparative in real time (Angom and Nakka, 2024, Bowley et al., 2022).

Before the discovery of the CRISPR-Cas9 system, genome editing in zebrafish mostly relied on Zinc Finger Nucleases (ZFNs) and Transcription Activator-Like Effector Nucleases (TALENs) (Doyon et al., 2008, Huang et al., 2011). While effective, both ZFN and TALEN have several limitations. First, they are more complex, costly, and labour-intensive to design and assemble. Second, they have lower targeting efficiency and are unsuitable for multiplexing (simultaneous targeting of multiple genes at once), with higher risk of off-target cleavage, which may lead to undesirable mutations. In contrast, CRISPR/Cas9 offers a simpler, faster, and more precise system for facilitating targeted mutations, allowing high-throughput screens, multiplexed gene mutagenesis, and modelling of human disease mutations (Mushtaq et al., 2018, Li et al., 2016).

In this chapter, I investigated the role of *ANXA2* in zebrafish embryonic development and cardiac regeneration following laser injury. As previously discussed in chapter 3, *ANXA2* was selected as a lead candidate based on its developmental gene expression and reactivation in the injured/diseased coronary vasculature across zebrafish, mice, and humans. This expression pattern suggests a possible conserved role in endothelial remodelling and repair. Based on the established roles of *ANXA2* in fibrinolysis, cytoskeleton organisation, cell migration and adhesion, and wound healing (Dallacasagrande and Hajjar, 2020, Hajjar, 2015), I hypothesised that the loss of *anxa2a/b* paralogues (representing the human homologue of *ANXA2*) would compromise normal embryonic and cardiovascular development, and impair cardiac regenerative capacity in zebrafish embryos.

To test this hypothesis, the zebrafish paralogues *anxa2a* and *anxa2b* were targeted using CRISPR/Cas9-mediated genome editing to generate F0 crispants in the double-transgenic line Tg(*fli1:eGFP*)^{y1tg} / Tg(*myl7:DsRed2-NLS*)^{f2}), which enables simultaneous visualisation of endothelial and myocardial structures. Crispants were generated by microinjecting pre-assembled AltR CRISPR dgRNA-Cas9 ribonucleoprotein (dgRNP) complexes at the one cell stage. Although allelic mosaicism can occur due to asymmetric editing of zygotic alleles, the use of crispants allow rapid and efficient assessment of gene function in a single generation of zebrafish (Daniel et al., 2023, Delbaere et al., 2020). This approach is ideal for preliminary functional validation, testing proof-of-concept for knockout models, and large-scale genetic analyses before committing to the generation of permanent mutant lines (Keeley et al., 2025, Debaenst et al., 2025).

I first aimed to examine and quantify the embryonic morphological defects and specific cardiovascular abnormalities in *anxa2a/b* crispants. In subsequent experiments, I combined crispant model with high-resolution SPIM imaging and laser-induced cardiac injury at 3 dpf to assess how the loss of *anxa2a/b* affects cardiac repair, endothelial and cardiomyocyte repopulation, and ventricular restoration. Finally, to understand the potential molecular mechanisms underlying the observed phenotypes in *anxa2a/b* crispants, I aimed to analyse transcriptional profiles of key genes involved in fibrinolysis, angiogenesis, and regeneration under both uninjured and injured conditions. By integrating CRISPR/Cas9-mediated gene disruption with live *in vivo* imaging and transcriptional profiling, this study provides functional and molecular insights into how *anxa2a/b* contributes to cardiac development and repair, and how its loss may disrupt angiogenic and regenerative processes in the larval zebrafish heart.

4.2 CRISPR/Cas9-mediated genome editing of *anxa2a/b* in zebrafish

CRISPR–Cas9-mediated knockdown of the zebrafish paralogues *anxa2a* and *anxa2b* – homologues of human *ANXA2* – was achieved using a pair of dgRNAs per paralogous gene. One-cell stage Tg(*fli1:eGFP*)^{y1tg} / Tg(*myl7:DsRed2-NLS*)^{f2}) embryos were microinjected with AltR CRISPR dgRNA-Cas9 ribonucleoprotein (dgRNP) complexes. Uninjected and cas9-only embryos served as controls.

Genomic DNA was isolated from zebrafish larvae, and mutagenesis was confirmed by T7 Endonuclease I (T7E1) assay. Primers spanning different exons of *anxa2a* and *anxa2b* were used to amplify target regions, and CRISPR–Cas9-induced mutations were detected by T7E1-mediated cleavage of mismatched heteroduplexes, generating band fragments. Clear changes in banding pattern were observed in *anxa2a/b* knockdown samples compared with uninjected controls (**Figure 8**).

At 3 dpf, brightfield imaging was used to assess developmental morphology across *anxa2ab* crispants, uninjected controls, and Cas9-only controls. Both control groups developed normally without visible abnormalities. In contrast, *anxa2a/b* crispants displayed a range of developmental defects and were categorised as mild, moderate, or severe. ***Table 16*** describes the criteria used to classify distinct phenotypes of crispants. **Table 17** shows the proportion of larvae in each phenotypic group. Mild crispants developed mostly normally but exhibited slightly reduced body length and smaller eye diameter; moderate phenotypes displayed bent or curled tails, pericardial oedema, and further size reductions; while severe crispants had extensive malformations, such as failed hatching, loss of craniofacial structures, complete absence of the tail, and severe body malformations.

To validate gene silencing, mRNA was extracted from pools of 5 dpf embryos (between 20-30 per group) for RT-qPCR analysis. *anxa2a/b* crispants were analysed both as a combined group (all phenotypes) and as separate pools based on phenotypic severity (mild, moderate, severe). Relative quantification values (RQ; $2^{-\Delta\Delta Ct}$) were $\log_2$-transformed, normalised to the housekeeping gene (*b2m* and *rply7*). Log_2 transformation of RQ was used for symmetric comparison, where a Log_2 fold change of 1 means a twofold increase, while a log2 fold change of -1 represents a twofold reduction.

In the combined crispants group, expression of both *anxa2a* and *anxa2b* was significantly reduced compared to uninjected controls (Log_2 fold change in *anxa2a* expression = -0.58 ± 0.23 versus $8.66e^{-12}$ ± 0.10, $P < 0.0001$; Log_2 fold change in *anxa2b* expression = -0.96 ± 0.56 versus $-1.77e^{-12}$± 0.17, $P < 0.0001$, ordinary one-way ANOVA with multiple comparisons). Cas9-only controls showed no change in expression for both genes compared to uninjected controls (Log_2 fold change in *anxa2a* expression = 0.03 ± 0.35 versus $8.66e^{-12}$ ± 0.10, $P > 0.9999$; Log_2 fold change in *anxa2b* expression = -0.06 ± 0.21 versus $-1.77e^{-12}$± 0.17, $P = 0.9994$; ordinary one-

way ANOVA with multiple comparisons). Both control groups developed normally without visible abnormalities (**Figure 8**).

Phenotype-specific analysis confirmed consistent gene suppression across all severity groups. Mild crispants exhibited reduced *anxa2a/b* expressions compared to uninjected control (Log_2 fold change in *anxa2a* expression = -0.99 ± 0.30 versus $8.66e^{-12}$ ± 0.10, P < 0.0001; Log_2 fold change in *anxa2b* expression = -0.64 ± 0.38 versus $-1.77e^{-12}$± 0.17, P = 0.0201, ordinary one-way ANOVA with multiple comparisons). Moderate crispants showed decreased *anxa2a*/b expressions compared to uninjected control (Log_2 fold change in *anxa2a* expression = -0.73 ± 0.05 versus $8.66e^{-12}$ ± 0.10, P = 0.0004; Log_2 fold change in *anxa2b* expression = -1.60 ± 0.16 versus $-1.77e^{-12}$± 0.17, P < 0.0001, ordinary one-way ANOVA with multiple comparisons). Severe crispants similarly displayed lower *anxa2a/b* expressions compared to uninjected control (Log_2 fold change in *anxa2a* expression = -1.03 ± 0.46 versus $8.66e^{-12}$ ± 0.10, P < 0.0001; Log_2 fold change in *anxa2b* expression = -1.22 ± 0.20 versus $-1.77e^{-12}$± 0.17, P = 0.001, ordinary one-way ANOVA with multiple comparisons) (**Figure 8**).

Table 16. Classification criteria for analysis of the gross developmental phenotype in anxa2a/b zebrafish crispants.

Category	Normal	Mild	Moderate	Severe
Features	Normal development with no abnormality	Slightly shorter body length Slightly small eyes Noninflated swim bladder (at 5dpf)	Short body length Curved body/tail Small eyes Underdeveloped head Pericardial oedema Small/noninflated swim bladder (at 5dpf)	Unhatched/chorion Shorter body length Curved body/tail Smaller/lack of eyes Underdeveloped head Larger pericardial oedema Yolk sack oedema (at 5dpf) Smaller/noninflated swim bladder (at 5dpf)

Table 17. The proportion of zebrafish larvae in each phenotypic category (normal, mild, moderate, severe, and dead) at 3 and 5 days post-fertilisation (dpf).

	Group	% normal	% mild	% moderate	% severe	% dead
3 dpf	Uninjected control	95.49 *(n=339)*	/	4.51 (n=16)	/	/
	Cas9-only controls	90.00 *(n=108)*	/	5.83 *(n=7)*	4.17 (n=5)	
	anxa2a/b crispants	/	51.44 *(n=143)*	26.98 *(n=75)*	19.78 *(n=55)*	1.8 *(n=5)*
5 dpf	Uninjected control	95.49 *(n=339)*	/	4.51 (n=16)	/	/
	Cas9-only controls	90.00 *(n=108)*	/	5.83 *(n=7)*	4.17 (n=5)	
	anxa2a/b crispants	/	45.32 *(n=126)*	23.74 *(n=66)*	21.22 *(n=59)*	9.71 *(n=27)*

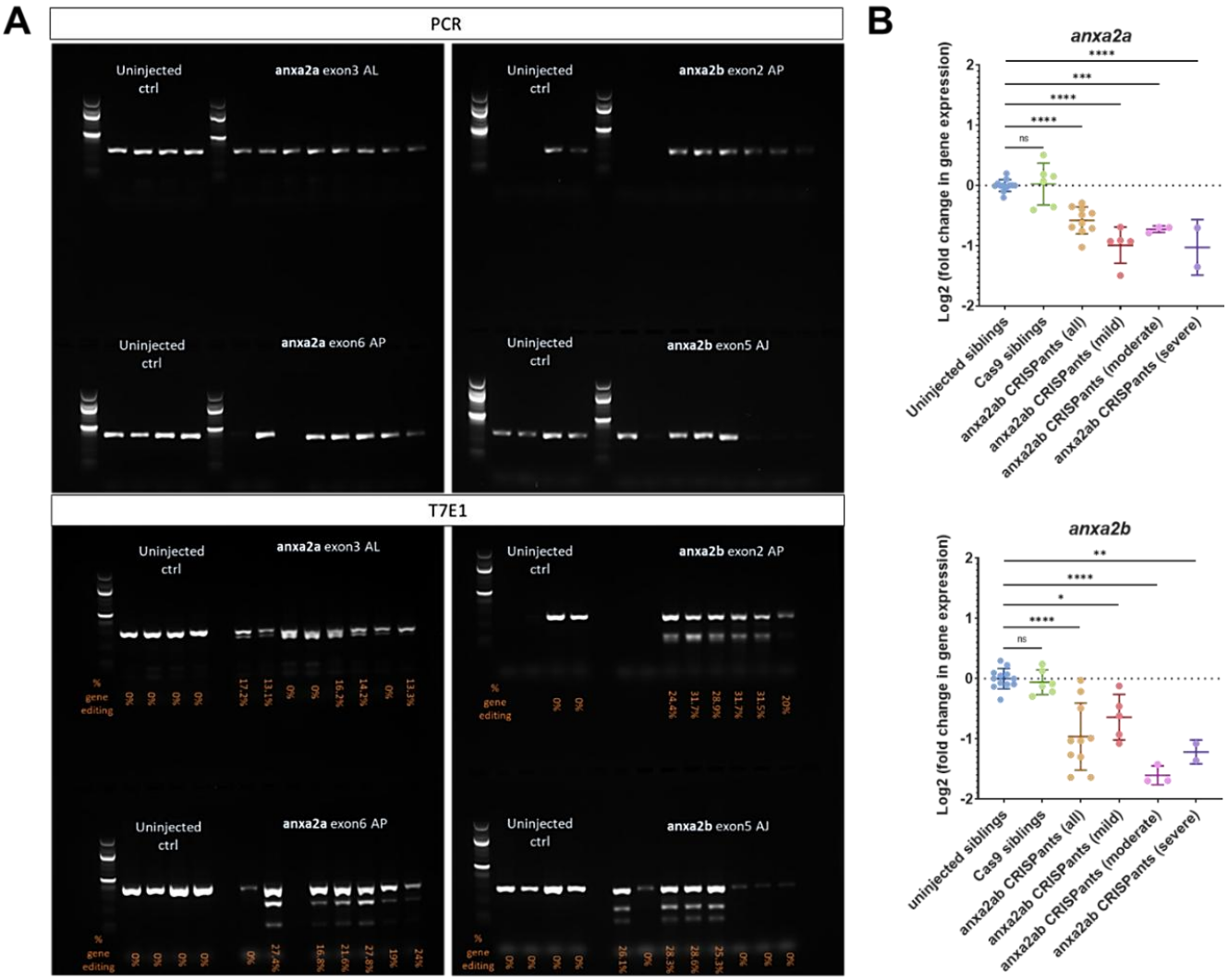

Figure 8. Generation of anxa2a/b knockdown in zebrafish using Alt-R CRISPR-Cas9 method. *(A) Electrophoresis gel showing PCR amplification product (top panel), and digested T7E1 products (bottom panel) from individual larvae – showing successful mutation (indicated by band fragments) of anxa2a and anxa2b. (B) Validation of anxa2a and anxa2b knockdown at the mRNA level via qPCR. Log2(fold change) relative to uninjected siblings. Scatter plots show mean with standard deviation, points = 20-30 pooled larva. Cas9 only controls showed no difference compared to uninjected controls. anxa2a/b crispants (all) included all phenotype groups and showed a significant downregulation at the mRNA level compared to uninjected siblings. anxa2a/b crispants with mild, moderate, severe phenotype all showed reduced anxa2a and anxa2b expressions compared to uninjected control. Only selected comparisons are shown on the graph for clarity; a full list of p-values is provided in* ***Table 18*** *and* ***Table 19****.*

Table 18. Summary of one-way ANOVA with multiple comparisons for anxa2a qPCR validation data (related to Figure 8).

anxa2a One-way ANOVA with multiple comparisons test	Mean Diff.	95.00% CI of diff.	Significant?	Adjusted P Value
Uninjected siblings vs. Cas9 siblings	-0.02546	-0.3786 to 0.3277	ns	>0.9999
Uninjected siblings vs. anxa2a/b crispants (all)	0.5791	0.2766 to 0.8815	****	<0.0001
Uninjected siblings vs. anxa2a/b crispants (mild)	0.9916	0.6157 to 1.368	****	<0.0001
Uninjected siblings vs. anxa2a/b crispants (moderate)	0.7257	0.2698 to 1.182	***	0.0004
Uninjected siblings vs. anxa2a/b crispants (severe)	1.028	0.4884 to 1.567	****	<0.0001
Cas9 siblings vs. anxa2a/b crispants (all)	0.6046	0.2398 to 0.9693	***	0.0003
Cas9 siblings vs. anxa2a/b crispants (mild)	1.017	0.5894 to 1.445	****	<0.0001
Cas9 siblings vs. anxa2a/b crispants (moderate)	0.7512	0.2517 to 1.251	***	0.0009
Cas9 siblings vs. anxa2a/b crispants (severe)	1.053	0.4766 to 1.630	****	<0.0001
anxa2a/b crispants (all) vs. anxa2a/b crispants (mild)	0.4126	0.02567 to 0.7994	*	0.0312
anxa2a/b crispants (all) vs. anxa2a/b crispants (moderate)	0.1466	-0.3183 to 0.6116	ns	0.9285
anxa2a/b crispants (all) vs. anxa2a/b crispants (severe)	0.4488	-0.09833	ns	0.1589

		to 0.9960		
anxa2a/b crispants (mild) vs. anxa2a/b crispants (moderate)	-0.2659	-0.7818 to 0.2499	ns	0.6286
anxa2a/b crispants (mild) vs. anxa2a/b crispants (severe)	0.03626	-0.5547 to 0.6272	ns	>0.9999
anxa2a/b crispants (moderate) vs. anxa2a/b crispants (severe)	0.3022	-0.3426 to 0.9470	ns	0.7152

Table 19. Summary of one-way ANOVA with multiple comparisons for anxa2b qPCR validation data (related to Figure 8).

anxa2b **One-way ANOVA with multiple comparisons test**	**Mean Diff.**	**95.00% CI of diff.**	**Significant?**	**Adjusted P Value**
uninjected siblings vs. Cas9 siblings	0.05877	-0.4753 to 0.5929	ns	0.9994
uninjected siblings vs. anxa2a/b CRISPants (all)	0.9622	0.5049 to 1.420	****	<0.0001
uninjected siblings vs. anxa2a/b crispants (mild)	0.6398	0.07126 to 1.208	*	0.0201
uninjected siblings vs. anxa2a/b crispants (moderate)	1.604	0.9146 to 2.294	****	<0.0001
uninjected siblings vs. anxa2a/b crispants (severe)	1.217	0.4016 to 2.033	**	0.001
Cas9 siblings vs. anxa2a/b crispants (all)	0.9035	0.3519 to 1.455	***	0.0003

Cas9 siblings vs. anxa2a/b crispants (mild)	0.5811	-0.06574 to 1.228	ns	0.0986
Cas9 siblings vs. anxa2a/b crispants (moderate)	1.545	0.7900 to 2.301	****	<0.0001
Cas9 siblings vs. anxa2a/b crispants (severe)	1.159	0.2865 to 2.031	**	0.0041
anxa2a/b CRISPants (all) vs. anxa2a/b crispants (mild)	-0.3224	-0.9075 to 0.2627	ns	0.561
anxa2a/b CRISPants (all) vs. anxa2a/b crispants (moderate)	0.6419	-0.06132 to 1.345	ns	0.0899
anxa2a/b CRISPants (all) vs. anxa2a/b crispants (severe)	0.2552	-0.5722 to 1.083	ns	0.9345
anxa2a/b crispants (mild) vs. anxa2a/b crispants (moderate)	0.9643	0.1842 to 1.744	**	0.0085
anxa2a/b crispants (mild) vs. anxa2a/b crispants (severe)	0.5776	-0.3161 to 1.471	ns	0.3878
anxa2a/b crispants (moderate) vs. anxa2a/b crispants (severe)	-0.3867	-1.362 to 0.5885	ns	0.833

4.3 *anxa2a/b* knockdown impaired embryonic and cardiovascular development

Quantitative analysis at 3 dpf confirmed these observations. Compared with uninjected control, mild crispants showed significantly shorter body length (body length (mm) = 9.67 ± 1.08 *versus* 10.70 ± 0.41, P < 0.0001, ordinary one-way ANOVA with multiple comparisons) and smaller eyes (eye diameter (mm) = 0.75 ± 0.18 *versus* 0.93 ± 0.04, P < 0.0001, ordinary one-way ANOVA with multiple comparisons) (**Figure 9**). Moderate crispants displayed further reductions in body length (body length (mm) = 7.73 ± 1.78 *versus* 10.70 ± 0.41, P < 0.0001) and eye size (eye diameter (mm) = 0.58 ± 0.16 *versus* 0.93 ± 0.04, P<0.0001). While severe crispants exhibited most marked reductions for both (body length (mm) = 5.96 ± 1.24 *versus* 10.70 ± 0.41, P < 0.0001; eye diameter (mm) = 0.54 ± 0.25 *versus* 0.93 ± 0.04, P < 0.0001; ordinary one-way ANOVA with multiple comparisons).

No significant differences were observed between uninjected and Cas9-only controls for both body length and eye diameter. Compared with Cas9-only control, mild crispants showed no significant difference in body length, but had significantly smaller eyes (eye diameter (mm) = 0.75 ± 0.18 versus 0.91 ± 0.04, P < 0.0001, ordinary one-way ANOVA with multiple comparisons). Moderate crispants were significantly shorter (body length (mm) = 7.73 ± 1.78 versus 10.34 ± 0.20, P < 0.0001) with smaller eyes (eye diameter (mm) = 0.58 ± 0.16 *versus* 0.91 ± 0.04, P<0.0001), compared to Cas9-only control. Similarly, severe crispants showed the most pronounced differences for both parameters compared to Cas9-only control (body length (mm) = 5.96 ± 1.24 versus 10.34 ± 0.20, P < 0.0001; eye diameter (mm) = 0.54 ± 0.25 versus 0.91 ± 0.04, P < 0.0001) (**Table 20**, **Table 21**).

By 5 dpf, additional developmental defects became evident. Mild crispants displayed uninflated swim bladders, in contrast to the fully inflated swim bladders observed in both control groups. Moderate and severe crispants developed worsening yolk sac and pericardial oedema, with no improvement in craniofacial or posterior structures (**Figure 9**). These findings indicate that *anxa2a/b* is required for normal zebrafish embryonic development.

Vascular development was assessed at 3 dpf using fluorescent stereomicroscopy. Controls displayed normal, well-organised vasculature, while mild crispants showed disorganised vessel patterning, thinning or loss of intersegmental vessels (ISVs), and reduced formation of parachordal vessels (PAVs) – developing lymphangioblasts – in the trunk. Quantification revealed significantly fewer complete ISVs (number of complete ISVs = 23.31 ± 3.05 *versus* 27.83 ± 1.36 *versus* 26.96 ± 1.54, P < 0.0001) and PAVs (number of parachordal vessels = 7.60 ± 4.40 *versus* 15.26 ± 7.25 *versus* 15.64 ± 4.91, P < 0.0001, ordinary one-way ANOVA with multiple comparisons) in mild crispants compared with uninjected and Cas9-only controls (**Figure 10**). Moderate and severe crispants exhibited more extensive vascular disruption; however, quantification

in these groups was limited by pronounced spinal curvature and severe body malformations.

In addition to vascular defects, mild *anxa2a/b* crispants exhibited impairments in cardiovascular development by 5 dpf. This was assessed in double transgenic Tg(*fli1:eGFP*)^{y1tg} / Tg(*myl7:DsRed2-NLS*)^{f2} larvae, where endothelial and endocardial cells were labelled with green fluorescence and cardiomyocyte nuclei with red fluorescence, enabling simultaneous visualisation of vascular and myocardial structures.

Zebrafish larvae were imaged *via* SPIM at 3 dpf, 4 and 5 dpf. SPIM z-stacks of the ventricles were reconstructed in Imaris to generate 3D surface renderings for quantitative analysis of cardiac development. This allowed precise measurement of diastolic ventricular volume and semi-automated counting of GFP^+ endothelial/endocardial cells and $DsRed^+$ cardiomyocytes. By 5 dpf, mild crispants exhibited a decline in cardiac endothelial cell number (GFP^+ endothelial cell counts = 86.81 ± 13.13 *versus* 99.00 ± 12.66, P = 0.049, two-way ANOVA with multiple comparisons) and diastolic ventricular volume (diastolic endocardial volume of ventricle (μm^3) = $8.60e^6$ ± $2.00e^6$ *versus* $1.17e^7$ ± $3.38e^6$, P = 0.0006) compared with uninjected siblings (**Figure 11**). Cardiomyocyte counts did not show a statistically significant change at this stage.

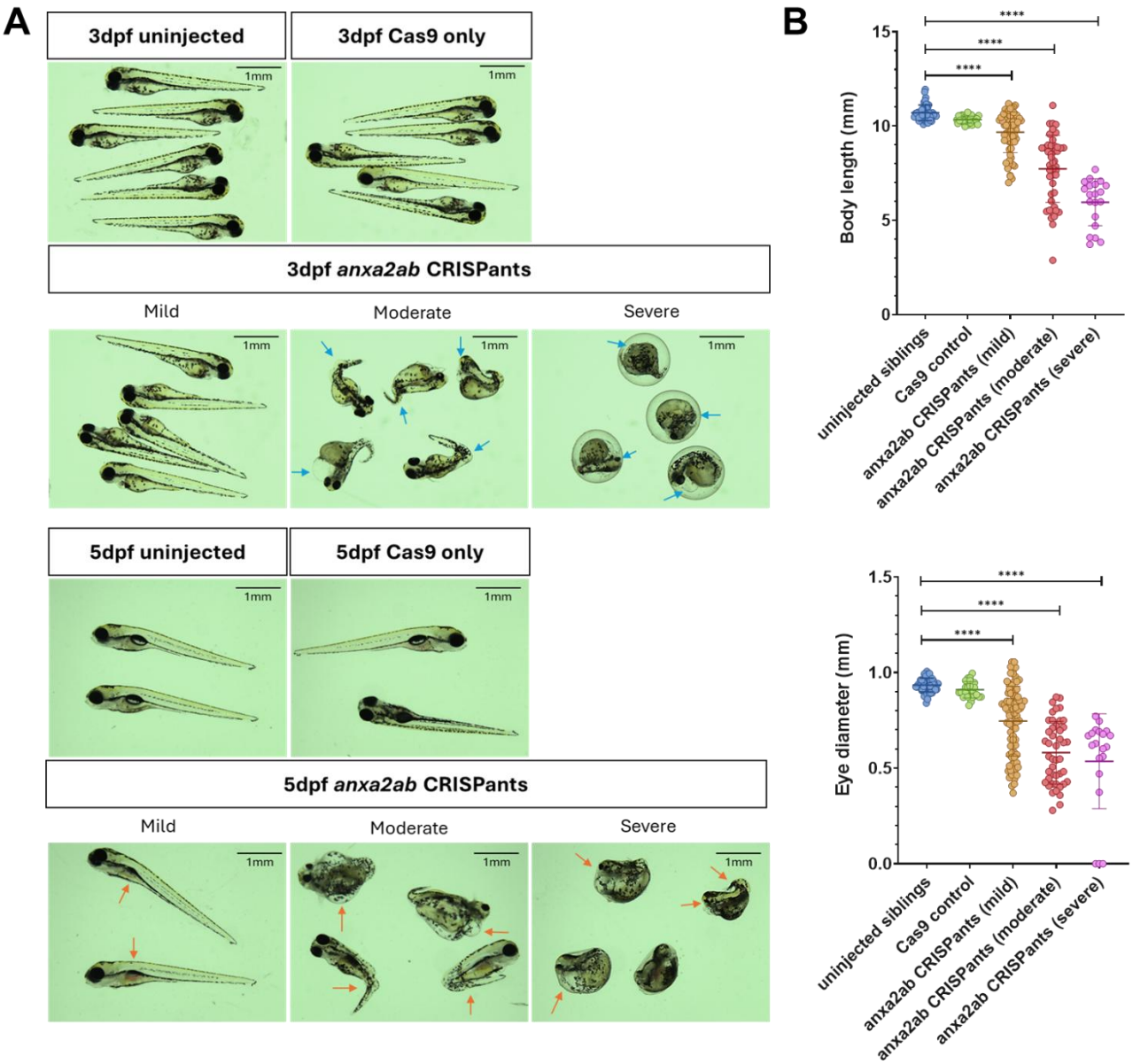

Figure 9. anxa2a/b crispants showed impaired embryonic development at 3 and 5 days post-fertilisation (dpf). *(A) Brightfield images showing the developmental growth of anxa2a/b crispants compared to uninjected and Cas9 only controls at 3 and 5 dpf. There was no phenotypic difference between the two control groups. At 3 dpf, crispants were grouped into 3 categories based on the severity of the developmental defect: mild (mostly normal), moderate (bent/curved tail, small eyes, small head, pericardial oedema), and severe (unhatched, full body malformation, missing tail, small eyes, and pericardial oedema) – indicated by blue arrows. At 5 dpf, crispants with mild phenotype had malformation in the swim bladder (uninflated), moderate and severe phenotypes exhibited yolk sac and pericardial oedema, bent/missing tail, small eyes, and head – indicated by orange arrows. Severe CRISPants were nonviable beyond 5 dpf. (B) Body length and eye diameter were quantified at 3dpf. Each datapoint represents individual larval zebrafish (n = 20-69); experimental repeat = 4. anxa2a/b crispants had smaller eyes and shorter body length compared to uninjected siblings. Cas9 only control showed no difference compared to uninjected control. Only selected comparisons are shown on the graph for clarity. Only selected comparisons*

are shown on the graph for clarity; a full list of p-values is provided in ***Table 20*** *and* ***Table 21Error! Reference source not found.****.*

Table 20. Summary of one-way ANOVA with multiple comparisons for body length quantitative data (related to Figure 9).

Body length (mm) One-way ANOVA with multiple comparisons test	Mean Diff.	95.00% CI of diff.	Significant?	Adjusted P Value
uninjected siblings vs. Cas9 control	0.365	-0.4023 to 1.132	ns	0.6855
uninjected siblings vs. anxa2a/b crispants (mild)	1.031	0.4344 to 1.628	****	<0.0001
uninjected siblings vs. anxa2a/b crispants (moderate)	2.971	2.314 to 3.628	****	<0.0001
uninjected siblings vs. anxa2a/b crispants (severe)	4.745	3.907 to 5.582	****	<0.0001
Cas9 control vs. anxa2a/b crispants (mild)	0.6662	-0.05057 to 1.383	ns	0.0822
Cas9 control vs. anxa2a/b crispants (moderate)	2.606	1.839 to 3.373	****	<0.0001
Cas9 control vs. anxa2a/b crispants (severe)	4.379	3.453 to 5.306	****	<0.0001
anxa2a/b crispants (mild) vs. anxa2a/b crispants (moderate)	1.94	1.343 to 2.537	****	<0.0001
anxa2a/b crispants (mild) vs. anxa2a/b crispants (severe)	3.713	2.922 to 4.504	****	<0.0001
anxa2a/b crispants (moderate) vs. anxa2a/b crispants (severe)	1.774	0.9365 to 2.611	****	<0.0001

Table 21. Summary of one-way ANOVA with multiple comparisons for eye diameter quantitative data (related to Figure 9).

Eye diameter (mm) One-way ANOVA with multiple comparisons test	Mean Diff.	95.00% CI of diff.	Significant?	Adjusted P Value
uninjected siblings vs. Cas9 control	0.02433	-0.08110 to 0.1298	ns	0.9692
uninjected siblings vs. anxa2a/b crispants (mild)	0.188	0.1084 to 0.2675	****	<0.0001
uninjected siblings vs. anxa2a/b crispants (moderate)	0.3532	0.2629 to 0.4434	****	<0.0001
uninjected siblings vs. anxa2a/b CRISPants (severe)	0.3981	0.2831 to 0.5131	****	<0.0001
Cas9 control vs. anxa2a/b crispants (mild)	0.1636	0.06715 to 0.2601	****	<0.0001
Cas9 control vs. anxa2a/b crispants (moderate)	0.3288	0.2234 to 0.4343	****	<0.0001
Cas9 control vs. anxa2a/b crispants (severe)	0.3738	0.2465 to 0.5011	****	<0.0001
anxa2a/b crispants (mild) vs. anxa2a/b crispants (moderate)	0.1652	0.08563 to 0.2448	****	<0.0001
anxa2a/b crispants (mild) vs. anxa2a/b crispants (severe)	0.2102	0.1033 to 0.3170	****	<0.0001
anxa2a/b crispants (moderate) vs. anxa2a/b crispants (severe)	0.04497	-0.07005 to 0.1600	ns	0.8188

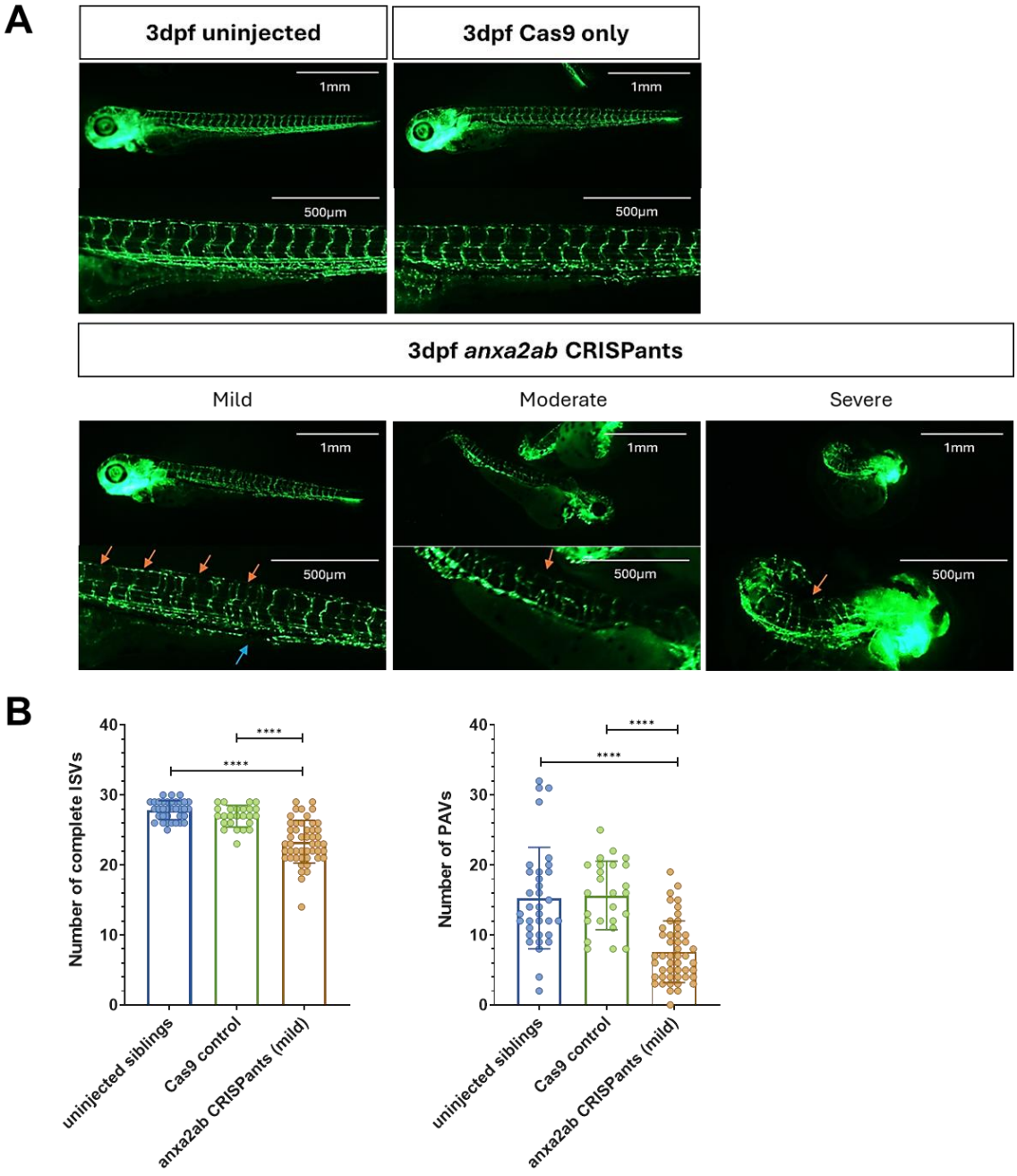

Figure 10. anxa2a/b crispants showed impaired trunk vascular development at 3 days post-fertilisation (dpf). *(A) Representative fluorescent images of Tg(fli1:eGFP)^{y1tg} / Tg(myl7:DsRed2-NLS)^{f2} zebrafish from uninjected control, Cas9 only control and anxa2a/b crispants. Uninjected and Cas9 control showed no vascular abnormality in the trunk. anxa2a/b crispants were categorised into 3 groups based on severity of malformation. anxa2a/b knockdown appeared to impair angiogenesis. Blue arrow indicates defective caudal vein. Orange arrows show disorganised vessel growth with missing/thinning vessels. (B) Vascular development of crispants with a mild phenotype was quantified compared to uninjected and Cas9-only controls. Vascular development was quantified by counting the total number of complete intersegmental vessels (ISVs; segmental blood vessels along the trunk) and parachordal vessels (PAVs; ventral vessels contributing to developing lymphangioblasts). Mild crispants showed reduced numbers of both ISVs and PAVs.*

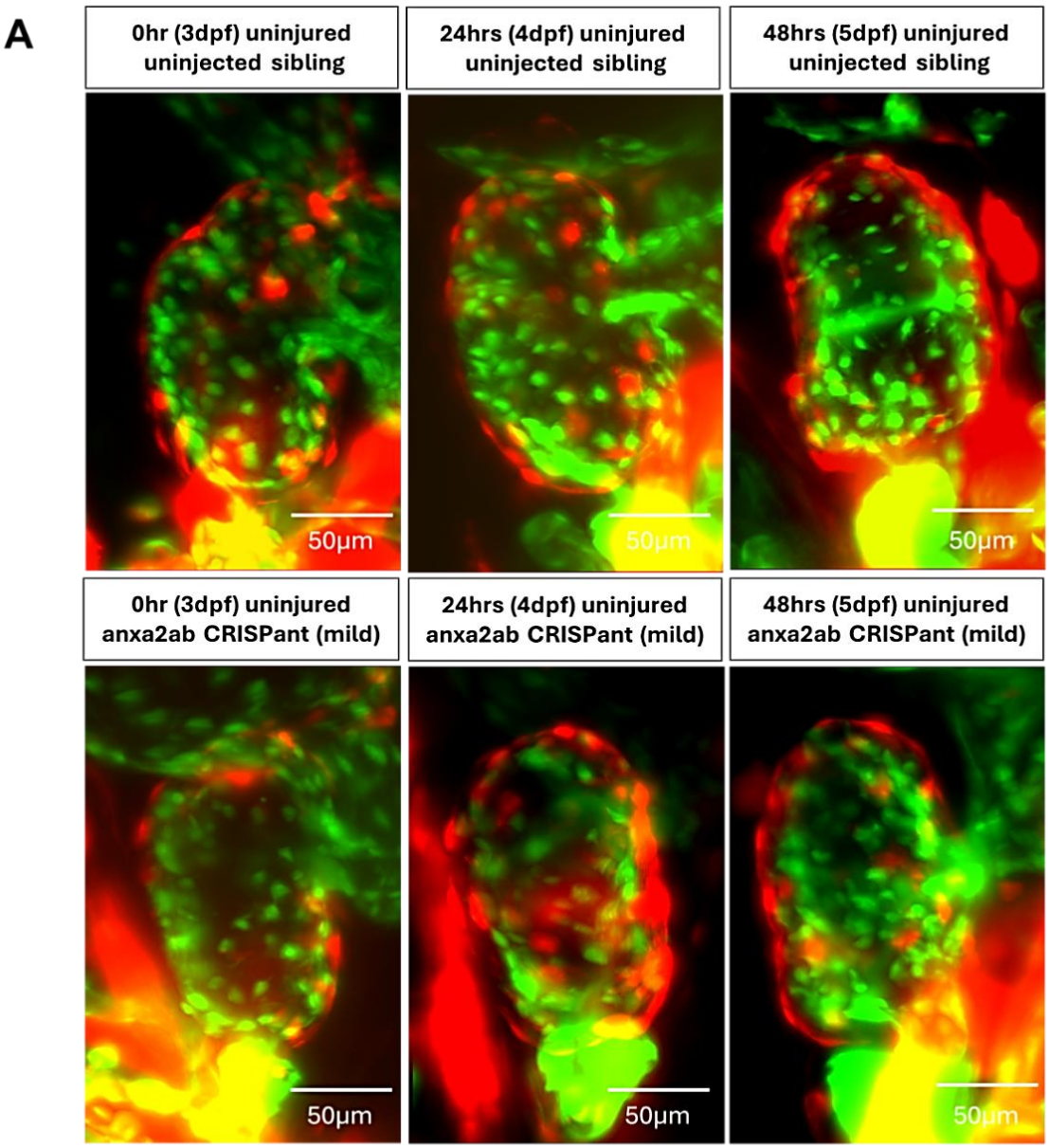
A
0hr (3dpf) uninjured uninjected sibling
24hrs (4dpf) uninjured uninjected sibling
48hrs (5dpf) uninjured uninjected sibling
0hr (3dpf) uninjured anxa2ab CRISPant (mild)
24hrs (4dpf) uninjured anxa2ab CRISPant (mild)
48hrs (5dpf) uninjured anxa2ab CRISPant (mild)
50µm
B
GFP+ endothelial cell counts #
mCherry+ cardiomyocyte counts#
Diastolic endocardial volume of ventricle (um3)
0hr
6hrs
24hrs
48hrs
Uninjured WT siblings
Uninjured anxa2ab CRISPants (mild)

Figure 11. anxa2a/b crispants showed impaired cardiovascular development at 5 days post-fertilisation (at 48 hours timepoint). *(A) Representative fluorescent images of Tg(fli1:eGFP)^{y1tg} / Tg(myl7:DsRed2-NLS)^{f2} zebrafish from uninjured uninjected control and anxa2a/b crispants with mild phenotype. Zebrafish larvae were first imaged when they reached 3 days post-fertilisation (0 hour), then at 24 hours and 48 hours. Green fluorescence = endothelial and endocardial cells. Red fluorescence = cardiomyocytes. (B) SPIM-acquired z-stacks of zebrafish ventricles were 3D surface-rendered via Imaris software to allow quantification of endothelial cell counts, cardiomyocytes counts and ventricular volume. Each datapoint represents individual larval zebrafish (n = 13-16); experimental repeat = 3. At 48 hours, anxa2a/b crispants (mild) showed reduced cardiac endothelial cell numbers and smaller diastolic ventricular volume compared to uninjected controls, indicating impaired cardiovascular development.*

4.4 A larval zebrafish cardiac laser injury and regeneration model

The PALM laser system was used to induce a localised injury at the ventricular apex of anesthetised 3 dpf wild type (WT) larvae (equivalent to uninjected siblings without CRISPR-Cas9-induced mutagenesis). Live cardiac imaging was performed using SPIM to assess structural and functional changes before and after injury. Laser-injured hearts demonstrated decreased ventricular contractility, whereas uninjured controls showed no significant changes in heart rate at any time point.

Quantitative analysis revealed that heart rate decreased significantly at 2 hours post-injury (hpi) compared with baseline (0 hpi) (heart rate in bpm = 159.41 ± 48.40 *versus* 200.74 ± 66.15, P = 0.0003, two-way repeated measures ANOVA with Tukey's multiple comparisons). Heart rate then increased significantly at 24 hpi relative to 2 hpi (heart rate in bpm = 199.05 ± 70.08 *versus*. 159.41 ± 48.40, P = 0.0009) and further increased at 48 hpi compared to 2 hpi (heart rate in bpm = 231.38 ± 63.78 *versus* 159.41 ± 48.40, P < 0.0001) . By 48 hpi, heart rate exceeded baseline (0 hpi) levels (heart rate in bpm = 231.38 ± 63.78 *versus* 200.74 ± 66.15, P = 0.0238). Larvae with a heart rate of 0 (n = 5) were excluded from the analysis (**Figure 12**).

SPIM-acquired z-stacks were surface-rendered and quantified using Imaris software (Bitplane). In healthy uninjured hearts, ECs within the endocardium showed a steady growth between 3 and 5 dpf, as expected (Samsa et al., 2015, Kemmler et al., 2021, Lowe et al., 2021). In contrast, laser injury caused a significant depletion in EC numbers at 2 hpi compared with 0 hpi (GFP^+ endothelial cell counts = 62.00 ± 28.27 *versus* 107.09 ± 29.46, P < 0.0001, two-way repeated measures ANOVA with Tukey's multiple comparisons). By 24 hpi, EC number had recovered to near-baseline levels (GFP^+ endothelial cell counts = 106.95 ± 49.73 *versus* 62.00 ± 28.27, P < 0.0001) and were fully repopulated by 48 hpi (GFP^+ endothelial cell counts = 108.31 ± 34.18 *versus* 62.00 ± 28.27, P < 0.0001) (**Figure 12**).

Quantification of diastolic endocardial ventricular surface volume revealed consistent measurements over time in uninjured WT hearts between 3 and 5 dpf. In contrast, laser-injured hearts exhibited a significant reduction in diastolic ventricular volume at both 2 and 6 hpi compared with baseline (0 hr) (diastolic endocardial volume of ventricle (μm^3) at 2 hpi = $3.02e^6 \pm 2.37e^6$ *versus* $7.29e^6 \pm 5.22e^6$, $P < 0.0001$; diastolic endocardial volume of ventricle (μm^3) at 6 hpi = $2.79e^6 \pm 2.22e^6$ *versus* $7.29e^6 \pm 5.22e^6$, $P = 0.0025$; two-way repeated measures ANOVA with Tukey's multiple comparisons). Ventricular volume then progressively increased during regeneration, with significant recovery evident by 24 hpi and further restoration by 48 hpi, compared to 2 hpi (diastolic endocardial volume of ventricle (μm^3) at 24 hpi = $5.51e^6 \pm 3.12e^6$ *versus* $3.02e^6 \pm 2.37e^6$, $P = 0.0002$; diastolic endocardial volume of ventricle (μm^3) at 48 hpi = $6.39e^6 \pm 3.63e^6$ *versus* 3.02e6 ± 2.37e6, $P < 0.0001$; two-way repeated measures ANOVA with Tukey's multiple comparisons). By 48 hpi, ventricular volume in injured hearts approached levels comparable to uninjured controls, indicating structural recovery of the ventricle following injury (**Figure 12**).

In summary, we established and optimised a larval zebrafish model of cardiac laser injury and regeneration. The injury induced a transient impairment in cardiac function and structure, characterised by reduced heart rate, decreased endothelial cell number, and reduced ventricular volume. All parameters showed substantial recovery by 48 hpi, demonstrating robust regenerative capacity in the larval zebrafish heart.

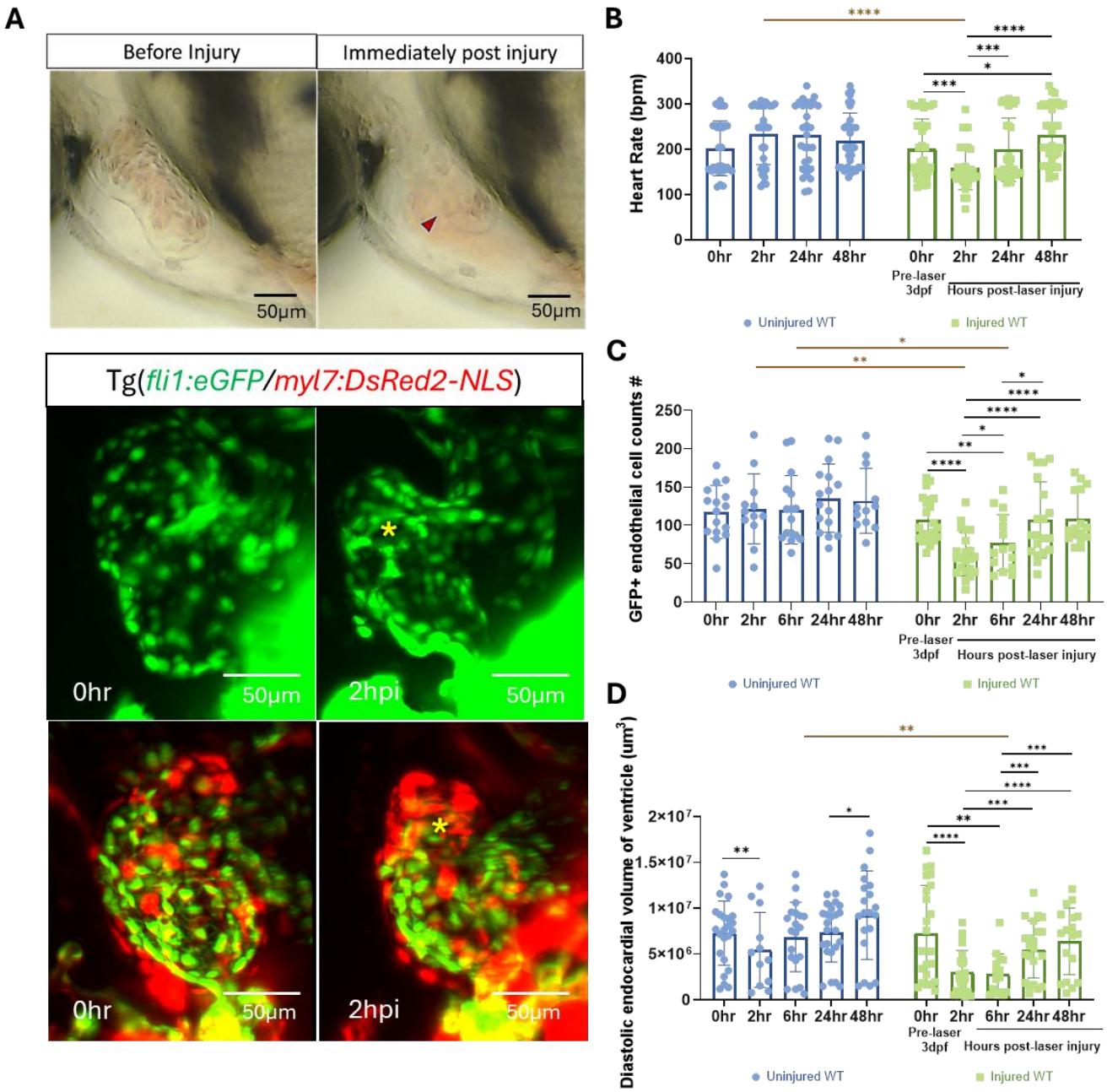

Figure 12. A larval zebrafish model of cardiac injury and regeneration. *(A) Representative brightfield and fluorescent images of Tg(fli1:eGFP)^{y1tg} / Tg(myl7:DsRed2-NLS)^{f2}) transgenic zebrafish, showing ventricles before and after laser injury at 3 days post-fertilisation (dpf). Yellow * indicates the site of laser lesion. Green fluorescence = endothelial and endocardial cells. Red fluorescence = cardiomyocytes. (B) Quantification of heart rate in uninjured and injured wild-type (WT) zebrafish larvae at 0, 2, 24 and 48 hours post-injury (hpi). Laser injury resulted in an immediate reduction in heart rate in WT zebrafish larvae, compared to uninjured controls. Heart rate was significantly decreased at 2 hours post-injury (hpi) relative to baseline (0 hpi), followed by a significant increase at 24 hpi and 48 hpi. Individual animals with heart rate of 0 (n = 5) were excluded from the analysis. Data represent individual larvae (n = 34 – 38 per group). Statistical analysis was performed using two-way repeated measures ANOVA analysis with Tukey's multiple comparisons. (C,D) SPIM-acquired z-stacks of zebrafish ventricles at 0hr, 2hr, 6hr, 24hr and 48hr were 3D*

surface-rendered via Imaris software to allow quantification of cell counts and ventricular volume. Laser injury immediately resulted in a significant reduction in cardiac endothelial cell counts and ventricular volume at 2hpi compared to uninjured controls, followed by recovery by 24 – 48 hpi. Data represent individual larvae (n = 16 – 24 per group). Statistical analysis was performed using two-way repeated measures ANOVA analysis with Tukey's multiple comparisons.

4.5 *anxa2a/b* knockdown impaired regeneration following cardiac laser injury

To determine whether *anxa2a/b* knockdown impaired cardiac regenerative capacity, ventricular laser injuries were performed at 3 dpf in Tg(*fli1:eGFP*)^{y1tg} / Tg(*myl7:DsRed2-NLS*)^{f2}) larvae comprising uninjected WT siblings and *anxa2a/b* crispants (mild and moderate phenotypes). In this transgenic background, endothelial and endocardial cells expressed green fluorescence (GFP), while cardiomyocyte nuclei expressed red fluorescence (mCherry). Longitudinal cardiac imaging at 0, 2, 24, and 48 hours post-injury (hpi) was conducted using SPIM, with z-stacks surface-rendered and quantified in Imaris.

Prior to injury (0 hpi), mild crispants already had reduced cardiomyocyte numbers compared with WT siblings (mCherry$^+$ cardiomyocyte count = 60.50 ± 19.88 *versus* 75.25 ± 18.43, P = 0.0416, two-way repeated measures ANOVA with Tukey's multiple comparisons, n = 24), with no significant difference in endothelial numbers and ventricular size compared to controls (GFP$^+$ endothelial cell counts = 80.88 ± 15.04 *versus* 90.63 ± 11.81, P = 0.0638; diastolic endocardial volume of ventricle (μm^3) = 7.56e^6 ± 1.74e^6 *versus* 8.92e^6 ± 3.03e^6 , P = 0.0958). Moderate crispants showed more severe baseline defects compared with WT siblings, including disrupted ventricular architecture, reduced endothelial and cardiomyocyte counts, and decreased diastolic ventricular volume (n = 24; GFP$^+$ endothelial cell counts = 52.67 ± 16.84 *versus* 84.75 ± 12.59; mCherry$^+$ cardiomyocyte counts = 29.05 ± 14.04 *versus* 60.3 ± 20.39; diastolic endocardial volume of ventricle (μm^3) = 6.57e^6 ± 1.84e^6 *versus* 1.02e^7 ± 3.03e^6; P < 0.0001, two-way repeated measures ANOVA with Tukey's multiple comparisons) (**Figure 13**).

At 2 hpi, the injury was evident in all groups, characterised by ventricular contraction and regional depletion of both ECs and cardiomyocytes. In mild crispants, EC and cardiomyocyte number and ventricular volume were significantly reduced compared to baseline (n = 24; GFP$^+$ endothelial cell counts = 34.67 ± 13.93 *versus* 80.88 ± 15.04; mCherry$^+$ cardiomyocyte counts = 36.29 ± 9.07 *versus* 60.50 ± 19.88; diastolic endocardial volume of ventricle (μm^3) = 3.21e^6 ± 1.26e^6 *versus* 7.56e^6 ± 1.74e^6; P < 0.0001, two-way repeated measures ANOVA with Tukey's multiple comparisons). Moderate crispants also displayed significant losses of ECs, cardiomyocytes and ventricular volume at 2 hpi versus 0 hpi (n = 21; GFP+ endothelial cell counts = 27.57 ± 12.07 *versus* 52.67 ± 16.84; mCherry$^+$ cardiomyocyte counts = 19.95 ± 9.47 *versus*

29.05 ± 14.04; diastolic endocardial volume of ventricle (μm^3) = $3.69e^6$ ± $1.62e^6$ *versus* $6.57e^6$ ± $1.84e^6$; P < 0.0001, two-way ANOVA with Tukey's multiple comparisons) (**Figure 13**).

WT siblings showed rapid regeneration, with full repopulation of ECs and cardiomyocytes and restoration of ventricular morphology by 48 hpi, often exceeding baseline values. In contrast, full regeneration was not achieved in *anxa2a/b* crispants. Although mild crispants exhibited significant improvements between 2 and 48 hpi, regeneration remained delayed and incomplete. At 48 hpi, they still demonstrated partial endothelial and cardiomyocyte repopulation, reduced ventricular volume, and localised contraction at the injury site compared with WT siblings (n = 24; GFP^+ endothelial cell counts = 61.70 ± 21.25 *versus* 89.00 ± 20.11, P = 0.0002; $mCherry^+$ cardiomyocyte count = 56.61 ± 17.03 *versus* 83.25 ± 14.06, P < 0.0001; diastolic endocardial volume of ventricle (μm^3) = $6.19e^6$ ± $2.00e^6$ *versus* $1.03e^7$ ± $2.62e^6$, P < 0.0001; two-way ANOVA with Tukey's multiple comparisons). In moderate crispants, no regeneration was observed between 2 and 48 hpi, with persistently low endothelial and cardiomyocyte counts and ventricular volumes, alongside distorted ventricular morphology and myocardial thinning (n = 21; GFP+ endothelial cell counts = 34.71 ± 19.21 *versus* 76.79 ± 13.01; mCherry+ cardiomyocyte count = 25.29 ± 17.01 *versus* 72.47 ± 13.34; diastolic endocardial volume of ventricle (μm^3) = $4.14e^6$ ± $2.49e^6$ *versus* $8.88e^6$ ± $2.00e^6$; P < 0.0001, two-way ANOVA with Tukey's multiple comparisons) (**Figure 13**).

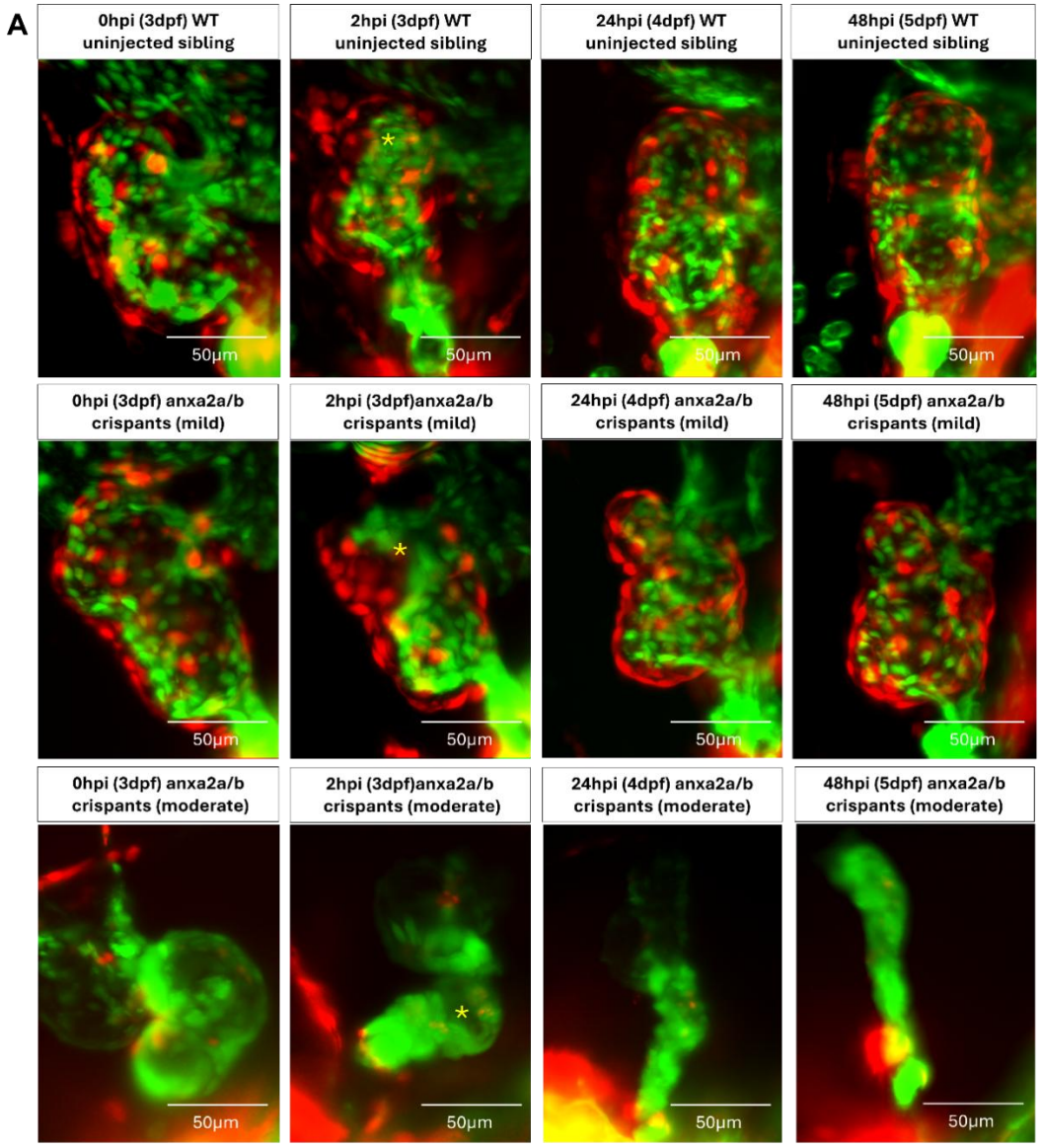
A
0hpi (3dpf) WT uninjected sibling
2hpi (3dpf) WT uninjected sibling
24hpi (4dpf) WT uninjected sibling
48hpi (5dpf) WT uninjected sibling
0hpi (3dpf) anxa2a/b crispants (mild)
2hpi (3dpf)anxa2a/b crispants (mild)
24hpi (4dpf) anxa2a/b crispants (mild)
48hpi (5dpf) anxa2a/b crispants (mild)
0hpi (3dpf) anxa2a/b crispants (moderate)
2hpi (3dpf)anxa2a/b crispants (moderate)
24hpi (4dpf) anxa2a/b crispants (moderate)
48hpi (5dpf) anxa2a/b crispants (moderate)
50µm

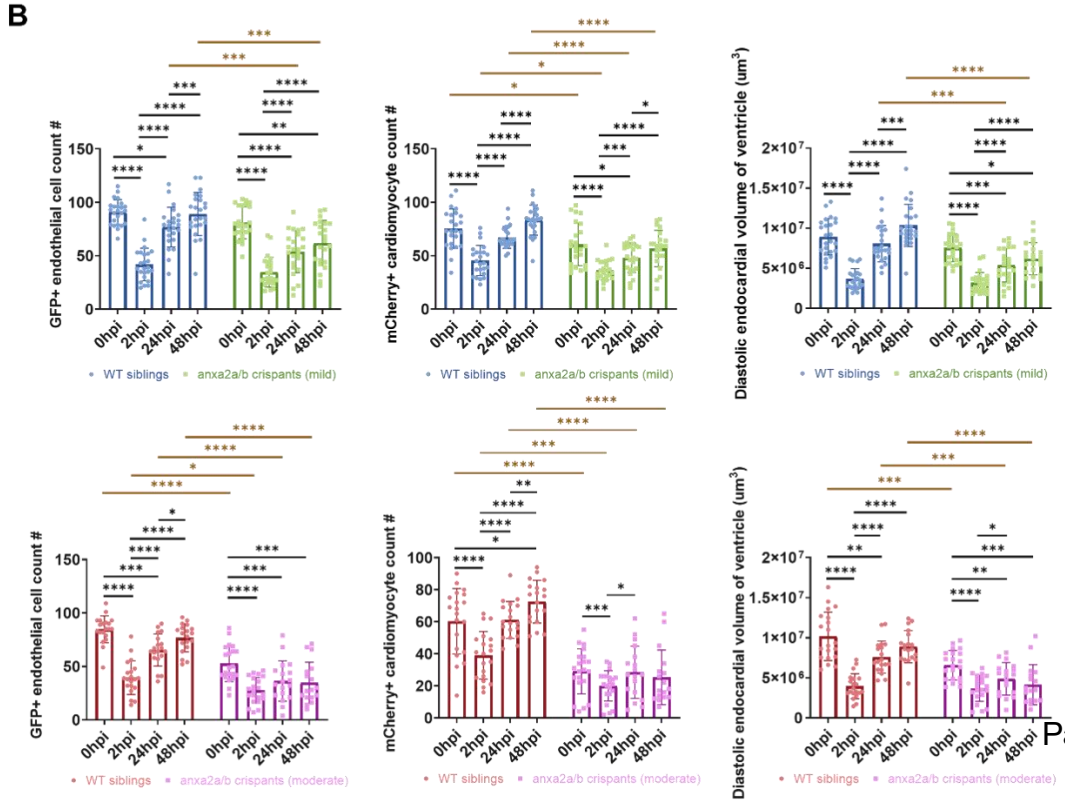
B
GFP+ endothelial cell count #
mCherry+ cardiomyocyte count #
Diastolic endocardial volume of ventricle (um3)
0hpi
2hpi
24hpi
48hpi
WT siblings
anxa2a/b crispants (mild)
anxa2a/b crispants (moderate)

Figure 13. anxa2a/b knockdown impaired cardiac regeneration within the 48-hour regenerative window in larval zebrafish. *(A) Representative brightfield and fluorescent images of Tg(fli1:eGFP)^{y1tg} / Tg(myl7:DsRed2-NLS)^{f2}) transgenic zebrafish ventricles at 0, 2, 24, and 48 hours post-injury (hpi). Endothelial and endocardial cells express GFP (green), and cardiomyocyte nuclei express DsRed2 (red). (B) At 2 hpi, laser injury was evident as a region of endothelial cell loss at the ventricular apex (yellow asterisks). By 48 hpi, anxa2a/b crispants with mild and moderate phenotypes (5 days post-fertilisation) displayed regenerative deficits, including incomplete endothelial repopulation, cardiomyocyte restoration, and ventricular volume recovery. Mild crispants exhibited a persistently shrunken ventricular apex adjacent to the injury site, whereas moderate crispants showed more severe abnormalities, characterised by distorted ventricular morphology and reduced chamber size. Data represent individual larvae (n = 20 – 24 per group). Statistical analysis was performed using two-way repeated measures ANOVA with Tukey's multiple comparisons. A mixed effects analysis (type III) was performed to examine the effect of sample type (WT siblings versus. crispants) and time on all parameters. There was a highly significant interaction between sample type (WT siblings versus. crispants) and timepoint (P < 0.0001). Significant main effects were also observed for sample type (P < 0.0001) and Timepoint (P < 0.0001).*

4.6 Transcriptional alterations in fibrinolytic, angiogenic, and regeneration-associated genes in *anxa2a/b* crispants prior to cardiac injury

To determine whether *anxa2a/b* knockdown affected the basal transcriptional profile of genes involved in fibrinolysis, angiogenesis, and cardiac regeneration in the absence of injury, RT-qPCR was performed on pooled uninjured 5 dpf zebrafish larvae (20–30 per group). The analysed genes included fibrinolytic genes – *s100a10a/b, serpine1, tpa/plat,* plasminogen *(plg);* angiogenic genes – tyrosine kinase with immunoglobulin like and EGF like domains 1 *(tie1), vegfab, cxcr4a, cxcl12b;* and regeneration-associated genes – notch receptor 1 *(notch1a/b), notch2, notch3,* transforming growth factor beta 1 *(tgfb1a),* transforming growth factor beta 2 *(tgfb2).*

Relative quantification values (RQ; $2^{-\Delta\Delta Ct}$) were $\log_2$-transformed and normalised to the housekeeping gene beta-2 microglobulin *(b2m)* and ribosomal protein L7 *(rpl7)*, then compared across uninjected siblings and *anxa2a/b* crispants exhibiting mild or moderate phenotypes. The $\log_2$ transformation enabled symmetric interpretation of expression changes, where a $\log_2$ fold change of +1 indicates a twofold increase, and –1 represents a twofold decrease.

As expected, both mild (Log_2 fold change in *anxa2a* expression = -0.84 ± 0.45 *versus* $8.00e^{-12}$ ± 0.09, P < 0.0001; one-way ANOVA with Tukey's multiple comparisons) and moderate (Log_2 fold change in *anxa2a* expression = -0.85 ± 0.28 *versus* $8.00e^{-12}$ ± 0.09, P < 0.0001) crispants displayed a marked reduction in *anxa2a* transcript levels. Similarly, *anxa2b* expression was significantly suppressed in mild (Log_2 fold change in

anxa2b expression = -0.78 ± 0.47 *versus* -1.63e^{-12} ± 0.09, P < 0.0001) and moderate crispants (Log_2 fold change in *anxa2b* expression = -0.85 ± 0.28 *versus* 8.00e^{-12} ± 0.09, P < 0.0001), validating efficient CRISPR/Cas9-mediated gene disruption. Within the fibrinolytic pathways, expression of *s100a10a* and *s100a10b* (orthologues of mammalian *S100A10*) remained unchanged in mild crispants. In contrast, *s100a10a* was significantly reduced in moderate crispants (Log_2 fold change in *s100a10a* expression = -0.63 ± 0.27 *versus* 6.17e^{-12} ± 0.18, P = 0.0145, one-way ANOVA with Tukey's multiple comparisons), while *s100a10b* expression remained unaffected. Transcript levels of *serpine1* and *plat/tpa* were unaffected by knockdown. By contrast, *plg* expression was significantly reduced in moderate crispants, compared to uninjected siblings (Log_2 fold change in *plg* expression = -0.59 ± 0.28 *versus* 8.46e^{-11} ± 0.33, P = 0.0416) and mild crispants (Log_2 fold change in *plg* expression = -0.59 ± 0.28 *versus* 0.23 ± 0.58, P = 0.0062), suggesting partial disruption of plasminogen availability or plasmin production in crispants with more severe phenotypes (**Figure 14**).

Genes associated with angiogenic signalling were particularly sensitive to *anxa2a/b* deficiency. Expression of *tie1* was significantly downregulated in moderate crispants, compared with uninjected siblings (Log_2 fold change in *tie1* expression = -1.05 ± 0.28 *versus* -2.26e^{-11} ± 0.16, P = 0.0013, one-way ANOVA with Tukey's multiple comparisons). Similarly, *vegfab* was reduced in moderate crispants, compared to both uninjected siblings (Log_2 fold change in *vegfab* expression = -0.62 ± 0.28 *versus* -2.37e^{-11} ± 0.19, P = 0.0121) and mild crispants (Log_2 fold change in *vegfab* expression = -0.62 ± 0.28 *versus* 0.20 ± 0.48, P = 0.0063). In contrast, *cxcr4a* and *cxcl12b* expression remained unchanged, indicating selective impairment of angiogenic pathways. Analysis of regeneration-associated genes revealed no significant changes in *notch1a, notch1b, notch2, notch3*, *tgfb1a* or *tgfb2* (**Figure 14**).

Overall, CRISPR/Cas9-mediated *anxa2a/b* deficiency led to consistent suppression of *anxa2ab* transcripts and downregulation of key angiogenic genes such as *tie1 and vegfab*, indicating that loss of *anxa2a/b* impairs endothelial signalling pathways critical for vessel formation and maintenance, even in the absence of cardiac injury. In parallel, expression reductions were also observed in co-regulatory and fibrinolytic genes, such as *s100a10a* and *plg*, suggesting secondary effects on the plasminogen activation system. This may establish a dysregulated pre-injury environment potentially predisposing to impaired neovascularisation and regenerative responses. The altered angiogenic signalling also supports a broader role for *anxa2a/b* in embryonic and cardiovascular development beyond its known function in fibrinolysis.

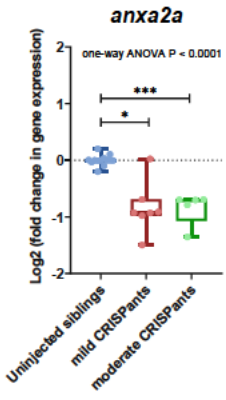
anxa2a
one-way ANOVA P < 0.0001
***
*
Log2 (fold change in gene expression)
2
1
0
-1
-2
Uninjected siblings
mild CRISPants
moderate CRISPants

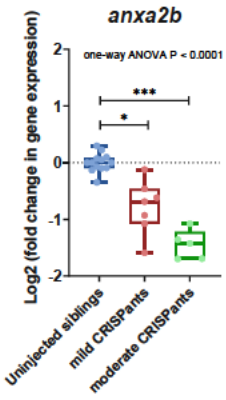
anxa2b
one-way ANOVA P < 0.0001
***
*
Log2 (fold change in gene expression)
2
1
0
-1
-2
Uninjected siblings
mild CRISPants
moderate CRISPants

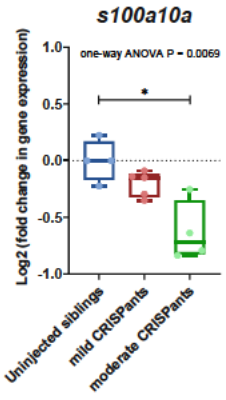
s100a10a
one-way ANOVA P = 0.0069
*
Log2 (fold change in gene expression)
1.0
0.5
0.0
-0.5
-1.0
Uninjected siblings
mild CRISPants
moderate CRISPants

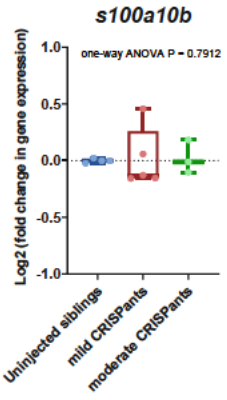
s100a10b
one-way ANOVA P = 0.7912
Log2 (fold change in gene expression)
1.0
0.5
0.0
-0.5
-1.0
Uninjected siblings
mild CRISPants
moderate CRISPants

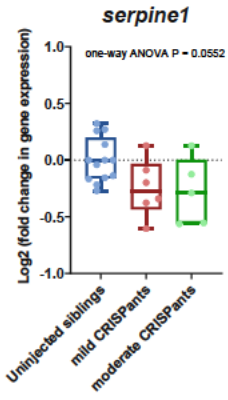
serpine1
one-way ANOVA P = 0.0552
Log2 (fold change in gene expression)
1.0
0.5
0.0
-0.5
-1.0
Uninjected siblings
mild CRISPants
moderate CRISPants

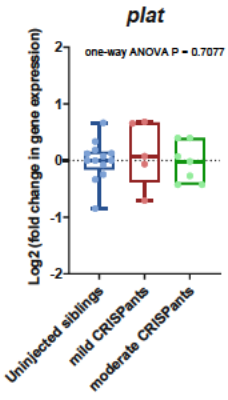
plat
one-way ANOVA P = 0.7077
Log2 (fold change in gene expression)
2
1
0
-1
-2
Uninjected siblings
mild CRISPants
moderate CRISPants

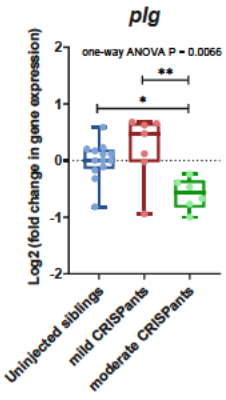
plg
one-way ANOVA P = 0.0066
**
*
Log2 (fold change in gene expression)
2
1
0
-1
-2
Uninjected siblings
mild CRISPants
moderate CRISPants

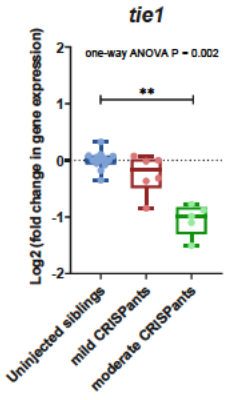
tie1
one-way ANOVA P = 0.002
**
Log2 (fold change in gene expression)
2
1
0
-1
-2
Uninjected siblings
mild CRISPants
moderate CRISPants

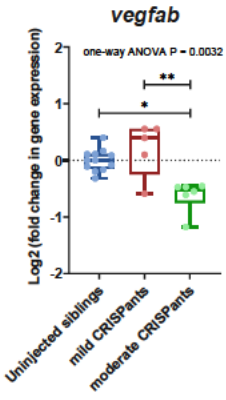
vegfab
one-way ANOVA P = 0.0032
**
*
Log2 (fold change in gene expression)
2
1
0
-1
-2
Uninjected siblings
mild CRISPants
moderate CRISPants

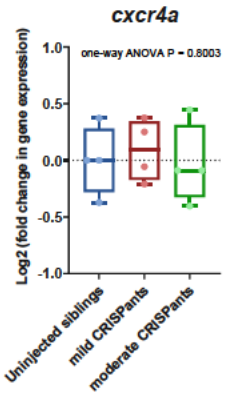
cxcr4a
one-way ANOVA P = 0.8003
Log2 (fold change in gene expression)
1.0
0.5
0.0
-0.5
-1.0
Uninjected siblings
mild CRISPants
moderate CRISPants

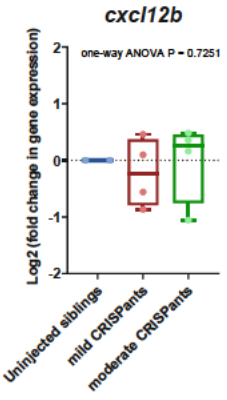
cxcl12b
one-way ANOVA P = 0.7251
Log2 (fold change in gene expression)
2
1
0
-1
-2
Uninjected siblings
mild CRISPants
moderate CRISPants

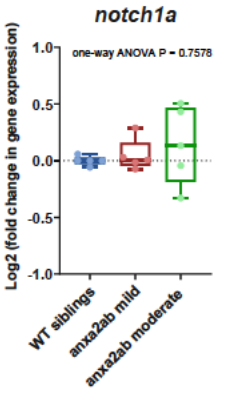
notch1a
one-way ANOVA P = 0.7578
Log2 (fold change in gene expression)
1.0
0.5
0.0
-0.5
-1.0
WT siblings
anxa2ab mild
anxa2ab moderate

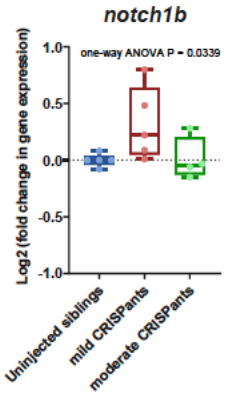
notch1b
one-way ANOVA P = 0.0339
Log2 (fold change in gene expression)
1.0
0.5
0.0
-0.5
-1.0
Uninjected siblings
mild CRISPants
moderate CRISPants

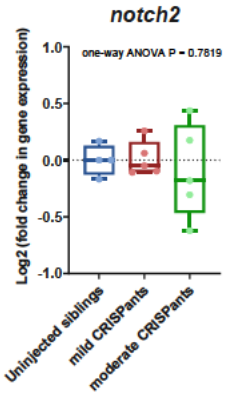
notch2
one-way ANOVA P = 0.7819
Log2 (fold change in gene expression)
1.0
0.5
0.0
-0.5
-1.0
Uninjected siblings
mild CRISPants
moderate CRISPants

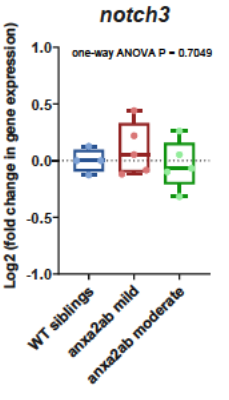
notch3
one-way ANOVA P = 0.7049
Log2 (fold change in gene expression)
1.0
0.5
0.0
-0.5
-1.0
WT siblings
anxa2ab mild
anxa2ab moderate

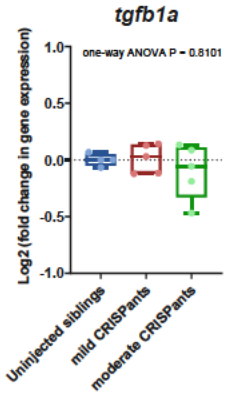
tgfb1a
one-way ANOVA P = 0.8101
Log2 (fold change in gene expression)
1.0
0.5
0.0
-0.5
-1.0
Uninjected siblings
mild CRISPants
moderate CRISPants

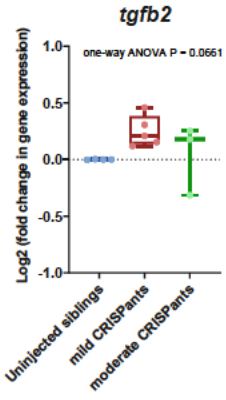
tgfb2
one-way ANOVA P = 0.0661
Log2 (fold change in gene expression)
1.0
0.5
0.0
-0.5
-1.0
Uninjected siblings
mild CRISPants
moderate CRISPants

Figure 14. Relative mRNA expression of fibrinolytic, angiogenic, and regenerative genes in uninjured 5 dpf anxa2a/b crispants. *Box plots display log_2-transformed relative quantification (RQ, 2^–ΔΔCt) of selected genes in uninjected siblings and anxa2a/b crispants with mild or moderate phenotypes, normalised to a housekeeping genes and expressed relative to uninjected controls. Horizontal bars represent medians; boxes represent interquartile ranges (IQR); whiskers extend to minimum and maximum values within 1.5× IQR. Knockdown efficiency was confirmed by significant reductions in anxa2a and anxa2b. Moderate crispants additionally showed decreased expression of s100a10a, plg, tie1, and vegfab, while serpine1, plat/tpa, cxcr4a, cxcl12b, tgfb1a/2, and pabpc1a/b were unchanged across groups. Statistical analysis was performed using one-way ANOVA with Tukey's multiple comparisons.*

4.7 Transcriptional alterations in fibrinolytic, angiogenic, and regeneration-associated genes in *anxa2a/b* crispants following cardiac injury

To evaluate whether the loss of *anxa2a/b* alters transcriptional responses to cardiac injury, RT-qPCR was performed at 48 hpi in uninjected WT siblings and *anxa2a/b* crispants with mild or moderate phenotypes (**Figure 15**).

Consistent with pre-injury findings, *anxa2a* expression was significantly reduced in both injured mild (Log_2 fold change in *anxa2a* expression = -0.70 ± 0.26 *versus.* $4.50e^{-11}$ ± 0.05, P = 0.0003) and moderate crispants (Log_2 fold change in *anxa2a* expression = -1.30 ± 0.35 *versus.* $4.50e^{-11}$ ± 0.05, P < 0.0001, one-way ANOVA with Tukey's multiple comparisons), compared with WT. *anxa2b* was similarly downregulated in both injured mild (Log_2 fold change in *anxa2b* expression = -0.55 ± 0.32 *versus.* 0.11 ± 0.31, P = 0.0290) and moderate crispants (Log_2 fold change in *anxa2b* expression = -1.38 ± 0.51 *versus.* 0.11 ± 0.31, P = 0.0003). Suppression was more pronounced in injured moderate compared to mild crispants for both *anxa2a* (Log_2 fold change in *anxa2a* expression = -1.30 ± 0.35 *versus.* -0.70 ± 0.26, P = 0.0058) and *anxa2b* (Log_2 fold change in *anxa2b* expression = -1.38 ± 0.51 *versus.* -0.55 ± 0.32, P = 0.0230), confirming progressive transcriptional impairment with increasing phenotype severity.

Within the fibrinolytic pathways, expression of *anxa2a/b* co-regulators, *s100a10a* and *s100a10b*, were downregulated in moderate crispants following cardiac injury, while expression of *s100a10a/b* remained unchanged in mild crispants. *s100a10a* was significantly reduced in moderate crispants, compared with WT (Log_2 fold change in *s100a10a* expression = -1.01 ± 0.46 *versus.* $-8.00e^{-11}$ ± 0.23, P = 0.0002) and mild crispants (Log_2 fold change in *s100a10a* expression = -1.01 ± 0.46 *versus.* 0.05 ± 0.05, P = 0.0002, one-way ANOVA with Tukey's multiple comparisons). Unlike pre-injury expression, *s100a10b* was also significantly decreased in 48hpi moderate crispants, relative to WT (Log_2 fold change in *s100a10b* expression = -0.48 ± 0.22 *versus.* $-3.33e^{-11}$ ± 0.08, P = 0.0023) and mild crispants (Log_2 fold change in *s100a10b* expression = -0.48 ± 0.22 *versus.* -0.15 ± 0.20, P = 0.0370) (**Figure 15**). These findings indicate injury-dependent dysregulation of *s100a10a/b*, with cumulative reductions observed specifically in moderate crispants.

For analysis of fibrinolytic pathways, *serpine1* expression remained unchanged, whereas *plg* levels, previously reduced in uninjured moderate crispants, were restored to control levels post-injury. Interestingly, *plat/tpa*, which was unaffected pre-injury, became significantly upregulated following injury in both mild (Log_2 fold change in *plat* expression = 0.26 ± 0.06 *versus.* 0.00 ± 0.00, P = 0.0002, one-way ANOVA with Tukey's multiple comparisons) and moderate crispants (Log_2 fold change in *plat* expression = 0.55 ± 0.01 *versus.* 0.00 ± 0.00, P < 0.0001) compared with WT. Furthermore, *plat/tpa* expression was higher in the moderate than mild phenotype (Log_2 fold change in *plat* expression = 0.55 ± 0.01 *versus.* 0.26 ± 0.06, P = 0.0002)

(**Figure 15**). These results suggest that loss of *anxa2a/b* disrupts normal regulation of fibrinolytic pathways in zebrafish larvae after cardiac injury. Importantly, the fibrinolytic pathways may encompass both fibrinolysis and angiogenesis, since plasmin activation can promote extracellular matrix modelling and endothelial migration (Liu and Hajjar, 2016a), which are crucial processes for neovascularisation and tissue regeneration.

Analysis of angiogenic gene expression revealed selective perturbations. Unlike the pre-injury state, *tie1* expression was unaltered across groups. However, *vegfab* remained significantly reduced in injured moderate crispants, compared with WT (Log_2 fold change in *vegfab* expression = -0.53 ± 0.19 *versus.* -0.08 ± 0.13, P = 0.0147) and mild crispants (Log_2 fold change in *vegfab* expression = -0.53 ± 0.19 *versus.* 0.13 ± 0.24, P = 0.0015; one-way ANOVA with multiple comparisons). While *cxcr4a* was unaffected post-injury, *cxcl12b* was exclusively downregulated post-injury in moderate crispants, relative to WT (Log_2 fold change in *cxcl12b* expression = -1.29 ± 0.75 *versus.* 0.00 ± 0.00, P = 0.0063) and mild (Log_2 fold change in *cxcl12b* expression = -1.29 ± 0.75 *versus.* 0.32 ± 0.17, P = 0.0017) (**Figure 15**). This pattern suggests impaired activation/regulation of key angiogenic signalling pathways in the absence of *anxa2a/b*.

Regeneration-associated genes showed further distinct changes following cardiac injury. *notch1a* was significantly downregulated in 48hpi moderate crispants, compared with WT (Log_2 fold change in *notch1a* expression = -1.18 ± 0.34 *versus.* 0.06 ± 0.18, P < 0.0001) and mild (Log_2 fold change in *notch1a* expression = -1.18 ± 0.34 *versus.* 0.00 ± 0.27, P < 0.0001). Notably, *notch3* was reduced following injury in both mild (Log_2 fold change in *notch3* expression = -0.26 ± 0.15 *versus.* 0.03 ± 0.10, P = 0.0162) and moderate crispants (Log_2 fold change in *notch3* expression = -0.51 ± 0.24 *versus.* 0.03 ± 0.10, P = 0.0005). Whereas *notch1b, notch2, tgfb1a*, and *tgfb2* remained unaltered, suggesting targeted disruption of notch-mediated signalling in *anxa2a/b* crispants post-injury (**Figure 15**).

These data demonstrate that *anxa2a/b* deficiency profoundly alters transcriptional responses to cardiac injury, and the transcriptional profile is different to what was seen in pre-injury conditions. In addition to persistent suppression of *anxa2a/b*, injury elicited further dysregulation of *anxa2a/b* co-regulators (*s100a10a/b*), fibrinolytic mediators (*plat/tpa*), angiogenic drivers (*vegfab, cxcl12b*), and regenerative effectors (*notch1a* and *notch3*), highlighting the important role of *anxa2a/b* in coordinating downstream endothelial and regenerative signalling.

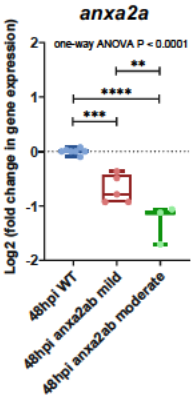
anxa2a
one-way ANOVA P < 0.0001
Log2 (fold change in gene expression)
48hpi WT
48hpi anxa2ab mild
48hpi anxa2ab moderate

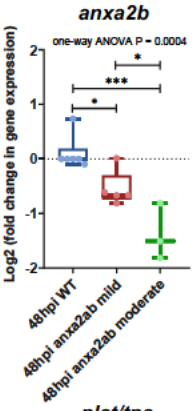
anxa2b
one-way ANOVA P = 0.0004
Log2 (fold change in gene expression)
48hpi WT
48hpi anxa2ab mild
48hpi anxa2ab moderate

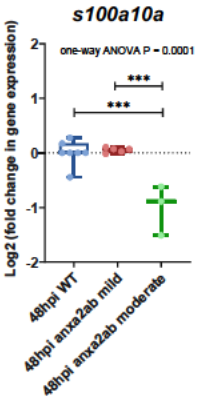
s100a10a
one-way ANOVA P = 0.0001
Log2 (fold change in gene expression)
48hpi WT
48hpi anxa2ab mild
48hpi anxa2ab moderate

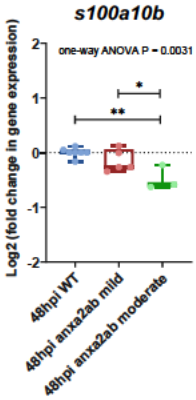
s100a10b
one-way ANOVA P = 0.0031
Log2 (fold change in gene expression)
48hpi WT
48hpi anxa2ab mild
48hpi anxa2ab moderate

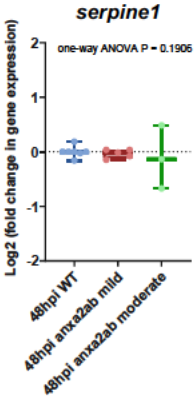
serpine1
one-way ANOVA P = 0.1906
Log2 (fold change in gene expression)
48hpi WT
48hpi anxa2ab mild
48hpi anxa2ab moderate

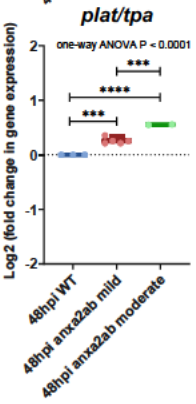
plat/tpa
one-way ANOVA P < 0.0001
Log2 (fold change in gene expression)
48hpi WT
48hpi anxa2ab mild
48hpi anxa2ab moderate

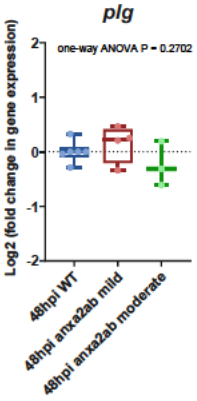
plg
one-way ANOVA P = 0.2702
Log2 (fold change in gene expression)
48hpi WT
48hpi anxa2ab mild
48hpi anxa2ab moderate

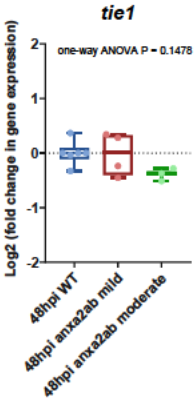
tie1
one-way ANOVA P = 0.1478
Log2 (fold change in gene expression)
48hpi WT
48hpi anxa2ab mild
48hpi anxa2ab moderate

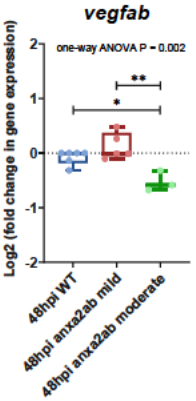
vegfab
one-way ANOVA P = 0.002
Log2 (fold change in gene expression)
48hpi WT
48hpi anxa2ab mild
48hpi anxa2ab moderate

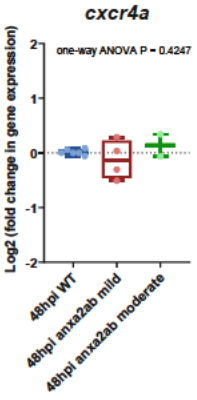
cxcr4a
one-way ANOVA P = 0.4247
Log2 (fold change in gene expression)
48hpi WT
48hpi anxa2ab mild
48hpi anxa2ab moderate

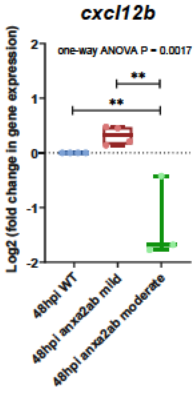
cxcl12b
one-way ANOVA P = 0.0017
Log2 (fold change in gene expression)
48hpi WT
48hpi anxa2ab mild
48hpi anxa2ab moderate

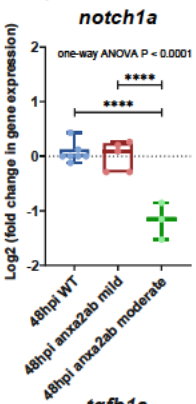
notch1a
one-way ANOVA P < 0.0001
Log2 (fold change in gene expression)
48hpi WT
48hpi anxa2ab mild
48hpi anxa2ab moderate

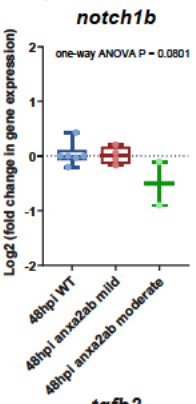
notch1b
one-way ANOVA P = 0.0801
Log2 (fold change in gene expression)
48hpi WT
48hpi anxa2ab mild
48hpi anxa2ab moderate

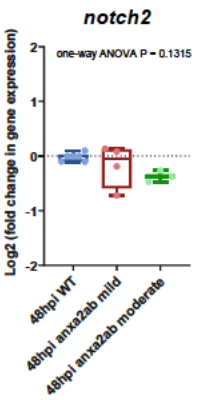
notch2
one-way ANOVA P = 0.1315
Log2 (fold change in gene expression)
48hpi WT
48hpi anxa2ab mild
48hpi anxa2ab moderate

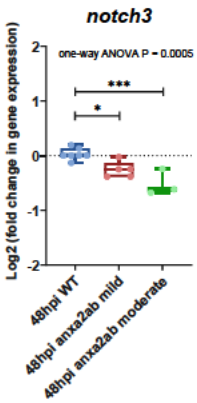
notch3
one-way ANOVA P = 0.0005
Log2 (fold change in gene expression)
48hpi WT
48hpi anxa2ab mild
48hpi anxa2ab moderate

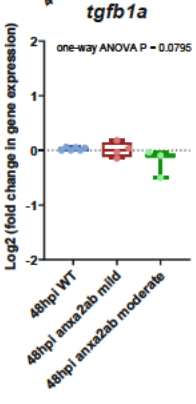
tgfb1a
one-way ANOVA P = 0.0795
Log2 (fold change in gene expression)
48hpi WT
48hpi anxa2ab mild
48hpi anxa2ab moderate

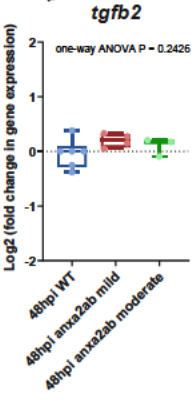
tgfb2
one-way ANOVA P = 0.2426
Log2 (fold change in gene expression)
48hpi WT
48hpi anxa2ab mild
48hpi anxa2ab moderate

Figure 15. Relative mRNA expression of fibrinolytic, angiogenic, and regenerative genes in anxa2a/b crispants following 48 hours post-injury (hpi). *Box plots show log-transformed relative quantification of mRNA expression levels for selected fibrinolytic, angiogenic, and regeneration-associated genes in three groups: uninjected siblings, anxa2a/b CRISPants with mild and moderate phenotypes. Data are normalised to housekeeping genes b2m and rpl7 and expressed as log_2 fold change relative to uninjected controls. Horizontal bars represent medians; boxes represent interquartile ranges (IQR); whiskers extend to minimum and maximum values within 1.5× IQR. Statistical analysis was performed using one-way ANOVA with Tukey's multiple comparisons.*

4.8 Discussion

The use of CRISP/Cas9 to generate first-generation (F0) mosaic mutant zebrafish (referred as crispants), provides significant advantages over the generation of stable knockout zebrafish lines. While the establishment of homozygous mutant lines typically requires at least two generations of breeding (6-9 months), F0 crispants can be generated around 3 months, thereby accelerating functional genetic screening (Debaenst et al., 2025). Previous studies have validated this approach: for instance, crispants generated for the osteoporosis gene low-density lipoprotein receptor-related protein 5 (*lrp5)* exhibited phenotypes and molecular signatures closely resembling those of stable germline knockouts while showing higher survival rates (Bek et al., 2021). Similarly, Watson et al, 2020 also reported strong phenotypic convergence between F0 crispants and homozygous germline mutants, despite crispants inherently display mosaic phenotypes due to variable editing across individual cells (Watson et al., 2020). Together, these findings support the utility of F0 crispants as reliable models for human disease biology, and powerful tool for reverse genetic screen of candidate genes. Additionally, F1 and F2 generations (the offspring of F0 crispants carrying heritable CRISPR-induced mutations) were generated in the laboratory with the aim of establishing stable *anxa2a/b* mutant lines (homozygous or heterozygous knockouts) for future mechanistic and rescue studies. However, this work will be beyond the timeframe of the current PhD project.

CRISPR/Cas9-mediated knockdown of paralogues *anxa2a* and *anxa2b* was confirmed by T7E1 assays and validated by RT-qPCR, which showed efficient mutagenesis at the targeted loci and transcript downregulation across crispants of varying phenotypic severity (**Figure 8**). Transcript quantification was performed on pooled larvae, since RNA yields from single larvae were insufficient for downstream assays. While pooling does not capture the full mosaicism at the single-embryo level, it improves statistical power and reduces stochastic variability. Crispants were grouped into mild, moderate, and severe groups, enabling phenotype–genotype associations to be drawn and revealing the gene dosage effects of *anxa2a/b*.

A critical component of this experimental framework was the inclusion of uninjected and Cas9-only controls which served to distinguish true gene-editing effects from potential artefacts introduced by the microinjection procedure or Cas9 toxicity. Uribe-Salazar et al (2022) reported that although Cas9 enzyme or mRNA injected without gRNA did not induce random somatic mutations, the injection process alone altered the expression of genes associated with stress responses, wound healing, and cytoskeletal organisation (Uribe-Salazar et al., 2022). In this study, Cas9-only controls did not show evidence of target gene suppression, confirming the specificity of the designed dgRNAs while ruled out Cas9 toxicity or off-target effects. Uninjected and Cas9-only controls also share identical phenotypes, supporting the absence of procedural artefacts. This validation step was essential to ensure the accuracy and interpretability of the results.

Knockdown of *anxa2a/b* consistently produced developmental abnormalities (**Figure 9**, **Figure 10**, **Figure 11**). The severity of phenotypic defects in crispants correlated with the extent of craniofacial, posterior body, angiogenic, and cardiac abnormalities, highlighting the essential role of *anxa2a/b* in coordinating systemic development, vascular patterning, and cardiac growth. The variability in phenotypes likely reflects the mosaic nature of CRISPR/Cas9 editing but also provided an opportunity to assess gene dosage effects (Naert et al., 2020). Mild crispants displayed reduced body length and eye size, whereas moderate and severe groups developed pericardial and yolk sac oedema, craniofacial malformations, spinal curvature, and defective tail formation. The progressive severity of defects suggests a dose-dependent requirement for ANXA2, where partial loss disrupts organogenesis, and more extensive loss leads to systemic developmental failure. Vascular analyses revealed clear impairment of angiogenesis, characterised by thinning or loss of ISVs and reduced PAVs formation at 3 dpf, indicating defects in both primary angiogenic sprouting and parachordal lymphangioblasts development (Veloso et al., 2024). Moderate and severe phenotypes were excluded from vascular quantification due to their pronounced morphological deformities, which may result in an under-characterisation of the most extreme angiogenic defects.

A double transgenic Tg(*fli1:eGFP*)^{y1tg} / Tg(*myl7:DsRed2-NLS*)^{f2} larvae was used in this study, in which endothelial and endocardial cells express green fluorescence (GFP) and cardiomyocyte nuclei express red fluorescence (mCherry), allowing simultaneous visualisation of vascular and myocardial structures. The developing heart consists of a myocardial tube lined by an inner endothelial layer known as the endocardium (Bussmann et al., 2007). The endocardial cells are a specialised subset of ECs that originate from the same *kdrl*$^{+}$*/fli1*$^{+}$ endothelial progenitor population giving rise to other vascular ECs (Brown et al., 2016, Lawson and Weinstein, 2002, Capon et al., 2022, Gurung et al., 2024). During early cardiac development, endocardial cells express key endothelial markers such as FLK1, CD31, VE-cadherin (Gurung et al., 2024, Milgrom-Hoffman et al., 2011). Hence, the endocardial cells observed in the larval ventricle are regarded as progenitor ECs in this study.

High-resolution SPIM imaging of double transgenic larvae further revealed that uninjured *anxa2a/b* crispants exhibited significantly reduced ventricular endothelial cell numbers and smaller diastolic volumes at 5 dpf, despite unchanged cardiomyocyte counts (**Figure 11**). Given that angiocrine signalling of cardiac ECs (e.g. endocardial cells, coronary ECs, and valve ECs) is essential for cardiac chamber ballooning, trabeculation, compaction, valve formation and cardiomyocyte cellular maturation during cardiac development (Kim et al., 2021, Rhee et al., 2021). The depletion of ECs observed in *anxa2a/b* crispants may impair expansion of the ventricular chamber and myocardial-endothelial cross talk, contributing to the observed ventricular growth defects and impaired contractility (Rhee et al., 2021). Mechanistically, disruption of the ANXA2-S100A10-tPA complex could inhibit vascular fibrinolysis and endothelial migration, thereby compromising vascularisation of the developing heart (Liu and Hajjar, 2016a).

The phenotypes observed in *anxa2a/b* crispants parallel those reported in ANXA2-deficient models, underscoring a conserved requirement for ANXA2 in coordinating morphogenesis, vascular homeostasis, and tissue repair. In humans, ANXA2 promotes embryo adhesion to endometrial epithelial cells by activating the RhoA/ROCK pathway and inducing F-actin rearrangement, a process essential for implantation (Garrido-Gómez et al., 2012). Consistently, ANXA2-null mice had impaired stromal decidualisation and defective placental formation, leading to foetal growth restriction, a hallmark of severe pre-eclampsia (Garrido-Gomez et al., 2020). Beyond reproductive development, ANXA2 contributed to central nervous system development in mice (Hamre et al., 1995, White et al., 2024), and was strongly upregulated in astrocytes and neurons after spinal cord injury in rats, which suggests an adaptive role in regulating biochemical and physiological responses to tissue damage (Chen et al., 2017). Together, these studies emphasise the broad developmental significance of ANXA2, in line with the craniofacial, angiogenic, and cardiac defects we observed in zebrafish *anxa2a/b* crispants.

The vascular phenotypes in crispants are also consistent with those in ANXA2 knockout mice, which despite being viable and fertile, showed reduced body weight by 13%, deposition of microvascular fibrin, defective clearance of arterial thrombi and collagen I matrix remodelling, which all attributable to impaired tPA-dependent plasmin generation at the EC surface (Ling et al., 2004). These mice exhibited compromised angiogenic capacity, including diminished corneal and retinal neovascularisation (Ling et al., 2004), mirroring the reduced ISV and PAV formation in zebrafish. Furthermore, ANXA2 loss compromised blood-brain barrier (BBB) integrity, with knockout mice displaying reduced endothelial junctional proteins and increased vascular leakage, whereas recombinant ANXA2 rescued hypoxia- and cytokine- induced cerebral trans-endothelial permeability in human brain ECs via F-actin, VE-cadherin, and roundabout guidance receptor 4 (Robo4)-paxillin-ADP-ribosylation factor 6 (ARF6) signalling (Li et al., 2019a). These findings reinforce the importance of ANXA2 in regulating vascular

homeostasis, angiogenesis, and barrier function, processes that may also be disrupted in zebrafish *anxa2a/b* crispants.

To assess regenerative capacity and the interplay between endothelial and myocardial compartments during repair, a controlled and reproducible cardiac laser injury model was established in larval zebrafish (**Figure 12**). Using the PALM laser system, focal injury was induced at the ventricular apex of 3 dpf larvae, creating regional damage while preserving overall embryo viability and structural integrity. This method generated transient yet quantifiable impairments in heart rate, ventricular volume, and both cardiomyocyte and EC numbers, all of which fully recovered within 48 hpi in WT siblings. These findings highlight the remarkable regenerative potential of the larval zebrafish heart and the suitability of this model for dissecting the impact of anxa2ab deficiency on cardiac repair. Although the laser lesion resembles regional myocardial damage caused by coronary artery ligation in mammals, it differs substantially from mouse or rat injury models (Matrone et al., 2013). Furthermore, fundamental differences in cardiac complexity between zebrafish and mammals limit direct translational relevance (Matrone et al., 2014). Nevertheless, the larval zebrafish offers unique advantages: at <5 dpf, larvae are optically transparent, genetically tractable, and capable of a rapid regenerative response (Yashaswini et al., 2025), enabling longitudinal live imaging at cellular resolution during cardiac development and regeneration (Zhang et al., 2023a). The capacity to study hundreds of larvae within a short period of time also provides strong statistical power and facilitates the investigation of severe developmental cardiac defects that would otherwise be lethal in mammalian models (Matrone et al., 2014).

Application of this model revealed that *anxa2a/b* knockdown disrupted multiple aspects of cardiac regeneration within the normal 48-hour regenerative window (**Figure 13**). In WT siblings, regeneration was rapid and efficient, with endothelial and cardiomyocyte populations replenished within 48 hpi, accompanied by restoration of ventricular morphology and function. By contrast, *anxa2a/b* crispants exhibited persistent deficits in endothelial repopulation, cardiomyocyte restoration, ventricular volume, and structural recovery. The severity of impairment correlated with baseline phenotype, with mild crispants showing delayed and partial regeneration, and moderate crispants displaying severe defects and distorted ventricular architecture. These results indicate that ANXA2 is required not only for developmental angiogenesis and cardiac morphogenesis, but also for orchestrating injury-induced cardiac regeneration.

A key strength of the regeneration study lies in the inclusion both mild and moderate *anxa2a/b* crispants. Because CRISPR/Cas9 mutagenesis in zebrafish produces mosaic embryos with variable mutation burdens (Mehravar et al., 2019), stratifying by severity allowed investigation of gene dosage effects. Mild crispants, which exhibited relatively normal cardiac development at baseline, suggested that even partial loss of ANXA2 impairs regenerative efficiency without grossly affecting cardiac morphogenesis, while moderate crispants, with baseline structural defects consistent

with near-complete loss of ANXA2 function, revealed how pre-existing developmental defects predisposes to regenerative failure. Importantly, this experimental design improves translational relevance, as it mirrors the clinical diversity in humans, where variable ANXA2 activity may arise from genetic variation, comorbidities, or environmental influences – thereby strengthening the applicability of these findings to human cardiac repair.

Mechanistically, ANXA2 functions as a co-receptor with S100A10 for plasminogen and tissue plasminogen activator, facilitating plasmin generation and vascular fibrinolysis at the endothelial surface (Liu and Hajjar, 2016a). Plasmin subsequently activates a proteolytic cascade involving matrix metalloproteinases, which are essential for fibrin clearance, ECM remodelling, and endothelial sprouting—processes fundamental for neovascularisation after cardiac injury (Ling et al., 2004). Loss of ANXA2 therefore likely compromises ECM degradation and vessel invasion, explaining the impaired endothelial recovery observed in injured crispants. In addition, phosphorylation of ANXA2 at Tyr23 regulated actin dynamics, promoting cell scattering, branching morphogenesis and EMT-related processes via cofilin-dependent cytoskeletal remodelling (de Graauw et al., 2008). Disruption of these pathways in *anxa2a/b* crispants may account for the distorted ventricular tissue architecture and incomplete myocardial regeneration observed. Together, these findings highlight ANXA2 as a central coordinator of myocardial–vascular repair, integrating fibrinolytic remodelling with cytoskeletal reorganisation to restore cardiac structure and function following injury.

In the boarder cardiovascular context, ANXA2 regulates vascular homeostasis and thrombosis. A rat carotid artery thrombosis model showed that recombinant ANXA2 administration improved vessel patency without disturbing systemic coagulation. By enhancing endothelial fibrinolytic activity, ANXA2 modulate the hypercoagulable state of atherosclerosis (Ishii et al., 2001). Beyond its role in fibrinolysis, ANXA2 expression was markedly increased in vascular neointima of carotid artery, where it mediated vascular smooth muscle cell migration and proliferation, thereby facilitating atherosclerotic plaque formation (Won et al., 2011). Similarly, in a mouse model of atherosclerosis, ANXA2 was markedly upregulated in atherosclerotic plaques, where its interaction with tenascin-c facilitated macrophage migration and VEGF expression via Akt, NF-κB and ERK1/2 pathways (Wang et al., 2018).

In the setting of MI, ANXA2 appears to exert reparative functions. Overexpression of ANXA2 promoted cardiac repair, improved ventricular function, and reduced infarct size by enhancing neovascularisation via its interaction with integrin β3 on cardiac microvascular ECs, and by modulating inflammation through YAP-dependent polarisation of macrophages from a pro-inflammatory (M1) to a reparative (M2) phenotype (Zhang et al., 2023b). Conversely, the protein ADAM8, which is overexpressed in macrophages during MI, binds to ANXA2 and causes phosphorylation of mammalian target of rapamycin (mTOR), resulting in the suppression of autophagy and angiogenesis, exacerbating inflammation and tissue

injury (Ji et al., 2025). However, the deficiency of ADAM8 facilitates cardiac repair by hindering the binding and phosphorylation of ANXA2, and activating the ANXA2-mToR-autophagy pathway, thereby enhancing the release of angiogenic factors and reducing inflammation(Ji et al., 2025) . Together, these studies position ANXA2 as a key regulator of vascular remodelling, fibrinolysis, and post-injury inflammatory responses. In the larval zebrafish model, the impaired myocardial-vascular recovery observed in injured *anxa2a/b* crispants likely reflects the loss of ANXA2's fibrinolytic, pro-migratory, and remodelling functions, indicating its conserved role in cardiac repair across species.

Beyond cardiovascular biology, ANXA2 contributes to tissue repair and regeneration across multiple organ systems. ANXA2 is highly expressed in invasive tumour cells. Invasive tumour cells rely on ANXA2 to repair membrane damage under shear stress, enabling invasion and metastasis in zebrafish and mouse models; genetic inhibition of ANXA2 disrupts this membrane repair, leading to cell death (Gounou et al., 2023). This parallels our zebrafish data, where ANXA2 deficiency impaired endothelial and cardiomyocyte dynamics during regeneration, suggesting a conserved role in supporting cell migration, remodelling, and survival under mechanical stress. Consistent with this, *anxa2a* and *anxa2b* were both upregulated during zebrafish caudal fin regeneration, with *anxa2b* showing a stronger and earlier response. Although *anxa2a* is more similar to human *ANXA2*, *anxa2b* appears more critical for fin regeneration, highlighting differential gene-specific regulation during the process (Saxena et al., 2016). Targeted CRISPR editing of these paralogues impaired caudal fin regeneration, reflecting their importance in cell-cell communication and ECM growth (Quoseena et al., 2020).

Additional studies further reinforce ANXA2's role as a key repair hub across tissue. In skeletal muscle, ANXA2 interacted with dysferlin in a calcium (Ca^{2+})-dependent manner to mediate vesicle aggregation and fusion at sarcolemmal injury sites; its loss impaired muscle membrane repair and contributed to muscular dystrophy (Lennon et al., 2003, Bittel et al., 2020). Similarly, ANXA2 knockout mice exhibited impaired blood-brain barrier development and elevated pro-inflammatory responses in macrophages (Li et al., 2019a). Following traumatic brain injury (TBI), ANXA2 expression was significantly upregulated at day three post-injury (Liu et al., 2019). The protective role of ANXA2 in neurovascular integrity was demonstrated by studies in ANXA2 knockout mice, which showed exacerbated neuroinflammation, neurovascular pro-inflammation, and worsened long-term neurological outcomes following TBI, including sensory and motor deficits, cognitive impairment and increased brain tissue loss (Liu et al., 2019). These findings suggest that enhancing ANXA2 activity may represent a potential therapeutic strategy to mitigate neuroinflammation and improve recovery following TBI.

Finally, our transcriptional analysis revealed that *anxa2a/b* knockdown induced broad dysregulation of vascular and fibrinolytic gene expression even in the absence of injury (**Figure 14**), suggesting that *ANXA2* functions not merely as an injury-responsive factor but as a fundamental regulator of endothelial homeostasis and developmental

angiogenesis. As expected, *anxa2a/b* transcript levels were strongly reduced, validating the CRISPR/Cas9 editing. Importantly, the suppression extended to *s100a10a* in moderate crispants, consistent with studies showing that ANXA2 stabilises S100A10/p11, which is required for tyrosine phosphorylation and cell-surface translocation of both proteins (Hedhli et al., 2012, He et al., 2008). Indeed, S100A10/P11 expression was very low in the absence of ANXA2 both *in vitro* and *in vivo* (He et al., 2008).

Within fibrinolytic pathways, moderate crispants exhibited selective reduction of plasminogen (plg) transcripts, suggesting impaired plasmin availability or activation. This mirrors findings in ANXA2 knockout mice, where loss of ANXA2 diminished endothelial tPA-dependent plasmin generation, leading to defective thrombus clearance and impaired matrix remodelling (Ling et al., 2004). Surprisingly, *serpine1* and *plat/tpa* expression remained unaltered, indicating that the primary disruption lies at the level of plasminogen regulation rather than its upstream activators or inhibitors. These findings argue against a direct transcriptional link between *ANXA2* and *SERPINE1*. Indeed, sc(n)RNA-seq analysis of COVID-19 lungs revealed endothelial downregulation of *ANXA2* alongside with reduced *PROCR* (protein C receptor) and *THBD* (thrombomodulin), which normally activate protein C and inhibit *SERPINE1*. This is accompanied by endothelial upregulation of SERPINE1, resulting in fibrinolytic shutdown and microvascular thrombosis (Lee et al., 2025). In our model, *serpine1* remained stable despite *anxa2a/b* suppression, suggesting *ANXA2* and *SERPINE1* do not directly regulate each other at the transcriptional level. Instead, their reciprocal expression balance appears essential for maintaining endothelial fibrinolytic competence. Disruption of this balance could compromise effective plasmin generation, ECM remodelling, and vascular repair. Notably, prior study reported that complete ANXA2 deficiency in mice abolished tPA cofactor activity (He et al., 2008).

The most interesting pre-injury changes were observed in angiogenic signalling. Downregulation of *tie1* and *vegfab* in moderate crispants suggests that *anxa2a/b* is required for endothelial growth and sprouting. TIE1, an endothelial angiopoietin receptor that modulates cell adhesion, angiogenesis and vascular stability (Korhonen et al., 2016), and VEGF-A, a master angiogenic regulator (Braile et al., 2020, Ferrara et al., 2003, Leung et al., 1989), are both essential for vascular development. Their suppression aligns with the defective ISV and PAV formation observed in crispants. In contrast, *cxcr4a* and *cxcl12b* remained unchanged, suggesting that chemotactic signalling via the CXCR4/CXCL12 axis remains intact and that ANXA2 exerts a more selective role in growth factor-driven angiogenesis. The CXCR4/CXCl12 axis is important for cardiovascular development: CXCR4 is the primary receptor for proper arterial patterning, while CXCL12 acts as chemoattractant that promotes endothelial recruitment and vascularisation (Ara et al., 2005, Kim et al., 2017). Importantly, regeneration-associated transcriptional programmes (Notch1-3, TGFβ isoforms, PABPC1 paralogues) were all unaffected under basal conditions, suggesting that ANXA2 deficiency alone does not prematurely activate or suppress regenerative gene

networks in the absence of injury (Gao et al., 2021, Chablais and Jaźwińska, 2012, Shi, 2023). During zebrafish heart regeneration, Notch signalling is activated by cardiac injury in either ventricular resection or cryoinjury models, leading to elevated expressions of *notch1a, notch1b, notch2*, and *notch3* (Münch et al., 2017). However, excessive or ubiquitous activation of the Notch pathway also compromises zebrafish cardiomyocyte proliferation and regeneration, indicating the exquisite sensitivity of cardiomyocyte renewal to Notch signalling perturbations (Zhao et al., 2014).

At 48 hours post-injury (hpi), transcriptional dysregulation became more pronounced and phenotype dependent (**Figure 15**). Both *anxa2a* and *anxa2b* remained suppressed, with injured moderate crispants exhibiting stronger downregulation. This suggests that injury reveals a functional requirement for *anxa2a/b* in transcriptional activation during regeneration, and that this injury-induced activation is defective in crispants. Failure to appropriately induce *anxa2a/b* would be predicted to impair proteolytic matrix clearance and endothelial migration, thereby limiting neovascularisation and tissue repair. Importantly, the enhanced suppression observed in moderate phenotype is unlikely to be solely attributable to a reduced number of *anxa2a/b*$^{+}$ cells, but instead reflects defective transcriptional induction following injury. Thus, phenotype severity modulates the capacity to transcriptionally activate *anxa2a/b* in response to injury, rather than simply reflecting baseline differences in *anxa2a/b*$^{+}$ cell abundance.

Both *s100a10a* and *s100a10b* were further downregulated in moderate crispants, reinforcing the requirement of the ANXA2/S100A10 complex in coordinating endothelial and myocardial repair responses (Liu and Hajjar, 2016a, de Graauw et al., 2008). Interestingly, *plat/tpa* was upregulated post-injury in both mild and moderate crispants, while *plg* levels were restored in previously deficient moderate embryos. This suggests an attempted compensatory response to promote fibrinolysis; however effective plasmin generation, ECM remodelling and endothelial sprouting are likely compromised in the absence of ANXA2, hence producing a maladaptive environment for regeneration. Changes in angiogenic and regenerative signalling further support this interpretation. In moderate crispants, *vegfab* and *cxcl12b* were downregulated, consistent with defective endothelial repopulation *in vivo* (Figure 6). notch signalling was selectively affected, with *notch1a* significantly reduced in moderate crispants, and *notch3* downregulated in both mild and moderate crispants, whereas other notch isoforms remained unchanged. This selective disruption implies that ANXA2 deficiency specifically interferes with notch-mediated endothelial and cardiomyocyte proliferation and cell-to-cell communication during heart regeneration (Zhao et al., 2014, Münch et al., 2017). Specifically, the activation of notch signalling improves cardiac function, minimizes myocardial fibrosis, suppresses cardiomyocytes apoptosis, and improves neovascularisation and regeneration (Li et al., 2010, Li et al., 2021a). Notch3 deficiency can cause ventricular hypertrophy and mild fibrosis, with impaired coronary microvascular maturation and reduced cardiac recovery after myocardial ischaemia (Del Gaudio et al., 2023, Tao et al., 2017). Moreover, *pabpc1a* and *pabpc1b*,

unaffected pre-injury, were suppressed post-injury, implying that ANXA2 is necessary not only for transcription regulation but also for sustaining translational capacity during regeneration. Given the role of PABPC1 proteins in promoting mRNA stabilisation and translation (Shi, 2023), their downregulation likely limit protein synthesis required for angiogenesis and myocardial repair, compounding the regenerative deficits.

In summary, my findings demonstrate that *anxa2a/b* paralogues are important for zebrafish embryogenesis, angiogenesis, and cardiac morphogenesis, with loss leading to dose-dependent developmental abnormalities, impaired endothelial growth, and compromised cardiac regeneration. Transcriptional profiling revealed that *anxa2a/b* deficiency disrupts fibrinolysis (*plg*), angiogenic signalling (*tie1*, *vegfab*), notch pathways (*notch1a, notch3*), and translational regulators (*pabpc1a/b*), creating a maladaptive molecular environment that cannot be compensated by injury-induced responses such as *plat/tpa* upregulation. Together, these molecular alterations offer a plausible mechanistic context for the observed *in vivo* phenotypes of reduced endothelial and cardiomyocyte repopulation, distorted ventricular architecture, and regenerative impairment. These findings supports a role for ANXA2 in coordinating cardiovascular development and injury-induced regenerative responses.

To further refine the mechanistic understanding of *anxa2a/b* function, future work could employ paralogue-specific gene editing to distinguish their individual contributions to cardiac repair (Saxena et al., 2016, Quoseena et al., 2020, Howe et al., 2013). Single-embryo or single-cell transcriptomic profiling of injured hearts at early and late regenerative phases could reveal downstream molecular pathways involved in endothelial migration, ECM remodelling, and inflammatory resolution (Cao et al., 2017, Honkoop et al., 2019). Complementary mRNA rescue or overexpression experiments using paralogue-specific constructs or the human ANXA2 orthologue could determine whether *anxa2a* or *anxa2b* can independently restore vascular and myocardial regeneration, while also assessing evolutionary conservation of function (Trinh and Stainier, 2004, Ablain and Zon, 2013). These approaches would provide mechanistic and translational insights into how ANXA2 facilitates cardiac neovascularisation and myocardial repair, with potential implications for therapeutic strategies in patients with cardiovascular diseases.

Chapter 5: Results – ANXA2 and SERPINE1 are induced during endogenous neovasculogenic responses in human heart

5.1 Introduction

In Chapters 3 and 4, I used a multi-species multi-omics approach combining sc(n)RNA-seq and spatial transcriptomics analyses, which identified *ANXA2* and *SERPINE1* as potential key mediators of coronary neovascularisation after myocardial injury. Both *ANXA2* and *SERPINE1* are dynamically regulated in cardiac ECs following myocardial injury in mice, zebrafish, and humans. Furthermore, I undertook *in vivo* functional studies using zebrafish *anxa2a/b* crispants which demonstrated that *anxa2a/b* are required for normal cardiovascular development and suggested a direct functional role in promoting cardiac regeneration following injury.

These findings highlighted ANXA2 and SERPINE1 as promising candidates in the context of cardiac repair, and so the next step was to investigate protein-level expression patterns and spatial localisation in the human heart after MI. This was important to both confirm that transcriptomic changes are reflected at the protein level in human hearts and to define the spatial localisation of ANXA2 and SERPINE1 – which I postulated to be within the infarct border zone, where endogenous neovascularisation is known to be most active.

To address this, I aimed to quantify protein-level expression of ANXA2 and SERPINE1 in human hearts. I performed double-immunofluorescence staining on tissue sections from MI patients and non-diseased controls, followed by quantitative analysis of protein expression, including in ECs, within the infarct border zone.

Based on my transcriptomic data and zebrafish *in vivo* functional data, I hypothesised that ANXA2 is reactivated in ECs of the infarcted adult human heart to promote neovascularisation, whereas SERPINE1 is also upregulated in ECs in the adult post-MI human heart to regulate neovascularisation, likely in a concerted action with ANXA2, and thus may be important in myocardial repair and remodelling.

This approach enables validation of the transcriptomic findings at the protein level and provides insight into the spatial context in which ANXA2 and SERPINE1 are induced during endogenous neovasculogenic responses in the adult human heart. Together, these data will bridge the gap between experimental models and human pathology, helping to evaluate the translational relevance of ANXA2 and SERPINE1 as potential therapeutic targets for post-MI vascular and myocardial repair and regeneration.

5.2 Co-localisation of ANXA2 and SERPINE1 with CD31+ cells in the infarct border zone of MI

To compare protein expression between healthy and infarcted human hearts, five regions of interests (ROIs) from each patient tissue section (n = 7) were selected, focusing on the infarct border zone – a region known for active neovascularisation following MI (Gu et al., 2006, Ma et al., 2025). Identification of ROIs was undertaken in Masson's Trichrome stained sections, serially adjacent to those used for immunofluorescence staining. Masson's Trichrome staining is a histological method used to selectively stain collagen, collagen fibres, fibrin, muscles, and erythrocytes (Van De Vlekkert et al., 2020, Garvey, 1984). Masson's Trichrome is particularly useful for studying fibrosis in the heart, as the muscle appears as red or pink, and the collagen fibres i.e. fibrosis stain blue. Immunofluorescence staining was performed for ANXA2 or SERPINE1 in combination with CD31, a pan-endothelial marker, to quantify expression in the coronary vasculature in patients with MI compared to age- and sex-matched healthy control hearts.

For ANXA2 immunostaining, the antibody was first optimised using rabbit IgG isotype control in human heart tissue (negative control) and confirmed using positive control staining of human colon and liver sections. This showed specific staining of ANXA2 in CD31+ ECs. In healthy control hearts, ANXA2 expression was minimal, as expected. In contrast, ANXA2 expression was significantly upregulated in the infarct border zone of MI patient tissue sections compared with healthy controls (% total $ANXA2^+$ cells = 73.37 ± 9.08 *versus* 55.57 ± 8.37, P = 0.0025; unpaired t-test) (**Figure 16**). The total proportion of CD31+ cells and the proportion of CD31+ cells of total ANXA2+ cells did not change across groups.

There was also a significant increase in ANXA2 expression in total CD31+ coronary ECs in MI patients compared to controls (% $ANXA2^+$ $CD31^+$ EC = 77.10 ± 12.13 *versus* 56.94 ± 9.20, P = 0.0018; unpaired t-test) (**Figure 16**). Notably, ANXA2 expression was not confined to ECs but was also detected in other cell types within the infarct border zone, including interstitial and perivascular fibrotic regions highlighted by Masson's Trichrome staining, suggestive of expression in fibroblasts, immune cells, or other stromal populations associated with myocardial remodelling.

To validate SERPINE1 primary antibody staining, rabbit IgG and mouse IgG kappa isotype controls were employed as negative controls. Like ANXA2, total SERPINE1 expression was significantly increased in the infarct border zone of MI patient tissue sections compared to control hearts (% $SERPINE1^+$ cells = 42.13 ± 15.12 *versus* 14.56 ± 8.94, P = 0.0021; unpaired t-test) (**Figure 17**). The total proportion of CD31+ cells and the proportion of CD31+ cells of total SERPINE1+ cells did not change across groups.

SERPINE1 expression was also significantly increased in coronary ECs in MI patients compared to healthy subjects (% $SERPINE1^+$ $CD31^+$ EC = 32.7 ± 11.7 *versus* 16.13

± 7.3, P = 0.0098; unpaired t-test). SERPINE1 staining was also observed outside of ECs, potentially in the vascular smooth muscle cells, inflammatory infiltrates, and fibroblast /myofibroblast, populations, identified using Masson's Trichrome (**Figure 17**).

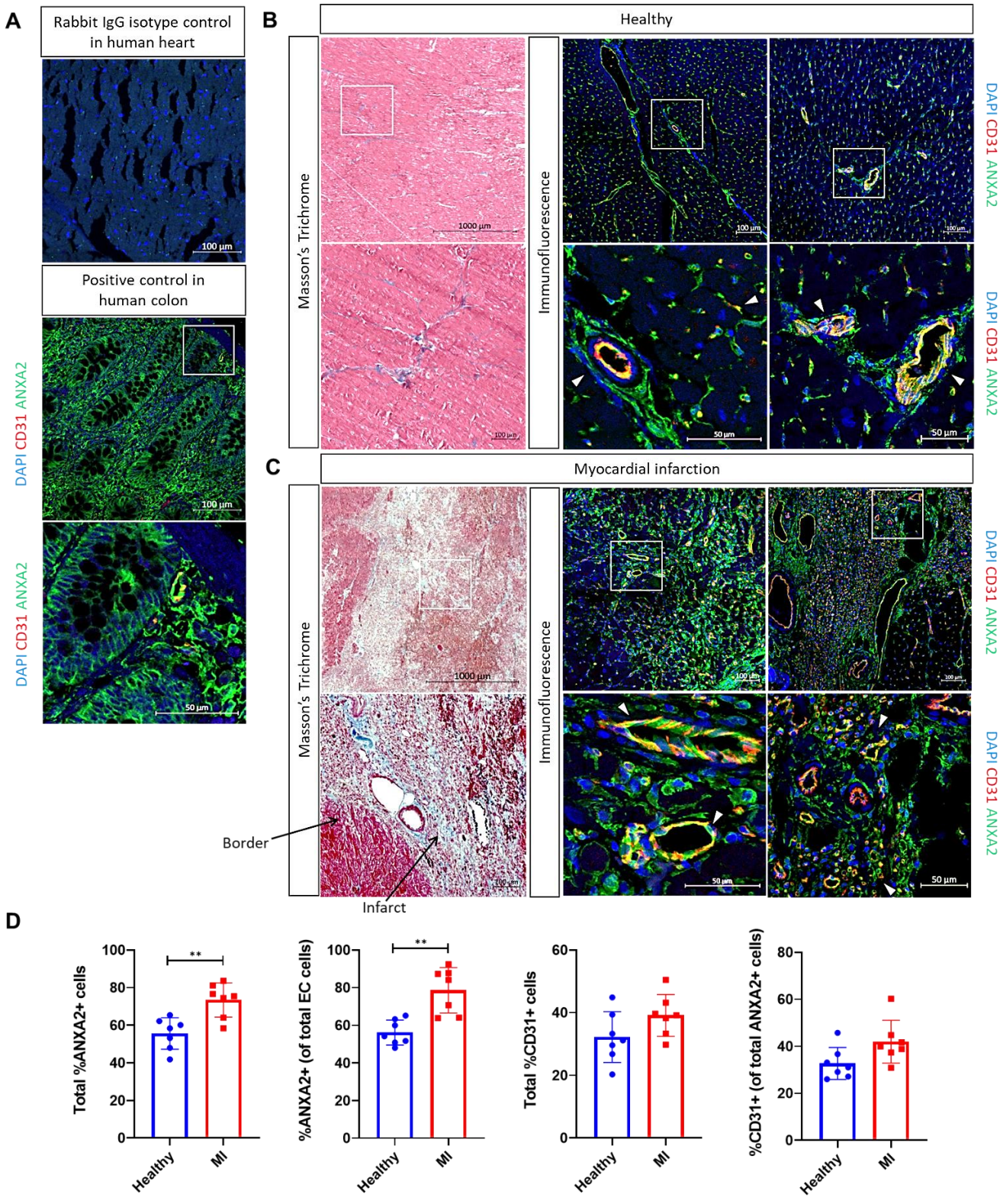

Figure 16. ANXA2 expression is upregulated in human cardiac tissues from myocardial infarction (MI) patients. *(A) Rabbit IgG isotype control and ANXA2 positive controls in human tissues. Left, representative low-power images of serial sections from the healthy human heart (B) and from patients with acute MI (C) stained using Masson's Trichrome. Right, representative images of human cardiac tissues stained by immunofluorescence for ANXA2 (green) and CD31 (red) with nuclei counterstain using DAPI (blue). The white boxes indicate the regions shown in the*

high-power images stained with ANXA2 and CD31. MI hearts showed elevated ANXA2 expression in endothelial cells and in interstitial/perivascular fibrosis. (D, E) Quantification of (i) total %ANXA2$^+$ cells, (ii) % ANXA2$^+$ cells within total CD31$^+$ population, (iii) total %CD31+ cells, and (iv) %CD31$^+$ cells within total ANXA2$^+$ population across healthy controls and MI hearts. Total ANXA2 expression and endothelial ANXA2 expression were significantly increased in MI compared with controls, indicating reactivation of ANXA2 in the infarcted human heart. Data are presented as mean ± SD.

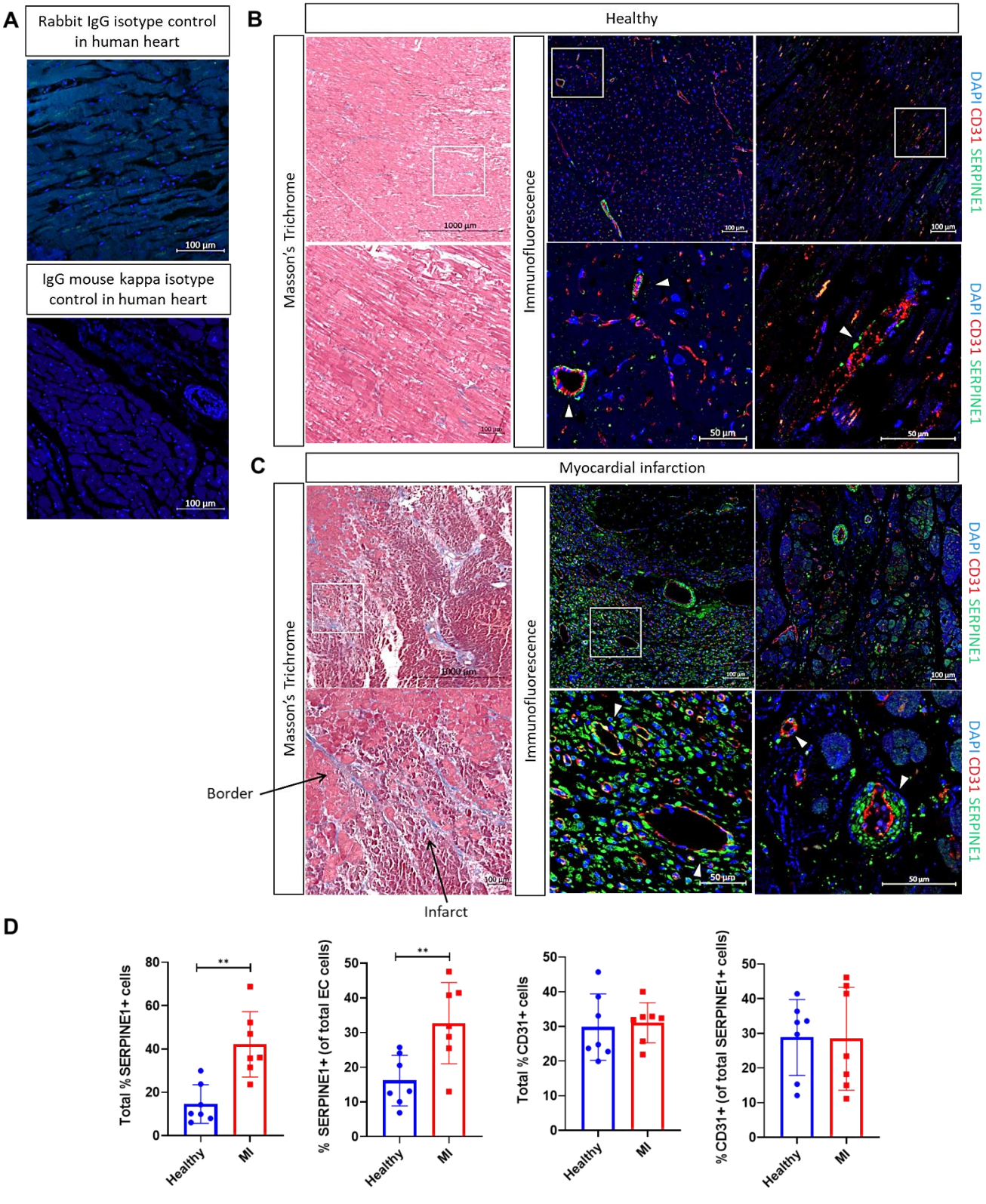

Figure 17. SERPINE1 expression is upregulated in human cardiac tissues from MI patients. *(A) Rabbit IgG isotype control and mouse IgG kappa isotype in human tissues. Left, representative low-power images of serial sections from the healthy human heart (B) and from patients with acute MI (C) stained using Masson's Trichrome. Right, representative images of human cardiac tissues stained by immunofluorescence for SERPINE1 (green) and CD31 (red) with nuclei counterstain*

using DAPI (blue). The white boxes indicate the regions shown in the high-power images stained with SERPINE1 and CD31. (D,E) Quantification of (i) total %SERPINE1⁺ cells, (ii) % SERPINE1⁺ cells within total CD31⁺ population, (iii) total %CD31+ cells, and (iv) %CD31⁺ cells within total SERPINE1⁺ population across healthy controls and MI hearts. Total SERPINE1 expression and endothelial SERPINE1 expression were significantly upregulated in MI compared to controls, indicating induction of SERPINE1 in the infarcted human heart. Data are presented as mean ± SD.

5.3 Co-localisation of ANXA2 with Vimentin+ cells in the infarct border zone of MI

As above, ANXA2 expression was not restricted to ECs but was also observed in other cell types within regions of interstitial and perivascular fibrosis. To characterise these non-endothelial ANXA2$^+$ cells, double immunofluorescence staining for ANXA2 and Vimentin was performed in human cardiac tissues (n = 2-3). Vimentin, an intermediate filament protein, is widely used as a marker of mesenchymal-derived cells, including fibroblasts, myofibroblasts, endothelial, and hematopoietic cells (Parvanian et al., 2023, Walker et al., 2019). Five ROIs were selected based on Masson's Trichrome staining, matching the same anatomical locations previously analysed for ANXA2 and CD31 co-staining. This approach ensured consistent sampling of the infarct border zone across analyses

As expected, there was minimal expression of Vimentin in healthy control hearts. In contrast, MI samples exhibited more extensive Vimentin$^+$ staining, particularly within the interstitial and perivascular regions of the infarct border zone. The total Vimentin expression appeared higher in MI hearts compared with controls (total % Vimentin$^+$ cells = 57.18 ± 11.81 versus 6.49 ± 0.11). The proportion of ANXA2$^+$ cells within the total Vimentin$^+$ population appeared comparable between MI and control samples (%ANXA2$^+$ cells within total Vimentin$^+$ population = 78.35 ± 7.53 versus 64.85 ± 2.48). In contrast, the proportion of Vimentin$^+$ cells within the total ANXA2$^+$ population appeared greater in MI hearts compared with controls (%Vimentin$^+$ cells within total ANXA2$^+$ population = 54.17 ± 9.58 versus 7.04 ± 0.04) (**Figure 18**).

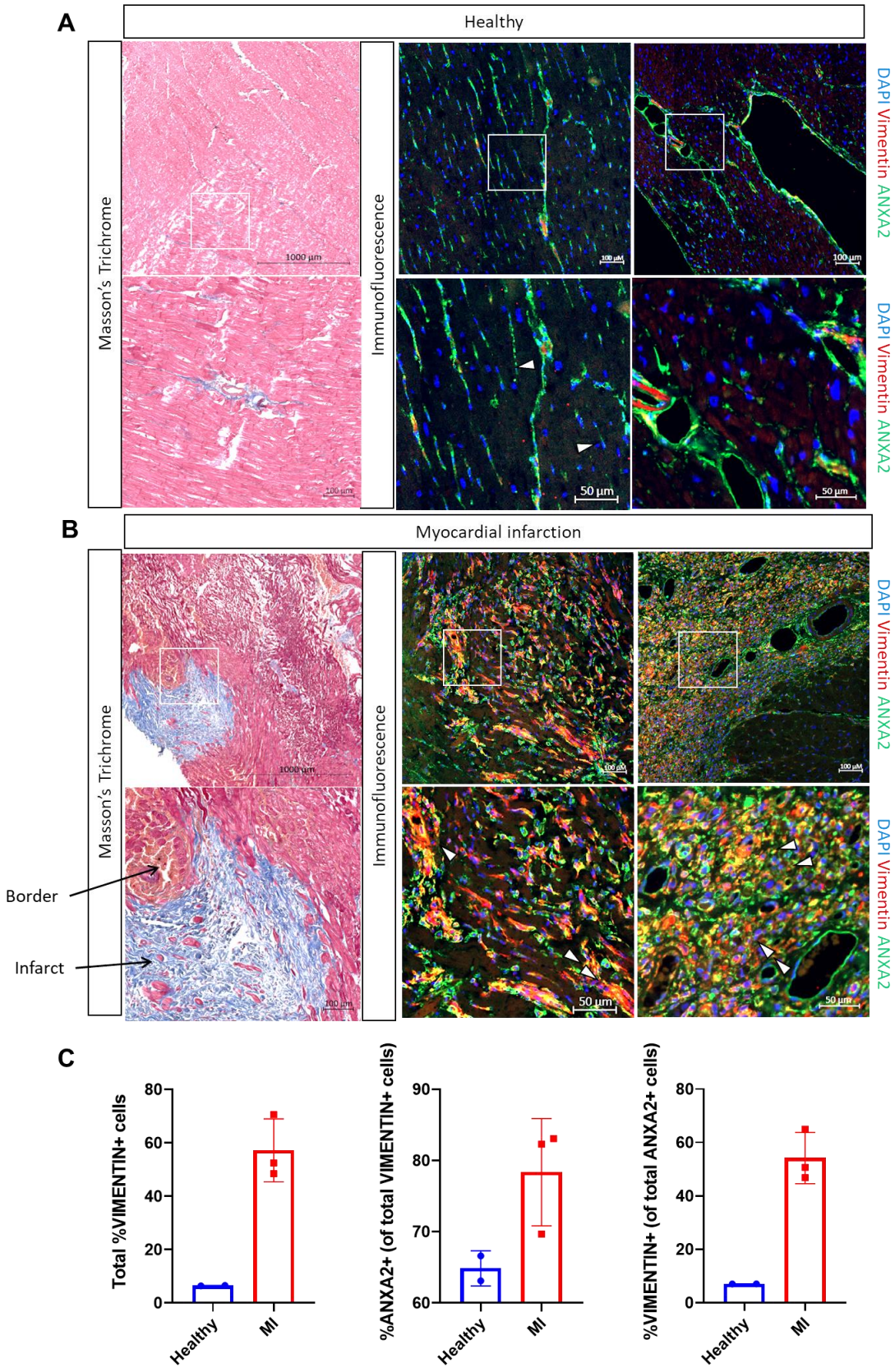

Figure 18. Co-expression of ANXA2 with Vimentin⁺ cells in human myocardial infarction (MI). *Representative images of Masson's Trichrome staining (left), and co-immunofluorescence for ANXA2 (green), Vimentin (red), and DAPI (blue) in healthy*

control hearts (A) and MI hearts (B). White boxes indicate regions of interest shown at higher magnification on the right. In MI hearts, extensive Vimentin⁺ staining was observed in interstitial and perivascular regions of the infarct border zone, with notable co-expression of ANXA2. (C) Descriptive quantification of (i) total %Vimentin⁺ cells, (ii) %ANXA2⁺ cells within total Vimentin⁺ population, and (iii) %Vimentin⁺ cells within total ANXA2⁺ population across healthy controls and MI hearts. Data are presented as mean ± SD. These data suggest an increased representation of Vimentin⁺ cells within the ANXA2⁺ population in MI hearts, consistent with enrichment of ANXA2 in mesenchymal-like cells (e.g. fibroblasts) following infarction.

5.4 *ANXA2* gene expression across cardiac cell types in control, ischaemic, and fibrotic zones.

Building on the findings from Chapter 3, where *ANXA2* and *SERPINE1* were identified as differentially expressed in the ischaemic and fibrotic zones of human hearts following MI, I next evaluated cell type-specific expression patterns in these zones using the same Kuppe dataset. This cell type analysis was performed to complement the immunofluorescence data and to determine the contribution of non-EC populations to *ANXA2* and *SERPINE1* expression in control (uninjured), ischaemic (IZ; necrotic myocardium), and fibrotic (FZ; late-stage post-MI scar) regions. The border zone (BZ; surrounding viable myocardium), and the remote zone (RZ; comprising unaffected myocardium) were excluded because ANXA2 and SERPINE1 were only differentially expressed in IZ and FZ. Focusing on IZ and FZ therefore is most likely to capture the cell populations directly involved in acute injury responses and scar formation, and thus, are relevant for understanding the roles of ANXA2 and SERPINE1 in post-MI repair.

Expression levels were assessed in two ways: i) the percentage of cells within each cell type-specific cluster that expressed the target gene and ii) the average expression level (log-transformed) in all cells in each cluster. Both EC and fibroblast clusters demonstrated significantly higher expression of *ANXA2* in the FZ compared to the IZ (%*ANXA2*⁺ ECs = 40.08 ± 14.04 *versus* 17.57 ± 10.81, P = 0.0046; %*ANXA2*⁺ fibroblasts = 43.77 ± 14.89 *versus* 20.62 ± 11.83, P = 0.0035; two-way ANOVA with Tukey's multiple comparisons) (**Figure 19**). Other cell types, including smooth muscle myoblasts, pericytes, mast cells, and immune cells, showed no statistically significant differences between different injury zones.

When analysing average expression (log-transformed), *ANXA2* expression remained relatively consistent across most cell types i.e. although the proportion of cells were significantly increased in ECs and fibroblasts- the level of expression within these cells was unchanged in response to MI. This was true for all cells except mast cells, which exhibited a significant increase in average expression in the IZ of MI patients compared with controls (log average expression = 2.83 ± 3.92 *versus* 0.51 ± 0.59, P = 0.0028) despite the proportion of cells that expressed *ANXA2* being unchanged.

Interestingly, *ANXA2 also* showed a significantly higher level of expression in mast cells in the IZ compared to FZ (log average expression = 2.83 ± 3.92 *versus* 0.92 ± 0.58, P = 0.0164; two-way ANOVA with Tukey's multiple comparisons) (**Figure 19**). Other cell types, including ECs, smooth muscle myoblasts, pericytes, fibroblasts, immature innate lymphoid cells, and cardiac myoblasts, showed no statistically significant differences in expression levels of *ANXA2* between injury zones.

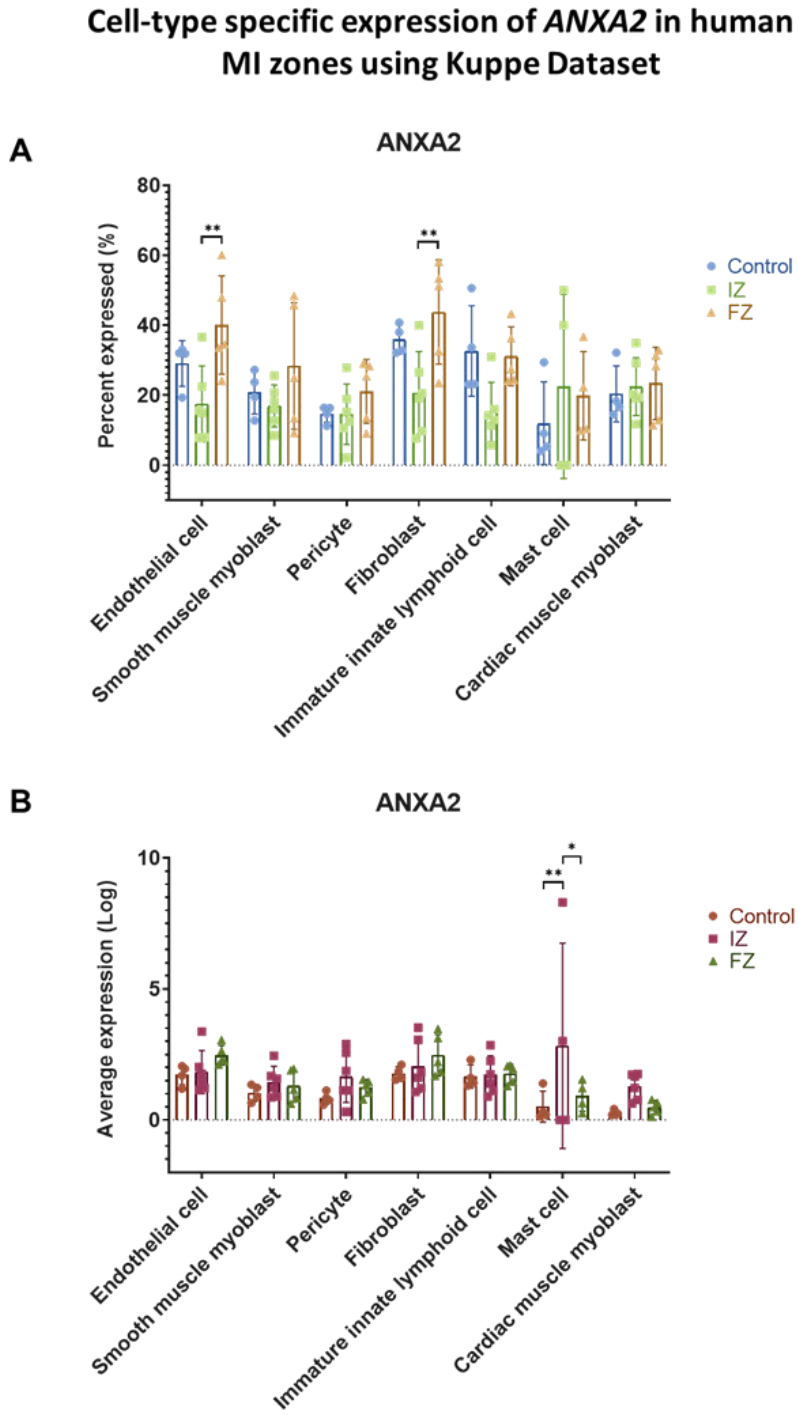

Figure 19. Single-cell transcriptomic profiling of ANXA2 across cardiac cell types in human control and myocardial infarction (MI). *(A) Percentage of cells expressing ANXA2 across different cardiac cell populations in control, infarct zone (IZ), and fibrotic zone (FZ) samples from human MI single-nucleus RNA-sequencing data*

(Kuppe et al., 2022). ANXA2 expression was enriched in endothelial cells and fibroblasts within the FZ compared with IZ. (B) Average ANXA2 expression levels (log-transformed) in the same cell populations show increased mast cell expression in IZ, compared with control and FZ. Statistical analysis was performed using two-way ANOVA with Tukey's multiple comparisons.

5.5 *SERPINE1* gene expression across cardiac cell types in control, ischaemic, and fibrotic zones.

The proportion of *SERPINE1*-expressing cells was significantly higher in all cardiac cell types in IZ regions of MI compared to control hearts, including in ECs, smooth muscle myoblasts, pericytes, fibroblasts, immature innate lymphoid cells, mast cells, and cardiac myoblasts. The largest change in the proportion of SERPINE1-expressing cell populations in IZ compared to controls were fibroblasts (% *SERPINE1*$^+$ fibroblasts = 47.83 ± 19.37 *versus* 4.40 ± 4.37, P = 0.0005), pericytes (%*SERPINE1*$^+$ pericytes = 42.28 ± 18.03 *versus* 1.62 ± 1.41, P = 0.0013) and cardiac muscle myoblasts (%*SERPINE1*$^+$ cardiac muscle myoblasts = 40.77 ± 19.18 *versus* 0.58 ± 0.27, P = 0.0014; two-way ANOVA multiple comparisons) (**Figure 20**).

Similarly, in the FZ of MI patient samples, the proportion of cells expressing *SERPINE1* was significantly elevated compared to healthy controls in multiple cell types, including ECs (%*SERPINE1*$^+$ = 29.97 ± 20.02 *versus* 2.29 ± 1.84, P = 0.0481), smooth muscle myoblasts (%*SERPINE1*$^+$ = 37.31 ± 22.67 *versus* 2.16 ± 1.88, P = 0.0085), pericytes (%*SERPINE1*$^+$ = 35.40 ± 23.93 *versus* 1.62 ± 1.41, P = 0.0120), and fibroblasts (%*SERPINE1*$^+$ = 43.95 ± 29.59 *versus* 4.40 ± 4.37, P = 0.0027; two-way ANOVA multiple comparisons) (**Figure 20**).

My analyses of average expression levels of *SERPINE1* in each cell type revealed a trend toward higher *SERPINE1* expression in most cell types in both IZ and FZ compared to healthy controls, although this did not reach statistical significance. The exception was fibroblasts, where *SERPINE1* average expression was significantly higher in FZ compared to controls (log average expression = 23.98 ± 30.68 *versus* 0.64 ± 0.85, P = 0.0002) and also significantly higher in FZ compared to IZ (log transformed average expression = 23.98 ± 30.68 *versus* 11.21 ± 6.34, P = 0.0322; two-way ANOVA multiple comparisons) (**Figure 20**).

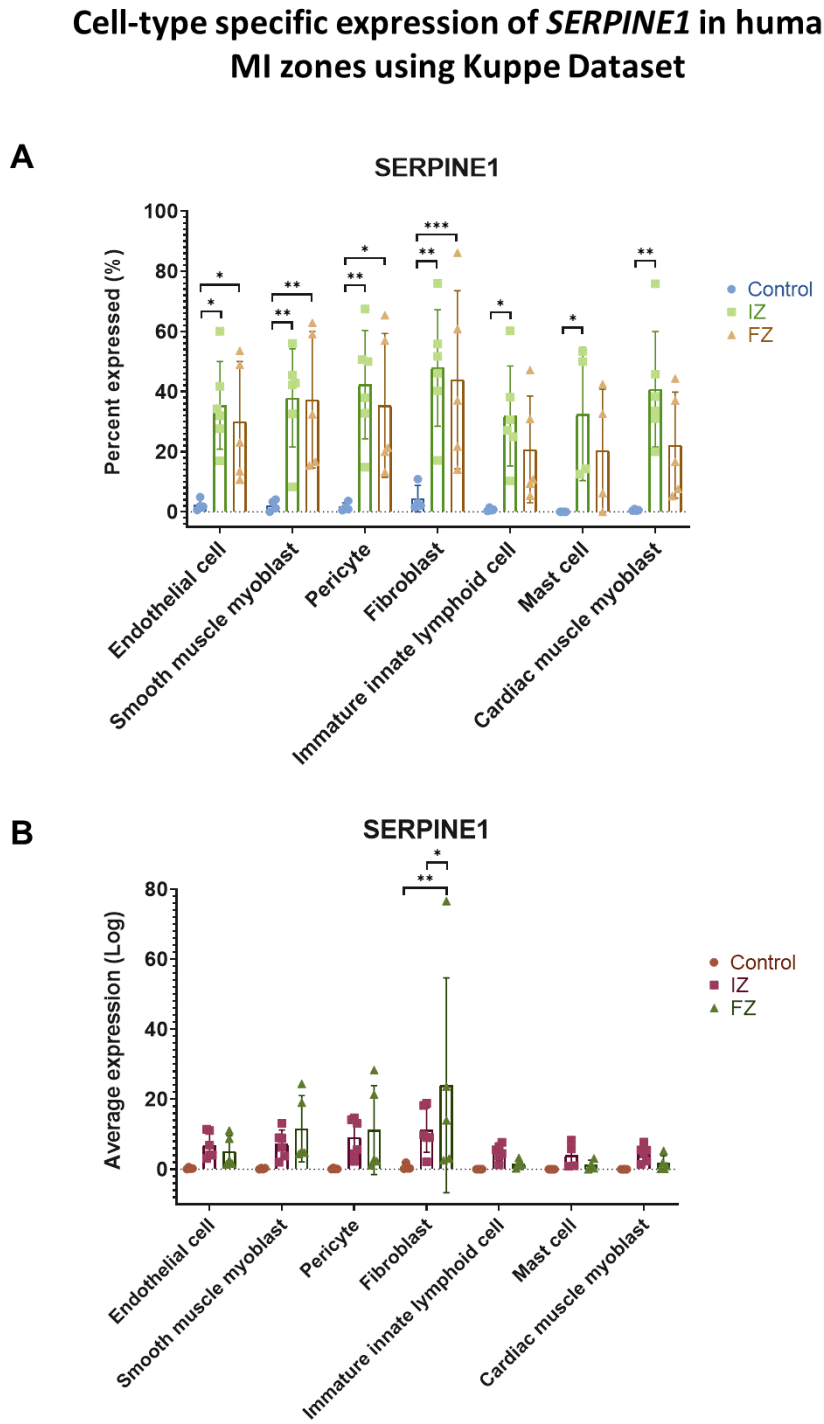

Figure 20. Single-cell transcriptomic profiling of SERPINE1 across cardiac cell types in human control and myocardial infarction (MI). *(A) Percentage of cells expressing SERPINE1 across different cardiac cell populations in control, infarct zone (IZ), and fibrotic zone (FZ) samples from human MI single-nucleus RNA-sequencing data (Kuppe et al., 2022). SERPINE1 expression was enriched in all cardiac cell types within the IZ compared with control. SERPINE1 expression was elevated in endothelial cells, smooth muscle myoblasts, pericytes, and fibroblasts within the FZ compared with control. (B) Average SERPINE1 expression levels (log-transformed) in the same cell populations show increased fibroblast expression in FZ, compared with control and IZ. Statistical analysis was performed using two-way ANOVA with Tukey's multiple comparisons.*

5.6 Discussion

In this chapter, I validated the transcriptomic findings from Chapters 3 and 4 by quantifying protein level expression of ANXA2 and SERPINE1 in the infarct border region of patients with MI, compared to the healthy heart. The results presented here provide supportive evidence that both ANXA2 and SERPINE1 were upregulated at the protein level in the infarct border zone of human MI hearts, including within ECs of the coronary vasculature, supporting their role in post-injury vascular and reparative processes.

The significant upregulation of ANXA2 within coronary vasculature of MI is consistent with my central hypothesis that *ANXA2* is a foetal endothelial gene reactivated after injury in the adult human heart. While enriched in ECs, ANXA2 was also observed in interstitial and perivascular fibrotic regions, suggesting expression in fibroblasts, immune cells, or other stromal populations involved in myocardial remodelling (**Figure 16**). Cell type analysis using the Kuppe dataset was able to confirm this identify of non-endothelial ANXA2^{+} cell populations (**Figure 19**). Given the established role of ANXA2 in plasmin generation, ECM remodelling, and angiogenesis; its upregulation likely facilitates neovascularisation and cardiovascular repair after MI (Liu and Hajjar, 2016b).

Double immunofluorescence staining of ANXA2 and Vimentin confirmed that many non-endothelial ANXA2^{+} cells were likely to be fibroblasts or myofibroblasts (**Figure 18**), which are critical mediators of wound healing and scar formation (Parvanian et al., 2023, Walker et al., 2019). The proportion of Vimentin^{+} cells within the ANXA2^{+} population significantly increased from 7% in controls to 54% in MI hearts, highlighting that ANXA2 may contribute to ECM turnover and fibroblast activation. This was further supported by cell type analysis using the Kuppe dataset, which further confirmed a significant enrichment of ANXA2-expressing fibroblasts and ECs in the fibrotic zone in patients with MI compared to the healthy heart.

Interestingly, cell type analysis (**Figure 19**) also revealed a mast cell-specific increase in *ANXA2* expression within the IZ in patients with MI. Cardiac mast cells are key regulators of both the initiation and resolution of inflammation; following MI, they increase in density, rapidly degranulate, and release bioactive mediators that drive cytokine cascades to promote early inflammatory healing (Shao et al., 2015). Mast cells also secrete anti-inflammatory factors that facilitate resolution and transition toward tissue repair, as well as growth factors, angiogenic mediators, and ECM regulators that influence matrix remodelling, granulation tissue formation, and neovascularisation (Jin et al., 2022, Frangogiannis, 2015). Mast cell-specific *ANXA2* upregulation suggests a role in immune-driven processes after MI, possibly immune-driven matrix remodelling and angiogenesis during early phase of inflammatory healing (Jin et al., 2022). Functionally, ANXA2 is known to facilitate leukocyte recruitment to site of inflammation, maintain VE-cadherin-mediated adherens junction

integrity, and promote angiogenesis for tissue repair, although dysregulation can lead to chronic inflammation (Dallacasagrande and Hajjar, 2020).

Previous studies of human heart failure support these observations. In human end-stage heart failure, ANXA2 mRNA and protein levels were increased by 67% and 41%, respectively (Song et al., 1998). And immunofluorescence studies revealed intense ANXA2 staining in ECs, the adventitia of coronary arteries, and the interstitial space between cardiomyocytes, but not in cardiomyocytes (Trouvé et al., 1999, Benevolensky et al., 2000). This interstitial localisation, combined with the known roles of ANXA2 in membrane trafficking and collagen binding, supports its involvement in ECM organisation and fibrosis development (Camors et al., 2005).

ANXA2 functions as a Ca^{2+}-dependent phospholipid-binding protein that regulates cellular processes involving membrane and cytoskeleton dynamics. By binding to the cell membranes, ANXA2 alters the membrane lipid rearrangements through modification in cholesterol distribution and lipid compaction, which may lead to an increase in order or disorder of the plasma membrane (Varyukhina et al., 2022, Camors et al., 2005). ANXA2 exists either as a monomer or as a heterotetrametric complex with S100A10, the latter reducing its calcium dependency and membrane interactions (Madureira et al., 2011, Bharadwaj et al., 2013). The absence of ANXA2 in cardiomyocytes from both non-failing and failing hearts indicates that its myocardial role likely does not involve direct regulation of cardiomyocyte Ca^{2+} handling but rather modulation of endothelial, stromal, and immune cell functions during injury and repair (Camors et al., 2005).

Similar to ANXA2, immunofluorescence showed that SERPINE1 protein expression was significantly upregulated in the infarct border zone of MI, specifically within ECs in the coronary vasculature, highlighting its potential role in endothelial activation and vascular regulation post-MI (**Figure 17**). Immunostaining and analyses of Masson's Trichrome-stained serial sections indicated that SERPINE1 expression was not restricted to ECs, but expression also appeared to be within vascular smooth muscle cells, infiltrating immune cells, fibroblasts, and myofibroblasts. This broad cellular distribution suggests a multifaceted role for SERPINE1, perhaps in coordinating tissue responses to injury. Previous studies in mice post-MI, showed that cardiomyocytes and fibroblasts in the infarct border zone exhibited abundant SERPINE1 mRNA, with additional expression observed in smooth muscle cells and perivascular mast cells surrounding coronary arteries (Takeshita et al., 2004). Immunohistochemical analysis further confirmed SERPINE1 antigen localisation within regions of interstitial fibrosis, consistent with a contribution of SERPINE1 to post-MI fibrotic remodelling and ECM stabilisation (Takeshita et al., 2004).

Cell type analysis using the Kuppe dataset revealed widespread *SERPINE1* induction in the IZ in patients with MI across multiple cell types, including smooth muscle myoblasts, pericytes, fibroblasts, immature innate lymphoid cells, mast cells, and cardiac myoblasts, confirming the identity of non-endothelial *SERPINE1*$^{+}$ cells

observed in immunofluorescence staining (**Figure 20**). This pattern indicated that SERPINE1 may coordinate a broad anti-fibrinolytic and tissue-stabilising response. Fibroblasts were the most significant *SERPINE1*-expressing cells in IZ, followed by pericytes and cardiac muscle myoblasts. In the FZ, the proportion of *SERPINE1* expression shifted, with ECs, smooth muscle myoblasts, pericytes, and fibroblasts showing significant upregulation compared to the healthy heart. However, only fibroblasts displayed a significant increase in average *SERPINE1* expression in the FZ, suggesting that they serve as a major source of *SERPINE1* during scar maturation. This aligns with the known roles of SERPINE1 in promoting collagen deposition and restricting matrix degradation, thereby contributing to ECM organisation and scar stability (Tuan et al., 2003, Ghosh and Vaughan, 2012).

As the principal inhibitor of plasminogen activators (tPA/uPA), SERPINE1 regulates fibrinolysis to maintain tissue homeostasis. During wound healing, elevated SERPINE1 limits protease activity, supporting repair, whereas excessive SERPINE1 in pathological conditions decreases fibrin degradation, promotes collagen and ECM accumulation, leading to fibrosis and persistent scarring (Ghosh and Vaughan, 2012, Tuan et al., 2003, Shaikh et al., 2024). Interestingly, in certain cardiomyopathies, SERPINE1 can also exert anti-fibrotic effects. In inflammatory-dilated cardiomyopathy (DCMi), elevated SERPINE1 diminished cardiac fibrosis by inhibiting TGF-β and myofibroblast activation, and correlates with a shift in macrophage populations from classical M1 toward non-classical M2 phenotypes (Baumeier et al., 2021). This dual functionality highlights SERPINE1 as a context-dependent regulator of ECM turnover, fibrosis, and tissue repair.

A key strength of this study lies in the multi-modal approach combining protein-level validation via immunofluorescence with single-nuclei transcriptomics and a cell type expression analysis. This chapter provides a multi-level view of ANXA2 and SERPINE1 regulation post-MI in the human heart, linking protein-level localisation and transcriptomic profiles, which strengthens confidence that observed mRNA upregulation is translated into functional protein responses in human tissues. The use of human MI samples further enhances the translational relevance of my findings. Moreover, the combination of endothelial-specific quantification, Vimentin co-localisation, and complementary bioinformatics analyses enables precise identification of the cell types expressing ANXA2 and SERPINE1 and allows for a more robust interpretation of their spatial distribution within the injured heart.

Several limitations should be considered. First, co-immunofluorescence with CD31 and target proteins was performed on a relatively small number of patient samples (n = 7), which may limit the generalisability of the findings and reduce the ability to capture inter-individual variation in MI pathology, comorbidities, or treatment history. Additionally, co-immunofluorescence analyses of Vimentin and ANXA2 were conducted on only 2 – 3 samples per group, providing only descriptive observations without sufficient statistical power. As a result, these data should be interpreted cautiously, as they may not fully reflect the broader spectrum of cellular responses or

pathological heterogeneity in human MI hearts. Future studies with larger patient cohorts will be necessary to validate these observations and allow robust quantitative comparisons. Second, although Vimentin is a widely recognised marker of fibroblasts and of epithelial-mesenchymal transition, it lacks specificity for fibroblasts/myofibroblasts as it also labels many stromal cells. Therefore, it would be ideal to include co-immunostaining with α-smooth muscle actin (α-SMA) or platelet-derived growth factor receptor alpha (PDGFRα) for a more precise and reliable indicator of fibroblast/myofibroblasts. Third, the cell type expression data were derived from the published Kuppe et al. (2022) dataset, which may not precisely match the timepoints post-MI or the exact histological regions analysed in our tissue sections. As it was not possible to get information of the timepoint post-MI for the human MI patients used in the immunostaining and histology study.

Finally, although protein expression and spatial localisation were quantified, functional validation using human cells was not performed, leaving the causal relationship between ANXA2/SERPINE1 upregulation and processes such as neovascularisation or ECM remodelling to be further established. However, this was already addressed using my *in vivo anxa2a/b* crispants zebrafish model, which provided functional insight into the role of ANXA2 in cardiovascular development and regeneration. Knockdown of *anxa2a/b* impaired embryonic growth, cardiovascular development, and ventricular recovery after laser-induced injury, with altered expression of angiogenic and regeneration-associated genes at 48 hpi. These findings provide direct evidence that ANXA2 contributes to injury-induced neovascularisation and functional cardiac regeneration. Importantly, these findings complement the human immunofluorescence and transcriptomic data by functionally demonstrating that ANXA2 is not merely a marker of injury response but an active regulator of vascular and myocardial repair. Nevertheless, additional mechanistic studies (such as cell type-specific knockdown or rescue experiments) will be necessary to determine the distinct functions of ANXA2/SERPINE1 in endothelial, fibroblast, and immune populations, and to understand how these proteins coordinate the balance between tissue repair and fibrosis in the injured human heart.

In conclusion, these results validated my multi-omics results presented from earlier chapters and demonstrated ANXA2 and SERPINE1 were reactivated/re-expressed at protein level in coronary ECs following MI. Their expression patterns, including localisation to both vascular and interstitial compartments, support potential roles in both endothelial activation and tissue remodelling post-MI. These observations suggest that *ANXA2* and *SERPINE1* may function as injury-response genes, contributing to the coordination of neovascularisation, inflammatory signalling, and reparative processes after injury. Together, the data revealed a dual role for these proteins in MI – mediating endothelial-dependent neovascularisation and potentially modulating fibroblast-driven scar remodelling. This positions *ANXA2* and *SERPINE1* as promising candidates for future mechanistic studies and potential therapeutic targeting to enhance post-MI repair.

Chapter 6: Results – Reactivation of the foetal endothelial gene *PABPC1* in myocardial infarction: implications for cardiac repair

6.1 Introduction

In Chapter 3, I highlighted how the application of scRNA-seq has transformed cardiovascular research by providing unprecedented molecular insight into coronary vessel development and vascular responses to ischaemic injury (Marín-Sedeño et al., 2021). I also introduced our in-house meta-analysis of integrated sc(n)RNA-seq data of coronary vascular ECs from both developing and adult mouse and human hearts, spanning healthy and diseased states (Li et al., 2022b). This comprehensive multi-species meta-analysis – referred to as CrescENDO – combined 18 independent studies comprising 14,482 ECs (12,231 mouse and 2,251 human) (**Table 1**). CrescENDO enabled us to characterise transcriptomic dynamics of coronary ECs across development, healthy, and disease, and to identify species-conserved, translationally relevant targets that may guide future strategies to enhance neovascularisation and cardiac regeneration (Li et al., 2022b).

From this work, we identified 752 (60.8%) genes that were upregulated in pro-regenerative (< postnatal day 7, P7) neonatal mouse coronary ECs but remained dormant in non-regenerative adult mouse coronary ECs post-MI. Similarly, in humans, seventeen differentially expressed genes (DEGs) were found to be highly expressed in coronary ECs from foetal hearts and in patients with dilated cardiomyopathy-induced heart failure (dHF), but expressed at low levels in ECs from uninjured adult human hearts (**Table 22**, **Figure 21**). These findings suggest that developmentally expressed genes or gene programmes can be reactivated under pathological conditions, leading to the hypothesis that such reactivation may stimulate developmental regenerative pathways and promote cardiac neovascularisation in the post-ischaemic adult heart.

Among the candidates identified in CrescENDO (**Table 22**, **Figure 21**), *PABPC1* (Poly(A)-binding protein cytoplasmic 1 or Polyadenylate-binding protein 1) emerged as a novel and understudied candidate, with its role in coronary neovascularisation post-MI yet to be defined. Therefore, I decided to further explore the role of *PABPC1* post-MI in the adult human heart.

In previous chapters, I have focused on ANXA2 and SERPINE1, which regulate fibrinolytic pathways and act through extracellular proteolysis and vascular remodelling. By contrast, PABPC1 represents a mechanistically distinct candidate, acting at the post-transcriptional level. PABPC1 is a well-established regulator of mRNA stability, translation, and cellular stress responses (Mangus et al., 2003), but its role in endothelial biology and cardiac regeneration remains poorly defined. Given its

upregulation during development and re-expression in disease states identified through CrescENDO, I aimed to investigate whether post-transcriptional regulation via PABPC1 could contribute to vascular regeneration after myocardial injury.

In this chapter, I therefore investigated *PABPC1* expression across complementary scRNA-seq datasets, including the human MI atlas published by Kuppe et al. (2022) and regenerating zebrafish heart dataset published by Ma et al. (2021). To gain further spatial and cellular resolution, I additionally integrated our in-house 10X Visium spatial transcriptomics data and performed cardiac cell type-specific expression analyses using the Kuppe dataset. Finally, I validated these transcriptomic findings at the protein level through immunofluorescence staining of human heart tissues (healthy and post-MI).

Building on these analyses, I next turned to the *anxa2a/b* zebrafish crispants, a model of impaired cardiac regeneration described in Chapter 4, to investigate whether the expression of PABPC1 paralogues (*pabpc1a* and *pabpc1b)* were influenced by *anxa2a/b* deficiency during development and/or in regeneration i.e. following laser-induced cardiac injury. Although the ANXA2-SERPINE1 axis has not previously been directly linked to PABPC1, the reactivation of *PABPC1* following myocardial injury across species made it an intriguing candidate to explore in the context of *anxa2a/b* loss. This allowed me to assess whether *PABPC1* paralogues form part of the broader translational and regenerative responses downstream of ANXA2.

Collectively, these studies build on the candidate gene framework established in earlier chapters, positioning *PABPC1* alongside *ANXA2* and *SERPINE1* as a complementary regulator of vascular repair. By integrating cross-species transcriptomics with analysis of *pabpc1a/b* mRNA expression in *anxa2a/b* crispants, this work provides a foundation for uncovering molecular pathways that may be harnessed to promote post-ischaemic neovascularisation and cardiac regeneration in humans.

Table 22. Common upregulated DEGs in foetal and dHF adult heart endothelial cells compared to the uninjured adult heart. *This shows the top expressed foetal genes, which have low expression in the healthy adult heart, but are re-activated*

(upregulated) in the injured adult heart, in dHF (heart failure caused by dilated cardiomyopathy). DEGs are ranked according to both P values and the average log2 fold change, with a summary of known role in neovascularisation post-MI (adapted from Li et al, 2022b).

Comparison	**Gene**	**log_2 fold change, (dHF/foetal)**	**Known role in neovascularisation post-MI**
Common upregulated DEGs between healthy foetal and dHF adult (vs. uninjured adult)	*RPL39 (ribosomal protein L39)*	0.35/2.61	n/a
	RPL11 (ribosomal protein L11)	0.36/1.91	n/a
	PTMA (*Prothymosin α*)	0.40/1.16	• PTMA was identified as a key paracrine factor released from cardiomyocytes in a ZEB2 (zinc finger E-box-binding homeobox 2)-dependent manner, where PTMA promotes angiogenesis and tissue repair following ischaemic injury (Gladka et al., 2021). • Overexpression of PTMA and TMSB4 (thymosin beta 4) promoted cardiomyocytes proliferation and preserved ejection fraction post-ischaemic injury in mice (Gladka et al., 2023).
	RPS11 (ribosomal protein S11)	0.37/1.19	n/a
	FN1 (*fibronectin 1*)	0.25/2.23	• Fibronectin is an extracellular matrix protein expressed along vertebrate endothelium-lined vasculature and is essential for embryonic cardiovascular development in both fish and mice (Astrof and Hynes, 2009). • Genetic inhibition of FN1 attenuated vasculogenesis and cardiogenesis in mice post-MI (Konstandin et al., 2013). • Paralogues fn1 and fn1b were deposited by injury-activated epicardial cells and were necessary

		for zebrafish cardiomyocyte proliferation and heart regeneration (Wang et al., 2013b). • FN1 expression was upregulated in the heart after myocardial ischemia/reperfusion injury (I/R). Pharmacological inhibition of FN1 attenuated I-R-induced cardiac infarction, myocyte apoptosis, inflammation, oxidative stress and fibrosis through activation of the AMP-LKB1-AMPK signalling pathway (Zhang et al., 2021).
NAP1L1 (Nucleosome assembly protein 1 like 1)	0.37/0.93	• NAP1L1 is upregulated in the hearts of patients with ischaemic cardiomyopathy and identified as a dysregulated hub protein in myocardial fibrosis post-myocardial infarction. Overexpression of NAP1L1 promoted cardiac fibroblasts proliferation, migration, and differentiation into myofibroblasts, leading to enhanced myocardial fibrosis (Li et al., 2023).
EFNB2 (EphrinB2)	0.47/0.63	• EphrinB2 plays an essential role in cardiovascular development, physiological and pathological postnatal angiogenesis, and cardiac remodelling after injuries (Su et al., 2019) • EphrinB2 protected ischaemic hearts post-myocardial infarction from remodelling and dysfunction through promoting cardiac lymphangiogenesis (Bai et al., 2024)
RPL10AP6 (ribosomal protein L10a pseudogene 6)	0.51/0.25	n/a
LTBP4 (latent transforming growth factor beta-binding protein 4)	0.55/1.02	LTBP4 regulates TGFβ activity and could protect against renal fibrosis by stimulating angiogenesis, suppressing inflammatory gene expression, and supporting mitochondrial structure in tubular epithelial cells (Su et al., 2021).
CCDC80	0.33/1.03	n/a

(Coiled-coil domain-containing protein 80)		
SOX4 (SRY-box transcription factor 4)	1.08/0.63	n/a
EEF2 (eukaryotic elongation factor 2)	0.61/1.01	n/a
HSPA5 (Heat Shock Protein Family A (Hsp70) Member 5)	0.40/0.86	n/a
FUS (fused in sarcoma)	0.76/0.77	n/a
PABPC1 (poly(A)-binding protein 1, cytoplasmic 1)	0.75/0.58	n/a
RTF1 (RTF1 homolog, Paf1/RNA polymerase II complex component)	0.27/0.43	n/a
TIMP2 (TIMP metallopeptidase inhibitor 2)	0.39/0.29	• TIMP-2 inhibits angiogenic factor-induced endothelial cell proliferation *in vitro* and angiogenesis in vivo (Seo et al., 2003) • TIMP2 deficiency significantly exacerbated left ventricular dilation and systolic dysfunction compared to WT mice post-MI (Kandalam et al., 2010).

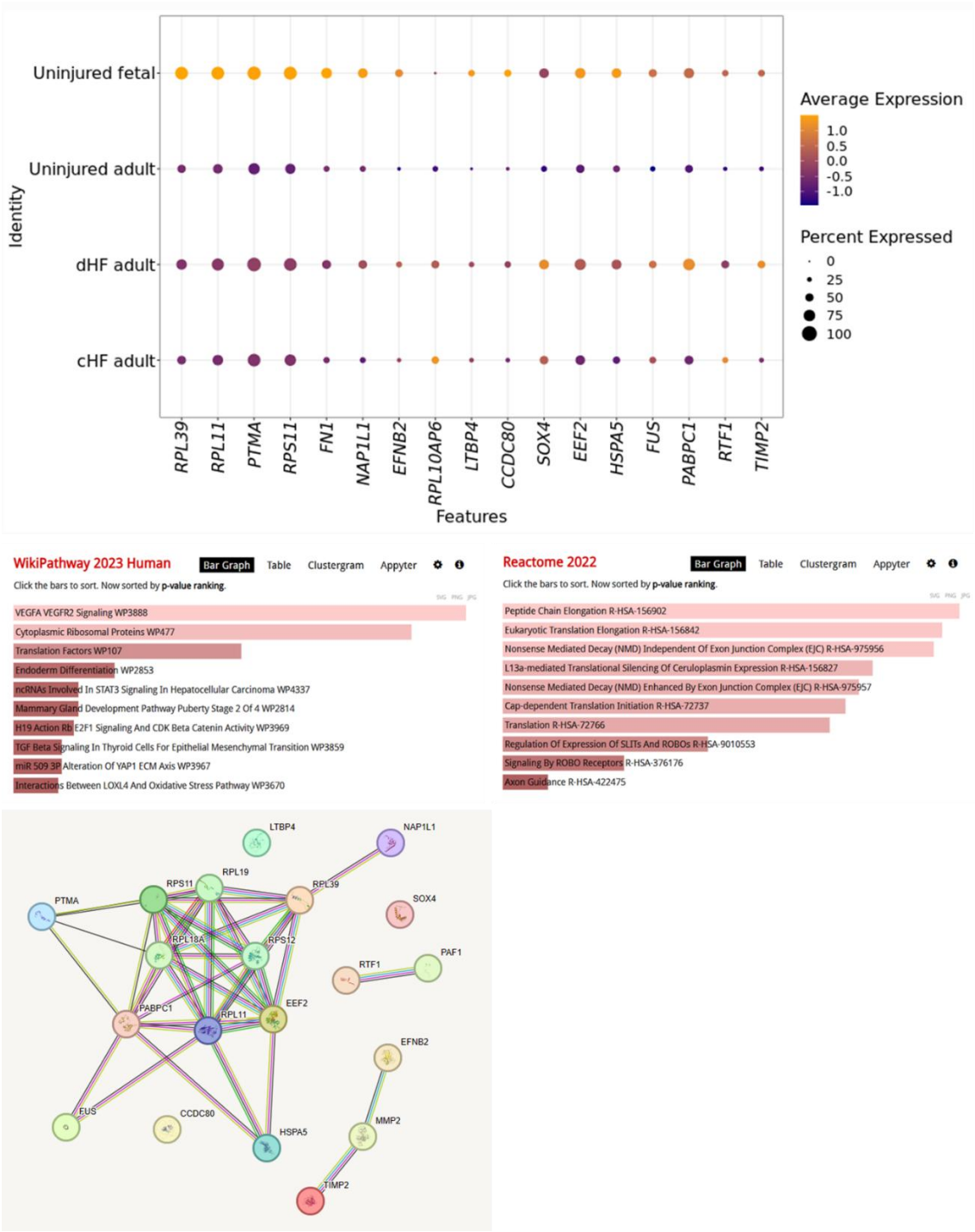

Figure 21. Dot plot generated from our coronary endothelial cell meta-atlas, CrescENDO, illustrating the common upregulated DEGs (n=17) in foetal and dHF/cHF adult heart ECs compared to the uninjured adult heart. *Dot size represents the percentage of ECs expressing target gene; colour indicates scaled average expression level (z-score). Bar graphs generated from EnrichR enrichment analysis (Kuleshov et al., 2016) show the common network / pathways shared between the 17 foetal genes. VEGFA/ VEGFR2 signalling ranks the highest which suggests angiogenic function. String network analysis shows potential functional links between the 17 foetal genes. For example, PABPC1 is co-expressed with the following proteins: EEF2, RPL11, RPS11, RPS12, HSPA5, FUS, and PTMA in humans, suggesting potential protein-protein associations.*

6.2 *PABPC1* as a novel candidate from CrescENDO and comparative gene expression analysis across multi-omics datasets

PABPC1 was first identified by the Brittan group as one of seventeen common DEGs in ECs in the foetal heart and in adult heart failure caused by dHF compared with uninjured adult hearts (**Table 22**, **Figure 21**) (Li et al., 2022b). *PABPC1* stood out as a candidate because it was consistently expressed at high levels in coronary ECs in both foetal and diseased/injured adult hearts but was almost absent in uninjured adult hearts. Given that its role in neovascularisation and cardiac repair has not been explored, *PABPC1* represented a novel and promising target for further investigation in post-ischaemic vascular regeneration.

Using the coronary EC meta-atlas, CrescENDO, I examined further both the expression levels of *PABPC1* and the percentage of ECs expressing the gene. In human foetal hearts, around 65% of coronary ECs exhibited strong *PABPC1* expression, whereas expression was very low in uninjured adult hearts. A similar pattern was observed in mice: around 52% of ECs expressed strong expression of *Pabpc1* in uninjured postnatal day 6 (P6) mouse hearts but became undetectable by P10 (**Figure 22**). In adult mice following MI, expression re-activated: around 90% of ECs upregulated *Pabpc1* at 14 days post-MI. In patients, *PABPC1* expression was very low in cHF, but around 75% of ECs expressed high levels in dHF (**Figure 22**).

To extend these findings, I analysed the Kuppe et al. (2022) endothelial-specific sc(n)RNA-seq dataset of the human heart after acute MI. This confirmed *PABPC1* upregulation in acute MI, with the highest expression observed in approximately 18% of ECs within the IZ, and the second highest in around 23% of ECs in the FZ (**Figure 22**). These results supported that *PABPC1* is “re-expressed” in endothelial populations following human MI.

Our in-house spatial transcriptomics dataset was then analysed to validate and complement the sc(n)RNA-seq findings. Although the study included a limited number of replicates (1-3 subjects per group; **Table 3**), which prevented robust quantification, the results were consistent across individuals and aligned with the transcriptomic analyses. Importantly, spatial transcriptomics provided additional localisation information: *PABPC1* was expressed at low levels in uninjured control hearts, but expression increased in both acute and chronic MI samples, with the highest levels appeared to be localised in the infarct border zone (**Figure 23**). This spatial enrichment is particularly relevant, as the border zone is the region most active in endogenous neovascularisation.

Finally, to assess evolutionary conservation and complement these murine and human datasets, I analysed *pabpc1* expression in regenerating adult zebrafish hearts using the endothelial-specific scRNA-seq dataset published by Ma et al. (2021). Temporal endothelial *pabpc1* expression was examined after cardiac injury by ventricular

resection (2, 7, and 14 days). Both zebrafish paralogues of *PABPC1* (*pabpc1a/b)* were upregulated following injury compared to uninjured hearts (day 0). *pabcp1a* was strongly expressed in 80% of ECs at 14 days post-injury (dpi), while *pabpc1b* showed peak expression in 20% of ECs at 7 dpi (**Figure 24**).

Taken together, these cross-species datasets, integrating both single-cell, single-nuclei, and spatial transcriptomics data, demonstrated *PABPC1* as a developmentally expressed endothelial gene that is re-expressed after myocardial injury. These findings provided a strong rationale for selecting *PABPC1* as a novel candidate target within the framework of my central hypothesis that reactivation of developmental genes may promote neovascularisation and cardiac regeneration in the injured adult heart.

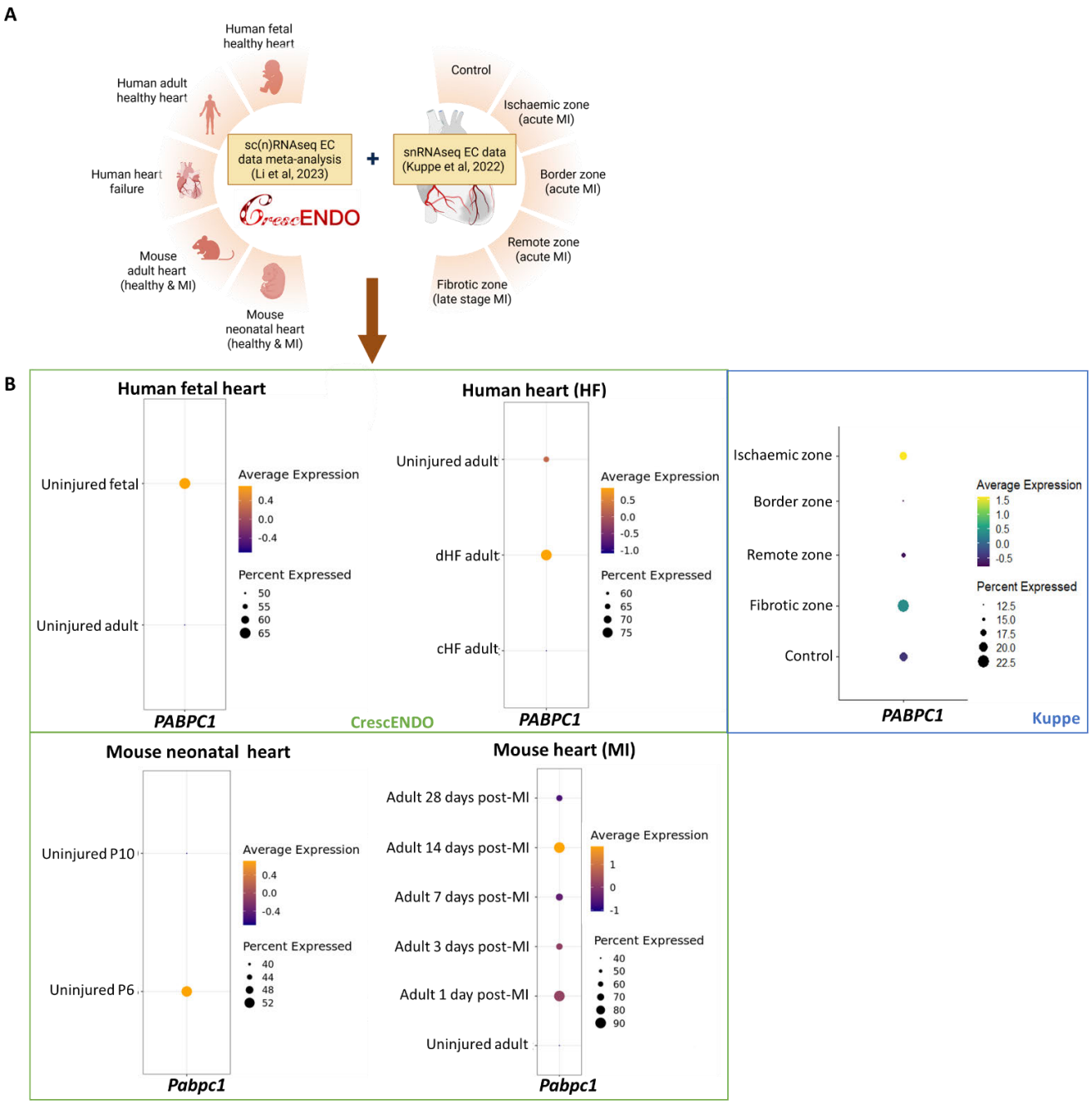

Figure 22. PABPC1, a foetal endothelial gene identified from CrescENDO, is reactivated in endothelial cells after myocardial injury across species and multi-omics datasets. *PABPC1 was first identified as one of the top 17 differentially expressed endothelial genes in CrescENDO, highly expressed during development, and reactivated after myocardial injury. (A) Schematic overview of datasets analysed, including the coronary EC meta-atlas CrescENDO (Li et al., 2022b) and the multi-omic map of human hearts after acute MI (Kuppe et al., 2022), covering foetal, adult healthy and diseased hearts. (B) Dot plots showing PABPC1 endothelial expression across (i) human foetal, adult, and heart failure (cHF, dHF), (ii) different myocardial zones post-acute MI (ischaemic, border, remote zone, fibrotic zone), (iii) neonatal mouse at P6 and P10, and (iv) adult mouse ECs at multiple time points post-MI. Dot size represents the percentage of ECs expressing PABPC1; dot colour indicates scaled average expression level (z-score).*

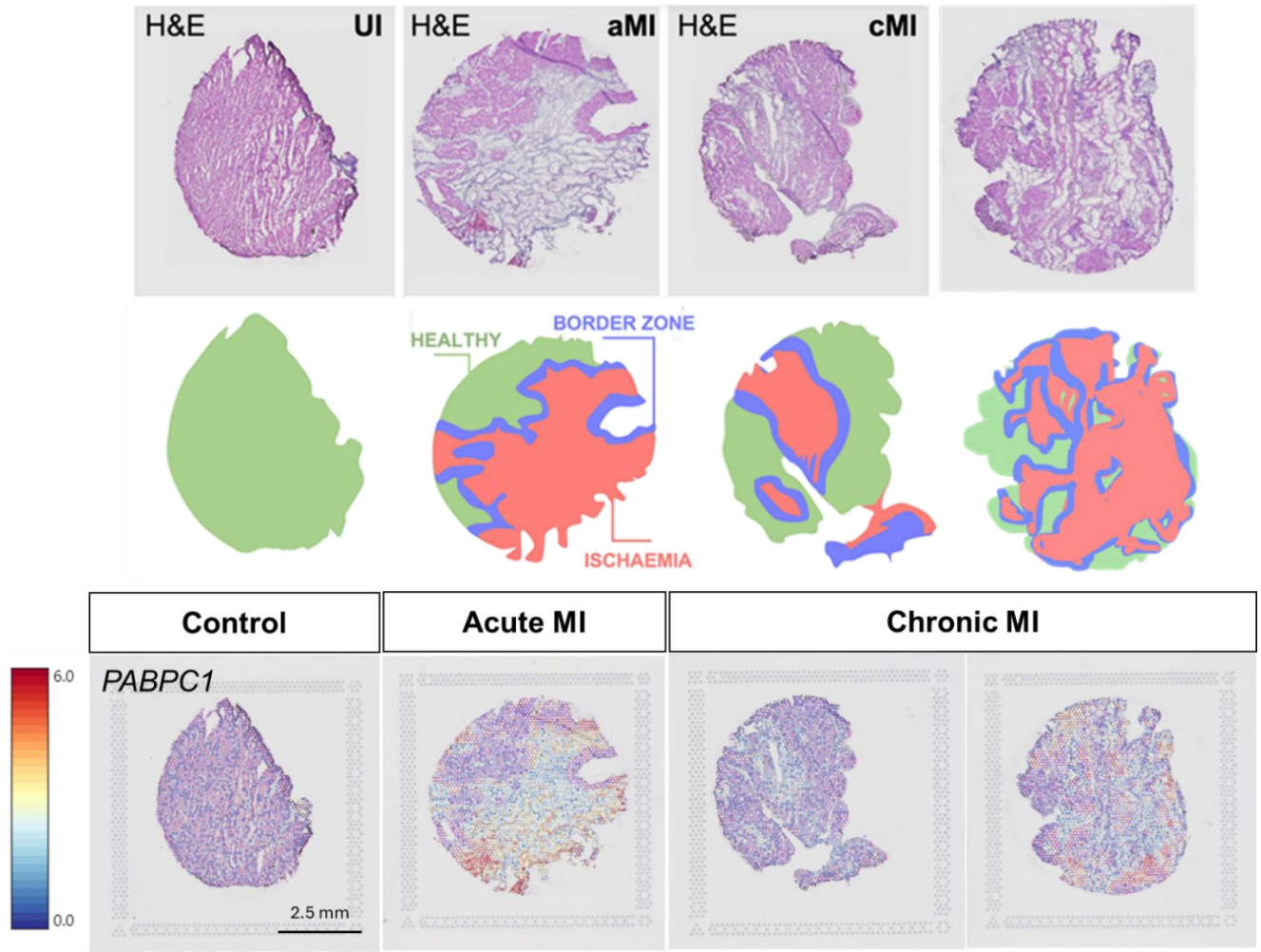

Figure 23. In-house spatial transcriptomic data showing sections of adult human heart tissue from an uninjured (UI), healthy control, patients presenting with acute MI (aMI) and chronic MI (cMI). *Panel 1 shows H&E staining of the tissue sections. Panel 2 highlights areas of healthy tissue (green), ischaemic damage (red), and ischaemic border zones (blue). Expression levels of PABPC1 are shown as the summed log-normalised counts (0-6). Each group included 1-3 subjects, and although the limited number of replicates precludes formal quantification, PABPC1 expression patterns were comparable across individuals, showing low expression in uninjured control hearts and increased expression in acute and chronic MI samples, with the highest expression localised to the infarct border zone.*

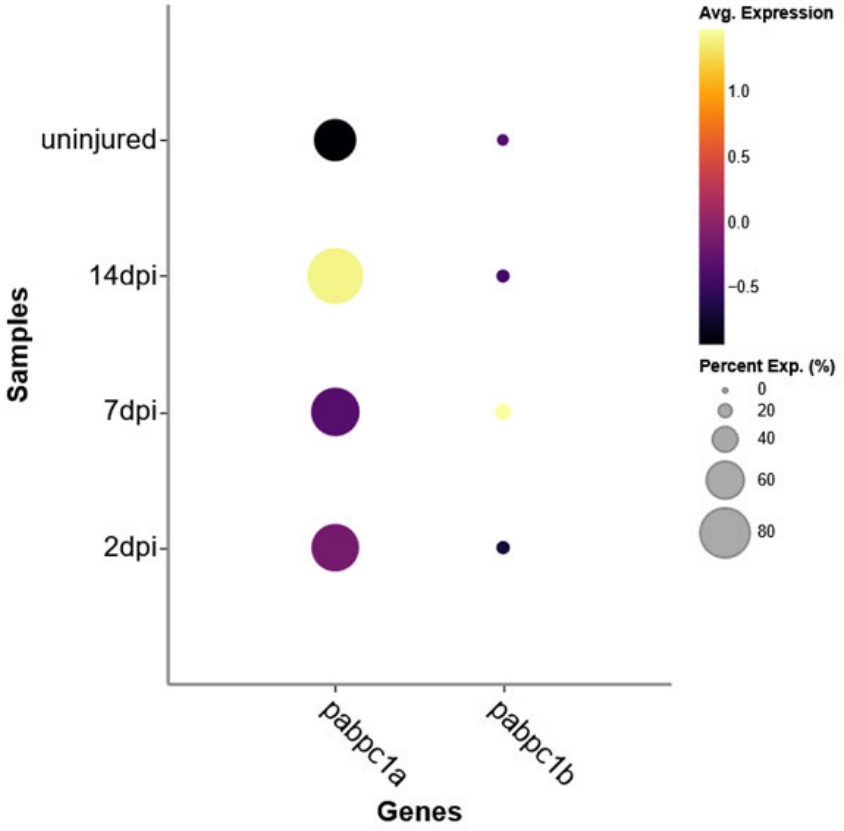

Figure 24. Expression of PABPC1 paralogues (pabpc1a and pabpc1b) from endothelial cell-specific adult zebrafish heart regeneration single cell transcriptomics data *(Ma et al., 2021). Dot plot showing the percentage of expressing cells and average expression level of pabpc1a and pabpc1b in zebrafish hearts at 2, 7, and 14 days post-injury (dpi) compared to uninjured controls. Dot size represents the percentage of ECs expressing pabcp1a/b; colour indicates scaled average expression level (z-score).*

6.3 Biological functions and mechanisms of PABPC1 and its potential implications in cardiovascular disease research

Poly(A) binding protein cytoplasmic 1 (PABPC1), also known as Polyadenylate-binding protein 1 (PABP1) acts as a multifunctional RNA-binding protein in the cytoplasm with central roles in post-transcriptional gene regulation (Sawazaki et al., 2018). *PABPC1* plays a critical role in post-transcriptional gene regulations such as transcription, transport, stability and translation through binding to the 3' poly(A) tails of mRNAs (Mangus et al., 2003). The best characterised function of PABPC1 is enhancement of translation by interacting with translation initiation factors at the 5'end of mRNA, promoting ribosome recruitment and hereby stimulating protein synthesis (Smith et al., 2014). Importantly, PABPC1 is not confined to the cytoplasm; it shuttles between the nucleus and cytoplasm, with RNA levels being a major determinant of its nucleocytoplasmic localisation (Gray et al., 2015). Beyond its primary function in translation, PABPC1 also regulates mRNA stability, trafficking, surveillance and nonsense-mediated mRNA decay, along with miRNA-induced translational repression and mRNA-specific activation (Smith et al., 2014, Hosoda et al., 2006). The gene-specific effects of *PABPC1* are very poorly defined; it usually needs other partner proteins/regulatory machinery e.g., eukaryotic initiation factor 4F (eIF4F) proteins for mRNA specific regulation (Zhai et al., 2023).

Emerging evidence suggests that PABPC1 is not only a regulator of mRNA dynamics but also a determinant of vascular cell function. Knockdown of *PABPC1* in human arterial ECs led to upregulation of $p16^{INK4a}$ with induced $p16^{INK4a}$ dependent cellular senescence, implicating *PABPC1* as a suppressor of cellular senescence and vascular ageing (Wu et al., 2021). In vascular smooth muscle cells (VSMCs), PABPC1 acts downstream of the long non-coding RNA (NONRATT011842), modulating VSMC proliferation and migration in a hypertensive rat model (Tan et al., 2020). Knockdown of PABPC1 significantly reduced rat VSMC proliferation and migration, whereas overexpression had the opposite effect (Tan et al., 2020). Together, these studies suggest that PABPC1 maintains vascular homeostasis and may influence pathological vascular responses.

Alterations in *PABPC1* expression and its function disrupts intra-tissue homeostasis and could contribute to the development of various tumour tissues and cancers. *PABPC1* expression is highly elevated in various tumours and associated with signalling pathways central to tumorigenesis, including Nfr2, Hippo, and PTEN signalling (Qi et al., 2022). For example, in oesophageal squamous cell carcinoma, *PABPC1* overexpression promotes angiogenesis and malignant progression by interacting with eukaryotic translation initiation factor 4G (eIF4G) to regulate eIF4G IFI27 mRNA stability via exosomal miR-21-5p/CXCL10 (Zhang et al., 2022). Such findings emphasise PABPC1 as a context-dependent regulator, capable of driving proliferation and angiogenesis in disease states.

The importance of PABPC1 in development is shown by animal and human studies. Morpholino-mediated knockdown of *PABPC1* in African clawed frog (*Xenopus laevis*) resulted in anterior and posterior developmental defects, embryonic lethality and impaired protein synthesis (Gorgoni et al., 2011). This highlights the critical role of *PABPC1* in embryonic development, likely through its role in mRNA-specific translation regulation and/or mRNA decay. In children, pathogenic variants in the PABP domain of *PABPC1* can lead to global developmental delay, movement coordination disorders, seizures, behavioural disorders, and mild facial dysmorphisms (Meret et al., 2022). This is likely due to disrupted translation initiation and impaired neurogenesis in cortical development. Additionally, the same study reported that *Pabpc1* knockdown in mouse embryo brains reduced neural progenitor cell proliferation, further highlighting its necessity for neurogenesis (Meret et al., 2022). These studies converge on the conclusion that *PABPC1* is essential for early development, largely through its role in translation regulation.

In the heart, PABPC1 has emerged as a key regulator of protein synthesis and growth. Another study demonstrated a key role for PABPC1 in modulating protein synthesis rates and hypertrophy in the heart. Chorghade et al found that PABPC1 is abundant in neonatal cardiomyocytes, where protein synthesis is high, but becomes reduced or silenced in adult cardiomyocytes, where protein synthesis is low due to limited cellular turnover. In adults, *PABPC1* expression is post-transcriptionally silenced through poly(A) tail shortening of its mRNA, reducing translation of *PABPC1* mRNA (Chorghade et al., 2017). Remarkably, in models of cardiac hypertrophy – whether induced by endurance exercise or disease – *PABPC1* expression and its poly(A) tail length are restored/enhanced, suggesting a critical role in cardiomyocyte proliferation and growth (Chorghade et al., 2017). These findings raise the possibility that targeted re-expression/overexpression of *PABPC1* could potentially be beneficial to a failing myocardium. Interestingly, while Chorghade et al. found that poly(A) tail shortening in adult mouse hearts was cardiomyocyte-specific, its role in other cardiac cell types, such as ECs and fibroblasts, remains unexplored. Since other cardiac cell types such as ECs and fibroblasts, can proliferate during pathological hypertrophy and influence the behaviour of cardiomyocytes (Gray and Gray, 2017). This raises the question of *PABPC1*'s broader function in other cardiac cell types.

Transcriptomic studies have further linked *PABPC1* to foetal gene reactivation in cardiovascular disease. D'Antonio et al. (2022) revealed that the reactivation of foetal-specific RNA-binding proteins, along with the accompanied re-expression of 1523 foetal-specific isoforms, has contributed to the transcriptome differences observed in heart failure when compared to healthy adult heart. Unlike the more relaxed transcriptional regulation seen in healthy adult cardiac tissue, foetal cardiac tissue demands a more stringent transcriptional regulation (D'Antonio et al., 2022). Similarly, during heart failure, there appears to be a return to this heightened level of transcriptional regulation. In line with this, *PABPC1* was differentially upregulated in induced pluripotent stem cell-derived cardiovascular progenitor cells compared to

adult heart or arterial tissue (D'Antonio et al., 2022). Our group's multi-species meta-analysis (CrescENDO) confirmed this finding, identifying *PABPC1* as a reactivated foetal endothelial gene after myocardial injury. This positions *PABPC1* as a candidate regulator of regenerative programmes in the adult heart. Finally, emerging evidence suggests RNA-binding PABPC1 might also have an interaction with N6-methyladenosine-single nucleotide polymorphisms that are associated with cardiovascular diseases including atrial fibrillation, MI, and myocardial hypertrophy (Huang et al., 2023).

In summary, PABPC1 emerges as a multifunctional regulator at the crossroads of RNA biology, development, and disease. Its canonical role in translation and mRNA turnover extends into vascular biology, cellular senescence, and cancer progression, emphasising its ability to influence cell proliferation, survival, and adaptation across diverse contexts. In the cardiovascular system, PABPC1 has a dual identity: abundant in the neonatal heart to support rapid growth, yet repressed in the adult myocardium until reactivated during hypertrophy or injury. Importantly, its re-expression in ECs after myocardial injury, as identified across multiple datasets, suggests a potential role in neovascularisation and tissue repair. However, the role of PABPC1 in ischaemic heart disease, especially in MI, remains largely unexplored. The precise mechanisms by which PABPC1 contributes to endothelial function, angiogenesis, and post-injury cardiac regeneration remain poorly defined. Its re-expression after myocardial injury, together with its known functions in translation, vascular cell biology, and hypertrophy, make it an intriguing target for future studies on neovascularisation and cardiac regeneration.

6.4 PABPC1 expression is induced during endogenous neovasculogenic responses in human heart

To assess PABPC1 protein expression in the human heart, immunofluorescence staining was performed on tissue sections from healthy controls and patients with MI. Five ROIs were analysed from each sample, focusing particularly on the infarct border zone, a known site of active neovascularisation post-MI (Gu et al., 2006, Ma et al., 2025). To avoid bias, adjacent sections stained with Masson's Trichrome were used to guide ROI selection and to confirm regions of infarct and scar formation. PABPC1 expression in the coronary endothelium in patients with MI were quantified using immunofluorescence staining for target protein combined with CD31 (a pan-endothelial cell marker).

Antibody specificity was first verified. A rabbit IgG isotype control showed no signal in human heart tissue, while positive control staining in mouse testes demonstrated the expected cytoplasmic localisation of PABPC1 in spermatocytes and round spermatids, consistent with previous reports (Kimura et al., 2009).

In healthy human hearts, PABPC1 expression appeared low, with some positive staining detected in ECs and surrounding interstitial cells. By contrast, in MI samples, PABPC1 expression was markedly upregulated, particularly in the infarct border zone. Quantitative analyses confirmed a significant increase in total $PABPC1^+$ cells in patients with MI compared to healthy controls (%$PABPC1^+$ cells = 59.63 ± 25.53 versus 31.50 ± 15.60, P=0.0492; unpaired t test) (**Figure 25**). Importantly, co-staining with CD31 revealed that endothelial PABPC1 expression was also significantly higher in patients with MI compared to controls (%$PABPC1^+$ CD31+ cells = 68.02 ± 15.56 *versus* 37.90 ± 18.57, P=0.0128; unpaired t test) (**Figure 25**). The proportion of ECs within the total PABPC1+ cell population was significantly higher in acute MI (%$CD31^+$ of total PABPC1+ cells = 51.40 ± 4.50 versus 40.00 ± 8.53, P=0.0212; unpaired t test). However, as per previous quantification of $CD31^+$ cell expression in MI compared to the healthy human heart, the overall proportion of $CD31^+$ ECs did not differ significantly between groups (**Figure 25**).

Although PABPC1 was strongly upregulated in vascular endothelium, it was not restricted to this cell type. PABPC1-positive staining was also observed in other cell populations within the infarcted tissue, likely inflammatory cells, fibroblasts, and myofibroblasts, as identified by their distinct morphology and distribution within collagen-rich scar areas identified by Masson's Trichrome staining (**Figure 25**).

Overall, these data demonstrate that PABPC1 protein expression is induced in the human heart following MI, with a pronounced increase in ECs at the infarct border zone. This supports transcriptomic findings of PABPC1 reactivation in injured endothelium and highlights its potential involvement in endogenous neovascularisation and tissue repair processes.

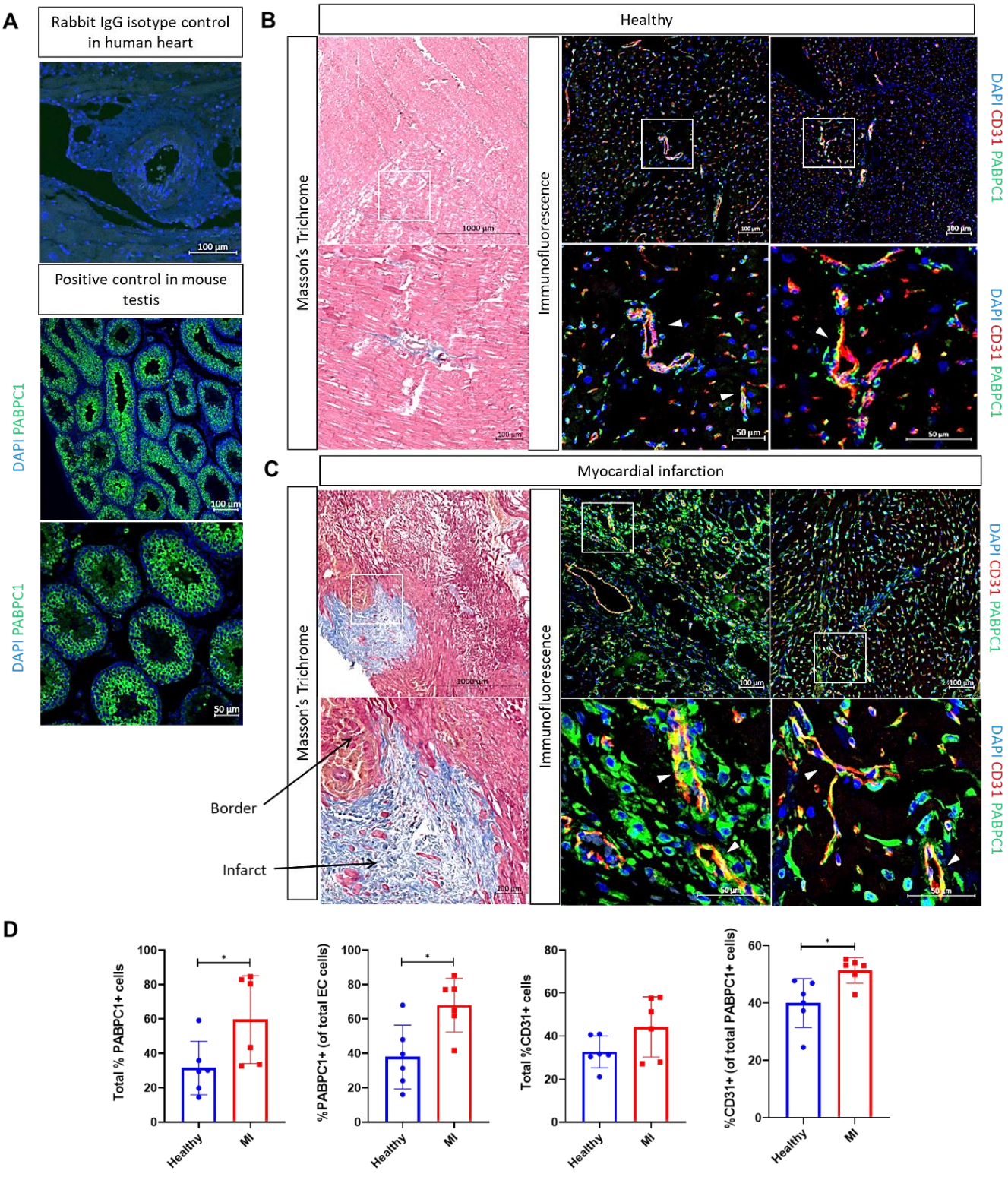

Figure 25. PABPC1 protein expression is induced in endothelial cells of the human heart following myocardial infarction (MI). (A) Representative images showing validation of antibody specificity: no signal in rabbit IgG isotype control (human heart, negative control) and strong cytoplasmic staining in mouse testis (positive control). (B, C) Middle panels show representative images of Masson's Trichrome staining of healthy and MI human heart tissue used to identify infarct and

border zones. Right panels show immunofluorescence staining for PABPC1 (green), endothelial marker CD31 (red), and nuclei (DAPI, blue) in healthy and MI hearts. PABPC1 immunostaining was not restricted to endothelial cells in MI. Staining also appeared to be in fibroblasts, myofibroblasts, and inflammatory cells within collagen-rich infarct and scar regions, implying PABPC1 upregulation may represent a broader injury-responsive program, potentially influencing fibroblast activation, extracellular matrix deposition, and immune responses. (D) Quantification of (i) total %PABPC1$^+$ cells, (ii) % PABPC1$^+$ cells within total CD31$^+$ population, (iii) total %CD31+ cells, and (iv) %CD31$^+$ cells within total PABPC1$^+$ population across healthy controls and MI hearts. Total PABPC1+ cells and endothelial PABPC1 expression in MI were significantly higher compared to healthy controls. The proportion of endothelial cells within the total PABPC1$^+$ cell population was significantly increased in MI hearts compared with controls.

6.5 *PABPC1* gene expression across cardiac cell types in control, ischaemic, and fibrotic zones.

To complement the immunofluorescence analysis and to determine the contribution of non-EC populations to PABPC1 expression, I next examined *PABPC1* expression across multiple cardiac cell types using the Kuppe dataset. Because ECs are not the only cell type activated during injury, it was important to evaluate whether other cardiac and immune populations also contribute to *PABPC1* expression. This cell type-specific expression analysis compared control (uninjured) myocardium with the ischaemic zone (IZ; necrotic myocardium) and fibrotic zone (FZ; late-stage scar). These regions were selected to capture cell populations actively engaged in acute injury responses and scar formation, thereby providing further insight into the potential roles of PABPC1 in post-MI repair.

Expression levels were evaluated in two ways: i) the percentage of cells within each cell type-specific cluster that expressed *PABPC1* and ii) the average expression level (log-transformed) in all cells in each cluster. Both immature innate lymphoid cell and cardiac muscle myoblast clusters showed higher expression of *PABPC1* in the FZ compared to the IZ (%*PABPC1*$^+$ immature innate lymphoid cells = 35.20 ± 8.78 *versus* 15.91 ± 9.50, P = 0.0077; %*PABPC1*$^+$ cardiac muscle myoblast = 36.05 ± 9.82 *versus* 18.72 ± 4.26, P = 0.0186; two-way ANOVA multiple comparisons). Notably, the immature innate lymphoid cell cluster showed a significantly lower expression of *PABPC1* in the IZ compared to control (%*PABPC1*$^+$ immature innate lymphoid cells = 15.91 ± 9.50 *versus* 38.64 ± 17.60, P = 0.0028, two-way ANOVA multiple comparisons) (**Figure 26**). In contrast, other major cell types, including ECs, smooth muscle myoblasts, pericytes, fibroblasts and mast cells, did not display significant differences in the percentage of PABPC1-expressing cells across zones. This contrasts with the original CrescENDO analysis, in which I identified *PABPC1* as upregulated in ECs in

dHF patients, and with my immunostaining results, which showed increased protein level of PABPC1 in the coronary vasculature post-MI.

When analysing average expression levels (log-transformed), no statistically significant changes in *PABPC1* expression were observed across any of the cardiac cell types when comparing diseased regions i.e., between control, IZ, and FZ. Thus, while shifts in the percentage of *PABPC1+* cells occurred in specific non-EC cell clusters such as immature innate lymphoid cells and cardiac muscle myoblasts, the average expression levels per cell did not substantially vary across myocardial zones (**Figure 26**).

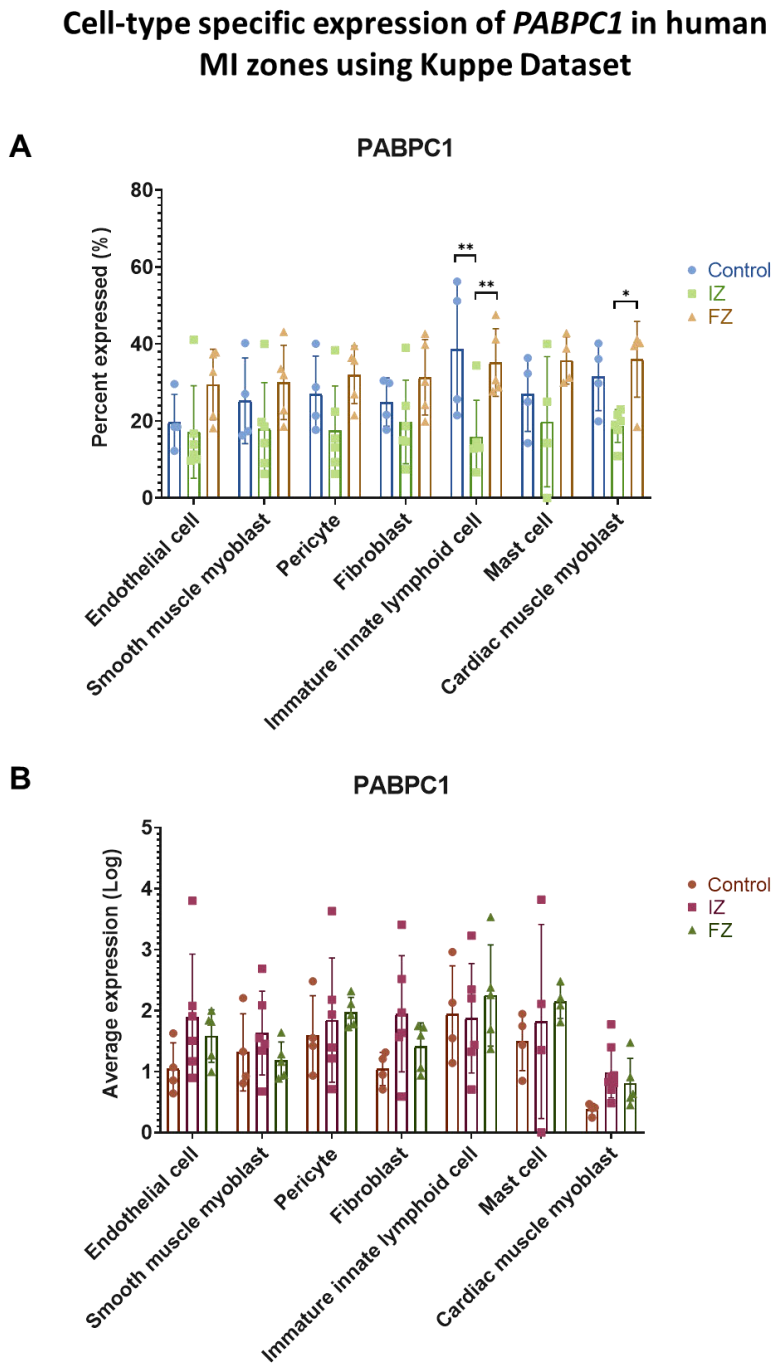

Figure 26. Cell type–specific expression of PABPC1 in control, ischaemic (IZ), and fibrotic (FZ) myocardial zones. *Analysis of the Kuppe et al. single-cell dataset was performed to assess PABPC1 expression across major cardiac cell populations. (A) Percentage of PABPC1+ cells within each cell type cluster. A higher proportion of PABPC1+ immature innate lymphoid cells and cardiac muscle myoblasts was observed in the fibrotic zone compared to the ischaemic zone, while immature innate lymphoid cells showed significantly reduced PABPC1 expression in the ischaemic zone compared to controls. (B) Average expression intensity (log-transformed) of PABPC1 across all cells within each cluster. No significant differences were detected across myocardial zones, suggesting that the main change lies in the proportion of PABPC1+ cells rather than in uniform upregulation across each population. Statistical analysis was performed using two-way ANOVA with Tukey's multiple comparisons.*

6.6 *PABPC1* paralogues expression in *anxa2a/b* crispants before and after cardiac laser injury

Given the consistent re-expression of *PABPC1* following myocardial injury across multiple species and datasets, I next investigated whether this translational regulator was affected by the loss of *anxa2a/b* during heart regeneration, and as described in Chapter 4, I examined their expression in *anxa2a/b* crispants at 48 hours post-injury (hpi) out of curiosity. While the *ANXA2-SERPINE1* axis has not previously been directly linked to *PABPC1*, the emerging role of *PABPC1* as a reactivated foetal gene made it an interesting candidate to assess in this model.

RT-qPCR was performed using cDNA generated from pooled 5 dpf larvae (20-30 per group), with expression normalised to housekeeping genes (*b2m*, *rpl7*) and relative quantification calculated using the ΔΔCt method, presented as $\log_2$ relative quantification (RQ; $2^{-\Delta\Delta Ct}$).

In uninjured zebrafish, the expression of *pabpc1a* and *pabpc1b* was unchanged in both mild and moderate *anxa2a/b* crispants compared to WT controls (Figure 6). However, this pattern shifted following laser-induced cardiac injury. At 48 hpi, *pabpc1a* expression was significantly downregulated in both mild (Log_2 fold change in *pabpc1a* expression = -0.16 ± 0.07 *versus* 0.00 ± 0.03, P = 0.0364) and moderate crispants (Log_2 fold change in *pabpc1a* expression = -0.39 ± 0.15 *versus* 0.00 ± 0.03, P = 0.0001; one-way ANOVA multiple comparisons) compared to WT (Figure 6). Moreover, *pabpc1a* levels were further reduced in moderate compared with mild crispants (Log_2 fold change in *pabpc1a* expression = -0.39 ± 0.15 *versus* -0.16 ± 0.07, P = 0.0099), consistent with a dose-dependent effect of *anxa2ab* deficiency. In contrast, *pabpc1b* was specifically downregulated in moderate crispants only, compared with WT at 48hpi (Log_2 fold change in *pabpc1b* expression = -0.26 ± 0.14 *versus* 0.01 ± 0.06, P = 0.0131) (**Figure 27**).

In summary, these data reveal that while *PABPC1* paralogues (*pabpc1a/b*) were unaffected by *anxa2a/b* loss in uninjured hearts, their expression fails to be maintained following injury in *anxa2a/b* crispants.

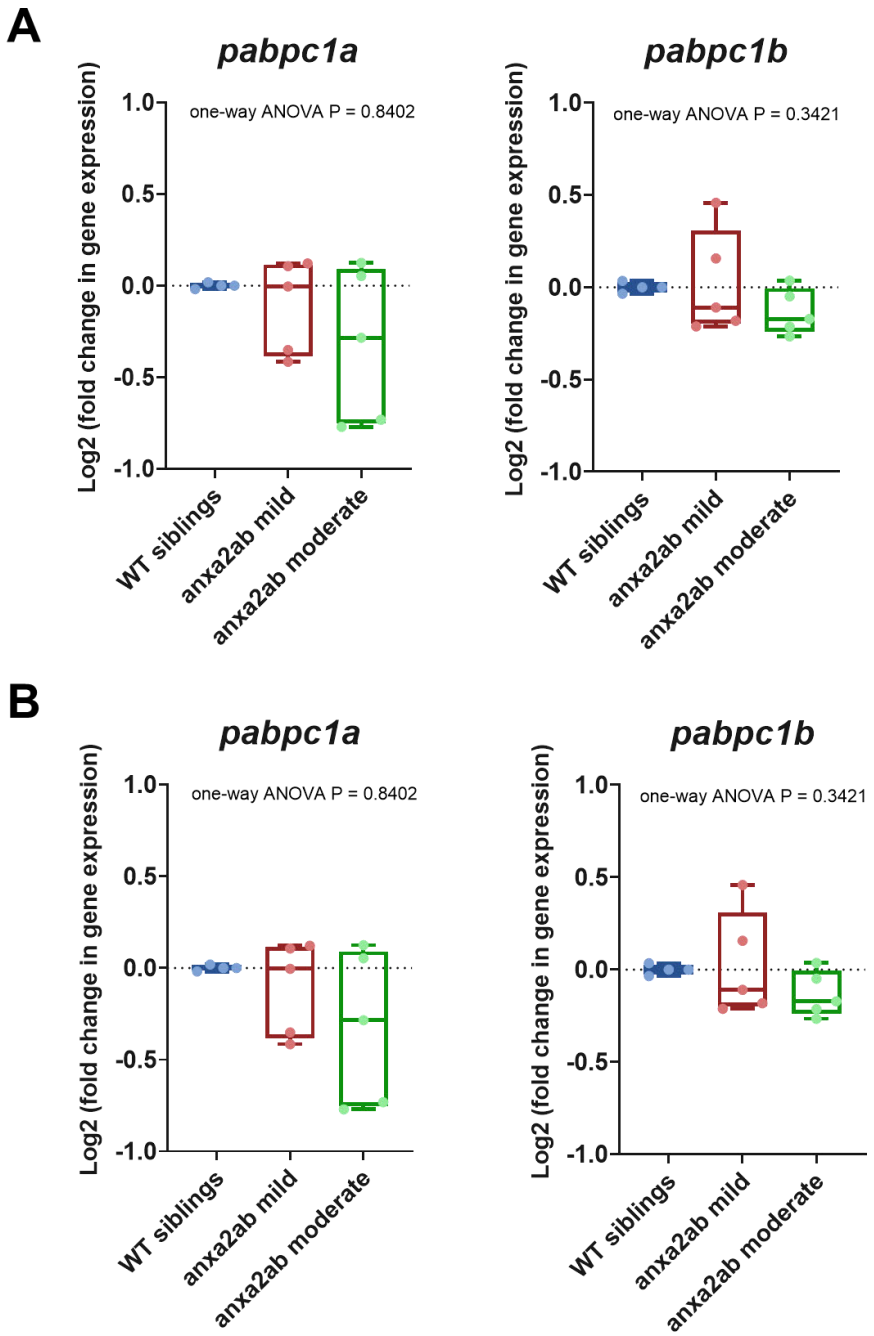

Figure 27. PABPC1 paralogues (pabpc1a/b) expression in anxa2a/b crispants before and after laser cardiac injury. *qPCR analysis of pabpc1a (left) and pabpc1b (right) in uninjured and injured (48 hours post-injury, hpi) zebrafish hearts. (A) In uninjured hearts, pabpc1a and pabpc1b expression was unchanged in both mild and moderate anxa2a/b crispants compared with uninjured sibling controls. (B) Following laser-induced cardiac injury, pabpc1a expression was significantly reduced in both mild and moderate crispants compared with wild-type (WT), with further suppression in moderate compared to mild phenotypes. pabpc1b expression was specifically downregulated in moderate crispants relative to WT. Data represent log_2 fold-change in expression relative to controls. Statistical analysis was performed using one-way ANOVA with Tukey's multiple comparisons.*

6.7 Discussion

The data presented in this chapter demonstrate that *PABPC1* is a developmentally expressed gene that is reactivated in ECs following myocardial injury across multiple species, supporting its candidacy as a regulator of post-ischaemic vascular regeneration. *PABPC1* was initially identified by the CrescENDO meta-analysis (Li et al., 2022b) as one of seventeen DEGs expressed by ECs in the foetal human heart and in patients with dHF, but not in patients cHF (***Table 1***, **Table 22**, **Figure 21**). The heart failure samples used in this CrescENDO originated from Wang et al., 2020 and included six male patients (range of ages was 21-52 years; median age 45.5 years), with two patients progressing from cHF and four progressing from dHF (Wang et al., 2020a). The same analysis showed that *PABPC1* was not expressed in the healthy adult human heart ECs. This suggests that *PABPC1* may play a role in coronary vascular development and becomes dormant in the adult healthy heart, but is reactivated under pathological stress. Notably, the low expression of *PABPC1* in cHF and contrasting pronounced expression in dHF, may imply that *PABPC1* re-expression is dependent on the type and severity of cardiac pathology, potentially reflecting differences in residual regenerative capacity or endothelial plasticity.

Cross-species analyses supported the potential role of *Pabpc1* during coronary vascular developmental and its re-induction after adult injury (**Figure 22**). In mice, *Pabpc1* expression was high in neonatal coronary ECs at postnatal day 6 (P6) but silenced by P10 and into adulthood (Li et al., 2022b), coinciding with a well-reported loss of cardiac regenerative capacity by postnatal day 7 in this species (Porrello et al., 2011, Haubner et al., 2012). Similar to the human heart endothelium, *Pabpc1* was reactivated in adult mouse ECs at 14 days post-MI.

Human MI sc(n)RNA-seq data (Kuppe et al., 2022) revealed an upregulation of *PABPC1* in ECs within the infarct and fibrotic zones, compared to the healthy human heart. The cardiac samples used in the Kuppe dataset included four control donors (range of ages was 44-61 years; median age 51 years; 75% male, 25% female), six patients for FZ (range of ages was 58-74 years; median age 63 years; 83.3% male, 16.7% female), twelve patients for IZ (range of ages was 29-66 year; median age 48.5 years; 66.7% male, 33.3% female) (**Figure 22**).

Analysis of in-house spatial transcriptomics datasets from patients with MI and healthy heart controls showed *PABPC1* expression was increased post-MI and was localised to the infarct border zone in MI – the region most active in neovascularisation (**Figure 23**). These data support a functional relevance in post-ischaemic repair and provide novel spatiotemporal context.

In regenerating adult zebrafish hearts (Ma et al., 2021), endothelial-specific scRNA-seq revealed upregulation of both paralogues, *pabpc1a* and *pabpc1b*, after ventricular apex amputation (**Figure 24**). The peak of *pabpc1b* expression was at day 7 post-injury, this may coincide with the onset of the proliferative and angiogenic phase (7-14 days post-injury) of cardiac regeneration, which follows the initial acute inflammatory

phase (1-3 days post-injury) (Lien et al., 2012, Kikuchi et al., 2010). This proliferative and angiogenic phase is characterised by active cardiomyocyte proliferation, endocardial activation, and neovascularisation (Lien et al., 2012, Ross Stewart et al., 2021). In contrast, the peak of *pabpc1a* expression at day 14 post-injury likely corresponds to a stage when substantial regeneration has already occurred, with active cardiomyocyte proliferation and vascular maturation, preceding the remodelling and maturation phase (14-30 days post-injury) (Ross Stewart et al., 2021, González-Rosa et al., 2011). These temporal expression differences indicate potential paralogue-specific contributions to distinct stages of zebrafish cardiac regeneration.

Mechanistically, *PABPC1* is a central regulator of post-transcriptional gene expression, enhancing translation through interactions with poly(A) tails and translation initiation factors while also modulating mRNA stability and decay (Mangus et al., 2003, Smith et al., 2014). Depletion of *PABPC1* disrupts the abundance and stability of specific mRNA populations, particularly those encoding proteins with regulatory or constitutive functions, by impairing the ability to prevent deadenylation-independent mRNA decay (Kajjo et al., 2022). This highlights a critical role for *PABPC1* in maintaining translational homeostasis and ensuring the sustained production of proteins essential for cellular function and stress responses. Its re-expression in diseased/injured ECs is therefore possibly crucial for stabilising mRNAs encoding proteins required for endothelial activation, neovascularisation, and coordinated repair programs.

Supporting evidence further shows that PABPC1 suppresses endothelial senescence (Wu et al., 2021) and regulates vascular smooth muscle proliferation and migration (Tan et al., 2020), emphasising its importance in vascular adaptation. In the heart, PABPC1 is abundant in neonatal cardiomyocytes but silenced in adulthood, only to be reactivated during hypertrophy or stress where it restores protein synthesis capacity (Chorghade et al., 2017). This developmental “switch” mirrors its post-injury reactivation in the endothelium observed in this Chapter. By controlling mRNA stability and translation efficiency, PABPC1 could coordinate the rapid production of pro-angiogenic factors and stress-response proteins, complementing extracellular pathways such as the ANXA2 in fibrinolysis and neovascularisation (Chorghade et al., 2017). However, my cell type-specific analysis using the Kuppe et al, 2022 dataset did not reveal any statistically significant expression of *PABPC1* in cardiomyocytes from MI patients. Thus, it is possible that *PABPC1* may operate different mechanisms in different diseased states.

Immunofluorescence analysis validated these transcriptomic findings and provided protein-level confirmation that PABPC1 is re-expressed in the human heart after MI, with specific enrichment in coronary ECs of the infarct border zone (**Figure 25**). Total $PABPC1^+$ cells, as well as $CD31^+$ $PABPC1^+$ cells were significantly higher in MI compared to healthy hearts. Importantly, the proportion of $CD31^+$ ECs within the $PABPC1^+$ population increased without a corresponding increase of total EC numbers, indicating selective upregulation within existing ECs rather than proliferation. This suggests that PABPC1 could contribute to an endothelial activation programme

triggered by myocardial injury, supporting pro-angiogenic and reparative responses in the infarct border zone.

PABPC1 immunostaining was not restricted to ECs in MI (**Figure 25**). Staining also appeared to be in fibroblasts, myofibroblasts, and inflammatory cells within collagen-rich infarct and scar regions, implying PABPC1 upregulation may represent a broader injury-responsive program, potentially influencing fibroblast activation, extracellular matrix deposition, and immune responses. Complementary cell type-specific analysis of the Kuppe dataset further revealed that the percentage of cells within each cluster that expressed *PABPC1* was significantly higher in immature innate lymphoid cells and cardiac muscle myoblasts within the FZ compared to the IZ (**Figure 26**). This suggests possible roles for PABPC1 in immune-mediated scar organisation, cytokine production, and myogenic adaptation during post-MI response. Studies have shown that PABPC1 links poly(A)-tail length to translational efficiency in early stages of development, while at later stages of development, its main function shifts toward protecting mRNAs and maintaining their stability (Xiang and Bartel, 2021). My findings suggest that the re-expression of *PABPC1* in injured cardiac populations likely serves a similar context-dependent function. In the acute injury phase, PABPC1 likely promotes rapid translation of pro-angiogenic and stress-response mRNAs. And subsequently, it stabilises mRNA to sustain protein synthesis to support vascular repair and scar formation. This mechanism aligns with the temporal and cell type-specific induction patterns observed across endothelial, immune, and myogenic populations in post-MI hearts.

Initially, I analysed the EC-specific snRNA-seq dataset from Kuppe et al., 2022, which showed *PABPC1* upregulation in ECs, with the highest expression in approximately 18% of cells in the IZ and the second highest in around 23% of cells in the FZ (**Figure 22**). However, a complementary cell type-specific analysis (**Figure 26**) comparing major cardiac cell types across IZ, FZ, and control zones, revealed no statistically significant difference in either the average log-transformed expression levels or the percentage of *PABPC1*-expressing cells within endothelial clusters. In contrast, immunofluorescence confirmed clear protein-level upregulation in the coronary vasculature post-MI in the human heart compared to the healthy heart. This inconsistency may reflect differences in post-transcriptional regulation of PABPC1, where mRNA levels do not always correlate directly with protein levels, and averaging across heterogeneous EC populations may mask subpopulation-specific increases. These observations highlight the importance of integrating transcriptomic and protein-level analyses to fully capture context-dependent regulation.

Functional investigation in *anxa2a/b* larval zebrafish crispants (< 5 dpf) revealed that *pabpc1a* and *pabpc1b* expression were largely unaffected at baseline (i.e. without injury) (**Figure 27**), indicating that *ANXA2* is not required for maintaining stable levels of *PABPC1* under normal, uninjured conditions. However, following laser-induced cardiac injury, both paralogues were downregulated in a dose-dependent manner, with *pabpc1a* more strongly affected and *pabpc1b* reduced only in moderate crispants

(**Figure 27**). This suggests differential sensitivity of the paralogues to *anxa2a/b* deficiency after injury. These findings indicate that injury-induced upregulation of *pabpc1a/b* requires intact *anxa2a/b* signalling. In the absence of ANXA2, the translational program normally activated during regeneration fails to engage, likely limiting neovascularisation and myocardial repair processes. Given the established roles of PABPC1 in mRNA stabilisation, translational efficiency, and stress response (Shi, 2023, Mangus et al., 2003), its downregulation in *anxa2a/b* crispants likely reduces the capacity for rapid protein synthesis necessary for angiogenesis, endothelial proliferation, and cardiomyocyte repopulation.

Together, these data suggest that ANXA2 functions beyond its well-characterised roles in fibrinolysis, possibly acting as an upstream facilitator of translational regulation during regenerative responses. The dose-dependent repression of *PABPC1* paralogues in crispants positions them as downstream effectors of *ANXA2*-dependent cardiac regeneration, providing a previously unrecognised mechanistic link between endothelial signalling and translational control. Future studies could explore whether targeted rescue of *PABPC1* paralogues in *anxa2a/b* crispants – via mRNA delivery or transgenic expression – can restore the regenerative deficit observed in crispants, offering direct evidence that translational regulation is a critical component of ANXA2-mediated neovascularisation and cardiac repair.

This study benefits from a cross-species and multi-modal datasets validation that integrates human, mouse, and zebrafish data, combining with sc(n)RNA-seq, spatial transcriptomics, and immunofluorescence. These complementary approaches provide convincing evidence that PABPC1 is a conserved injury-responsive gene involved in neovascularisation, which is validated at both RNA and protein levels.

The study of *anxa2a/b* crispants suggests a novel mechanistic association between *ANXA2* deficiency and *PABPC1* downregulation following cardiac laser injury, suggesting *PABPC1* acts downstream of *ANXA2* to promote neovascularisation and cardiac regeneration. However, direct mechanistic evidence in human ECs is lacking. Additional *in vitro* functional assays (such as PABPC1 gain- or -loss-of-function studies) will help to validate the proposed ANXA2-PABPC1 regulatory axis, and to confirm whether PABPC1 directly stimulates angiogenic or regenerative behaviours in ECs.

The transcriptomic analyses were based on both publicly available (Kuppe) and in-house (CrescENDO) sc(n)RNA-seq datasets generated from small and heterogeneous patient cohorts ($n < 6$ per sample group). This limited sample size may reduce statistical power and generalisability of the findings, and increases susceptibility to inter-patient variability, including differences in age, sex, and underlying health conditions, all of which can influence endothelial transcriptional states. Furthermore, sc(n)RNA-seq data only provides a snapshot of steady-state mRNA levels, and may not accurately correspond to the dynamic changes in translation or protein turnover. This is particularly relevant for PABPC1, given its cytoplasmic localisation and role in post-translational regulation. In addition, clustering

and averaging of expression across all endothelial populations may mask subpopulation-specific regulation (e.g. arterial EC, venous EC, capillary EC) and underrepresenting potentially meaningful heterogeneity in PABPC1 expression.

Immunofluorescence can provide qualitative and semi-quantitative evidence for PABPC1 protein localisation within the coronary endothelial after MI. However, the quantification is restricted to fixed tissue sections at static timepoints, preventing assessment of the temporal expression patterns of PABPC1 during the post-MI response. Additionally, PABPC1 was only co-stained with endothelial marker CD31, other lineage-specific markers (e.g. fibroblast, myofibroblast, or inflammatory cells) were not included, limiting the ability to definitively assign PABPC1 expression to other non-endothelial populations within the same region of interest.

In summary, the data presented in this chapter identify PABPC1 as a conserved, injury-responsive translational regulator re-activated in diseased/injured coronary endothelium across species following MI. PABPC1 likely functions as a downstream effector of ANXA2, supporting neovascularisation by regulating protein translation and synthesis, which are critical for myocardial repair. These findings establish PABPC1 as a key mediator of post-ischaemic vascular repair in the heart and provide a strong rationale for future studies to investigate its downstream targets, temporal regulation, cell-type specific functions, and interactions with well-known regenerative pathways, with potential implications for enhancing cardiac regeneration post-MI in humans.

Chapter 7: Investigation of the cardioprotective properties of blue mussel-derived drug N2-01 in collaboration with N2 Pharmaceuticals (External Partner Organisation)

7.1 Introduction

This PhD project included an industrial collaboration with External Partner Organisation (EPO) – N2 Pharmaceuticals, who developed a bioactive compound extracted from blue mussel (*Mytilus edulis)* meat via enzyme-acid hydrolysis (for more detail see Chapter 1.8).

Blue mussels are a sustainable marine resource rich in bioactive peptides with proven antioxidant, anti-inflammatory, antithrombotic, and cardioprotective properties. Their hydrolysates inhibit key metabolic enzymes, including pancreatic cholesterol esterase, pancreatic lipase, and α-glucosidase (Lu et al., 2025, Wang et al., 2013a), suggesting a potential role to modulate lipid and glucose metabolism, and reduce oxidative stress. This means *Mytilus edulis* hydrolysates may serve as natural therapeutic for metabolic and cardiovascular disorders.

Furthermore, *Mytilus edulis* hydrolysates have shown to improve endothelial function across multiple disease models, including sepsis, preeclampsia, cancer, and kidney failure. They exert anti-inflammatory and cytoprotective effects by suppressing pro-inflammatory cytokine production, reducing ROS and NO generation, and inhibiting apoptosis (Kim et al., 2016, Cheong et al., 2017, Suryaningtyas et al., 2021). Additionally, *Mytilus edulis* derivatives protect ECs from oxidative injury and thrombosis by inhibiting caspase-3 activation and apoptosis (Oh et al., 2019, Qiao et al., 2018), Hence, this suggests *Mytilus edulis* hydrolysates may be effective in protecting oxidative stress-mediated endothelial dysfunction or related cardiovascular disease such as atherosclerosis.

Enzyme-assisted hydrolysates of *Mytilus edulis* have shown strong potential to attenuate muscle atrophy in both *in vitro* and *in vivo* zebrafish models (Amarasiri et al., 2023). Alcalase-assisted *Mytilus edulis* hydrolysate enhanced C2C12 myoblast proliferation, increased myotube size and nuclear number, upregulated hypertrophy markers, and suppressed levels of proteins responsible for muscle atrophy (Amarasiri et al., 2023). In zebrafish, treatment with alcalase-assisted *Mytilus edulis* hydrolysate improved locomotor performance and increased body weight, confirming its efficacy in promoting muscle maintenance and growth *in vivo* (Amarasiri et al., 2023). Moreover, mussel-derived peptides exhibited antioxidant and anti-inflammatory properties that may protect against atherosclerosis by preventing oxidative modification of ox-LDL cholesterol, and reducing vascular inflammation. Specifically, blue mussel alcalase

hydrolysate inhibited ox-LDL-induced foam cell formation in macrophages by modulating cholesterol influx and efflux pathways, while mitigating inflammation and oxidative stress via inhibiting NF-κB and activating HO-1/Nrf2 signalling (Marasinghe et al., 2023).

Dietary consumption of blue mussels was associated with cardiovascular benefits including blood pressure reduction, particularly in Southeast and East Asian populations (Je et al., 2005). *In vivo* studies showed that angiotensin I-converting enzyme inhibitory peptides derived from fermented blue mussel sauce significantly lowered blood pressure in spontaneously hypertensive rats, supporting potential antihypertensive effects (Je et al., 2005, DAI et al., 2012). Additionally, continuous subcutaneous administration of small doses (1.0 µl/hour) of N2-01 protected mice against Lipopolysaccharide-D-Galactosamine-induced acute liver injury, achieving 100% survival rate by suppressing pro-inflammatory cytokines, regulating NO production, and reducing VCAM-1 expression and vascular permeability (Starikova et al., 2021).

N2-01 is currently registered in Russia as a veterinary medicine, with over 25,000 animals treated successfully for pathologies linked to endothelial dysfunction (https://www.n2pharma.co.uk). This preclinical success suggests potential translation for cardiovascular diseases related to endothelial dysfunction, including hypertension, heart failure, and coronary artery disease. The vascular endothelium is central to cardiovascular homeostasis, regulating vascular tone, permeability, and angiogenesis (Galley and Webster, 2004, Sun et al., 2020). Endothelial dysfunction, characterised by NO dysregulation, oxidative stress, inflammation, and apoptosis, contributes to the progression of atherogenesis and hypertension, and heart failure (Premer et al., 2019). Following MI, ischaemic injury triggers endothelial dysfunction, impeding neovascularisation and cardiac recovery. This process is exacerbated by endoplasmic reticulum (ER) stress, which promotes apoptosis and disrupts angiogenic signalling. Recent findings identified endothelial protein arginine methyltransferase 7 (PRMT7) as a key regulator of ER stress and apoptosis, essential for vascular homeostasis, EC survival and cardiac recovery post-MI (Tran et al., 2025).

Previous sc(n)RNA-seq analyses from the Brittan group revealed upregulation of genes associated with pathways regulating oxidative stress response and endothelial permeability in coronary ECs at 7 days post-MI compared to healthy controls, (Li et al., 2019b, Li et al., 2022b). These findings provided the foundation for this collaboration with N2 Pharmaceuticals, aimed at exploring N2-01's ability to restore endothelial integrity and function following cardiac injury.

Given its multifunctional bioactivity and endothelial-protective properties, N2-01 represents a promising candidate for cardiovascular regeneration. However, the cellular and molecular mechanisms underlying its protective effects remain poorly understood. This study therefore investigates the effects of N2-01 on EC function and cardiovascular development, using *in vitro* assays with human cardiac microvascular

endothelial cells (HCMECs) and *in vivo* zebrafish models. Specifically, this chapter examines whether N2-01 enhances endothelial proliferation and angiogenesis *in vitro*, and whether it can rescue developmental and vascular defects in *anxa2a/b* zebrafish crispants or promote cardiac regeneration following laser-induced myocardial injury.

It was hypothesised that N2-01 exerts cardioprotective and endothelial-preserving effects by modulating pathways involved in oxidative stress, inflammation, and angiogenesis. By integrating cell-based and zebrafish studies, this chapter aimed to elucidate N2-01's mechanisms of action and provide preclinical insights into its translational relevance for endothelial protection and cardiovascular regeneration.

7.2 N2-01 drug modulates endothelial behaviour by suppressing cell proliferation while enhancing angiogenic network formation

To investigate the functional effects of N2-01 on HCMECs under baseline conditions, I first evaluated its ability to stimulate proliferation using an EdU incorporation assay. HCMECs were cultured under two nutrient conditions: i) complete Endothelial Cell Growth Medium MV2 (Basal MV2 Medium added with supplement growth kit) and ii) Endothelial Cell Basal Medium MV2 containing 5% foetal bovine serum (FBS). This approach allowed me to assess the influence of growth supplements on HCMEC proliferation and determine the most appropriate medium for preparation of N2-01 for use in later assays.

N2-01 was supplied in batches from N2 Pharmaceuticals, but the concentration details were not made available. Hence cells were treated with N2-01 at dilutions of 1/3, 1/6, and 1/12 (v/v) in cell culture medium. This is prepared by diluting the same volume of N2-01 stock into culture medium to a constant final volume across all conditions. Thus, all wells received equal volumes of medium, and the only variable was the relative dilution of N2-01.

Two independent production batches of N2-01 (N2-01-014 and N2-01-015) were tested. VEGF-165 (10 ng/ml), a well-established endothelial mitogen known to stimulate cell proliferation and angiogenesis (Barr et al., 2015), was included as a positive control. EdU incorporation per cell was quantified after 24 and 48 hours to assess proliferation relative to untreated controls.

Cell proliferation was quantified by EdU incorporation and data were presented as fold change relative to the untreated control, which was set to 1. Across three biological and three technical HCMEC replicates, N2-01 treatment caused a dose-dependent decrease in EdU incorporation at both 24- and 48-hours following N2-01 treatment compared to control MV2 medium, indicating reduced cell proliferation. In nutrient-rich complete MV2 medium with supplements, proliferation was significantly inhibited

following treatment with 1/3 N2-01-014 at both 24 hours (Fold change of %EdU$^+$ HCMECs = 0.38 ± 0.27 vs 1.00, P = 0.0407) and 48 hours (Fold change of %EdU$^+$ HCMECs = 0.40 ± 0.02 vs 1.00, P = 0.0223; two-way ANOVA with multiple comparisons) (**Figure 28**). The 1/3 N2-01-015 treatment also significantly reduced proliferation at 24 hours (Fold change of %EdU$^+$ HCMECs = 0.40 ± 0.23 vs 1.00, P = 0.0234, two-way ANOVA with multiple comparisons), although the reduction at 48 hours was not significant. Despite a clear trend for increased proliferation, VEGF-165 treatment did not show any statistically significance in cell proliferation compared to the complete MV2 control.

Under nutrient-limited conditions (5% FBS in basal medium MV2), the effects of N2-01 were less pronounced (**Figure 28**). Only 1/3 N2-01-015 significantly reduced cell proliferation at 48 hours (Fold change of %EdU$^+$ HCMECs = 0.43 ± 0.171 vs 1.00, P = 0.0224, two-way ANOVA with Tukey's multiple comparisons test). Other dilutions and timepoints showed no significant changes, and again, VEGF-165 did not significantly affect proliferation relative to the basal control.

To determine whether N2-01 influences angiogenic behaviour in HCMECs (two biological replicates with three technical replicates), a Matrigel-based tube formation assay was performed (Kubota et al., 1988, DeCicco-Skinner et al., 2014). HCMECs were seeded on Matrigel matrix (growth factor reduced), and cell were treated with: i) complete MV2 medium alone ii) complete MV2 medium supplemented with VEGF-165 iii) complete MV2 Medium supplemented with 1/3 N2-01 (either N2-01-014 or N2-01-015). Tubular network formation was quantified at 5- and 22-hours post-treatment using phase-contrast microscopy.

After an initial 5 hours of treatment, HCMECs (n = 2, with 3 technical replicates) treated with both N2-14 (number of tubules = 109.8 ± 15.79 vs 83.83 ± 12.96) and N2-15 (number of tubules = 104.8 ± 21.92 vs 83.83 ± 12.96) appeared to promote tubular network formation compared to the control MV2 media alone group (**Figure 29**). In contrast, VEGF-165 treatment did not seem to change the number of tubules compared to control. This lack of effect is likely due to the presence of growth factors already presented in the MV2 medium supplement kit (including epidermal growth factor, basic fibroblast growth factor, insulin-like growth factor, and VEGF-165 (PromoCell Inc., 2025)). This means that additional VEGF-165 treatment at an increased concentrations may not further promote endothelial cell proliferation or tubule formation.

By 22 hours post-treatment, tubular structures had largely dissolved or disassembled in all groups, this appeared particularly prominent in the N2-01 treated condition. Thus, the 5-hour time point was considered optimal for quantifying the pro-angiogenic effect of N2-01 (**Figure 29**).

In summary, N2-01 treatment resulted in a reduction of EC proliferation in HCMECs as measured by EdU incorporation. In contrast, Matrigel-based tube formation assays showed that N2-01 significantly enhanced tubule formation within 5 hours. These

findings suggest that, although N2-01 suppressed EC proliferation, it may exert additional and potentially more potent effects on endothelial function, such as cell survival and migration, thereby promoting angiogenesis.

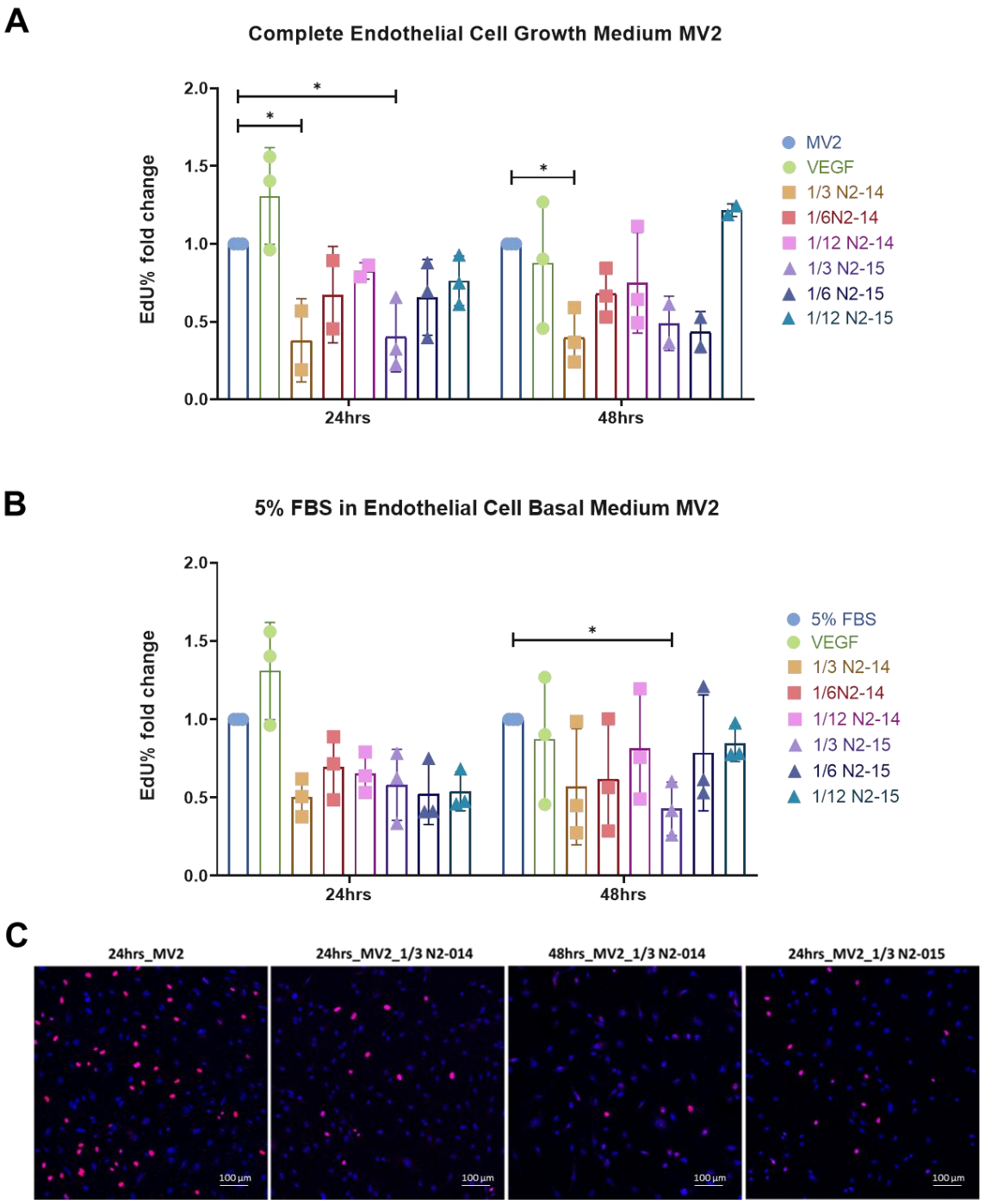

Figure 28. Higher concentration of N2-01 appears to inhibit coronary endothelial cell proliferation following 24 hours of treatment. *(A, B) Fold change of %EdU+ cells with three different doses of N2-01. HCMECs (n = 3, with three technical replicates) were cultured in either endothelial cell growth media MV2 (A) or 5% FBS (B) to compare the impact of the growth supplements supplied with the media, and to assess the best media for dilution of N2-01. Two time points (24 hours vs 48 hours)*

were conducted. Treatment of N2-01 reduced proliferation assessed by EdU incorporation assay, in a dose dependent manner. When diluted in MV2, 1/3 N2-014 significantly inhibited cell proliferation at 24 hours and 48 hours. Whereas 1/3 N2-015 diluted in MV2 only showed significant reduction in cell proliferation at 24 hours, but not at 48 hours. When diluted in 5% FBS, only 1/3 N2-15 showed significant reduction in cell proliferation at 48 hours. (C) Representative immunofluorescence images showing EdU⁺ nuclei (magenta) and total nuclei counterstained with DAPI (blue) in control and 1/3 N2-01-treated HCMECs at 24 hours. N2-01-treated cells exhibited visibly reduced EdU incorporation compared to control.

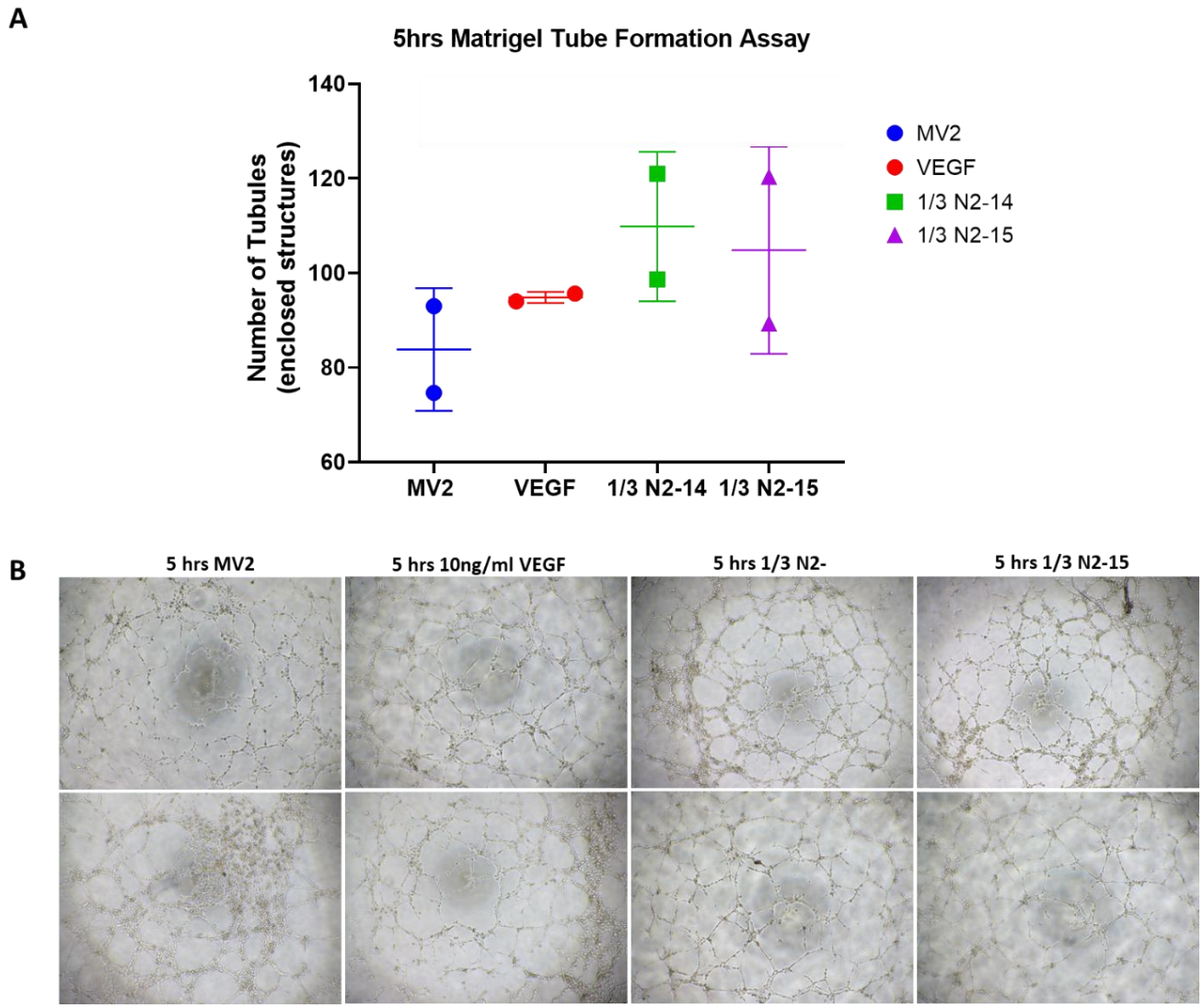

Figure 29. N2-01 promoted endothelial tubule network formation at 5 hours post-treatment*. (A) HCMECs (n = 2, with 3 technical replicates) were cultured in complete Endothelial Cell Growth Medium MV2 on Matrigel matrix. Three 4X objective images were taken per well and networks measured for each technical replicate. At 5 hours, both batches of N2-01 appeared to promote network formation, compared to control. (B) Representative images of network formation in HCMECs following 5 hours of N2-*

01 treatment. (C) Representative images of HCMECs following 22 hours of N2-01 treatment. In all groups, networks became dispersed at this timepoint.

7.3 N2-01 treatment resulted in delayed development and early embryonic lethality in zebrafish

I previously observed non-vascular and vascular developmental defects in *anxa2a/b* crispants in Chapter 4. Most *anxa2a/b* crispants developed smaller eyes and shortened body length, pericardial oedema, curved body axis, and tail malformation. Vascularly, *anxa2a/b* crispants exhibited a reduced number of complete intersegmental and parachordal vessels in the trunk.

To investigate whether N2-01 could reverse or rescue these developmental abnormalities, I treated zebrafish embryos with N2-01 immediately following CRISPR dgRNPs microinjection at 1-cell stage. Embryos (n=15 per group) were exposed to a 1/3 dilution of N2-015 (3.33ml N2-01 in 6.67ml fish medium) and monitored for morphological changes using brightfield stereomicroscopy at 1-day post-fertilisation (dpf). This concentration was chosen based on its prior efficacy in *in vitro* assays. Uninjected embryos with or without N2-01 treatment were used as controls.

Unexpectedly, for both uninjected controls and *anxa2a/b* crispants, treatment with 1/3 N2-01 resulted in a significant developmental delay compared to non-treated embryos, and these embryos appeared to be stuck at the epiboly or early somite stage (Kimmel et al., 1995). None of the embryos treated with this concentration survived beyond 2 dpf (**Figure 30**). To evaluate whether a lower concentration might improve survival, a separate group of embryos at 2dpf was treated with a 1/6 dilution of N2-015. However, even at this reduced concentration, embryos showed delayed development and failed to survive beyond 3 dpf (**Figure 30**).

In summary, N2-01 exposure during early embryogenesis led to delayed development and loss of viability of zebrafish embryos, suggesting potential developmental toxicity at the tested concentrations.

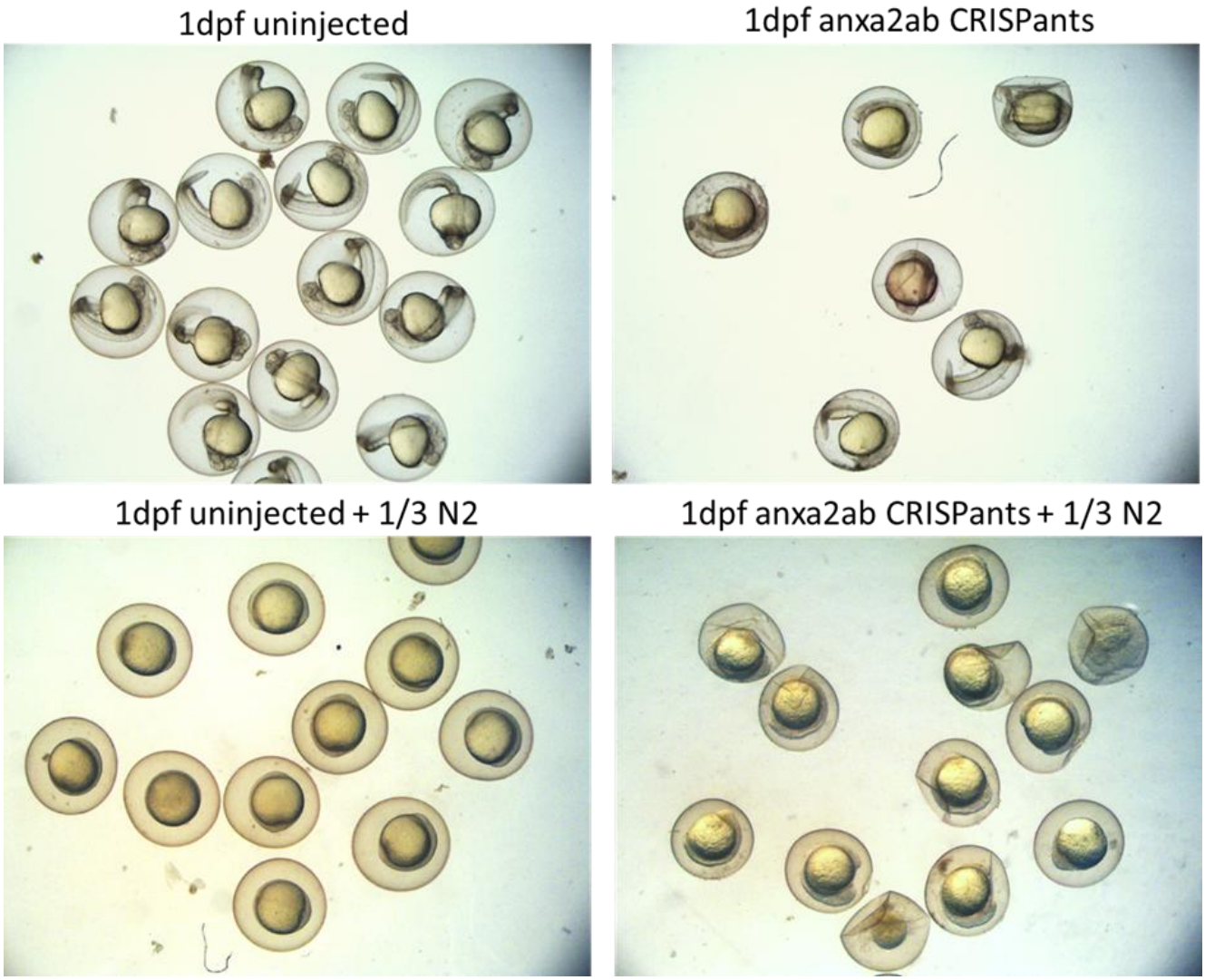

Figure 30. N2-01 treatment delays zebrafish embryonic development and reduces survival. *Representative brightfield images of zebrafish embryos at 1 day post-fertilisation (dpf) following exposure to 1/3 N2-01 (3.33 mL N2-01 in 6.67 mL fish medium) immediately after fertilisation, in either uninjured controls or embryos microinjected with anxa2a/b dgRNPs at 1-cell stage. Control embryos without N2-01 treatment (top left) displayed normal developmental progression with well-formed somites and tail extension, while anxa2a/b crispants (top right) exhibited growth defects consistent with those described in earlier chapters. At 1 dpf both uninjected and anxa2a/b crispant embryos treated with N2-01 showed delayed development and abnormal morphology, appearing arrested at the epiboly or early somite stage. By 2dpf, all N2-01 treated embryos were non-viable.*

7.4 Discussion

There is increasing interest in marine-derived bioactive peptides as sustainable sources of therapeutic compounds. Mussels represent a promising source due to their abundance, environmental sustainability, and high nutritional value. Mussel-derived peptides have demonstrated antioxidant, anti-inflammatory, antihypertensive, immunomodulatory, and cardiovascular health-promoting properties, making them valuable candidates for functional food, nutraceutical, and biomedical applications (Suryaningtyas et al., 2025). Optimising extraction and purification strategies, improving bioavailability, and expanding research into therapeutic mechanisms remain key for fully realising their translational potential (Koodathil et al., 2025).

The findings presented in this chapter demonstrated that blue mussel-derived drug N2-01 had distinct functional effects on HCMECs. Using an EdU incorporation assay, N2-01 significantly suppressed endothelial proliferation in a dose-dependent manner, particularly at the highest concentration tested (1/3 dilution) (**Figure 28**). Interestingly, under nutrient-limited conditions (5% FBS in basal medium), this antiproliferative effect was attenuated, suggesting that N2-01 activity may depend on growth factor availability or modulation of growth factor-associated signalling pathways (**Figure 28**).

Despite its inhibitory effects on proliferation, N2-01 appeared to increase tubule formation in a Matrigel-based angiogenesis assay at early timepoints (5 hours), suggesting a pro-angiogenic or pro-migratory influence on ECs. However, by 22 hours, the tubular networks had largely dissembled, indicating a loss of structural stability and possible onset of apoptosis. While VEGF-165 and MV2-only positive and negative controls, respectively, also exhibited some structure disintegration over time, their tubular structures appeared to remain more intact compared to those treated with N2-01 (**Figure 29**).

The inclusion of VEGF-165 as a positive control helped confirm that some degree of tubule dissemblance was expected *in vitro*; as it was previously reported that endothelial tube formation typically peaks between 18-24 hours before regressing as cells detach from the Matrigel and undergo apoptosis (Kelley et al., 2022). However, the more pronounced and premature tubule disintegration observed with N2-01 treatment suggests that it may promote EC detachment and apoptosis, rather than sustaining angiogenic activation, although further study of these mechanisms is warranted. These contrasting effects imply that N2-01 may transiently activate cellular processes associated with cytoskeletal rearrangement, cell adhesion, and migration, but fails to maintain pro-survival or adhesion signalling necessary for network stability.

Mechanistically, these findings are consistent with previous report of N2-01 modulation of NO signalling and vascular adhesion. NO is a key regulator of vascular tone, permeability, and endothelial survival. Transient increases in NO levels can promote cytoskeletal reorganisation and migration, which are important for repair and angiogenesis, but it simultaneously inhibits cell proliferation (Walford and Loscalzo, 2003, Cooke and Losordo, 2002, Tousoulis et al., 2012). Additionally, previous

research showed that *Mytilus edulis* hydrolysates possess anti-inflammatory properties by inhibiting the activation of inflammatory signalling pathways, such as NF-κB, and downregulating pro-inflammatory cytokines like TNF-α, IL-6, and IL-1β in cell models such as RAW264.7 mouse macrophages, human umbilical vein endothelial cells, and THP-1 human macrophages (Kim et al., 2016, Starikova et al., 2021, Liu et al., 2017). N2-01 has also been associated with reduced expression of adhesion molecules such as VCAM-1 (Starikova et al., 2021), which may alter cell-matrix interactions and modulate the balance between endothelial quiescence and an activated, migratory state. Therefore, my observed early promotion of tubule formation followed by network disintegration may indicate that N2-01 initially stimulates endothelial activation and migration, but may later fails to maintain cell-matrix adhesion and/or survival signals required for vascular network stability and maintenance.

A key strength of this study was the use of multiple N2-01 production batches and two different EC culture media (complete MV2 media with supplement kit and 5% FBS in basal MV2), providing a broader understanding of the drug's biological effects and its dependence on environmental context e.g. growth factors. The use of both proliferation and angiogenesis assays allowed for functional comparison, revealing that N2-01's effects are not simply pro- or anti-angiogenic but depend on cellular processes and the environmental context. These insights lay the groundwork for future exploration of how N2-01 might modulate vascular behaviour in cardiovascular regenerative settings.

However, several limitations should be acknowledged. First, these assays were performed under baseline, non-injury conditions in cultured cells, which may not fully capture the regenerative environment N2-01 is designed to modulate. Second, evaluation of mechanistic markers of apoptosis or cytoskeletal remodelling, (e.g. Ki67, cleaved caspase-3, and F-actin) (Nanev et al., 2024, De Silva et al., 2022) was not possible due to time-constraints of this project. This limits our understanding of specific cellular pathways that might have directly led to the observed results. Third, N2-01 is an undefined and complex molecular mixture, making it difficult to directly link observed phenotypic effects to specific biological or molecular mechanisms and complicating mechanistic interpretation, reproducibility, and dose standardisation. Fourth, although promising biological effects were observed *in vitro*, translation of N2-01 to MI therapy would likely be challenging, as effective clinical application would likely require targeted or local administration to the injured myocardium. Finally, although the Matrigel tube formation assay is a useful model for assessing early-stage angiogenesis, such as the initial sprouting a migration of ECs. However, this model does not capture later, more complex processes of vessel maturation, lumen formation, and functional perfusion (Irvin et al., 2014, Brown et al., 2023). Moreover, due to the limited number of biological replicates available for N2-01 treatment in this assay (n = 2), the findings are necessarily descriptive and could not be subjected to statistical

analysis. Therefore, more advanced models or further assays are needed to study the complete, long-term development of functional blood vessels and effects of N2-01.

In zebrafish, early embryonic exposure to N2-01 caused severe developmental delay and lethality, with embryos failing to progress beyond epiboly or early somite stages and losing viability entirely (**Figure 30**). These findings suggest that N2-01 disrupts key morphogenetic processes. Notably, this phenotype occurred in both uninjected controls and *anxa2a/b* CRISPants, indicating that toxicity was independent of *anxa2a/b* loss of function and contradicting the initial hypothesis that N2-01 might rescue *anxa2*-deficient developmental defects.

The arrest during gastrulation and somitogenesis implies interference with fundamental cellular pathways required for morphogenesis and organogenesis. As N2-01 has been shown to modulate endothelial nitric oxide (NO) production and cell-matrix interactions (Walford and Loscalzo, 2003, Cooke and Losordo, 2002, Tousoulis et al., 2012). One plausible explanation is that early embryonic exposure to N2-01 disrupted NO-dependent signalling essential for embryonic patterning and vascular development (Krause et al., 2011, Rajendran et al., 2022).

NO plays multifaceted and context-dependent roles in zebrafish embryogenesis, regulating cardiovascular formation, neurogenesis, haematopoiesis, and organ positioning (Locascio et al., 2023, Veerkamp et al., 2013, Li et al., 2014). During zebrafish tail fin regeneration, NO synthase translocated to the nucleus and altered the nuclear S-nitrosylated proteome, highlighting its role in regeneration-associated signalling (Matrone et al., 2021). Acting as a “double-edged sword,” NO can exert either pro-survival or pro-apoptotic effects depending on concentration and context. At low or physiological levels, NO supports normal development by preventing apoptosis via S-nitrosylation of caspases and induction of anti-apoptotic proteins. However, excessive or dysregulated NO triggers oxidative stress, mitochondrial dysfunction, and caspase- or p53-dependent apoptosis, leading to developmental arrest and cell death (Chung et al., 2001, Zhang et al., 2025, Raghul Kannan et al., 2024). Given that N2-01 modulates NO signalling, the observed developmental toxicity may stem from NO-induced redox imbalance and cytotoxicity.

From a developmental toxicology perspective, these findings highlight the sensitivity of early zebrafish embryos to N2-01. In contrast, N2-01 or *Mytilus edulis* hydrolysates have been demonstrated to be safe and well-tolerated in rodent models (Azad et al., 2023, Starikova et al., 2021, Wang et al., 2022). The concentrations used (1/3 and 1/6 dilutions) were based on effective doses in adult HCMECs assays but may have exceeded tolerable thresholds for embryonic stages. A strength of this study is inclusion of both *anxa2a/b* crispants and uninjected controls, allowing the differentiation between general toxicity and genotype-specific effects. The consistent developmental arrest and lethality across both groups confirms that N2-01 embryotoxicity is independent of *ANXA2* knockdown. Early embryos are particularly

sensitive to oxidative stress and metabolic imbalance, highlighting the importance of optimising dose and exposure timing in future work.

Some limitations include narrow concentration range tested and lack of mechanistic molecular analyses. Assessing markers of apoptosis, oxidative stress, and endothelial differentiation markers (e.g. caspase-3, p53, foetal liver kinase 1, ETS variant transcription factor 2, SRY-box transcription factor 17) could clarify the processes disrupted by N2-01 (Meadows et al., 2011, Zhang et al., 2017, Aragon and Hirschi, 2022). Moreover, delayed administration of N2-01 at later developmental stages (e.g. post- 3 dpf) might reduce toxicity and sensitivity, revealing potential regenerative effects of N2-01.

My initial hypothesis proposed that N2-01 exerts cardioprotective and endothelial-preserving effects by modulating oxidative stress, inflammation, and angiogenic pathways, thereby enhancing endothelial function and promoting cardiovascular regeneration. The current findings partially support this hypothesis. *In vitro*, N2-01 promoted endothelial migration and early angiogenic organisation – processes relevant to regenerative repair – but suppressed cell proliferation, likely due to NO-mediated oxidative or apoptotic signalling. In contrast, despite the absence of toxicity in previous rodent studies, zebrafish embryonic exposure to N2-01 exposure caused developmental arrest and lethality, consistent with disruption of essential NO, vascular adhesion pathways, or other essential developmental regulatory processes. Rather than uniformly protective, N2-01 appears to exert a biphasic influence: transiently activating endothelial remodelling at sublethal doses, while inducing oxidative or apoptotic responses when signalling thresholds are exceeded. These results refine the original hypothesis, indicating that the potential pro-regenerative effects of N2-01 may depend critically on dose, timing, and cellular context.

To move N2-01 towards therapeutic application, further experiments are needed to determine the optimal concentration and temporal window at which N2-01 promotes vascular regeneration without inducing cytotoxicity *in vivo*. These should be supported by broader mechanistic and functional assays, such as evaluating oxidative stress, apoptotic signalling, and endothelial adhesion.

Future pre-clinical *in vivo* studies should investigate whether N2-01 and its associated gene targets enhance cardiac repair and functional recovery in infarcted hearts, for example using endothelial cell-specific Confetti mouse models (Li et al., 2019b). Parallel zebrafish studies could further assess how N2-01 influences cardiac regeneration following laser-induced injury, including assessing its potential to restore regenerative capacity in *anxa2a/b* crispant hearts. In addition, bulk RNA sequencing could provide mechanical insight into the signalling pathways by which N2-01 modulates endothelial protection and cardiac regeneration.

Chapter 8: General discussion

8.1 Summary of findings

Despite major advances in treatments, which have significantly improved short-term survival rates, MI remains a leading cause of death globally. The main challenges surrounding MI include high pre-hospital mortality, post-MI complications, limitations in diagnosis and treatment, and the increased prevalence and global disparity of MI (Salari et al., 2023, Farah and Barbagelata, 2017, Ojha and Dhamoon, 2023). Most importantly the adult heart has a very limited capacity to regenerate. Current treatments can only delay or prevent the progression to HF, but they cannot halt or reverse cardiac fibrosis or restore the lost myocardium. Hence, the ultimate therapeutic goal is to promote effective heart repair without the accumulation of scar tissues (Cahill et al., 2017).

Complete heart regeneration cannot rely solely on cardiomyocyte proliferation; the rapid reconstruction of a functional vasculature is equally important (Cochain et al., 2013). However, the molecular mechanisms controlling post-injury neovascularisation are not fully understood. There is growing evidence to suggest that reactivation of genes involved in embryonic development may support tissue repair after injury (Goldman and Poss, 2020). A better understanding of how these developmental programmes are redeployed in the adult heart could reveal new therapeutic targets to enhance cardiac regeneration.

This first aim of this thesis was to identify developmental genes reactivated in the injured adult coronary vasculature that could regulate cardiovascular repair, then to validate and compare the gene and protein expression of candidate genes in human cardiac tissue from healthy and MI hearts. Using a multi-species multi-omics approach combining sc(n)RNA-seq and spatial transcriptomics data from zebrafish, mouse, and human heart, I identified three promising endothelial genes (*ANXA2*, *SERPINE1* and *PABPC1)* that aligned with my central hypothesis that reactivation of developmental genes in the adult coronary endothelium promotes neovascularisation and cardiac regeneration following MI.

ANXA2 was identified as an endothelial gene with expression during development that is reactivated in the injured/diseased adult coronary vasculature. *SERPINE1* was less prominent as a developmentally expressed gene, but was highly upregulated in coronary ECs and other cardiac cells post-injury. ANXA2 promotes plasmin generation and ECM degradation, creating a proteolytic, pro-angiogenic environment (Dallacasagrande and Hajjar, 2020), while SERPINE1 acts as a counter-regulator to prevent excessive proteolysis and main scar stability (Sillen and Declerck, 2020). They may form a regulatory axis that tightly coordinates fibrinolysis, ECM turnover, and neovascularisation, to ensure a balanced tissue repair process after MI. Disrupting this balance could impair vascular regeneration or promote pathological fibrosis. Thus,

both ANXA2 and SERPINE1 represent promising therapeutic targets for improving cardiac regeneration while minimising adverse remodelling. Given ANXA2's vital role in this regulatory axis, it was prioritised for further functional validation.

The second aim of this thesis was to investigate *ANXA2* further through CRISPR-Cas9-mediated mutagenesis and functional analysis in zebrafish F0 crispants, exploring its role in embryogenesis and cardiac regeneration. My findings demonstrate that *anxa2a/b* paralogues are important for zebrafish development, angiogenesis, and cardiac morphogenesis. Loss of *anxa2a/b* led to dose-dependent developmental abnormalities such as smaller eyes, shorter body length, disrupted growth of intersegmental and parachordal vessels, and compromised cardiac regeneration. Transcriptional profiling via RT-qPCR revealed that *anxa2a/b* deficiency disrupts fibrinolytic (*plg*), angiogenic (*tie1*, *vegfab*), notch (*notch1a, notch3*) signalling. This suggests a failure to activate the molecular pathways required for tissue repair. These molecular impairments may explain the observed *in vivo* phenotypes of *anxa2a/b* crispants, which include reduced endothelial and cardiomyocyte repopulation, distorted ventricular architecture, and poor regenerative outcome. However, *serpine1* expression remained unaltered before and after injury despite *anxa2a/b* loss, which suggests *ANXA2* and *SERPINE1* do not directly regulate each other at the transcriptional level. *ANXA2* does not act upstream of *SERPINE1* but mainly act upstream of a network of endothelial and regenerative signalling genes, so that the loss of *ANXA2* compromises repair responses. This establishes ANXA2's role as a central regulator of cardiovascular development and injury-induced repair.

PABPC1 emerged as another interesting target. It was first identified by the Brittan group as one of top seventeen common differentially expressed genes in ECs of the foetal heart and in adult hearts with dHF, compared with uninjured adult hearts. With a function distinct from ANXA2 and SERPINE1, PABPC1 acts through post-transcriptional mechanisms to regulate mRNA stability, translation, and stress responses (Smith et al., 2014). Based on its upregulation during development and re-expression in disease states, I investigated whether post-transcriptional regulation via PABPC1 contributes to vascular regeneration after myocardial injury. My results suggest that ANXA2 functions beyond its well-characterised role in fibrinolysis, potentially facilitating the activation of translational regulators such as PABPC1 during tissue repair. Transcript analysis of 5 dpf *anxa2a/b* crispants after laser-induced cardiac injury revealed a dose-dependent reduction in *pabpc1a* and *pabpc1b* expression. This indicates that injury-induced upregulation of *pabpc1a/b* requires intact *anxa2a/b* signalling. Given the established roles of PABPC1 in mRNA stabilisation, translational efficiency, and stress response (Shi, 2023, Mangus et al., 2003), its downregulation in *anxa2a/b* crispants likely impairs process of protein synthesis crucial for angiogenesis, endothelial proliferation, and cardiomyocyte repopulation. My findings reveal a previously unrecognised ANXA2-PABPC1 regulatory axis crucial for bridging endothelial signalling and translational control in neovascularisation and cardiac regeneration.

To validate these multi-omics findings at the protein level using double immunofluorescence staining of human heart tissue from MI patients and non-diseased controls. All three targets (ANXA2, SERPINE1 and PABPC1) were significantly upregulated in the coronary vasculature within the infarct border zone. While their protein expressions were enriched in $CD31^+$ ECs, they were also present in other cardiac cell types, likely to be immune cells, fibroblasts and myofibroblast in the fibrotic region. Co-immunostaining with Vimentin confirmed many $ANXA2^+$ non-ECs were fibroblasts or myofibroblast, supporting a broader role in ECM remodelling and scar formation.

As a collaborative project with N2 Pharmaceuticals (EPO), I investigated the effects of the drug N2-01 on endothelial function and *anxa2a/b* embryos, specifically testing its potential to rescue developmental defects in *vivo*. My initial hypothesis was that N2-01 would exert cardioprotective and endothelial-preserving effects by modulating oxidative stress, inflammation, and angiogenic pathways, thus enhancing cardiovascular regeneration. My results partially support this, showing that N2-01 modulated endothelial cell behaviour by enhancing endothelial migration and angiogenic network formation *in vitro*, while inhibiting cell proliferation. Unexpectedly, exposure during early zebrafish embryogenesis (< 2 dpf) caused delayed development and loss of viability, suggesting potential embryonic toxicity and sensitivity to the tested concentrations. These findings demonstrate that N2-01's influence is biphasic: it can transiently activate endothelial remodelling at sublethal doses but induces oxidative or apoptotic responses when signalling thresholds are surpassed. This refines our original hypothesis, indicating that the potential pro-regenerative effects of N2-01 are highly dependent on dose, timing, and cellular context.

8.2 Clinical implications

By integrating multi-species multimodal omics data analyses, with functional *in vivo* studies in zebrafish, and further protein level validations in human cardiac tissue, I provide novel evidence of foetal gene reactivation in the adult coronary endothelium to promote cardiac neovascularisation and repair following MI. My findings have several important clinical and translational implications for improving cardiac neovascularisation, repair, and improve post-MI outcomes.

Using a multi-omics approach integrating human, mouse, and zebrafish datasets, *ANXA2* was identified as a developmentally regulated endothelial gene that is silenced in adulthood and re-expressed following myocardial injury. This injury-induced re-expression in ECs most likely to support both proteolytic clearance of fibrin deposits and vascular sprouting which ultimately facilitate reperfusion and cardiac repair. (Liu and Hajjar, 2016a, Dassah et al., 2009).

Annexin A2 is a multifunctional repair protein that preserves cellular integrity by coordinating plasma membrane repair and forming a complex with S100A10 to facilitate ECM degradation, fibrinolysis, and angiogenesis, all of which are crucial for effective cardiac healing (Kayejo et al., 2023). Clinically, the loss of ANXA2 function increases cellular degeneration, contributing to muscular dystrophy and cardiovascular disease (Kayejo et al., 2023). In the heart, ANXA2 binds to extracellular collagen and promote cell-cell adhesion to support post-injury remodelling of the myocardial interstitium and prevent perivascular fibrosis (Camors et al., 2005). Therefore, making ANXA2 a promising therapeutic target for reducing excessive fibrosis, resolving inflammation, and promoting cardiovascular repair.

Clinical insights into myocardial healing can be drawn from the historical use of fibrinolytic therapies in MI management (Baig and Bodle, 2025). Fibrinolytic agents such as tPA, streptokinase, and tenecteplase promote thrombus dissolution and early reperfusion, thereby limiting infarct size and supporting favourable remodelling (Halvorsen and Huber, 2014, Johanson et al., 2009). However, these therapies has been associated with increased risk of myocardial rupture compared with primary PCI, highlighting that excessive or poorly regulated fibrinolysis may destabilise infarct repair (Bueno et al., 2005). Together, these clinical insights highlight the importance of tightly balancing fibrinolysis with ECM remodelling during cardiac healing. Possibly, ANXA2 and SERPINE1 may act as endogenous modulators by coordinating fibrinolysis, ECM remodelling, and vascular growth to promote sufficient repair.

One potential therapeutic application could involve the delivery of recombinant ANXA2, or small-molecule activators specifically activate ANXA2 or its associated signalling pathway, maybe possible to stimulate controlled matrix remodelling and neovascularisation in ischaemic tissue. Supporting this idea, adeno-associated virus-mediated ANXA2 overexpression in mice post-MI improved left ventricular function, increased microvessel density, and reduced infarct size (Zhang et al., 2023b). The clinical challenge lies in its multifaceted nature and its involvement in other diseases such as cancer. This is because ANXA2 is often overexpressed by cancer cells, which hijacked its protective activity to promote their own survival and metastasis (Huang et al., 2025, Li et al., 2021c). Therefore, understanding the optimal dose and timing of ANXA2 delivery would be important to maximise benefits.

Future therapeutic strategies must focus on endothelial- or cardiac- specific gene delivery methods to minimise unwanted adverse effects. This methods include: engineering viral vectors that recognise and bind to specific cell receptors, equipping vectors with tissue-specific promoters or enhancer sequences, or designing targeted lipid nanoparticles (Katz et al., 2011, Liu et al., 2023). Some major barriers to successful cardiac gene therapy include: inefficient gene transfer, host immune responses, and a lack of durable transgene expression. These challenges are often a result of the chosen vector, dose, and delivery method. Thus, achieving effective therapy requires a careful balance between maximising gene transfer for efficacy and minimising risks by staying within safe limits (Katz et al., 2011). To reduce toxicity and

immunogenicity while enhancing therapeutic efficacy, future advancements will need further improvements in tissue-specific delivery, potentially through chemical modifications, bioconjugation, and the use of nanocarriers (Van Linthout et al., 2025).

Although this thesis initially proposed an ANXA2-SERPINE1 co-regulatory axis in neovascularisation and cardiac repair, however my data show that *serpine1* expression was unchanged in *anxa2a/b* zebrafish crispants, both before and after cardiac laser injury. This suggests *ANXA2* and *SERPINE1* do not directly regulate each other transcriptionally. Instead, my findings position ANXA2 as an upstream modulator of multiple endothelial and regenerative signalling pathways, independent of SERPINE1 and associated fibrinolytic pathway. Therapeutically, selective enhancement of ANXA2 activity might promote cardiovascular repair without affecting SERPINE1-dependent scar stability, thus achieving a balance between repair and fibrosis limitation. This is supported by zebrafish studies that showed *serpine1* is an early endocardial injury-response gene essential for regulating endocardial and myocardial proliferation during heart regeneration (Münch et al., 2017). Therefor balancing regeneration and fibrosis is key to promote beneficial remodelling (angiogenesis, clearing of dead tissue) while preventing pathological remodelling (excessive fibrosis, which leads to heart failure).

Broader insights into tissue regeneration can be gained by comparing the heart with other organs. For example, liver regeneration involves both hepatocyte proliferation and contributions from liver sinusoidal ECs, which provide critical angiocrine signals to coordinate vascular reconstruction and tissue regrowth (Liu et al., 2016, Kostallari and Shah, 2016). In contrast, the adult brain exhibits minimal regenerative capacity; although vascular activation and neovascularisation occur after injury, these responses are insufficient to restore tissue function (Yao et al., 2021, Vanacore et al., 2024). These differences suggest that successful regeneration depends not only on parenchymal progenitors but also on endothelial plasticity and the ability of ECs to re-activate developmental signalling programs (Tombor and Dimmeler, 2022). ECs exhibit tissue-specific adaptations from development that persist into adulthood. Brain ECs guide neuronal differentiation and maintain a selective barrier to protect against neurotoxicity, whereas heart ECs supply fatty acids to cardiomyocytes to support continuous contraction (Jambusaria et al., 2020, Hennigs et al., 2021). It is therefore possible that cardiac and brain ECs share intrinsic features that limit regenerative capacity compared with liver ECs (Pasut et al., 2021). Understanding these organ-specific differences may reveal conserved or divergent molecular checkpoints that could be therapeutically exploited to enhance cardiac repair.

Finally, this thesis uncovers a previously unrecognised ANXA2-PABPC1 regulatory axis that bridges endothelial signalling with translational control. The observed downregulation of *pabpc1a/b* in *anxa2a/b* knockdown crispants implicates that ANXA2 acts upstream of PABPC1, to facilitates translational reprogramming required for tissue repair. Given the known roles of PABPC1 in mRNA stabilisation, protein synthesis, and cellular stress response (Sawazaki et al., 2018), my finding indicates

that post-transcriptional regulation could be a novel layer of control in cardiovascular regeneration. Clinically, targeting this axis could offer new strategies to stimulate regenerative capacity by improving protein synthesis and cardiac cell survival after ischemic injury.

8.3 Conclusion

This thesis provides robust evidence that reactivation of developmental genes in the adult coronary endothelium critically drives neovascularisation and cardiac regeneration. Through a multi-species, multi-omics approach, I identified *ANXA2* and *PABPC1* as pivotal endothelial regulatory genes, alongside *SERPINE1*, which together coordinate distinct but complementary process in heart repair. ANXA2 promotes fibrinolysis and neovascularisation, SERPINE1 preserves ECM integrity and scar stability, and PABPC1 governs post-transcriptional control of protein synthesis essential for vascular regeneration.

An antagonistic balance between ANXA2 and SERPINE1 is crucial for efficient cardiac repair following injury. Disruption of this balance, caused by excess SERPINE1 or reduced ANXA2, results in a pro-coagulant, anti-fibrinolytic, and anti-angiogenic environment. This environment favours fibrosis and adverse remodelling, which can drive the progression to HF. Targeting this regulatory axis may therefore offer a promising therapeutic strategy for promoting cardiac regeneration and improving HF patient outcomes.

Functional studies using *anxa2a/b* zebrafish crispants showed that ANXA2 is crucial for embryonic development, angiogenesis, and injury-induced cardiac regeneration. Importantly, ANXA2 modulates endothelial and regenerative networks independently of SERPINE1 and the classical fibrinolytic pathway. The discovery of the ANXA2-PABPC1 regulatory axis uncovers a novel link between endothelial signalling and translational control, highlighting the critical role of post-transcriptional regulation in cardiac regeneration. This discovery reveals a promising therapeutic avenue that requires further research to dissect the mechanisms through which ANXA2 regulates endothelial responses to injury and develop effective regenerative therapies.

Validation in human MI tissues confirmed the clinical relevance of these candidate genes, with ANXA2, SERPINE1, and PABPC1 all significantly upregulated in the infarct border zone. Their localisation to both vascular and interstitial compartments, supports their involvement in both endothelial activation and tissue remodelling following MI.

Furthermore, collaborative studies with N2-01 pharmaceuticals demonstrated that N2-01 drug modulates endothelial behaviour by suppressing cell proliferation while enhancing angiogenic network formation, in a dose-, timing-, and context- dependent

manner, highlighting the complexity of endothelial responses to therapeutic intervention.

Together, this work shed light on fundamental mechanisms that link developmental reprogramming with cardiac regeneration. By identifying and studying novel endothelial targets that orchestrate neovascularisation and cardiac repair, these findings provide a foundation for developing regenerative therapies. These insights could ultimately redefine the treatment of cardiovascular disease like MI and HF, bringing us closer to the long-standing goal of transforming MI from an irreversible injury into a curable, regenerative condition.

References

ABLAIN, J. & ZON, L. I. 2013. Of fish and men: using zebrafish to fight human diseases. *Trends Cell Biol,* 23**,** 584-6.

ABPLANALP, W. T., TUCKER, N. & DIMMELER, S. 2022. Single-cell technologies to decipher cardiovascular diseases. *Eur Heart J,* 43**,** 4536-4547.

AHMAD, M., MEHTA, P., REDDIVARI, A. K. R. & MUNGEE, S. 2022. Percutaneous Coronary Intervention. *StatPearls.* Treasure Island (FL): StatPearls Publishing

Copyright © 2022, StatPearls Publishing LLC.

AMACHER, S. L. 2008. Emerging gene knockout technology in zebrafish: zinc-finger nucleases. *Brief Funct Genomic Proteomic,* 7**,** 460-4.

AMARASIRI, R. P. G. S. K., HYUN, J., LEE, S.-W., KIM, J., JEON, Y.-J. & LEE, J.-S. 2023. Alcalase-Assisted Mytilus edulis Hydrolysate: A Nutritional Approach for Recovery from Muscle Atrophy. *Marine Drugs,* 21**,** 623.

ANGOM, R. S. & NAKKA, N. M. R. 2024. Zebrafish as a Model for Cardiovascular and Metabolic Disease: The Future of Precision Medicine. *Biomedicines,* 12**,** 693.

ARA, T., TOKOYODA, K., OKAMOTO, R., KONI, P. A. & NAGASAWA, T. 2005. The role of CXCL12 in the organ-specific process of artery formation. *Blood,* 105**,** 3155-3161.

ARAGON, J. W. & HIRSCHI, K. K. 2022. Endothelial Cell Differentiation and Hemogenic Specification. *Cold Spring Harb Perspect Med,* 12.

ARELLANO MENDOZA, M. G., ROBLES, H. V., ROMO, E., RIOS, A. & ESCALANTE, B. 2007. Nitric oxide-dependent neovascularization role in the lower extremity disease. *Current Pharmaceutical Design,* 13**,** 3591-3596.

ASNANI, A. & PETERSON, R. T. 2014. The zebrafish as a tool to identify novel therapies for human cardiovascular disease. *Dis Model Mech,* 7**,** 763-7.

ASTROF, S. & HYNES, R. O. 2009. Fibronectins in vascular morphogenesis. *Angiogenesis,* 12**,** 165-75.

AZAD, A. M., BERNHARD, A., SHEN, A., MYRMEL, L. S., LUNDEBYE, A. K., LECAUDEY, L. A., FJÆRE, E., TRI HO, Q., SVEIER, H., KRISTIANSEN, K., LIMBORG, M. T. & MADSEN, L. 2023. Metabolic effects of diet containing blue mussel (Mytilus edulis) and blue mussel-fed salmon in a mouse model of obesity. *Food Res Int,* 169**,** 112927.

BAI, Y., CHEN, L., GUO, F., ZHANG, J., HU, J., TAO, X., LU, Q., LI, W., CHEN, X., GONG, T., QIU, N., JIN, Y., YANG, L., LEI, Y., RUAN, C., JING, Q., COOKE, J. P., WANG, S., ZOU, Y. & GE, J. 2024. EphrinB2-mediated CDK5/ISL1 pathway enhances cardiac lymphangiogenesis and alleviates ischemic injury by resolving post-MI inflammation. *Signal Transduct Target Ther,* 9**,** 326.

BAIG, M. U. & BODLE, J. 2025. Thrombolytic Therapy. *StatPearls.* Treasure Island (FL): StatPearls Publishing

Copyright © 2025, StatPearls Publishing LLC.

BAKKERS, J. 2011. Zebrafish as a model to study cardiac development and human cardiac disease. *Cardiovascular Research,* 91**,** 279-288.

BALBI, C., LODDER, K., COSTA, A., MOIMAS, S., MOCCIA, F., VAN HERWAARDEN, T., ROSTI, V., CAMPAGNOLI, F., PALMERI, A., DE BIASIO, P., SANTINI, F., GIACCA, M., GOUMANS, M.-J., BARILE, L., SMITS, A. M. & BOLLINI, S. 2019. Reactivating endogenous mechanisms of cardiac regeneration via paracrine boosting using the human amniotic fluid stem cell secretome. *International Journal of Cardiology,* 287**,** 87-95.

BARR, M. P., GRAY, S. G., GATELY, K., HAMS, E., FALLON, P. G., DAVIES, A. M., RICHARD, D. J., PIDGEON, G. P. & O'BYRNE, K. J. 2015. Vascular endothelial growth factor is an autocrine growth factor, signaling through neuropilin-1 in non-small cell lung cancer. *Molecular Cancer,* 14**,** 45.

BARTUNEK, J., TERZIC, A., DAVISON, B. A., FILIPPATOS, G. S., RADOVANOVIC, S., BELESLIN, B., MERKELY, B., MUSIALEK, P., WOJAKOWSKI, W., ANDREKA, P., HORVATH, I. G., KATZ, A., DOLATABADI, D., EL NAKADI, B., ARANDJELOVIC, A., EDES, I., SEFEROVIC, P. M., OBRADOVIC, S., VANDERHEYDEN, M., JAGIC, N., PETROV, I., ATAR, S., HALABI, M., GELEV, V. L., SHOCHAT, M. K., KASPRZAK, J. D., SANZ-RUIZ, R., HEYNDRICKX, G. R., NYOLCZAS, N., LEGRAND, V., GUÉDÈS, A., HEYSE, A., MOCCETTI, T., FERNANDEZ-AVILES, F., JIMENEZ-QUEVEDO, P., BAYES-GENIS, A., HERNANDEZ-GARCIA, J. M., RIBICHINI, F., GRUCHALA, M., WALDMAN, S. A., TEERLINK, J. R., GERSH, B. J., POVSIC, T. J., HENRY, T. D., METRA, M., HAJJAR, R. J., TENDERA, M., BEHFAR, A., ALEXANDRE, B., SERON, A., STOUGH, W. G., SHERMAN, W., COTTER, G. & WIJNS, W. 2017. Cardiopoietic cell therapy for advanced ischaemic heart failure: results at 39 weeks of the prospective, randomized, double blind, sham-controlled CHART-1 clinical trial. *Eur Heart J,* 38**,** 648-660.

BAUMEIER, C., ESCHER, F., ALESHCHEVA, G., PIETSCH, H. & SCHULTHEISS, H.-P. 2021. Plasminogen activator inhibitor-1 reduces cardiac fibrosis and promotes M2 macrophage polarization in inflammatory cardiomyopathy. *Basic Research in Cardiology,* 116**,** 1.

BECKER, R. O., CHAPIN, S. & SHERRY, R. 1974. Regeneration of the ventricular myocardium in amphibians. *Nature,* 248**,** 145-7.

BEDELL, V. M., WANG, Y., CAMPBELL, J. M., POSHUSTA, T. L., STARKER, C. G., KRUG II, R. G., TAN, W., PENHEITER, S. G., MA, A. C., LEUNG, A. Y. H., FAHRENKRUG, S. C., CARLSON, D. F., VOYTAS, D. F., CLARK, K. J., ESSNER, J. J. & EKKER, S. C. 2012. In vivo genome editing using a high-efficiency TALEN system. *Nature,* 491**,** 114-118.

BEK, J. W., SHOCHAT, C., DE CLERCQ, A., DE SAFFEL, H., BOEL, A., METZ, J., RODENBURG, F., KARASIK, D., WILLAERT, A. & COUCKE, P. J. 2021. Lrp5 Mutant and Crispant Zebrafish Faithfully Model Human Osteoporosis, Establishing the Zebrafish as a Platform for CRISPR-Based Functional Screening of Osteoporosis Candidate Genes. *J Bone Miner Res,* 36**,** 1749-1764.

BENEVOLENSKY, D., BELIKOVA, Y., MOHAMMADZADEH, R., TROUVÉ, P., MAROTTE, F., RUSSO-MARIE, F., SAMUEL, J.-L. & CHARLEMAGNE, D. 2000. Expression and Localization of the Annexins II, V, and VI in Myocardium from Patients with End-Stage Heart Failure. *Laboratory Investigation,* 80**,** 123-133.

BERGMANN, O., BHARDWAJ, R. D., BERNARD, S., ZDUNEK, S., BARNABÉ-HEIDER, F., WALSH, S., ZUPICICH, J., ALKASS, K., BUCHHOLZ, B. A., DRUID, H., JOVINGE, S. & FRISÉN, J. 2009. Evidence for cardiomyocyte renewal in humans. *Science,* 324**,** 98-102.

BERGMANN, O., ZDUNEK, S., FELKER, A., SALEHPOUR, M., ALKASS, K., BERNARD, S., SJOSTROM, S. L., SZEWCZYKOWSKA, M., JACKOWSKA, T., DOS REMEDIOS, C., MALM, T., ANDRÄ, M., JASHARI, R., NYENGAARD, J. R., POSSNERT, G., JOVINGE, S., DRUID, H. & FRISÉN, J. 2015. Dynamics of Cell Generation and Turnover in the Human Heart. *Cell,* 161**,** 1566-75.

BERKELEY, B., TANG, M. N. H. & BRITTAN, M. 2023. Mechanisms regulating vascular and lymphatic regeneration in the heart after myocardial infarction. *The Journal of Pathology,* 260**,** 666-678.
BHARADWAJ, A., BYDOUN, M., HOLLOWAY, R. & WAISMAN, D. 2013. Annexin A2 heterotetramer: structure and function. *Int J Mol Sci,* 14**,** 6259-305.
BITTEL, D. C., CHANDRA, G., TIRUNAGRI, L. M. S., DEORA, A. B., MEDIKAYALA, S., SCHEFFER, L., DEFOUR, A. & JAISWAL, J. K. 2020. Annexin A2 Mediates Dysferlin Accumulation and Muscle Cell Membrane Repair. *Cells,* 9.
BOGIC, L. V., OHIRA, R. H., YAMAMOTO, S. Y., OKAZAKI, K. J., MILLAR, K. & BRYANT-GREENWOOD, G. D. 1999. Tissue Plasminogen Activator and Its Receptor in the Human Amnion, Chorion, and Decidua at Preterm and Term1. *Biology of Reproduction,* 60**,** 1006-1012.
BOWLEY, G., KUGLER, E., WILKINSON, R., LAWRIE, A., VAN EEDEN, F., CHICO, T. J. A., EVANS, P. C., NOËL, E. S. & SERBANOVIC-CANIC, J. 2022. Zebrafish as a tractable model of human cardiovascular disease. *British Journal of Pharmacology,* 179**,** 900-917.
BRAILE, M., MARCELLA, S., CRISTINZIANO, L., GALDIERO, M. R., MODESTINO, L., FERRARA, A. L., VARRICCHI, G., MARONE, G. & LOFFREDO, S. 2020. VEGF-A in Cardiomyocytes and Heart Diseases. *Int J Mol Sci,* 21.
BREITENSTEIN, A. & STEFFEL, J. 2019. Devices in Heart Failure Patients-Who Benefits From ICD and CRT? *Front Cardiovasc Med,* 6**,** 111.
BROWN, D. R., SAMSA, L. A., QIAN, L. & LIU, J. 2016. Advances in the Study of Heart Development and Disease Using Zebrafish. *J Cardiovasc Dev Dis,* 3.
BROWN, K. C., LIGHT, R. S., MODI, K. J., CONELY, K. B., SUGRUE, A. M., COX, A. J., MILES, S. L., VALENTOVIC, M. A. & DASGUPTA, P. 2023. An Improved Protocol for the Matrigel Duplex Assay: A Method to Measure Retinal Angiogenesis. *Bio Protoc,* 13**,** e4899.
BRYL, R., KULUS, M., BRYJA, A., DOMAGAŁA, D., MOZDZIAK, P., ANTOSIK, P., BUKOWSKA, D., ZABEL, M., DZIĘGIEL, P. & KEMPISTY, B. 2024. Cardiac progenitor cell therapy: mechanisms of action. *Cell Biosci,* 14**,** 30.
BUENO, H., MARTÍNEZ-SELLÉS, M., PÉREZ-DAVID, E. & LÓPEZ-PALOP, R. 2005. Effect of thrombolytic therapy on the risk of cardiac rupture and mortality in older patients with first acute myocardial infarction. *Eur Heart J,* 26**,** 1705-11.
BUSSMANN, J., BAKKERS, J. & SCHULTE-MERKER, S. 2007. Early endocardial morphogenesis requires Scl/Tal1. *PLoS Genet,* 3**,** e140.
BUTLER, J., HAMMONDS, K., TALHA, K. M., ALHAMDOW, A., BENNETT, M. M., BOMAR, J. V. A., ETTLINGER, J. A., TRABA, M. M., PRIEST, E. L., SCHMEDT, N., ZEBALLOS, C., SHAVER, C. N., AFZAL, A., WIDMER, R. J., GOTTLIEB, R. L., MACK, M. J. & PACKER, M. 2025. Incident heart failure and recurrent coronary events following acute myocardial infarction. *European Heart Journal,* 46**,** 1540-1550.
CAHILL, T. J., CHOUDHURY, R. P. & RILEY, P. R. 2017. Heart regeneration and repair after myocardial infarction: translational opportunities for novel therapeutics. *Nature Reviews Drug Discovery,* 16**,** 699-717.
CAHILL, T. J. & KHARBANDA, R. K. 2017. Heart failure after myocardial infarction in the era of primary percutaneous coronary intervention: Mechanisms, incidence and identification of patients at risk. *World journal of cardiology,* 9**,** 407-415.
CAI, Y., ZANG, G. Y., HUANG, Y., SUN, Z., ZHANG, L. L., QIAN, Y. J., YUAN, W. & WANG, Z. Q. 2022. Advances in neovascularization after diabetic ischemia. *World J Diabetes,* 13**,** 926-939.

CAMORS, E., MONCEAU, V. & CHARLEMAGNE, D. 2005. Annexins and Ca2+ handling in the heart. *Cardiovascular Research,* 65**,** 793-802.
CAO, J., PACKER, J. S., RAMANI, V., CUSANOVICH, D. A., HUYNH, C., DAZA, R., QIU, X., LEE, C., FURLAN, S. N., STEEMERS, F. J., ADEY, A., WATERSTON, R. H., TRAPNELL, C. & SHENDURE, J. 2017. Comprehensive single-cell transcriptional profiling of a multicellular organism. *Science,* 357**,** 661-667.
CAPON, S. J., URIBE, V., DOMINADO, N., EHRLICH, O. & SMITH, K. A. 2022. Endocardial identity is established during early somitogenesis by Bmp signalling acting upstream of npas4l and etv2. *Development,* 149.
CAPORALI, A., BÄCK, M., DAEMEN, M. J., HOEFER, I. E., JONES, E. A., LUTGENS, E., MATTER, C. M., BOCHATON-PIALLAT, M. L., SIEKMANN, A. F., SLUIMER, J. C., STEFFENS, S., TUÑÓN, J., VINDIS, C., WENTZEL, J. J., YLÄ-HERTTUALA, S. & EVANS, P. C. 2018. Future directions for therapeutic strategies in post-ischaemic vascularization: a position paper from European Society of Cardiology Working Group on Atherosclerosis and Vascular Biology. *Cardiovasc Res,* 114**,** 1411-1421.
CARLSSON, L., CLARKE, J. C., YEN, C., GREGOIRE, F., ALBERY, T., BILLGER, M., EGNELL, A. C., GAN, L. M., JENNBACKEN, K., JOHANSSON, E., LINHARDT, G., MARTINSSON, S., SADIQ, M. W., WITMAN, N., WANG, Q. D., CHEN, C. H., WANG, Y. P., LIN, S., TICHO, B., HSIEH, P. C. H., CHIEN, K. R. & FRITSCHE-DANIELSON, R. 2018. Biocompatible, Purified VEGF-A mRNA Improves Cardiac Function after Intracardiac Injection 1 Week Post-myocardial Infarction in Swine. *Mol Ther Methods Clin Dev,* 9**,** 330-346.
CARMELIET, P. 2000. Mechanisms of angiogenesis and arteriogenesis. *Nature Medicine,* 6**,** 389-395.
CHABLAIS, F. & JAŹWIŃSKA, A. 2012. The regenerative capacity of the zebrafish heart is dependent on TGFβ signaling. *Development,* 139**,** 1921-1930.
CHEN, J., CUI, Z., YANG, S., WU, C., LI, W., BAO, G., XU, G., SUN, Y., WANG, L. & ZHANG, J. 2017. The upregulation of annexin A2 after spinal cord injury in rats may have implication for astrocyte proliferation. *Neuropeptides,* 61**,** 67-76.
CHEN, Q. F., CHEN, L., KATSOURAS, C. S., LIU, C., SHI, J., LIANG, D., XIANG, G., ZHU, H., LIAO, H., LIN, W., ZHOU, X. & ZHOU, X. D. 2025. Global burden of heart failure and its underlying causes in 204 countries and territories, 1990-2021. *Eur Heart J Qual Care Clin Outcomes,* 11**,** 493-509.
CHEN, Y., LIU, Y. & GAO, X. 2021. The Application of Single-Cell Technologies in Cardiovascular Research. *Frontiers in Cell and Developmental Biology,* Volume 9 - 2021.
CHENG, C., WANG, X., JIANG, Y., LI, Y., LIAO, Z., LI, W., YU, Z., WHALEN, M. J., LOK, J., DUMONT, A. S., LIU, N. & WANG, X. 2021. Recombinant Annexin A2 Administration Improves Neurological Outcomes After Traumatic Brain Injury in Mice. *Front Pharmacol,* 12**,** 708469.
CHEONG, S. H., LEE, S. H., JEON, Y. J. & LEE, D. S. 2017. Mussel (Mytilus coruscus) Water Extract Containing Taurine Prevents LPS-Induced Inflammatory Responses in Zebrafish Model. *Adv Exp Med Biol,* 975 Pt 2**,** 931-942.
CHOLAN, P., CARTLAND, S. & KAVURMA, M. 2017. NADPH oxidases, angiogenesis, and peripheral artery disease. Antioxidants 6 (3): 56.
CHORGHADE, S., SEIMETZ, J., EMMONS, R., YANG, J., BRESSON, S. M., LISIO, M. D., PARISE, G., CONRAD, N. K. & KALSOTRA, A. 2017. Poly(A) tail length regulates PABPC1 expression to tune translation in the heart. *eLife,* 6**,** e24139.

CHUGH, S., OUZOUNIAN, M., LU, Z., MOHAMED, S., LI, W., BOUSETTE, N., LIU, P. P. & GRAMOLINI, A. O. 2013. Pilot study identifying myosin heavy chain 7, desmin, insulin-like growth factor 7, and annexin A2 as circulating biomarkers of human heart failure. *Proteomics,* 13**,** 2324-34.

CHUNG, H.-T., PAE, H.-O., CHOI, B.-M., BILLIAR, T. R. & KIM, Y.-M. 2001. Nitric Oxide as a Bioregulator of Apoptosis. *Biochemical and Biophysical Research Communications,* 282**,** 1075-1079.

COCHAIN, C., CHANNON, K. M. & SILVESTRE, J.-S. 2013. Angiogenesis in the Infarcted Myocardium. *Antioxidants & Redox Signaling,* 18**,** 1100-1113.

COLLÉN, A., BERGENHEM, N., CARLSSON, L., CHIEN, K. R., HOGE, S., GAN, L. M. & FRITSCHE-DANIELSON, R. 2022. VEGFA mRNA for regenerative treatment of heart failure. *Nat Rev Drug Discov,* 21**,** 79-80.

COLLINS, L. R., PRIEST, C., CARAS, I., LITTMAN, N. & KADYK, L. 2015. Proceedings: Moving Toward Cell-Based Therapies for Heart Disease. *Stem Cells Transl Med,* 4**,** 863-7.

CONSORTIUM, T. M. 2018. Single-cell transcriptomics of 20 mouse organs creates a Tabula Muris. *Nature,* 562**,** 367-372.

COOKE, J. P. & LOSORDO, D. W. 2002. Nitric Oxide and Angiogenesis. *Circulation,* 105**,** 2133-2135.

CORLISS, B. A., AZIMI, M. S., MUNSON, J. M., PEIRCE, S. M. & MURFEE, W. L. 2016. Macrophages: An Inflammatory Link Between Angiogenesis and Lymphangiogenesis. *Microcirculation,* 23**,** 95-121.

CROSS, M. J. & CLAESSON-WELSH, L. 2001. FGF and VEGF function in angiogenesis: signalling pathways, biological responses and therapeutic inhibition. *Trends in Pharmacological Sciences,* 22**,** 201-207.

CUBBON, R. M., GALE, C. P., KEARNEY, L. C., SCHECHTER, C. B., BROOKSBY, W. P., NOLAN, J., FOX, K. A., RAJWANI, A., BAIG, W., GROVES, D., BARLOW, P., FISHER, A. C., BATIN, P. D., KAHN, M. B., ZAMAN, A. G., SHAH, A. M., BYRNE, J. A., LINDSAY, S. J., SAPSFORD, R. J., WHEATCROFT, S. B., WITTE, K. K. & KEARNEY, M. T. 2011. Changing characteristics and mode of death associated with chronic heart failure caused by left ventricular systolic dysfunction: a study across therapeutic eras. *Circ Heart Fail,* 4**,** 396-403.

CUBBON, R. M., YULDASHEVA, N. Y., VISWAMBHARAN, H., MERCER, B. N., BALIGA, V., STEPHEN, S. L., ASKHAM, J., SUKUMAR, P., SKROMNA, A., MUGHAL, R. S., WALKER, A. M. N., BRUNS, A., BAILEY, M. A., GALLOWAY, S., IMRIE, H., GAGE, M. C., RAKOBOWCHUK, M., LI, J., PORTER, K. E., PONNAMBALAM, S., WHEATCROFT, S. B., BEECH, D. J. & KEARNEY, M. T. 2014. Restoring Akt1 Activity in Outgrowth Endothelial Cells From South Asian Men Rescues Vascular Reparative Potential. *Stem Cells,* 32**,** 2714-2723.

D'ANTONIO, M., NGUYEN, J. P., ARTHUR, T. D., MATSUI, H., DONOVAN, M. K. R., D'ANTONIO-CHRONOWSKA, A. & FRAZER, K. A. 2022. In heart failure reactivation of RNA-binding proteins is associated with the expression of 1,523 fetal-specific isoforms. *PLoS Comput Biol,* 18**,** e1009918.

DAI, Z.-Y., ZHANG, Y.-P., ZHANG, H. & LU, Y.-B. 2012. PREPARATION AND CHARACTERIZATION OF MUSSEL (MYTILUS EDULIS) PROTEIN HYDROLYSATES WITH ANGIOTENSIN-I-CONVERTING ENZYME (ACE) INHIBITORY ACTIVITY BY ENZYMATIC HYDROLYSIS. *Journal of Food Biochemistry,* 36**,** 66-74.

DALLACASAGRANDE, V. & HAJJAR, K. A. 2020. Annexin A2 in Inflammation and Host Defense. *Cells,* 9.

DANIEL, J. G., YU, X., FERGUSON, A. C. & SHAVIT, J. A. 2023. CRISPR/Cas9-Mediated Genome Editing in Zebrafish. *Methods Mol Biol,* 2631**,** 371-380.

DASSAH, M., DEORA, A. B., HE, K. & HAJJAR, K. A. 2009. The endothelial cell annexin A2 system and vascular fibrinolysis. *Gen Physiol Biophys,* 28 Spec No Focus**,** F20-8.

DE GRAAUW, M., TIJDENS, I., SMEETS, M. B., HENSBERGEN, P. J., DEELDER, A. M. & VAN DE WATER, B. 2008. Annexin A2 phosphorylation mediates cell scattering and branching morphogenesis via cofilin Activation. *Mol Cell Biol,* 28**,** 1029-40.

DE LUCA, L. 2020. Established and Emerging Pharmacological Therapies for Post-Myocardial Infarction Patients with Heart Failure: a Review of the Evidence. *Cardiovascular Drugs and Therapy,* 34**,** 723-735.

DE MUINCK, E. D. & SIMONS, M. 2004. Re-evaluating therapeutic neovascularization. *Journal of Molecular and Cellular Cardiology,* 36**,** 25-32.

DE SILVA, E., PAUL, M. & KIM, H. 2022. Apoptosis in platelets is independent of the actin cytoskeleton. *PLoS One,* 17**,** e0276584.

DEBAENST, S., JARAYSEH, T., DE SAFFEL, H., BEK, J. W., BOONE, M., JOSIPOVIC, I., KIBLEUR, P., KWON, R. Y., COUCKE, P. J. & WILLAERT, A. 2025. Crispant analysis in zebrafish as a tool for rapid functional screening of disease-causing genes for bone fragility. *Elife,* 13.

DECICCO-SKINNER, K. L., HENRY, G. H., CATAISSON, C., TABIB, T., GWILLIAM, J. C., WATSON, N. J., BULLWINKLE, E. M., FALKENBURG, L., O'NEILL, R. C., MORIN, A. & WIEST, J. S. 2014. Endothelial cell tube formation assay for the in vitro study of angiogenesis. *J Vis Exp***,** e51312.

DEFOUR, A., MEDIKAYALA, S., VAN DER MEULEN, J. H., HOGARTH, M. W., HOLDREITH, N., MALATRAS, A., DUDDY, W., BOEHLER, J., NAGARAJU, K. & JAISWAL, J. K. 2017. Annexin A2 links poor myofiber repair with inflammation and adipogenic replacement of the injured muscle. *Human Molecular Genetics,* 26**,** 1979-1991.

DEL GAUDIO, F., LIU, D., ANDALOUSSI MÄE, M., BRAUNE, E.-B., HANSSON, E. M., WANG, Q.-D., BETSHOLTZ, C. & LENDAHL, U. 2023. Left ventricular hypertrophy and metabolic resetting in the Notch3-deficient adult mouse heart. *Scientific Reports,* 13**,** 15022.

DELBAERE, S., VAN DAMME, T., SYX, D., SYMOENS, S., COUCKE, P., WILLAERT, A. & MALFAIT, F. 2020. Hypomorphic zebrafish models mimic the musculoskeletal phenotype of β4GalT7-deficient Ehlers-Danlos syndrome. *Matrix Biology,* 89**,** 59-75.

DERNTL, M. & WEIDINGER, F. 2012. Managing no-reflow during percutaneous coronary intervention. *Interventional Cardiology,* 4**,** 461-472.

DICKSTEIN, K., VARDAS, P. E., AURICCHIO, A., DAUBERT, J. C., LINDE, C., MCMURRAY, J., PONIKOWSKI, P., PRIORI, S. G., SUTTON, R. & VAN VELDHUISEN, D. J. 2010. 2010 Focused Update of ESC Guidelines on device therapy in heart failure: an update of the 2008 ESC Guidelines for the diagnosis and treatment of acute and chronic heart failure and the 2007 ESC guidelines for cardiac and resynchronization therapy. Developed with the special contribution of the Heart Failure Association and the European Heart Rhythm Association. *Eur Heart J,* 31**,** 2677-87.

DIRKX, E., DA COSTA MARTINS, P. A. & DE WINDT, L. J. 2013. Regulation of fetal gene expression in heart failure. *Biochimica et Biophysica Acta (BBA) - Molecular Basis of Disease,* 1832**,** 2414-2424.

DOYON, Y., MCCAMMON, J. M., MILLER, J. C., FARAJI, F., NGO, C., KATIBAH, G. E., AMORA, R., HOCKING, T. D., ZHANG, L., REBAR, E. J., GREGORY, P. D., URNOV, F. D. & AMACHER, S. L. 2008. Heritable targeted gene disruption in zebrafish using designed zinc-finger nucleases. *Nat Biotechnol,* 26**,** 702-8.

DROZD, M., PUJADES-RODRIGUEZ, M., SUN, F., FRANKS, K. N., LILLIE, P. J., WITTE, K. K., KEARNEY, M. T. & CUBBON, R. M. 2021. Causes of Death in People With Cardiovascular Disease: A UK Biobank Cohort Study. *J Am Heart Assoc,* 10**,** e023188.

DUBÉ, K. N., THOMAS, T. M., MUNSHAW, S., ROHLING, M., RILEY, P. R. & SMART, N. 2017. Recapitulation of developmental mechanisms to revascularize the ischemic heart. *JCI Insight,* 2.

DUELEN, R. & SAMPAOLESI, M. 2017. Stem Cell Technology in Cardiac Regeneration: A Pluripotent Stem Cell Promise. *EBioMedicine,* 16**,** 30-40.

EREN, M., PAINTER, C. A., ATKINSON, J. B., DECLERCK, P. J. & VAUGHAN, D. E. 2002. Age-Dependent Spontaneous Coronary Arterial Thrombosis in Transgenic Mice That Express a Stable Form of Human Plasminogen Activator Inhibitor-1. *Circulation,* 106**,** 491-496.

ERICKSON, L. A., FICI, G. J., LUND, J. E., BOYLE, T. P., POLITES, H. G. & MAROTTI, K. R. 1990. Development of venous occlusions in mice transgenic for the plasminogen activator inhibitor-1 gene. *Nature,* 346**,** 74-6.

EULALIO, A., MANO, M., FERRO, M. D., ZENTILIN, L., SINAGRA, G., ZACCHIGNA, S. & GIACCA, M. 2012. Functional screening identifies miRNAs inducing cardiac regeneration. *Nature,* 492**,** 376-381.

FAIROOZY, R. H., COOPER, J., WHITE, J., GIAMBARTOLOMEI, C., FOLKERSEN, L., WANNAMETHEE, S. G., JEFFERIS, B. J., WHINCUP, P., BEN-SHLOMO, Y., KUMARI, M., KIVIMAKI, M., WONG, A., HARDY, R., KUH, D., GAUNT, T. R., CASAS, J. P., MCLACHLAN, S., PRICE, J. F., HINGORANI, A., FRANCO-CERECEDA, A., GREWAL, T., KALEA, A. Z. & HUMPHRIES, S. E. 2017. Identifying low density lipoprotein cholesterol associated variants in the Annexin A2 (ANXA2) gene. *Atherosclerosis,* 261**,** 60-68.

FARAH, A. & BARBAGELATA, A. 2017. Unmet goals in the treatment of Acute Myocardial Infarction: Review. *F1000Res,* 6.

FARBEHI, N., PATRICK, R., DORISON, A., XAYMARDAN, M., JANBANDHU, V., WYSTUB-LIS, K., HO, J. W., NORDON, R. E. & HARVEY, R. P. 2019. Single-cell expression profiling reveals dynamic flux of cardiac stromal, vascular and immune cells in health and injury. *Elife,* 8.

FAUSETT, B. V. & GOLDMAN, D. 2006. A role for alpha1 tubulin-expressing Müller glia in regeneration of the injured zebrafish retina. *J Neurosci,* 26**,** 6303-13.

FERNÁNDEZ-AVILÉS, F., SANZ-RUIZ, R., CLIMENT, A. M., BADIMON, L., BOLLI, R., CHARRON, D., FUSTER, V., JANSSENS, S., KASTRUP, J., KIM, H. S., LÜSCHER, T. F., MARTIN, J. F., MENASCHÉ, P., SIMARI, R. D., STONE, G. W., TERZIC, A., WILLERSON, J. T. & WU, J. C. 2017. Global position paper on cardiovascular regenerative medicine. *Eur Heart J,* 38**,** 2532-2546.

FERRARA, N., GERBER, H. P. & LECOUTER, J. 2003. The biology of VEGF and its receptors. *Nat Med,* 9**,** 669-76.

FORMAN-RUBINSKY, R., PAUL, A., FENG, W., SCHLEGEL, B. T., ZUPPO, D. A., KEDZIORA, K., STOLTZ, D. B., WATKINS, S. C., RAJASUNDARAM, D., LI, G. & TSANG, M. 2025. Cited4a limits cardiomyocyte dedifferentiation and proliferation during zebrafish heart regeneration. *Development,* 152.

FRANGOGIANNIS, N. G. 2015. Pathophysiology of Myocardial Infarction. *Compr Physiol,* 5**,** 1841-75.
GABISONIA, K., PROSDOCIMO, G., AQUARO, G. D., CARLUCCI, L., ZENTILIN, L., SECCO, I., ALI, H., BRAGA, L., GORGODZE, N., BERNINI, F., BURCHIELLI, S., COLLESI, C., ZANDONÀ, L., SINAGRA, G., PIACENTI, M., ZACCHIGNA, S., BUSSANI, R., RECCHIA, F. A. & GIACCA, M. 2019. MicroRNA therapy stimulates uncontrolled cardiac repair after myocardial infarction in pigs. *Nature,* 569**,** 418-422.
GALLEY, H. F. & WEBSTER, N. R. 2004. Physiology of the endothelium. *British Journal of Anaesthesia,* 93**,** 105-113.
GANCZ, D., RAFTREY, B. C., PERLMOTER, G., MARÍN-JUEZ, R., SEMO, J., MATSUOKA, R. L., KARRA, R., RAVIV, H., MOSHE, N., ADDADI, Y., GOLANI, O., POSS, K. D., RED-HORSE, K., STAINIER, D. Y. & YANIV, K. 2019. Distinct origins and molecular mechanisms contribute to lymphatic formation during cardiac growth and regeneration. *Elife,* 8.
GAO, J., FAN, L., ZHAO, L. & SU, Y. 2021. The interaction of Notch and Wnt signaling pathways in vertebrate regeneration. *Cell Regeneration,* 10**,** 11.
GAONAC'H-LOVEJOY, V., BOSCHER, C., DELISLE, C. & GRATTON, J.-P. 2020. Rap1 is involved in angiopoietin-1-induced cell-cell junction stabilization and endothelial cell sprouting. *Cells,* 9**,** 155.
GARRIDO-GÓMEZ, T., DOMINGUEZ, F., QUIÑONERO, A., ESTELLA, C., VILELLA, F., PELLICER, A. & SIMON, C. 2012. Annexin A2 is critical for embryo adhesiveness to the human endometrium by RhoA activation through F-actin regulation. *The FASEB Journal,* 26**,** 3715-3727.
GARRIDO-GOMEZ, T., QUIÑONERO, A., DOMINGUEZ, F., RUBERT, L., PERALES, A., HAJJAR, K. A. & SIMON, C. 2020. Preeclampsia: a defect in decidualization is associated with deficiency of Annexin A2. *American Journal of Obstetrics & Gynecology,* 222**,** 376.e1-376.e17.
GARVEY, W. 1984. Modified Elastic Tissue-Masson Trichrome Stain. *Stain Technology,* 59**,** 213-216.
GASPARD-BOULINC, L. C., GORTANA, L., WALTER, T., BARILLOT, E. & CAVALLI, F. M. G. 2025. Cell-type deconvolution methods for spatial transcriptomics. *Nature Reviews Genetics,* 26**,** 828-846.
GEMBERLING, M., BAILEY, T. J., HYDE, D. R. & POSS, K. D. 2013. The zebrafish as a model for complex tissue regeneration. *Trends Genet,* 29**,** 611-20.
GERBIN, K. A. & MURRY, C. E. 2015. The winding road to regenerating the human heart. *Cardiovasc Pathol,* 24**,** 133-40.
GERKE, V., CREUTZ, C. E. & MOSS, S. E. 2005. Annexins: linking Ca2+ signalling to membrane dynamics. *Nat Rev Mol Cell Biol,* 6**,** 449-61.
GHOSH, A. K. & VAUGHAN, D. E. 2012. PAI-1 in tissue fibrosis. *Journal of cellular physiology,* 227**,** 493-507.
GIDH-JAIN, M., HUANG, B., JAIN, P., GICK, G. & EL-SHERIF, N. 1998. Alterations in cardiac gene expression during ventricular remodeling following experimental myocardial infarction. *J Mol Cell Cardiol,* 30**,** 627-37.
GLADKA, M. M., JOHANSEN, A. K. Z., VAN KAMPEN, S. J., PETERS, M. M. C., MOLENAAR, B., VERSTEEG, D., KOOIJMAN, L., ZENTILIN, L., GIACCA, M. & VAN ROOIJ, E. 2023. Thymosin β4 and prothymosin α promote cardiac regeneration post-ischaemic injury in mice. *Cardiovasc Res,* 119**,** 802-812.
GLADKA, M. M., KOHELA, A., MOLENAAR, B., VERSTEEG, D., KOOIJMAN, L., MONSHOUWER-KLOOTS, J., KREMER, V., VOS, H. R., HUIBERS, M. M. H.,

HAIGH, J. J., HUYLEBROECK, D., BOON, R. A., GIACCA, M. & VAN ROOIJ, E. 2021. Cardiomyocytes stimulate angiogenesis after ischemic injury in a ZEB2-dependent manner. *Nat Commun,* 12**,** 84.
GOLDMAN, J. A. & POSS, K. D. 2020. Gene regulatory programmes of tissue regeneration. *Nat Rev Genet,* 21**,** 511-525.
GONZÁLEZ-ROSA, J. M. 2022. Zebrafish Models of Cardiac Disease: From Fortuitous Mutants to Precision Medicine. *Circ Res,* 130**,** 1803-1826.
GONZÁLEZ-ROSA, J. M., BURNS, C. E. & BURNS, C. G. 2017. Zebrafish heart regeneration: 15 years of discoveries. *Regeneration (Oxf),* 4**,** 105-123.
GONZÁLEZ-ROSA, J. M., MARTÍN, V., PERALTA, M., TORRES, M. & MERCADER, N. 2011. Extensive scar formation and regression during heart regeneration after cryoinjury in zebrafish. *Development,* 138**,** 1663-1674.
GORGONI, B., RICHARDSON, W. A., BURGESS, H. M., ANDERSON, R. C., WILKIE, G. S., GAUTIER, P., MARTINS, J. P. S., BROOK, M., SHEETS, M. D. & GRAY, N. K. 2011. Poly(A)-binding proteins are functionally distinct and have essential roles during vertebrate development. *Proceedings of the National Academy of Sciences,* 108**,** 7844-7849.
GRAY, G. A. & GRAY, N. K. 2017. A tail of translational regulation. *eLife,* 6**,** e29104.
GRAY, NICOLA K., HRABÁLKOVÁ, L., SCANLON, J. P. & SMITH, RICHARD W. P. 2015. Poly(A)-binding proteins and mRNA localization: who rules the roost? *Biochemical Society Transactions,* 43**,** 1277-1284.
GU, X., CHENG, L., CHUENG, W. L., YAO, X., LIU, H., QI, G. & LI, M. 2006. Neovascularization of ischemic myocardium by newly isolated tannins prevents cardiomyocyte apoptosis and improves cardiac function. *Mol Med,* 12**,** 275-83.
GUPTA, K. K., DONAHUE, D. L., SANDOVAL-COOPER, M. J., CASTELLINO, F. J. & PLOPLIS, V. A. 2017. Plasminogen Activator Inhibitor-1 Protects Mice Against Cardiac Fibrosis by Inhibiting Urokinase-type Plasminogen Activator-mediated Plasminogen Activation. *Scientific Reports,* 7**,** 365.
GURUNG, S., RESTREPO, N. K. & SUMANAS, S. 2024. Endocardium gives rise to blood cells in zebrafish embryos. *Cell Reports,* 43**,** 113736.
HAJJAR, K. A. 2015. The Biology of Annexin A2: From Vascular Fibrinolysis to Innate Immunity. *Trans Am Clin Climatol Assoc,* 126**,** 144-55.
HALVORSEN, S. & HUBER, K. 2014. Fibrinolytic treatment of ST-elevation myocardial infarction. Update 2014. *Hamostaseologie,* 34**,** 47-53.
HAMRE, K. M., CHEPENIK, K. P. & GOLDOWITZ, D. 1995. The annexins: specific markers of midline structures and sensory neurons in the developing murine central nervous system. *J Comp Neurol,* 352**,** 421-35.
HARRISON, M. R., BUSSMANN, J., HUANG, Y., ZHAO, L., OSORIO, A., BURNS, C. G., BURNS, C. E., SUCOV, H. M., SIEKMANN, A. F. & LIEN, C. L. 2015. Chemokine-guided angiogenesis directs coronary vasculature formation in zebrafish. *Dev Cell,* 33**,** 442-54.
HARRISON, M. R., FENG, X., MO, G., AGUAYO, A., VILLAFUERTE, J., YOSHIDA, T., PEARSON, C. A., SCHULTE-MERKER, S. & LIEN, C. L. 2019. Late developing cardiac lymphatic vasculature supports adult zebrafish heart function and regeneration. *Elife,* 8.
HAUBNER, B. J., ADAMOWICZ-BRICE, M., KHADAYATE, S., TIEFENTHALER, V., METZLER, B., AITMAN, T. & PENNINGER, J. M. 2012. Complete cardiac regeneration in a mouse model of myocardial infarction. *Aging (Albany NY),* 4**,** 966-77.

HAUBNER, B. J., SCHNEIDER, J., SCHWEIGMANN, U., SCHUETZ, T., DICHTL, W., VELIK-SALCHNER, C., STEIN, J. I. & PENNINGER, J. M. 2016. Functional Recovery of a Human Neonatal Heart After Severe Myocardial Infarction. *Circ Res,* 118**,** 216-21.

HE, K.-L., DEORA, A. B., XIONG, H., LING, Q., WEKSLER, B. B., NIESVIZKY, R. & HAJJAR, K. A. 2008. Endothelial Cell Annexin A2 Regulates Polyubiquitination and Degradation of Its Binding Partner S100A10/p11*. *Journal of Biological Chemistry,* 283**,** 19192-19200.

HE, L., HUANG, X., KANISICAK, O., LI, Y., WANG, Y., LI, Y., PU, W., LIU, Q., ZHANG, H., TIAN, X., ZHAO, H., LIU, X., ZHANG, S., NIE, Y., HU, S., MIAO, X., WANG, Q. D., WANG, F., CHEN, T., XU, Q., LUI, K. O., MOLKENTIN, J. D. & ZHOU, B. 2017. Preexisting endothelial cells mediate cardiac neovascularization after injury. *J Clin Invest,* 127**,** 2968-2981.

HE, Q., ZHU, J., YANG, G., LIU, X., LI, L., WANG, Y., XIONG, X., ZHENG, Y., ZHENG, H. & QU, H. 2023. Serum Annexin A2 concentrations are increased in patients with diabetic cardiomyopathy and are linked to cardiac dysfunctions. *Diabetes Research and Clinical Practice,* 195**,** 110196.

HEDHLI, N., FALCONE, D. J., HUANG, B., CESARMAN-MAUS, G., KRAEMER, R., ZHAI, H., TSIRKA, S. E., SANTAMBROGIO, L. & HAJJAR, K. A. 2012. The annexin A2/S100A10 system in health and disease: emerging paradigms. *J Biomed Biotechnol,* 2012**,** 406273.

HEDHLI, N., HUANG, Q., KALINOWSKI, A., PALMERI, M., HU, X., RUSSELL, R. R. & RUSSELL, K. S. 2011. Endothelium-derived neuregulin protects the heart against ischemic injury. *Circulation,* 123**,** 2254-2262.

HEDMAN, M., HARTIKAINEN, J., SYVÄNNE, M., STJERNVALL, J., HEDMAN, A., KIVELÄ, A., VANNINEN, E., MUSSALO, H., KAUPPILA, E., SIMULA, S., NÄRVÄNEN, O., RANTALA, A., PEUHKURINEN, K., NIEMINEN, M. S., LAAKSO, M. & YLÄ-HERTTUALA, S. 2003. Safety and feasibility of catheter-based local intracoronary vascular endothelial growth factor gene transfer in the prevention of postangioplasty and in-stent restenosis and in the treatment of chronic myocardial ischemia: phase II results of the Kuopio Angiogenesis Trial (KAT). *Circulation,* 107**,** 2677-83.

HENNIGS, J. K., MATUSZCAK, C., TREPEL, M. & KÖRBELIN, J. 2021. Vascular Endothelial Cells: Heterogeneity and Targeting Approaches. *Cells,* 10.

HENRY, T. D., GRINES, C. L., WATKINS, M. W., DIB, N., BARBEAU, G., MOREADITH, R., ANDRASFAY, T. & ENGLER, R. L. 2007. Effects of Ad5FGF-4 in patients with angina: an analysis of pooled data from the AGENT-3 and AGENT-4 trials. *J Am Coll Cardiol,* 50**,** 1038-46.

HONKOOP, H., DE BAKKER, D. E., AHARONOV, A., KRUSE, F., SHAKKED, A., NGUYEN, P. D., DE HEUS, C., GARRIC, L., MURARO, M. J., SHOFFNER, A., TESSADORI, F., PETERSON, J. C., NOORT, W., BERTOZZI, A., WEIDINGER, G., POSTHUMA, G., GRÜN, D., VAN DER LAARSE, W. J., KLUMPERMAN, J., JASPERS, R. T., POSS, K. D., VAN OUDENAARDEN, A., TZAHOR, E. & BAKKERS, J. 2019. Single-cell analysis uncovers that metabolic reprogramming by ErbB2 signaling is essential for cardiomyocyte proliferation in the regenerating heart. *Elife,* 8.

HOSHIJIMA, K., JURYNEC, M. J., KLATT SHAW, D., JACOBI, A. M., BEHLKE, M. A. & GRUNWALD, D. J. 2019. Highly Efficient CRISPR-Cas9-Based Methods for Generating Deletion Mutations and F0 Embryos that Lack Gene Function in Zebrafish. *Developmental Cell,* 51**,** 645-657.e4.

HOSODA, N., LEJEUNE, F. & MAQUAT, L. E. 2006. Evidence that Poly(A) Binding Protein C1 Binds Nuclear Pre-mRNA Poly(A) Tails. *Molecular and Cellular Biology,* 26**,** 3085-3097.

HOWE, K., CLARK, M. D., TORROJA, C. F., TORRANCE, J., BERTHELOT, C., MUFFATO, M., COLLINS, J. E., HUMPHRAY, S., MCLAREN, K., MATTHEWS, L., MCLAREN, S., SEALY, I., CACCAMO, M., CHURCHER, C., SCOTT, C., BARRETT, J. C., KOCH, R., RAUCH, G. J., WHITE, S., CHOW, W., KILIAN, B., QUINTAIS, L. T., GUERRA-ASSUNÇÃO, J. A., ZHOU, Y., GU, Y., YEN, J., VOGEL, J. H., EYRE, T., REDMOND, S., BANERJEE, R., CHI, J., FU, B., LANGLEY, E., MAGUIRE, S. F., LAIRD, G. K., LLOYD, D., KENYON, E., DONALDSON, S., SEHRA, H., ALMEIDA-KING, J., LOVELAND, J., TREVANION, S., JONES, M., QUAIL, M., WILLEY, D., HUNT, A., BURTON, J., SIMS, S., MCLAY, K., PLUMB, B., DAVIS, J., CLEE, C., OLIVER, K., CLARK, R., RIDDLE, C., ELLIOT, D., THREADGOLD, G., HARDEN, G., WARE, D., BEGUM, S., MORTIMORE, B., KERRY, G., HEATH, P., PHILLIMORE, B., TRACEY, A., CORBY, N., DUNN, M., JOHNSON, C., WOOD, J., CLARK, S., PELAN, S., GRIFFITHS, G., SMITH, M., GLITHERO, R., HOWDEN, P., BARKER, N., LLOYD, C., STEVENS, C., HARLEY, J., HOLT, K., PANAGIOTIDIS, G., LOVELL, J., BEASLEY, H., HENDERSON, C., GORDON, D., AUGER, K., WRIGHT, D., COLLINS, J., RAISEN, C., DYER, L., LEUNG, K., ROBERTSON, L., AMBRIDGE, K., LEONGAMORNLERT, D., MCGUIRE, S., GILDERTHORP, R., GRIFFITHS, C., MANTHRAVADI, D., NICHOL, S., BARKER, G., et al. 2013. The zebrafish reference genome sequence and its relationship to the human genome. *Nature,* 496**,** 498-503.

HSING, D. D., STOCK, A. C., GREENWALD, B. M., BACHA, E. A., FLYNN, P. A., CARROLL, S. J., DAYTON, J. D., PROCKOP, S. E., QIU, Y., ALMEIDA, D., TAMURA, S. & HAJJAR, K. A. 2023. Annexin A2 Loss After Cardiopulmonary Bypass and Development of Acute Postoperative Respiratory Dysfunction in Children. *Crit Care Explor,* 5**,** e0862.

HU, B. & CHENG, S. Y. 2009. Angiopoietin-2: development of inhibitors for cancer therapy. *Curr Oncol Rep,* 11**,** 111-6.

HUANG, L., XU, K., YANG, Q., DING, Z., SHAO, Z. & LI, E. 2025. ANXA2 in cancer: aberrant regulation of tumour cell apoptosis and its immune interactions. *Cell Death Discov,* 11**,** 174.

HUANG, P., XIAO, A., ZHOU, M., ZHU, Z., LIN, S. & ZHANG, B. 2011. Heritable gene targeting in zebrafish using customized TALENs. *Nat Biotechnol,* 29**,** 699-700.

HUANG, Y., TAN, Y., YAO, Y., GU, L., HUANG, L. & SONG, T. 2023. Genome-wide detection of m6A-associated SNPs in atrial fibrillation pathogenesis. *Front Cardiovasc Med,* 10**,** 1152851.

HUTCHINGS, G., KRUSZYNA, Ł., NAWROCKI, M. J., STRAUSS, E., BRYL, R., SPACZYŃSKA, J., PEREK, B., JEMIELITY, M., MOZDZIAK, P., KEMPISTY, B., NOWICKI, M. & KRASIŃSKI, Z. 2021. Molecular Mechanisms Associated with ROS-Dependent Angiogenesis in Lower Extremity Artery Disease. *Antioxidants,* 10**,** 735.

IISMAA, S. E., KAIDONIS, X., NICKS, A. M., BOGUSH, N., KIKUCHI, K., NAQVI, N., HARVEY, R. P., HUSAIN, A. & GRAHAM, R. M. 2018. Comparative regenerative mechanisms across different mammalian tissues. *NPJ Regen Med,* 3**,** 6.

INGASON, A. B., GOLDSTONE, A. B., PAULSEN, M. J., THAKORE, A. D., TRUONG, V. N., EDWARDS, B. B., ESKANDARI, A., BOLLIG, T., STEELE, A. N. & WOO,

Y. J. 2018. Angiogenesis precedes cardiomyocyte migration in regenerating mammalian hearts. *The Journal of thoracic and cardiovascular surgery,* 155**,** 1118-1127.e1.
IRVIN, M. W., ZIJLSTRA, A., WIKSWO, J. P. & POZZI, A. 2014. Techniques and assays for the study of angiogenesis. *Exp Biol Med (Maywood),* 239**,** 1476-88.
ISHII, H., YOSHIDA, M., HIRAOKA, M., HAJJAR, K. A., TANAKA, A., YASUKOCHI, Y. & NUMANO, F. 2001. Recombinant annexin II modulates impaired fibrinolytic activity in vitro and in rat carotid artery. *Circ Res,* 89**,** 1240-5.
ISNER, J. M. & ASAHARA, T. 1999. Angiogenesis and vasculogenesis as therapeutic strategies for postnatal neovascularization. *J Clin Invest,* 103**,** 1231-6.
JACOBI, A. M., RETTIG, G. R., TURK, R., COLLINGWOOD, M. A., ZEINER, S. A., QUADROS, R. M., HARMS, D. W., BONTHUIS, P. J., GREGG, C., OHTSUKA, M., GURUMURTHY, C. B. & BEHLKE, M. A. 2017. Simplified CRISPR tools for efficient genome editing and streamlined protocols for their delivery into mammalian cells and mouse zygotes. *Methods,* 121-122**,** 16-28.
JAMBUSARIA, A., HONG, Z., ZHANG, L., SRIVASTAVA, S., JANA, A., TOTH, P. T., DAI, Y., MALIK, A. B. & REHMAN, J. 2020. Endothelial heterogeneity across distinct vascular beds during homeostasis and inflammation. *eLife,* 9**,** e51413.
JASIN, M. & ROTHSTEIN, R. 2013. Repair of strand breaks by homologous recombination. *Cold Spring Harb Perspect Biol,* 5**,** a012740.
JE, J.-Y., PARK, P.-J., BYUN, H.-G., JUNG, W.-K. & KIM, S.-K. 2005. Angiotensin I converting enzyme (ACE) inhibitory peptide derived from the sauce of fermented blue mussel, Mytilus edulis. *Bioresource Technology,* 96**,** 1624-1629.
JENČA, D., MELENOVSKÝ, V., STEHLIK, J., STANĚK, V., KETTNER, J., KAUTZNER, J., ADÁMKOVÁ, V. & WOHLFAHRT, P. 2021. Heart failure after myocardial infarction: incidence and predictors. *ESC Heart Fail,* 8**,** 222-237.
JEON, H., XIE, J., JEON, Y., JUNG, K. J., GUPTA, A., CHANG, W. & CHUNG, D. 2023. Statistical Power Analysis for Designing Bulk, Single-Cell, and Spatial Transcriptomics Experiments: Review, Tutorial, and Perspectives. *Biomolecules,* 13**,** 221.
JI, Z., GUO, J., ZHANG, R., ZUO, W., XU, Y., QU, Y., TAO, Z., LI, X., LI, Y., YAO, Y. & MA, G. 2024. ADAM8 deficiency in macrophages promotes cardiac repair after myocardial infarction via ANXA2-mTOR-autophagy pathway. *Journal of Advanced Research*.
JI, Z., GUO, J., ZHANG, R., ZUO, W., XU, Y., QU, Y., TAO, Z., LI, X., LI, Y., YAO, Y. & MA, G. 2025. ADAM8 deficiency in macrophages promotes cardiac repair after myocardial infarction via ANXA2-mTOR-autophagy pathway. *Journal of Advanced Research,* 73**,** 483-499.
JIN, J., JIANG, Y., CHAKRABARTI, S. & SU, Z. 2022. Cardiac Mast Cells: A Two-Head Regulator in Cardiac Homeostasis and Pathogenesis Following Injury. *Front Immunol,* 13**,** 963444.
JOHANSON, P., FU, Y., WAGNER, G. S., GOODMAN, S. G., GRANGER, C. B., WALLENTIN, L., VAN DE WERF, F. & ARMSTRONG, P. W. 2009. ST resolution 1 hour after fibrinolysis for prediction of myocardial infarct size: insights from ASSENT 3. *Am J Cardiol,* 103**,** 154-8.
JONES, R. C., KARKANIAS, J., KRASNOW, M. A., PISCO, A. O., QUAKE, S. R., SALZMAN, J., YOSEF, N., BULTHAUP, B., BROWN, P., HARPER, W., HEMENEZ, M., PONNUSAMY, R., SALEHI, A., SANAGAVARAPU, B. A., SPALLINO, E., AARON, K. A., CONCEPCION, W., GARDNER, J. M., KELLY, B., NEIDLINGER, N., WANG, Z., CRASTA, S., KOLLURU, S., MORRI, M., TAN,

S. Y., TRAVAGLINI, K. J., XU, C., ALCÁNTARA-HERNÁNDEZ, M., ALMANZAR, N., ANTONY, J., BEYERSDORF, B., BURHAN, D., CALCUTTAWALA, K., CARTER, M. M., CHAN, C. K. F., CHANG, C. A., CHANG, S., COLVILLE, A., CULVER, R. N., CVIJOVIĆ, I., D'AMATO, G., EZRAN, C., GALDOS, F. X., GILLICH, A., GOODYER, W. R., HANG, Y., HAYASHI, A., HOUSHDARAN, S., HUANG, X., IRWIN, J. C., JANG, S., JUANICO, J. V., KERSHNER, A. M., KIM, S., KISS, B., KONG, W., KUMAR, M. E., KUO, A. H., LI, B., LOEB, G. B., LU, W. J., MANTRI, S., MARKOVIC, M., MCALPINE, P. L., DE MORREE, A., MROUJ, K., MUKHERJEE, S., MUSER, T., NEUHÖFER, P., NGUYEN, T. D., PEREZ, K., PULUCA, N., QI, Z., RAO, P., RAQUER-MCKAY, H., SCHAUM, N., SCOTT, B., SEDDIGHZADEH, B., SEGAL, J., SEN, S., SIKANDAR, S., SPENCER, S. P., STEFFES, L. C., SUBRAMANIAM, V. R., SWARUP, A., SWIFT, M., VAN TREUREN, W., TRIMM, E., VEIZADES, S., VIJAYAKUMAR, S., VO, K. C., VORPERIAN, S. K., WANG, W., WEINSTEIN, H. N. W., WINKLER, J., WU, T. T. H., XIE, J., YUNG, A. R., ZHANG, Y., DETWEILER, A. M., et al. 2022. The Tabula Sapiens: A multiple-organ, single-cell transcriptomic atlas of humans. *Science,* 376**,** eabl4896.

JOPLING, C., SLEEP, E., RAYA, M., MARTÍ, M., RAYA, A. & IZPISÚA BELMONTE, J. C. 2010. Zebrafish heart regeneration occurs by cardiomyocyte dedifferentiation and proliferation. *Nature,* 464**,** 606-9.

KAHN, M. B., YULDASHEVA, N. Y., CUBBON, R. M., SMITH, J., RASHID, S. T., VISWAMBHARAN, H., IMRIE, H., ABBAS, A., RAJWANI, A., AZIZ, A., BALIGA, V., SUKUMAR, P., GAGE, M., KEARNEY, M. T. & WHEATCROFT, S. B. 2011. Insulin resistance impairs circulating angiogenic progenitor cell function and delays endothelial regeneration. *Diabetes,* 60**,** 1295-303.

KAJJO, S., SHARMA, S., CHEN, S., BROTHERS, W. R., COTT, M., HASAJ, B., JOVANOVIC, P., LARSSON, O. & FABIAN, M. R. 2022. PABP prevents the untimely decay of select mRNA populations in human cells. *Embo j,* 41**,** e108650.

KAJSTURA, J., ROTA, M., HOSODA, T., ANVERSA, P. & LERI, A. 2012. Response to Bergmann et al: Carbon 14 Birth Dating of Human Cardiomyocytes. *Circ Res,* 110**,** e19-e21.

KALUCKA, J., DE ROOIJ, L., GOVEIA, J., ROHLENOVA, K., DUMAS, S. J., META, E., CONCHINHA, N. V., TAVERNA, F., TEUWEN, L. A., VEYS, K., GARCÍA-CABALLERO, M., KHAN, S., GELDHOF, V., SOKOL, L., CHEN, R., TREPS, L., BORRI, M., DE ZEEUW, P., DUBOIS, C., KARAKACH, T. K., FALKENBERG, K. D., PARYS, M., YIN, X., VINCKIER, S., DU, Y., FENTON, R. A., SCHOONJANS, L., DEWERCHIN, M., EELEN, G., THIENPONT, B., LIN, L., BOLUND, L., LI, X., LUO, Y. & CARMELIET, P. 2020. Single-Cell Transcriptome Atlas of Murine Endothelial Cells. *Cell,* 180**,** 764-779.e20.

KANDALAM, V., BASU, R., ABRAHAM, T., WANG, X., SOLOWAY, P. D., JAWORSKI, D. M., OUDIT, G. Y. & KASSIRI, Z. 2010. TIMP2 Deficiency Accelerates Adverse Post–Myocardial Infarction Remodeling Because of Enhanced MT1-MMP Activity Despite Lack of MMP2 Activation. *Circulation Research,* 106**,** 796-808.

KARLSSON, J., VON HOFSTEN, J. & OLSSON, P. E. 2001. Generating transparent zebrafish: a refined method to improve detection of gene expression during embryonic development. *Mar Biotechnol (NY),* 3**,** 522-7.

KATZ, M. G., SWAIN, J. D., TOMASULO, C. E., SUMAROKA, M., FARGNOLI, A. & BRIDGES, C. R. 2011. Current strategies for myocardial gene delivery. *J Mol Cell Cardiol,* 50**,** 766-76.

KAVEH, A., BRUTON, F. A., BUCKLEY, C., OREMEK, M. E. M., TUCKER, C. S., MULLINS, J. J., TAYLOR, J. M., ROSSI, A. G. & DENVIR, M. A. 2020. Live Imaging of Heart Injury in Larval Zebrafish Reveals a Multi-Stage Model of Neutrophil and Macrophage Migration. *Front Cell Dev Biol,* 8**,** 579943.

KAYEJO, V. G., FELLNER, H., THAPA, R. & KEYEL, P. A. 2023. Translational implications of targeting annexin A2: From membrane repair to muscular dystrophy, cardiovascular disease and cancer. *Clin Transl Discov,* 3.

KEELEY, S., FERNÁNDEZ-LAJARÍN, M., BERGEMANN, D., JOHN, N., PARROTT, L., ANDREA, B. E. & GONZÁLEZ-ROSA, J. M. 2025. Rapid and robust generation of cardiomyocyte-specific crispants in zebrafish using the cardiodeleter system. *Cell Reports Methods,* 5**,** 101003.

KELLEY, M., FIERSTEIN, S., PURKEY, L. & DECICCO-SKINNER, K. 2022. Endothelial Cell Tube Formation Assay: An In Vitro Model for Angiogenesis. *Methods Mol Biol,* 2475**,** 187-196.

KEMMLER, C. L., RIEMSLAGH, F. W., MORAN, H. R. & MOSIMANN, C. 2021. From Stripes to a Beating Heart: Early Cardiac Development in Zebrafish. *Journal of Cardiovascular Development and Disease,* 8**,** 17.

KHOUKAZ, H. B., JI, Y., BRAET, D. J., VADALI, M., ABDELHAMID, A. A., EMAL, C. D., LAWRENCE, D. A. & FAY, W. P. 2020. Drug Targeting of Plasminogen Activator Inhibitor-1 Inhibits Metabolic Dysfunction and Atherosclerosis in a Murine Model of Metabolic Syndrome. *Arterioscler Thromb Vasc Biol,* 40**,** 1479-1490.

KIESSLING, P. & KUPPE, C. 2024. Spatial multi-omics: novel tools to study the complexity of cardiovascular diseases. *Genome Medicine,* 16**,** 14.

KIKUCHI, K., HOLDWAY, JENNIFER E., MAJOR, ROBERT J., BLUM, N., DAHN, RANDALL D., BEGEMANN, G. & POSS, KENNETH D. 2011a. Retinoic Acid Production by Endocardium and Epicardium Is an Injury Response Essential for Zebrafish Heart Regeneration. *Developmental Cell,* 20**,** 397-404.

KIKUCHI, K., HOLDWAY, J. E., MAJOR, R. J., BLUM, N., DAHN, R. D., BEGEMANN, G. & POSS, K. D. 2011b. Retinoic acid production by endocardium and epicardium is an injury response essential for zebrafish heart regeneration. *Dev Cell,* 20**,** 397-404.

KIKUCHI, K., HOLDWAY, J. E., WERDICH, A. A., ANDERSON, R. M., FANG, Y., EGNACZYK, G. F., EVANS, T., MACRAE, C. A., STAINIER, D. Y. & POSS, K. D. 2010. Primary contribution to zebrafish heart regeneration by gata4(+) cardiomyocytes. *Nature,* 464**,** 601-5.

KIM, B.-G., KIM, Y. H., STANLEY, E. L., GARRIDO-MARTIN, E. M., LEE, Y. J. & OH, S. P. 2017. CXCL12-CXCR4 signalling plays an essential role in proper patterning of aortic arch and pulmonary arteries. *Cardiovascular Research,* 113**,** 1677-1687.

KIM, H., WANG, M. & PAIK, D. T. 2021. Endothelial-Myocardial Angiocrine Signaling in Heart Development. *Front Cell Dev Biol,* 9**,** 697130.

KIM, J., WU, Q., ZHANG, Y., WIENS, K. M., HUANG, Y., RUBIN, N., SHIMADA, H., HANDIN, R. I., CHAO, M. Y., TUAN, T.-L., STARNES, V. A. & LIEN, C.-L. 2010. PDGF signaling is required for epicardial function and blood vessel formation in regenerating zebrafish hearts. *Proceedings of the National Academy of Sciences,* 107**,** 17206-17210.

KIM, Y.-W. & BYZOVA, T. V. 2014. Oxidative stress in angiogenesis and vascular disease. *Blood,* 123**,** 625-631.
KIM, Y. S., AHN, C. B. & JE, J. Y. 2016. Anti-inflammatory action of high molecular weight Mytilus edulis hydrolysates fraction in LPS-induced RAW264.7 macrophage via NF-κB and MAPK pathways. *Food Chem,* 202**,** 9-14.
KIMMEL, C. B., BALLARD, W. W., KIMMEL, S. R., ULLMANN, B. & SCHILLING, T. F. 1995. Stages of embryonic development of the zebrafish. *Dev Dyn,* 203**,** 253-310.
KIR, D., PATEL, M. J. & MUNAGALA, M. R. 2021. What Is the Status of Regenerative Therapy in Heart Failure? *Curr Cardiol Rep,* 23**,** 146.
KOBAYASHI, K., MAEDA, K., TAKEFUJI, M., KIKUCHI, R., MORISHITA, Y., HIRASHIMA, M. & MUROHARA, T. 2017. Dynamics of angiogenesis in ischemic areas of the infarcted heart. *Sci Rep,* 7**,** 7156.
KOCHER, A. A., SCHUSTER, M. D., SZABOLCS, M. J., TAKUMA, S., BURKHOFF, D., WANG, J., HOMMA, S., EDWARDS, N. M. & ITESCU, S. 2001. Neovascularization of ischemic myocardium by human bone-marrow-derived angioblasts prevents cardiomyocyte apoptosis, reduces remodeling and improves cardiac function. *Nat Med,* 7**,** 430-6.
KONSTANDIN, M. H., TOKO, H., GASTELUM, G. M., QUIJADA, P., DE LA TORRE, A., QUINTANA, M., COLLINS, B., DIN, S., AVITABILE, D., VÖLKERS, M., GUDE, N., FÄSSLER, R. & SUSSMAN, M. A. 2013. Fibronectin is essential for reparative cardiac progenitor cell response after myocardial infarction. *Circ Res,* 113**,** 115-25.
KOODATHIL, J., ELAVARASAN, K., MUNUSAMY, H., ARIVUKKARASU, N. K., SENDHIL MURUGAN, K. & JEYASANKAR, D. 2025. Mussels: a treasure trove of nutrients, bioactive peptides, and minerals-a review of their applications in food, pharmaceuticals, and biomedicine. *Future Journal of Pharmaceutical Sciences,* 11**,** 88.
KORHONEN, E. A., LAMPINEN, A., GIRI, H., ANISIMOV, A., KIM, M., ALLEN, B., FANG, S., D'AMICO, G., SIPILÄ, T. J., LOHELA, M., STRANDIN, T., VAHERI, A., YLÄ-HERTTUALA, S., KOH, G. Y., MCDONALD, D. M., ALITALO, K. & SAHARINEN, P. 2016. Tie1 controls angiopoietin function in vascular remodeling and inflammation. *J Clin Invest,* 126**,** 3495-510.
KOSTALLARI, E. & SHAH, V. H. 2016. Angiocrine signaling in the hepatic sinusoids in health and disease. *Am J Physiol Gastrointest Liver Physiol,* 311**,** G246-51.
KOTH, J., WANG, X., KILLEN, A. C., STOCKDALE, W. T., POTTS, H. G., JEFFERSON, A., BONKHOFER, F., RILEY, P. R., PATIENT, R. K., GÖTTGENS, B. & MOMMERSTEEG, M. T. M. 2020. Runx1 promotes scar deposition and inhibits myocardial proliferation and survival during zebrafish heart regeneration. *Development,* 147.
KRAUSE, B. J., HANSON, M. A. & CASANELLO, P. 2011. Role of nitric oxide in placental vascular development and function. *Placenta,* 32**,** 797-805.
KRISHNAN, S., DEORA, A. B., ANNES, J. P., OSORIA, J., RIFKIN, D. B. & HAJJAR, K. A. 2004. Annexin II-mediated plasmin generation activates TGF-beta3 during epithelial-mesenchymal transformation in the developing avian heart. *Dev Biol,* 265**,** 140-54.
KUBOTA, Y., KLEINMAN, H. K., MARTIN, G. R. & LAWLEY, T. J. 1988. Role of laminin and basement membrane in the morphological differentiation of human endothelial cells into capillary-like structures. *J Cell Biol,* 107**,** 1589-98.

KUKUŁA, K., CHOJNOWSKA, L., DĄBROWSKI, M., WITKOWSKI, A., CHMIELAK, Z., SKWAREK, M., KĄDZIELA, J., TERESIŃSKA, A., MAŁECKI, M., JANIK, P., LEWANDOWSKI, Z., KŁOPOTOWSKI, M., WNUK, J. & RUŻYŁŁO, W. 2011. Intramyocardial plasmid-encoding human vascular endothelial growth factor A165/basic fibroblast growth factor therapy using percutaneous transcatheter approach in patients with refractory coronary artery disease (VIF-CAD). *Am Heart J,* 161**,** 581-9.

KULESHOV, M. V., JONES, M. R., ROUILLARD, A. D., FERNANDEZ, N. F., DUAN, Q., WANG, Z., KOPLEV, S., JENKINS, S. L., JAGODNIK, K. M., LACHMANN, A., MCDERMOTT, M. G., MONTEIRO, C. D., GUNDERSEN, G. W. & MA'AYAN, A. 2016. Enrichr: a comprehensive gene set enrichment analysis web server 2016 update. *Nucleic Acids Res,* 44**,** W90-7.

KUMAR, A. A., BUCKLEY, B. J. & RANSON, M. 2022. The Urokinase Plasminogen Activation System in Pancreatic Cancer: Prospective Diagnostic and Therapeutic Targets. *Biomolecules,* 12.

KUPPE, C., RAMIREZ FLORES, R. O., LI, Z., HAYAT, S., LEVINSON, R. T., LIAO, X., HANNANI, M. T., TANEVSKI, J., WÜNNEMANN, F., NAGAI, J. S., HALDER, M., SCHUMACHER, D., MENZEL, S., SCHÄFER, G., HOEFT, K., CHENG, M., ZIEGLER, S., ZHANG, X., PEISKER, F., KAESLER, N., SARITAS, T., XU, Y., KASSNER, A., GUMMERT, J., MORSHUIS, M., AMRUTE, J., VELTROP, R. J. A., BOOR, P., KLINGEL, K., VAN LAAKE, L. W., VINK, A., HOOGENBOEZEM, R. M., BINDELS, E. M. J., SCHURGERS, L., SATTLER, S., SCHAPIRO, D., SCHNEIDER, R. K., LAVINE, K., MILTING, H., COSTA, I. G., SAEZ-RODRIGUEZ, J. & KRAMANN, R. 2022. Spatial multi-omic map of human myocardial infarction. *Nature,* 608**,** 766-777.

KUWAHARA, K., NISHIKIMI, T. & NAKAO, K. 2012. Transcriptional Regulation of the Fetal Cardiac Gene Program. *Journal of Pharmacological Sciences,* 119**,** 198-203.

LAWSON, N. D. & WEINSTEIN, B. M. 2002. In Vivo Imaging of Embryonic Vascular Development Using Transgenic Zebrafish. *Developmental Biology,* 248**,** 307-318.

LEE, J. T. H., BARNETT, S. N., ROBERTS, K., ASHWIN, H., MILROSS, L., CHO, J. W., HUSEYNOV, A., WOODHAMS, B., AIVAZIDIS, A., LI, T., MAJO, J., CHAVES, P., LEE, M., MIRANDA, A. M. A., JABLONSKA, Z., ARENA, V., HANLEY, B., OSBORN, M., UHLMANN, V., XU, X. N., MCLEAN, G. R., TEICHMANN, S. A., RANDI, A. M., FILBY, A., KAYE, P. M., FISHER, A. J., HEMBERG, M., NOSEDA, M. & BAYRAKTAR, O. A. 2025. Integrated histopathology, spatial and single cell transcriptomics resolve cellular drivers of early and late alveolar damage in COVID-19. *Nat Commun,* 16**,** 1979.

LEE, S., LEE, D. H., PARK, B.-W., KIM, R., HOANG, A. D., WOO, S.-K., XIONG, W., LEE, Y. J., BAN, K. & PARK, H.-J. 2019. In vivo transduction of ETV2 improves cardiac function and induces vascular regeneration following myocardial infarction. *Experimental & Molecular Medicine,* 51**,** 1-14.

LENNON, N. J., KHO, A., BACSKAI, B. J., PERLMUTTER, S. L., HYMAN, B. T. & BROWN, R. H., JR. 2003. Dysferlin Interacts with Annexins A1 and A2 and Mediates Sarcolemmal Wound-healing *. *Journal of Biological Chemistry,* 278**,** 50466-50473.

LEPILINA, A., COON, A. N., KIKUCHI, K., HOLDWAY, J. E., ROBERTS, R. W., BURNS, C. G. & POSS, K. D. 2006. A dynamic epicardial injury response

supports progenitor cell activity during zebrafish heart regeneration. *Cell,* 127**,** 607-19.
LEUNG, D. W., CACHIANES, G., KUANG, W. J., GOEDDEL, D. V. & FERRARA, N. 1989. Vascular endothelial growth factor is a secreted angiogenic mitogen. *Science,* 246**,** 1306-9.
LI, C., ZHAO, Z. & ZHAO, S. 2022a. Annexin A2 promotes development of retinal neovascularization through PI3K/ AKT signaling pathway. *Current Eye Research,* 47**,** 579-589.
LI, H., CHANG, C., LI, X. & ZHANG, R. 2021a. The roles and activation of endocardial Notch signaling in heart regeneration. *Cell Regeneration,* 10**,** 3.
LI, J., JIA, W. & ZHAO, Q. 2014. Excessive nitrite affects zebrafish valvulogenesis through yielding too much NO signaling. *PLoS One,* 9**,** e92728.
LI, L., LU, M., GUO, L., ZHANG, X., LIU, Q., ZHANG, M., GAO, J., XU, M., LU, Y., ZHANG, F., LI, Y., ZHANG, R., LIU, X., PAN, S., ZHANG, X., LI, Z., CHEN, Y., SU, X., ZHANG, N., GUO, W., YANG, T., CHEN, J., QIN, Y., ZHANG, Z., CUI, W., YU, L., GU, Y., YANG, H., XU, X., WANG, J., BURNS, C. E., BURNS, C. G., HAN, K., ZHAO, L., FAN, G. & SU, Y. 2025. An organ-wide spatiotemporal transcriptomic and cellular atlas of the regenerating zebrafish heart. *Nat Commun,* 16**,** 3716.
LI, M., ZHAO, L., PAGE-MCCAW, P. S. & CHEN, W. 2016. Zebrafish Genome Engineering Using the CRISPR-Cas9 System. *Trends Genet,* 32**,** 815-827.
LI, Q., LAUMONNIER, Y., SYROVETS, T. & SIMMET, T. 2007. Plasmin triggers cytokine induction in human monocyte-derived macrophages. *Arterioscler Thromb Vasc Biol,* 27**,** 1383-9.
LI, T., NIU, Z., YU, T., LI, J., LU, X., HUANG, M., WANG, Q., YU, X., FENG, J., XU, B., BING, D., LI, X., LU, L., LIANG, H., YANG, R., WANG, B. & SHAN, H. 2023. Nucleosome assembly protein 1 like 1 (NAP1L1) promotes cardiac fibrosis by inhibiting YAP1 ubiquitination and degradation. *MedComm (2020),* 4**,** e348.
LI, W., CHEN, Z., YUAN, J., YU, Z., CHENG, C., ZHAO, Q., HUANG, L., HAJJAR, K. A., CHEN, Z. & LO, E. H. 2019a. Annexin A2 is a Robo4 ligand that modulates ARF6 activation-associated cerebral trans-endothelial permeability. *Journal of Cerebral Blood Flow & Metabolism,* 39**,** 2048-2060.
LI, Y., CHEN, X., JIN, R., CHEN, L., DANG, M., CAO, H., DONG, Y., CAI, B., BAI, G., GOODING, J. J., LIU, S., ZOU, D., ZHANG, Z. & YANG, C. 2021b. Injectable hydrogel with MSNs/microRNA-21-5p delivery enables both immunomodification and enhanced angiogenesis for myocardial infarction therapy in pigs. *Sci Adv,* 7.
LI, Y., HIROI, Y. & LIAO, J. K. 2010. Notch signaling as an important mediator of cardiac repair and regeneration after myocardial infarction. *Trends Cardiovasc Med,* 20**,** 228-31.
LI, Z., SOLOMONIDIS, E. G., BERKELEY, B., TANG, M. N. H., STEWART, K. R., PEREZ-VICENCIO, D., MCCRACKEN, I. R., SPIROSKI, A.-M., GRAY, G. A., BARTON, A. K., SELLERS, S. L., RILEY, P. R., BAKER, A. H. & BRITTAN, M. 2022b. Multi-species meta-analysis identifies transcriptional signatures associated with cardiac endothelial responses in the ischaemic heart. *Cardiovascular Research,* 119**,** 136-154.
LI, Z., SOLOMONIDIS, E. G., MELONI, M., TAYLOR, R. S., DUFFIN, R., DOBIE, R., MAGALHAES, M. S., HENDERSON, B. E. P., LOUWE, P. A., D'AMICO, G., HODIVALA-DILKE, K. M., SHAH, A. M., MILLS, N. L., SIMONS, B. D., GRAY, G. A., HENDERSON, N. C., BAKER, A. H. & BRITTAN, M. 2019b. Single-cell

transcriptome analyses reveal novel targets modulating cardiac neovascularization by resident endothelial cells following myocardial infarction. *Eur Heart J,* 40**,** 2507-2520.

LI, Z., SOLOMONIDIS, E. G., MELONI, M., TAYLOR, R. S., DUFFIN, R., DOBIE, R., MAGALHAES, M. S., HENDERSON, B. E. P., LOUWE, P. A., D'AMICO, G., HODIVALA-DILKE, K. M., SHAH, A. M., MILLS, N. L., SIMONS, B. D., GRAY, G. A., HENDERSON, N. C., BAKER, A. H. & BRITTAN, M. 2019c. Single-cell transcriptome analyses reveal novel targets modulating cardiac neovascularization by resident endothelial cells following myocardial infarction. *European Heart Journal,* 40**,** 2507-2520.

LI, Z., YU, L., HU, B., CHEN, L., JV, M., WANG, L., ZHOU, C., WEI, M. & ZHAO, L. 2021c. Advances in cancer treatment: a new therapeutic target, Annexin A2. *J Cancer,* 12**,** 3587-3596.

LIAO, Z., CHEN, Y., DUAN, C., ZHU, K., HUANG, R., ZHAO, H., HINTZE, M., PU, Q., YUAN, Z., LV, L., CHEN, H., LAI, B., FENG, S., QI, X. & CAI, D. 2021. Cardiac telocytes inhibit cardiac microvascular endothelial cell apoptosis through exosomal miRNA-21-5p-targeted cdip1 silencing to improve angiogenesis following myocardial infarction. *Theranostics,* 11**,** 268-291.

LIEN, C. L., HARRISON, M. R., TUAN, T. L. & STARNES, V. A. 2012. Heart repair and regeneration: recent insights from zebrafish studies. *Wound Repair Regen,* 20**,** 638-46.

LIM, H. I. & HAJJAR, K. A. 2021. Annexin A2 in Fibrinolysis, Inflammation and Fibrosis. *Int J Mol Sci,* 22.

LIM, J., PARK, C., KIM, M., KIM, H., KIM, J. & LEE, D. S. 2024. Advances in single-cell omics and multiomics for high-resolution molecular profiling. *Exp Mol Med,* 56**,** 515-526.

LIN, H., LI, W., SHEN, Z., BEI, Y., WEI, T., YU, Z., DAI, Y. & DAI, H. 2023. Annexin A2 promotes angiogenesis after ischemic stroke via annexin A2 receptor – AKT/ERK pathways. *Neuroscience Letters,* 792**,** 136941.

LING, Q., JACOVINA, A. T., DEORA, A., FEBBRAIO, M., SIMANTOV, R., SILVERSTEIN, R. L., HEMPSTEAD, B., MARK, W. H. & HAJJAR, K. A. 2004. Annexin II regulates fibrin homeostasis and neoangiogenesis in vivo. *J Clin Invest,* 113**,** 38-48.

LITVIŇUKOVÁ, M., TALAVERA-LÓPEZ, C., MAATZ, H., REICHART, D., WORTH, C. L., LINDBERG, E. L., KANDA, M., POLANSKI, K., HEINIG, M., LEE, M., NADELMANN, E. R., ROBERTS, K., TUCK, L., FASOULI, E. S., DELAUGHTER, D. M., MCDONOUGH, B., WAKIMOTO, H., GORHAM, J. M., SAMARI, S., MAHBUBANI, K. T., SAEB-PARSY, K., PATONE, G., BOYLE, J. J., ZHANG, H., ZHANG, H., VIVEIROS, A., OUDIT, G. Y., BAYRAKTAR, O. A., SEIDMAN, J. G., SEIDMAN, C. E., NOSEDA, M., HUBNER, N. & TEICHMANN, S. A. 2020. Cells of the adult human heart. *Nature,* 588**,** 466-472.

LIU, F., ZHANG, X., LI, Y., CHEN, Q., LIU, F., ZHU, X., MEI, L., SONG, X., LIU, X., SONG, Z., ZHANG, J., ZHANG, W., LING, P. & WANG, F. 2017. Anti-Inflammatory Effects of a Mytilus coruscus α-d-Glucan (MP-A) in Activated Macrophage Cells via TLR4/NF-κB/MAPK Pathway Inhibition. *Mar Drugs,* 15.

LIU, G. W., GUZMAN, E. B., MENON, N. & LANGER, R. S. 2023. Lipid Nanoparticles for Nucleic Acid Delivery to Endothelial Cells. *Pharm Res,* 40**,** 3-25.

LIU, N., JIANG, Y., CHUNG, J. Y., LI, Y., YU, Z., KIM, J. W., LOK, J. M., WHALEN, M. J. & WANG, X. 2019. Annexin A2 Deficiency Exacerbates Neuroinflammation

and Long-Term Neurological Deficits after Traumatic Brain Injury in Mice. *International Journal of Molecular Sciences,* 20**,** 6125.
LIU, W. & HAJJAR, K. A. 2016a. The annexin A2 system and angiogenesis. *Biological Chemistry,* 397**,** 1005-1016.
LIU, W. & HAJJAR, K. A. 2016b. The annexin A2 system and angiogenesis. *Biol Chem,* 397**,** 1005-16.
LIU, W. H., REN, L. N., WANG, T., NAVARRO-ALVAREZ, N. & TANG, L. J. 2016. The Involving Roles of Intrahepatic and Extrahepatic Stem/Progenitor Cells (SPCs) to Liver Regeneration. *Int J Biol Sci,* 12**,** 954-63.
LOCASCIO, A., ANNONA, G., CACCAVALE, F., D'ANIELLO, S., AGNISOLA, C. & PALUMBO, A. 2023. Nitric Oxide Function and Nitric Oxide Synthase Evolution in Aquatic Chordates. *Int J Mol Sci,* 24.
LÓPEZ-CAMARILLO, C., RUIZ-GARCÍA, E., STARLING, N. & MARCHAT, L. A. 2020. Editorial: Neovascularization, Angiogenesis and Vasculogenic Mimicry in Cancer. *Front Oncol,* 10**,** 1140.
LOSORDO, D. W., VALE, P. R., HENDEL, R. C., MILLIKEN, C. E., FORTUIN, F. D., CUMMINGS, N., SCHATZ, R. A., ASAHARA, T., ISNER, J. M. & KUNTZ, R. E. 2002. Phase 1/2 placebo-controlled, double-blind, dose-escalating trial of myocardial vascular endothelial growth factor 2 gene transfer by catheter delivery in patients with chronic myocardial ischemia. *Circulation,* 105**,** 2012-8.
LOWE, V., WISNIEWSKI, L. & PELLET-MANY, C. 2021. The Zebrafish Cardiac Endothelial Cell-Roles in Development and Regeneration. *J Cardiovasc Dev Dis,* 8.
LU, J., SHI, P., CAO, Y., SHI, B., SHEN, H., ZHAO, S., GAO, Y., CHI, H., WANG, L. & SHI, Y. 2025. Isolation and Purification of Novel Antioxidant Peptides from Mussel (Mytilus edulis) Prepared by Marine Bacillus velezensis Z-1 Protease. *Mar Drugs,* 23.
LUPU, I.-E., DE VAL, S. & SMART, N. 2020. Coronary vessel formation in development and disease: mechanisms and insights for therapy. *Nature Reviews Cardiology,* 17**,** 790-806.
MA, D. & LIU, F. 2015. Genome Editing and Its Applications in Model Organisms. *Genomics Proteomics Bioinformatics,* 13**,** 336-44.
MA, H., LIU, Z., YANG, Y., FENG, D., DONG, Y., GARBUTT, T. A., HU, Z., WANG, L., LUAN, C., COOPER, C. D., LI, Y., WELCH, J. D., QIAN, L. & LIU, J. 2021. Functional coordination of non-myocytes plays a key role in adult zebrafish heart regeneration. *EMBO reports,* 22**,** e52901.
MA, J., CHEN, Q., LIN, D. & MA, S. 2025. The Role of Infarct Border Zone Remodelling in Ventricular Arrhythmias: Bridging Basic Research and Clinical Applications. *J Cell Mol Med,* 29**,** e70526.
MADEN, S. K., KWON, S. H., HUUKI-MYERS, L. A., COLLADO-TORRES, L., HICKS, S. C. & MAYNARD, K. R. 2023. Challenges and opportunities to computationally deconvolve heterogeneous tissue with varying cell sizes using single cell RNA-sequencing datasets. *ArXiv*.
MADUREIRA, P. A., SURETTE, A. P., PHIPPS, K. D., TABOSKI, M. A. S., MILLER, V. A. & WAISMAN, D. M. 2011. The role of the annexin A2 heterotetramer in vascular fibrinolysis. *Blood,* 118**,** 4789-4797.
MANAVSKI, Y., LUCAS, T., GLASER, S. F., DORSHEIMER, L., GÜNTHER, S., BRAUN, T., RIEGER, M. A., ZEIHER, A. M., BOON, R. A. & DIMMELER, S. 2018. Clonal Expansion of Endothelial Cells Contributes to Ischemia-Induced Neovascularization. *Circ Res,* 122**,** 670-677.

MANGUS, D. A., EVANS, M. C. & JACOBSON, A. 2003. Poly(A)-binding proteins: multifunctional scaffolds for the post-transcriptional control of gene expression. *Genome Biol,* 4**,** 223.
MARASINGHE, C. K., YOON, S.-D. & JE, J.-Y. 2023. Blue mussel (Mytilus edulis) hydrolysates attenuate oxidized-low density lipoproteins (ox-LDL)-induced foam cell formation, inflammation, and oxidative stress in RAW264.7 macrophages. *Process Biochemistry,* 134**,** 131-140.
MARÍN-JUEZ, R., EL-SAMMAK, H., HELKER, C. S. M., KAMEZAKI, A., MULLAPULI, S. T., BIBLI, S. I., FOGLIA, M. J., FLEMING, I., POSS, K. D. & STAINIER, D. Y. R. 2019. Coronary Revascularization During Heart Regeneration Is Regulated by Epicardial and Endocardial Cues and Forms a Scaffold for Cardiomyocyte Repopulation. *Dev Cell,* 51**,** 503-515.e4.
MARÍN-JUEZ, R., MARASS, M., GAUVRIT, S., ROSSI, A., LAI, S. L., MATERNA, S. C., BLACK, B. L. & STAINIER, D. Y. 2016. Fast revascularization of the injured area is essential to support zebrafish heart regeneration. *Proc Natl Acad Sci U S A,* 113**,** 11237-11242.
MARÍN-SEDEÑO, E., DE MORENTIN, X. M., PÉREZ-POMARES, J. M., GÓMEZ-CABRERO, D. & RUIZ-VILLALBA, A. 2021. Understanding the Adult Mammalian Heart at Single-Cell RNA-Seq Resolution. *Front Cell Dev Biol,* 9**,** 645276.
MATRONE, G., JUNG, S. Y., CHOI, J. M., JAIN, A., LEUNG, H.-C. E., RAJAPAKSHE, K., COARFA, C., RODOR, J., DENVIR, M. A., BAKER, A. H. & COOKE, J. P. 2021. Nuclear S-nitrosylation impacts tissue regeneration in zebrafish. *Nature Communications,* 12**,** 6282.
MATRONE, G., MAQSOOD, S., TAYLOR, J., MULLINS, J. J., TUCKER, C. S. & DENVIR, M. A. 2014. Targeted laser ablation of the zebrafish larval heart induces models of heart block, valvular regurgitation, and outflow tract obstruction. *Zebrafish,* 11**,** 536-41.
MATRONE, G., TAYLOR, J. M., WILSON, K. S., BAILY, J., LOVE, G. D., GIRKIN, J. M., MULLINS, J. J., TUCKER, C. S. & DENVIR, M. A. 2013. Laser-targeted ablation of the zebrafish embryonic ventricle: a novel model of cardiac injury and repair. *Int J Cardiol,* 168**,** 3913-9.
MCCURLEY, A. T. & CALLARD, G. V. 2008. Characterization of housekeeping genes in zebrafish: male-female differences and effects of tissue type, developmental stage and chemical treatment. *BMC Molecular Biology,* 9**,** 102.
MEADOWS, S. M., MYERS, C. T. & KRIEG, P. A. 2011. Regulation of endothelial cell development by ETS transcription factors. *Semin Cell Dev Biol,* 22**,** 976-84.
MEHDIABADI, N. R., BOON SIM, C., PHIPSON, B., KALATHUR, R. K. R., SUN, Y., VIVIEN, C. J., TER HUURNE, M., PIERS, A. T., HUDSON, J. E., OSHLACK, A., WEINTRAUB, R. G., KONSTANTINOV, I. E., PALPANT, N. J., ELLIOTT, D. A. & PORRELLO, E. R. 2022. Defining the Fetal Gene Program at Single-Cell Resolution in Pediatric Dilated Cardiomyopathy. *Circulation,* 146**,** 1105-1108.
MEHRAVAR, M., SHIRAZI, A., NAZARI, M. & BANAN, M. 2019. Mosaicism in CRISPR/Cas9-mediated genome editing. *Developmental Biology,* 445**,** 156-162.
MELLY, L., BOCCARDO, S., ECKSTEIN, F., BANFI, A. & MARSANO, A. 2012. Cell and gene therapy approaches for cardiac vascularization. *Cells,* 1**,** 961-75.
MERET, W., XIANGBIN, J., MARIELLE, A., ARJAN, B., JIA, C., XINYU, D., JULIE, L. L., INGE, B. M., HEINRICH, S., STEFFEN, S., SENWEI, T., HUI, G. & RAMI

2022. De novo variants in the PABP domain of PABPC1 lead to developmental delay. *Genetics in Medicine,* 24**,** 1761-1773.
MILGROM-HOFFMAN, M., HARRELSON, Z., FERRARA, N., ZELZER, E., EVANS, S. M. & TZAHOR, E. 2011. The heart endocardium is derived from vascular endothelial progenitors. *Development,* 138**,** 4777-87.
MITROUSIS, N., FOKINA, A. & SHOICHET, M. S. 2018. Biomaterials for cell transplantation. *Nature Reviews Materials,* 3**,** 441-456.
MOLLA DESTA, G. & BIRHANU, A. G. 2025. Advancements in single-cell RNA sequencing and spatial transcriptomics: transforming biomedical research. *Acta Biochimica Polonica,* Volume 72 - 2025.
MORANGE, P. E., SAUT, N., ALESSI, M. C., YUDKIN, J. S., MARGAGLIONE, M., MINNO, G. D., HAMSTEN, A., HUMPHRIES, S. E., TREGOUET, D. A. & JUHAN-VAGUE, I. 2007. Association of Plasminogen Activator Inhibitor (PAI)-1 (SERPINE1) SNPs With Myocardial Infarction, Plasma PAI-1, and Metabolic Parameters. *Arteriosclerosis, Thrombosis, and Vascular Biology,* 27**,** 2250-2257.
MORROW, G. B., WHYTE, C. S. & MUTCH, N. J. 2021. A Serpin With a Finger in Many PAIs: PAI-1's Central Function in Thromboinflammation and Cardiovascular Disease. *Frontiers in Cardiovascular Medicine,* 8.
MÜNCH, J., GRIVAS, D., GONZÁLEZ-RAJAL, Á., TORREGROSA-CARRIÓN, R. & DE LA POMPA, J. L. 2017. Notch signalling restricts inflammation and serpine1 expression in the dynamic endocardium of the regenerating zebrafish heart. *Development,* 144**,** 1425-1440.
MUSHTAQ, M., BHAT, J. A., MIR, Z. A., SAKINA, A., ALI, S., SINGH, A. K., TYAGI, A., SALGOTRA, R. K., DAR, A. A. & BHAT, R. 2018. CRISPR/Cas approach: A new way of looking at plant-abiotic interactions. *Journal of Plant Physiology,* 224-225**,** 156-162.
NAERT, T., TULKENS, D., EDWARDS, N. A., CARRON, M., SHAIDANI, N. I., WLIZLA, M., BOEL, A., DEMUYNCK, S., HORB, M. E., COUCKE, P., WILLAERT, A., ZORN, A. M. & VLEMINCKX, K. 2020. Maximizing CRISPR/Cas9 phenotype penetrance applying predictive modeling of editing outcomes in Xenopus and zebrafish embryos. *Sci Rep,* 10**,** 14662.
NANEV, V., MILEV, H., DIMITROVA, D., NANEVA, S., STRASHILOV, S. A., YORDANOV, A., MIHAILOVA, M., IVANOVA, S., KARCHEVA, M. & IVANOV, I. 2024. Evaluation of cleaved caspase-3 and Ki-67 index on diagnostic biopsy in response to neoadjuvant chemotherapy in the context of post-treatment tumour ypT stage, ypN stage, grade, and molecular subtype. *Prz Menopauzalny,* 23**,** 31-40.
NAQVI, N., LI, M., CALVERT, JOHN W., TEJADA, T., LAMBERT, JONATHAN P., WU, J., KESTEVEN, SCOTT H., HOLMAN, SARA R., MATSUDA, T., LOVELOCK, JOSHUA D., HOWARD, WESLEY W., IISMAA, SIIRI E., CHAN, ANDREA Y., CRAWFORD, BRIAN H., WAGNER, MARY B., MARTIN, DAVID I. K., LEFER, DAVID J., GRAHAM, ROBERT M. & HUSAIN, A. 2014. A Proliferative Burst during Preadolescence Establishes the Final Cardiomyocyte Number. *Cell,* 157**,** 795-807.
NDREPEPA, G. 2023. Angiographic coronary no-reflow after primary percutaneous coronary intervention – a combination of an insensitive diagnostic method, inappropriate timing and rushed judgement. *EuroIntervention,* 19**,** e368-e370.
OBERPRILLER, J. O. & OBERPRILLER, J. C. 1974. Response of the adult newt ventricle to injury. *J Exp Zool,* 187**,** 249-53.

OH, Y., AHN, C. B., NAM, K. H., KIM, Y. K., YOON, N. Y. & JE, J. Y. 2019. Amino Acid Composition, Antioxidant, and Cytoprotective Effect of Blue Mussel (Mytilus edulis) Hydrolysate through the Inhibition of Caspase-3 Activation in Oxidative Stress-Mediated Endothelial Cell Injury. *Mar Drugs,* 17.

OJHA, N. & DHAMOON, A. S. 2023. Myocardial Infarction. *StatPearls.* Treasure Island (FL): StatPearls Publishing

Copyright © 2023, StatPearls Publishing LLC.

OJHA, N., DHAMOON, A. S. & CHAPAGAIN, R. 2022. Myocardial Infarction (Nursing). *StatPearls.* Treasure Island (FL): StatPearls Publishing

Copyright © 2022, StatPearls Publishing LLC.

PARVANIAN, S., COELHO-RATO, L. S., ERIKSSON, J. E. & PATTESON, A. E. 2023. The molecular biophysics of extracellular vimentin and its role in pathogen-host interactions. *Curr Opin Cell Biol,* 85**,** 102233.

PASUT, A., BECKER, L. M., CUYPERS, A. & CARMELIET, P. 2021. Endothelial cell plasticity at the single-cell level. *Angiogenesis,* 24**,** 311-326.

PETZ, A., GRANDOCH, M., GORSKI, D. J., ABRAMS, M., PIROTH, M., SCHNECKMANN, R., HOMANN, S., MÜLLER, J., HARTWIG, S., LEHR, S., YAMAGUCHI, Y., WIGHT, T. N., GORRESSEN, S., DING, Z., KÖTTER, S., KRÜGER, M., HEINEN, A., KELM, M., GÖDECKE, A., FLÖGEL, U. & FISCHER, J. W. 2019. Cardiac Hyaluronan Synthesis Is Critically Involved in the Cardiac Macrophage Response and Promotes Healing After Ischemia Reperfusion Injury. *Circulation Research,* 124**,** 1433-1447.

PIÑEIRO, A. J., HOUSER, A. E. & JI, A. L. 2022. Research Techniques Made Simple: Spatial Transcriptomics. *Journal of Investigative Dermatology,* 142**,** 993-1001.e1.

PITULESCU, M. E., SCHMIDT, I., GIAIMO, B. D., ANTOINE, T., BERKENFELD, F., FERRANTE, F., PARK, H., EHLING, M., BILJES, D. & ROCHA, S. F. 2017. Dll4 and Notch signalling couples sprouting angiogenesis and artery formation. *Nature cell biology,* 19**,** 915-927.

PONTES-QUERO, S., FERNÁNDEZ-CHACÓN, M., LUO, W., LUNELLA, F. F., CASQUERO-GARCIA, V., GARCIA-GONZALEZ, I., HERMOSO, A., ROCHA, S. F., BANSAL, M. & BENEDITO, R. 2019. High mitogenic stimulation arrests angiogenesis. *Nature communications,* 10**,** 2016.

PORRELLO, E. R., MAHMOUD, A. I., SIMPSON, E., HILL, J. A., RICHARDSON, J. A., OLSON, E. N. & SADEK, H. A. 2011. Transient regenerative potential of the neonatal mouse heart. *Science,* 331**,** 1078-80.

PORRELLO, E. R., MAHMOUD, A. I., SIMPSON, E., JOHNSON, B. A., GRINSFELDER, D., CANSECO, D., MAMMEN, P. P., ROTHERMEL, B. A., OLSON, E. N. & SADEK, H. A. 2013. Regulation of neonatal and adult mammalian heart regeneration by the miR-15 family. *Proceedings of the National Academy of Sciences of the United States of America,* 110**,** 187-192.

PORTO, I., ASHAR, V. & MITCHELL, A. R. 2006. Pharmacological management of no reflow during percutaneous coronary intervention. *Curr Vasc Pharmacol,* 4**,** 95-100.

POSS, K. D., KEATING, M. T. & NECHIPORUK, A. 2003. Tales of regeneration in zebrafish. *Developmental Dynamics,* 226**,** 202-210.

POSS, K. D., WILSON, L. G. & KEATING, M. T. 2002. Heart Regeneration in Zebrafish. *Science,* 298**,** 2188-2190.

PREMER, C., KANELIDIS, A. J., HARE, J. M. & SCHULMAN, I. H. 2019. Rethinking Endothelial Dysfunction as a Crucial Target in Fighting Heart Failure. *Mayo Clinic Proceedings: Innovations, Quality & Outcomes,* 3**,** 1-13.

PRICE, E. L., VIEIRA, J. M. & RILEY, P. R. 2019. Model organisms at the heart of regeneration. *Dis Model Mech,* 12.

QI, Y., WANG, M. & JIANG, Q. 2022. PABPC1--mRNA stability, protein translation and tumorigenesis. *Front Oncol,* 12**,** 1025291.

QIAO, M., TU, M., WANG, Z., MAO, F., CHEN, H., QIN, L. & DU, M. 2018. Identification and Antithrombotic Activity of Peptides from Blue Mussel (Mytilus edulis) Protein. *Int J Mol Sci,* 19.

QUOSEENA, M., VUPPALADADIUM, S., HUSSAIN, S., BANU, S., BHARATHI, S. & IDRIS, M. M. 2020. Functional role of annexins in zebrafish caudal fin regeneration – A gene knockdown approach in regenerating tissue. *Biochimie,* 175**,** 125-131.

RAFII, S., BUTLER, J. M. & DING, B.-S. 2016. Angiocrine functions of organ-specific endothelial cells. *Nature,* 529**,** 316-325.

RAGHUL KANNAN, S., LATHA LAXMI, I. P., AHMAD, S. F. & TAMIZHSELVI, R. 2024. Embryonic ethanol exposure induces oxidative stress and inflammation in zebrafish model: A dose-dependent study. *Toxicology,* 506**,** 153876.

RAJENDRAN, S., SUNDARESAN, L., VENKATACHALAM, G., RAJENDRAN, K., BEHERA, J. & CHATTERJEE, S. 2022. Temporal dynamics of nitric oxide wave in early vasculogenesis. *Vascular Medicine,* 27**,** 3-12.

RAN, F. A., HSU, P. D., WRIGHT, J., AGARWALA, V., SCOTT, D. A. & ZHANG, F. 2013. Genome engineering using the CRISPR-Cas9 system. *Nat Protoc,* 8**,** 2281-2308.

RASSIER, G. T., SILVEIRA, T. L. R., REMIÃO, M. H., DANELUZ, L. O., MARTINS, A. W. S., DELLAGOSTIN, E. N., ORTIZ, H. G., DOMINGUES, W. B., KOMNINOU, E. R., KÜTTER, M. T., MARINS, L. F. F. & CAMPOS, V. F. 2020. Evaluation of qPCR reference genes in GH-overexpressing transgenic zebrafish (Danio rerio). *Scientific Reports,* 10**,** 12692.

RAYA, Á., KOTH, C. M., BÜSCHER, D., KAWAKAMI, Y., ITOH, T., RAYA, R. M., STERNIK, G., TSAI, H.-J., RODRÍGUEZ-ESTEBAN, C. & IZPISÚA-BELMONTE, J. C. 2003. Activation of Notch signaling pathway precedes heart regeneration in zebrafish. *Proceedings of the National Academy of Sciences,* 100**,** 11889-11895.

REEVES, S. A., CHAVEZ-KAPPEL, C., DAVIS, R., ROSENBLUM, M. & ISRAEL, M. A. 1992. Developmental regulation of annexin II (Lipocortin 2) in human brain and expression in high grade glioma. *Cancer Res,* 52**,** 6871-6.

RHEE, S., PAIK, D. T., YANG, J. Y., NAGELBERG, D., WILLIAMS, I., TIAN, L., ROTH, R., CHANDY, M., BAN, J., BELBACHIR, N., KIM, S., ZHANG, H., PHANSALKAR, R., WONG, K. M., KING, D. A., VALDEZ, C., WINN, V. D., MORRISON, A. J., WU, J. C. & RED-HORSE, K. 2021. Endocardial/endothelial angiocrines regulate cardiomyocyte development and maturation and induce features of ventricular non-compaction. *Eur Heart J,* 42**,** 4264-4276.

RIZZI, A., BENAGIANO, V. & RIBATTI, D. 2017. Angiogenesis versus arteriogenesis. *Rom J Morphol Embryol,* 58**,** 15-19.

ROGOZIŃSKA, E., GARGON, E., OLMEDO-REQUENA, R., ASOUR, A., COOPER, N. A. M., VALE, C. L. & VAN'T HOOFT, J. 2020. Methods used to assess outcome consistency in clinical studies: A literature-based evaluation. *PLoS One,* 15**,** e0235485.

ROMEO, S. G., SECCO, I., SCHNEIDER, E., REUMILLER, C. M., SANTOS, C. X. C., ZOCCARATO, A., MUSALE, V., POONI, A., YIN, X., THEOFILATOS, K., TREVELIN, S. C., ZENG, L., MANN, G. E., PATHAK, V., HARKIN, K., STITT, A. W., MEDINA, R. J., MARGARITI, A., MAYR, M., SHAH, A. M., GIACCA, M. & ZAMPETAKI, A. 2023. Human blood vessel organoids reveal a critical role for CTGF in maintaining microvascular integrity. *Nature Communications,* 14**,** 5552.

ROSS STEWART, K. M., WALKER, S. L., BAKER, A. H., RILEY, P. R. & BRITTAN, M. 2021. Hooked on heart regeneration: the zebrafish guide to recovery. *Cardiovascular Research,* 118**,** 1667-1679.

ROTTBAUER, W., SAURIN, A. J., LICKERT, H., SHEN, X., BURNS, C. G., WO, Z. G., KEMLER, R., KINGSTON, R., WU, C. & FISHMAN, M. 2002. Reptin and pontin antagonistically regulate heart growth in zebrafish embryos. *Cell,* 111**,** 661-672.

RUIKAR, K., KHODE, V., SHETTY, S. S., SARATHKUMAR, E., PATIL, P., PATIL, S., BARGALE, A., SADASHIV, R. & SHETTY, P. 2023. Association of pro-fibrinolytic receptor AnnexinA2 with tissue plasminogen activator/Inhibitor-1 in pre-eclampsia. *Afr Health Sci,* 23**,** 309-319.

RYAN, R., MOYSE, B. R. & RICHARDSON, R. J. 2020. Zebrafish cardiac regeneration-looking beyond cardiomyocytes to a complex microenvironment. *Histochemistry and cell biology,* 154**,** 533-548.

SABRA, M., KARBASIAFSHAR, C., ABOULGHEIT, A., RAJ, S., ABID, M. R. & SELLKE, F. W. 2021. Clinical Application of Novel Therapies for Coronary Angiogenesis: Overview, Challenges, and Prospects. *Int J Mol Sci,* 22.

SALARI, N., MORDDARVANJOGHI, F., ABDOLMALEKI, A., RASOULPOOR, S., KHALEGHI, A. A., HEZARKHANI, L. A., SHOHAIMI, S. & MOHAMMADI, M. 2023. The global prevalence of myocardial infarction: a systematic review and meta-analysis. *BMC Cardiovascular Disorders,* 23**,** 206.

SALERNO, N., SALERNO, L., MARINO, F., SCALISE, M., CHIEFALO, A., PANUCCIO, G., DE ANGELIS, A., CIANFLONE, E., URBANEK, K. & TORELLA, D. 2022. Myocardial regeneration protocols towards the routine clinical scenario: An unseemly path from bench to bedside. *EClinicalMedicine,* 50**,** 101530.

SAMSA, L. A., GIVENS, C., TZIMA, E., STAINIER, D. Y., QIAN, L. & LIU, J. 2015. Cardiac contraction activates endocardial Notch signaling to modulate chamber maturation in zebrafish. *Development,* 142**,** 4080-91.

SAVARESE, G., BECHER, P. M., LUND, L. H., SEFEROVIC, P., ROSANO, G. M. C. & COATS, A. J. S. 2023. Global burden of heart failure: a comprehensive and updated review of epidemiology. *Cardiovasc Res,* 118**,** 3272-3287.

SAWAZAKI, R., IMAI, S., YOKOGAWA, M., HOSODA, N., HOSHINO, S.-I., MIO, M., MIO, K., SHIMADA, I. & OSAWA, M. 2018. Characterization of the multimeric structure of poly(A)-binding protein on a poly(A) tail. *Scientific Reports,* 8**,** 1455.

SAXENA, S., PURUSHOTHAMAN, S., MEGHAH, V., BHATTI, B., PORURI, A., MEENA LAKSHMI, M. G., SARATH BABU, N., NARASIMHA MURTHY CH, L., MANDAL, K. K., KUMAR, A. & IDRIS, M. M. 2016. Role of annexin gene and its regulation during zebrafish caudal fin regeneration. *Wound Repair Regen,* 24**,** 551-9.

SEIDAH, N. G., POIRIER, S., DENIS, M., PARKER, R., MIAO, B., MAPELLI, C., PRAT, A., WASSEF, H., DAVIGNON, J., HAJJAR, K. A. & MAYER, G. 2012. Annexin A2 is a natural extrahepatic inhibitor of the PCSK9-induced LDL receptor degradation. *PLoS One,* 7**,** e41865.

SEO, D. W., LI, H., GUEDEZ, L., WINGFIELD, P. T., DIAZ, T., SALLOUM, R., WEI, B. Y. & STETLER-STEVENSON, W. G. 2003. TIMP-2 mediated inhibition of angiogenesis: an MMP-independent mechanism. *Cell,* 114**,** 171-80.

SEROPIAN, I. M., TOLDO, S., VAN TASSELL, B. W. & ABBATE, A. 2014. Anti-inflammatory strategies for ventricular remodeling following ST-segment elevation acute myocardial infarction. *J Am Coll Cardiol,* 63**,** 1593-603.

SEYHAN, A. A. 2024. Trials and Tribulations of MicroRNA Therapeutics. *Int J Mol Sci,* 25.

SHAIKH, S. B., BALAYA, R. D. A., DAGAMAJALU, S., BHANDARY, Y. P., UNWALLA, H., PRASAD, T. S. K. & RAHMAN, I. 2024. A signaling pathway map of plasminogen activator inhibitor-1 (PAI-1/SERPINE-1): a review of an innovative frontier in molecular aging and cellular senescence. *Cell Communication and Signaling,* 22**,** 544.

SHAO, Z., NAZARI, M., GUO, L., LI, S. H., SUN, J., LIU, S. M., YUAN, H. P., WEISEL, R. D. & LI, R. K. 2015. The cardiac repair benefits of inflammation do not persist: evidence from mast cell implantation. *J Cell Mol Med,* 19**,** 2751-62.

SHEN, K., MIAO, J., GAO, Q., LING, X., LIANG, Y., ZHOU, Q., SONG, Q., LUO, Y., WU, Q., SHEN, W., WANG, X., LI, X., LIU, Y., ZHOU, S., TANG, Y. & ZHOU, L. 2022. Annexin A2 plays a key role in protecting against cisplatin-induced AKI through β-catenin/TFEB pathway. *Cell Death Discovery,* 8**,** 430.

SHI, D. L. 2023. RNA-Binding Proteins as Critical Post-Transcriptional Regulators of Cardiac Regeneration. *Int J Mol Sci,* 24.

SI, X., ZHENG, H., WEI, G., LI, M., LI, W., WANG, H., GUO, H., SUN, J., LI, C., ZHONG, S., LIAO, W., LIAO, Y., HUANG, S. & BIN, J. 2020. circRNA Hipk3 Induces Cardiac Regeneration after Myocardial Infarction in Mice by Binding to Notch1 and miR-133a. *Molecular Therapy Nucleic Acids,* 21**,** 636-655.

SILLEN, M. & DECLERCK, P. J. 2020. Targeting PAI-1 in Cardiovascular Disease: Structural Insights Into PAI-1 Functionality and Inhibition. *Frontiers in Cardiovascular Medicine,* 7.

SILLEN, M. & DECLERCK, P. J. 2021. A Narrative Review on Plasminogen Activator Inhibitor-1 and Its (Patho)Physiological Role: To Target or Not to Target? *International Journal of Molecular Sciences,* 22**,** 2721.

SILVESTRE, J.-S., SMADJA, D. M. & LÉVY, B. I. 2013. Postischemic Revascularization: From Cellular and Molecular Mechanisms to Clinical Applications. *Physiological Reviews,* 93**,** 1743-1802.

SIMÕES, F. C. & RILEY, P. R. 2022. Immune cells in cardiac repair and regeneration. *Development,* 149.

SIMONE, T. M., HIGGINS, C. E., CZEKAY, R. P., LAW, B. K., HIGGINS, S. P., ARCHAMBEAULT, J., KUTZ, S. M. & HIGGINS, P. J. 2014. SERPINE1: A Molecular Switch in the Proliferation-Migration Dichotomy in Wound-"Activated" Keratinocytes. *Adv Wound Care (New Rochelle),* 3**,** 281-290.

SKELLY, D. A., SQUIERS, G. T., MCLELLAN, M. A., BOLISETTY, M. T., ROBSON, P., ROSENTHAL, N. A. & PINTO, A. R. 2018. Single-Cell Transcriptional Profiling Reveals Cellular Diversity and Intercommunication in the Mouse Heart. *Cell Rep,* 22**,** 600-610.

SMART, N., BOLLINI, S., DUBÉ, K. N., VIEIRA, J. M., ZHOU, B., DAVIDSON, S., YELLON, D., RIEGLER, J., PRICE, A. N., LYTHGOE, M. F., PU, W. T. & RILEY, P. R. 2011. De novo cardiomyocytes from within the activated adult heart after injury. *Nature,* 474**,** 640-4.

SMART, N., DUBÉ, K. N. & RILEY, P. R. 2009. Coronary vessel development and insight towards neovascular therapy. *Int J Exp Pathol,* 90**,** 262-83.
SMITH, RICHARD W. P., BLEE, TAJEKESA K. P. & GRAY, NICOLA K. 2014. Poly(A)-binding proteins are required for diverse biological processes in metazoans. *Biochemical Society Transactions,* 42**,** 1229-1237.
SONG, C., BURGESS, S., EICHER, J. D., O'DONNELL, C. J. & JOHNSON, A. D. 2017. Causal Effect of Plasminogen Activator Inhibitor Type 1 on Coronary Heart Disease. *J Am Heart Assoc,* 6.
SONG, G., CAMPOS, B., WAGONER, L. E., DEDMAN, J. R. & WALSH, R. A. 1998. Altered cardiac annexin mRNA and protein levels in the left ventricle of patients with end-stage heart failure. *J Mol Cell Cardiol,* 30**,** 443-51.
SRIDHARAN, D., PRACHA, N., DOUGHERTY, J. A., AKHTAR, A., ALVI, S. B. & KHAN, M. 2022. A One-Stop Protocol to Assess Myocardial Fibrosis in Frozen and Paraffin Sections. *Methods Protoc,* 5.
STARIKOVA, E., MAMMEDOVA, J., OZHIGANOVA, A., LEBEDEVA, A., MALASHICHEVA, A., SEMENOVA, D., KHOKHLOVA, E., MAMELI, E., CAPORALI, A., WILLS, J. & SOKOLOV, A. 2021. Protective Role of Mytilus edulis Hydrolysate in Lipopolysaccharide-Galactosamine Acute Liver Injury. *Frontiers in Pharmacology,* 12.
STEWART, D. J., KUTRYK, M. J., FITCHETT, D., FREEMAN, M., CAMACK, N., SU, Y., DELLA SIEGA, A., BILODEAU, L., BURTON, J. R., PROULX, G. & RADHAKRISHNAN, S. 2009. VEGF gene therapy fails to improve perfusion of ischemic myocardium in patients with advanced coronary disease: results of the NORTHERN trial. *Mol Ther,* 17**,** 1109-15.
STOCKDALE, W. T., LEMIEUX, M. E., KILLEN, A. C., ZHAO, J., HU, Z., RIEPSAAME, J., HAMILTON, N., KUDOH, T., RILEY, P. R., VAN AERLE, R., YAMAMOTO, Y. & MOMMERSTEEG, M. T. M. 2018. Heart Regeneration in the Mexican Cavefish. *Cell Rep,* 25**,** 1997-2007.e7.
STREISINGER, G., WALKER, C., DOWER, N., KNAUBER, D. & SINGER, F. 1981. Production of clones of homozygous diploid zebra fish (Brachydanio rerio). *Nature,* 291**,** 293-296.
SU, C.-T., JAO, T.-M., URBAN, Z., HUANG, Y.-J., SEE, D. H. W., TSAI, Y.-C., LIN, W.-C. & HUANG, J.-W. 2021. LTBP4 affects renal fibrosis by influencing angiogenesis and altering mitochondrial structure. *Cell Death & Disease,* 12**,** 943.
SU, S. A., XIE, Y., ZHANG, Y., XI, Y., CHENG, J. & XIANG, M. 2019. Essential roles of EphrinB2 in mammalian heart: from development to diseases. *Cell Commun Signal,* 17**,** 29.
SUI, X., LO, J. A., LUO, S., HE, Y., TANG, Z., LIN, Z., ZHOU, Y., WANG, W. X., LIU, J. & WANG, X. 2024. Scalable spatial single-cell transcriptomics and translatomics in 3D thick tissue blocks. *bioRxiv*.
SUN, H.-J., WU, Z.-Y., NIE, X.-W. & BIAN, J.-S. 2020. Role of Endothelial Dysfunction in Cardiovascular Diseases: The Link Between Inflammation and Hydrogen Sulfide. *Frontiers in Pharmacology,* Volume 10 - 2019.
SUN, J., PETERSON, E. A., CHEN, X. & WANG, J. 2023. hapln1a+ cells guide coronary growth during heart morphogenesis and regeneration. *Nature Communications,* 14**,** 3505.
SUN, M., LIU, Y. & GIBB, W. 1996. Distribution of annexin I and II in term human fetal membranes, decidua and placenta. *Placenta,* 17**,** 181-4.

SUN, N., NING, B., HANSSON, K. M., BRUCE, A. C., SEAMAN, S. A., ZHANG, C., RIKARD, M., DEROSA, C. A., FRASER, C. L., WÅGBERG, M., FRITSCHE-DANIELSON, R., WIKSTRÖM, J., CHIEN, K. R., LUNDAHL, A., HÖLTTÄ, M., CARLSSON, L. G., PEIRCE, S. M. & HU, S. 2018. Modified VEGF-A mRNA induces sustained multifaceted microvascular response and accelerates diabetic wound healing. *Scientific Reports,* 8**,** 17509.

SURYANINGTYAS, I. T., AHN, C.-B. & JE, J.-Y. 2021. Cytoprotective Peptides from Blue Mussel Protein Hydrolysates: Identification and Mechanism Investigation in Human Umbilical Vein Endothelial Cells Injury. *Marine drugs,* 19**,** 609.

SURYANINGTYAS, I. T., JASMADI, DAYARATHNE, L. A., MARASINGHE, C. K. & JE, J.-Y. 2025. Mussels as sustainable marine resources for bioactive peptides for health and the food industry. *Food & Function,* 16**,** 3255-3272.

TAKESHITA, K., HAYASHI, M., IINO, S., KONDO, T., INDEN, Y., IWASE, M., KOJIMA, T., HIRAI, M., ITO, M., LOSKUTOFF, D. J., SAITO, H., MUROHARA, T. & YAMAMOTO, K. 2004. Increased expression of plasminogen activator inhibitor-1 in cardiomyocytes contributes to cardiac fibrosis after myocardial infarction. *Am J Pathol,* 164**,** 449-56.

TAN, J., XIE, Y., YAO, A., QIN, Y., LI, L., SHEN, L., ZHANG, X., XU, C., JIANG, X., WANG, A. & YAN, Z. 2020. Long noncoding RNA-dependent regulation of vascular smooth muscle cell proliferation and migration in hypertension. *The International Journal of Biochemistry & Cell Biology,* 118**,** 105653.

TAN, W. L. W., SEOW, W. Q., ZHANG, A., RHEE, S., WONG, W. H., GREENLEAF, W. J. & WU, J. C. 2023. Current and future perspectives of single-cell multi-omics technologies in cardiovascular research. *Nat Cardiovasc Res,* 2**,** 20-34.

TAO, Y.-K., ZENG, H., ZHANG, G.-Q., CHEN, S. T., XIE, X.-J., HE, X., WANG, S., WEN, H. & CHEN, J.-X. 2017. Notch3 deficiency impairs coronary microvascular maturation and reduces cardiac recovery after myocardial ischemia. *International Journal of Cardiology,* 236**,** 413-422.

TAYLOR, J., SAUNTER, C., LOVE, G., GIRKIN, J., HENDERSON, D. & CHAUDHRY, B. 2011. Real-time optical gating for three-dimensional beating heart imaging. *Journal of Biomedical Optics,* 16**,** 116021.

TAYLOR, J. M., NELSON, C. J., BRUTON, F. A., KAVEH, A., BUCKLEY, C., TUCKER, C. S., ROSSI, A. G., MULLINS, J. J. & DENVIR, M. A. 2019a. Adaptive prospective optical gating enables day-long 3D time-lapse imaging of the beating embryonic zebrafish heart. *Nature Communications,* 10**,** 5173.

TAYLOR, S. C., NADEAU, K., ABBASI, M., LACHANCE, C., NGUYEN, M. & FENRICH, J. 2019b. The Ultimate qPCR Experiment: Producing Publication Quality, Reproducible Data the First Time. *Trends in Biotechnology,* 37**,** 761-774.

THUILLIEZ, C., MOQUIN-BEAUDRY, G., KHNEISSER, P., MARQUES DA COSTA, M. E., KARKAR, S., BOUDHOUCHE, H., DRUBAY, D., AUDINOT, B., GEOERGER, B., SCOAZEC, J.-Y., GASPAR, N. & MARCHAIS, A. 2024. CellsFromSpace: a fast, accurate, and reference-free tool to deconvolve and annotate spatially distributed omics data. *Bioinformatics Advances,* 4.

TOFLER, G. H., MASSARO, J., O'DONNELL, C. J., WILSON, P. W. F., VASAN, R. S., SUTHERLAND, P. A., MEIGS, J. B., LEVY, D. & D'AGOSTINO, R. B., SR. 2016. Plasminogen activator inhibitor and the risk of cardiovascular disease: The Framingham Heart Study. *Thromb Res,* 140**,** 30-35.

TOMBOR, L. S. & DIMMELER, S. 2022. Why is endothelial resilience key to maintain cardiac health? *Basic Res Cardiol,* 117**,** 35.

TOUSOULIS, D., KAMPOLI, A. M., TENTOLOURIS, C., PAPAGEORGIOU, N. & STEFANADIS, C. 2012. The role of nitric oxide on endothelial function. *Curr Vasc Pharmacol,* 10**,** 4-18.

TRAN, T. T. V., ZHANG, Y., WEI, S., LEE, J., JEONG, Y., VUONG, T. A., LEE, S.-J., RYU, D., BAE, G.-U. & KANG, J.-S. 2025. Endothelial PRMT7 prevents dysfunction, promotes revascularization and enhances cardiac recovery post-myocardial infarction. *Experimental & Molecular Medicine,* 57**,** 1759-1774.

TRINH, L. A. & STAINIER, D. Y. 2004. Fibronectin regulates epithelial organization during myocardial migration in zebrafish. *Dev Cell,* 6**,** 371-82.

TROUVÉ, P., LEGOT, S., BÉLIKOVA, I., MAROTTE, F., BÉNÉVOLENSKY, D., RUSSO-MARIE, F., SAMUEL, J. L. & CHARLEMAGNE, D. 1999. Localization and quantitation of cardiac annexins II, V, and VI in hypertensive guinea pigs. *Am J Physiol,* 276**,** H1159-66.

TU, C., MEZYNSKI, R. & WU, J. C. 2020. Improving the engraftment and integration of cell transplantation for cardiac regeneration. *Cardiovascular research,* 116**,** 473-475.

TUAN, T.-L., WU, H., HUANG, E. Y., CHONG, S. S. N., LAUG, W., MESSADI, D., KELLY, P. & LE, A. 2003. Increased Plasminogen Activator Inhibitor-1 in Keloid Fibroblasts May Account for their Elevated Collagen Accumulation in Fibrin Gel Cultures. *The American Journal of Pathology,* 162**,** 1579-1589.

TUCKER, N. R., CHAFFIN, M., FLEMING, S. J., HALL, A. W., PARSONS, V. A., BEDI, K. C., JR., AKKAD, A. D., HERNDON, C. N., ARDUINI, A., PAPANGELI, I., ROSELLI, C., AGUET, F., CHOI, S. H., ARDLIE, K. G., BABADI, M., MARGULIES, K. B., STEGMANN, C. M. & ELLINOR, P. T. 2020. Transcriptional and Cellular Diversity of the Human Heart. *Circulation,* 142**,** 466-482.

TZAHOR, E. & POSS, K. D. 2017. Cardiac regeneration strategies: Staying young at heart. *Science,* 356**,** 1035-1039.

UBIL, E., DUAN, J., PILLAI, I. C., ROSA-GARRIDO, M., WU, Y., BARGIACCHI, F., LU, Y., STANBOULY, S., HUANG, J., ROJAS, M., VONDRISKA, T. M., STEFANI, E. & DEB, A. 2014. Mesenchymal-endothelial transition contributes to cardiac neovascularization. *Nature,* 514**,** 585-90.

URIBE-SALAZAR, J. M., KAYA, G., SEKAR, A., WEYENBERG, K., INGAMELLS, C. & DENNIS, M. Y. 2022. Evaluation of CRISPR gene-editing tools in zebrafish. *BMC Genomics,* 23**,** 12.

UYGUR, A. & LEE, R. T. 2016. Mechanisms of Cardiac Regeneration. *Developmental cell,* 36**,** 362-374.

VALLS, M. D., SOLDADO, M., ARASA, J., PEREZ-ASO, M., WILLIAMS, A. J., CRONSTEIN, B. N., NOGUERA, M. A., TERENCIO, M. C. & MONTESINOS, M. C. 2021. Annexin A2-Mediated Plasminogen Activation in Endothelial Cells Contributes to the Proangiogenic Effect of Adenosine A(2A) Receptors. *Front Pharmacol,* 12**,** 654104.

VAN DE VLEKKERT, D., MACHADO, E. & D'AZZO, A. 2020. Analysis of Generalized Fibrosis in Mouse Tissue Sections with Masson's Trichrome Staining. *Bio Protoc,* 10**,** e3629.

VAN LINTHOUT, S., STELLOS, K., GIACCA, M., BERTERO, E., CANNATA, A., CARRIER, L., GARCIA-PAVIA, P., GHIGO, A., GONZÁLEZ, A., HAUGAA, K. H., IMAZIO, M., LOPES, L. R., MOST, P., POLLESELLO, P., SCHUNKERT, H., STRECKFUSS-BÖMEKE, K., THUM, T., TOCCHETTI, C. G., TSCHÖPE, C., VAN DER MEER, P., VAN ROOIJ, E., METRA, M., ROSANO, G. M. C. & HEYMANS, S. 2025. State of the art and perspectives of gene therapy in heart

failure. A scientific statement of the Heart Failure Association of the ESC, the ESC Council on Cardiovascular Genomics and the ESC Working Group on Myocardial & Pericardial Diseases. *Eur J Heart Fail,* 27**,** 5-25.
VAN ROYEN, N., PIEK, J. J., BUSCHMANN, I., HOEFER, I., VOSKUIL, M. & SCHAPER, W. 2001. Stimulation of arteriogenesis; a new concept for the treatment of arterial occlusive disease. *Cardiovascular Research,* 49**,** 543-553.
VAN WIJK, B., GUNST, Q. D., MOORMAN, A. F. & VAN DEN HOFF, M. J. 2012. Cardiac regeneration from activated epicardium. *PLoS One,* 7**,** e44692.
VANACORE, G., CHRISTENSEN, J. B. & BAYIN, N. S. 2024. Age-dependent regenerative mechanisms in the brain. *Biochem Soc Trans,* 52**,** 2243-2252.
VARYUKHINA, S., LAMAZIÈRE, A., DELAUNAY, J. L., DE WREEDE, A. & AYALA-SANMARTIN, J. 2022. The Ca(2+)- and phospholipid-binding protein Annexin A2 is able to increase and decrease plasma membrane order. *Biochim Biophys Acta Biomembr,* 1864**,** 183810.
VAUGHAN, D. E., RAI, R., KHAN, S. S., EREN, M. & GHOSH, A. K. 2017. Plasminogen Activator Inhibitor-1 Is a Marker and a Mediator of Senescence. *Arteriosclerosis, Thrombosis, and Vascular Biology,* 37**,** 1446-1452.
VEERKAMP, J., RUDOLPH, F., CSERESNYES, Z., PRILLER, F., OTTEN, C., RENZ, M., SCHAEFER, L. & ABDELILAH-SEYFRIED, S. 2013. Unilateral dampening of Bmp activity by nodal generates cardiac left-right asymmetry. *Dev Cell,* 24**,** 660-7.
VELOSO, A., BLEUART, A., CONRARD, L., ORBAN, T., BRUYR, J., CABOCHETTE, P., GERMANO, R. F. V., SCHEVENELS, G., BERNARD, A., ZINDY, E., DEMEYER, S., VANHOLLEBEKE, B., DEQUIEDT, F. & MARTIN, M. 2024. The cytoskeleton adaptor protein Sorbs1 controls the development of lymphatic and venous vessels in zebrafish. *BMC Biology,* 22**,** 51.
VENUGOPAL, J. R., PRABHAKARAN, M. P., MUKHERJEE, S., RAVICHANDRAN, R., DAN, K. & RAMAKRISHNA, S. 2012. Biomaterial strategies for alleviation of myocardial infarction. *J R Soc Interface,* 9**,** 1-19.
VERMEULEN, Z., MATEIU, L., DUGAUCQUIER, L., KEULENAER, G. W. D. & SEGERS, V. F. M. 2019. Cardiac endothelial cell transcriptome in neonatal, adult, and remodeling hearts. *Physiological Genomics,* 51**,** 186-196.
VIEIRA, J. M., HOWARD, S., VILLA DEL CAMPO, C., BOLLINI, S., DUBÉ, K. N., MASTERS, M., BARNETTE, D. N., ROHLING, M., SUN, X., HANKINS, L. E., GAVRIOUCHKINA, D., WILLIAMS, R., METZGER, D., CHAMBON, P., SAUKA-SPENGLER, T., DAVIES, B. & RILEY, P. R. 2017. BRG1-SWI/SNF-dependent regulation of the Wt1 transcriptional landscape mediates epicardial activity during heart development and disease. *Nat Commun,* 8**,** 16034.
WAGNER, K.-D., WAGNER, N., BONDKE, A., NAFZ, B., FLEMMING, B., THERES, H. & SCHOLZ, H. 2002. The Wilms' tumor suppressor Wt1 is expressed in the coronary vasculature after myocardial infarction. *The FASEB Journal,* 16**,** 1117-1119.
WALFORD, G. & LOSCALZO, J. 2003. Nitric oxide in vascular biology. *Journal of Thrombosis and Haemostasis,* 1**,** 2112-2118.
WALKER, E. J., HEYDET, D., VELDRE, T. & GHILDYAL, R. 2019. Transcriptomic changes during TGF-β-mediated differentiation of airway fibroblasts to myofibroblasts. *Scientific Reports,* 9**,** 20377.
WANG, B., LI, L., CHI, C. F., MA, J. H., LUO, H. Y. & XU, Y. F. 2013a. Purification and characterisation of a novel antioxidant peptide derived from blue mussel (Mytilus edulis) protein hydrolysate. *Food Chem,* 138**,** 1713-9.

WANG, H., LA RUSSA, M. & QI, L. S. 2016. CRISPR/Cas9 in Genome Editing and Beyond. *Annu Rev Biochem,* 85**,** 227-64.
WANG, J., CAO, J., DICKSON, A. L. & POSS, K. D. 2015. Epicardial regeneration is guided by cardiac outflow tract and Hedgehog signalling. *Nature,* 522**,** 226-230.
WANG, J., KARRA, R., DICKSON, A. L. & POSS, K. D. 2013b. Fibronectin is deposited by injury-activated epicardial cells and is necessary for zebrafish heart regeneration. *Dev Biol,* 382**,** 427-35.
WANG, L., YU, P., ZHOU, B., SONG, J., LI, Z., ZHANG, M., GUO, G., WANG, Y., CHEN, X., HAN, L. & HU, S. 2020a. Single-cell reconstruction of the adult human heart during heart failure and recovery reveals the cellular landscape underlying cardiac function. *Nat Cell Biol,* 22**,** 108-119.
WANG, Q., LIU, F.-J., WANG, X.-M., ZHAO, G.-H., CAI, D., YU, J.-H., YIN, F.-W. & ZHOU, D.-Y. 2022. Preparation and Hepatoprotective Activities of Peptides Derived from Mussels (Mytilus edulis) and Clams (Ruditapes philippinarum). *Marine Drugs,* 20**,** 719.
WANG, Z., CUI, M., SHAH, A. M., TAN, W., LIU, N., BASSEL-DUBY, R. & OLSON, E. N. 2020b. Cell-Type-Specific Gene Regulatory Networks Underlying Murine Neonatal Heart Regeneration at Single-Cell Resolution. *Cell Rep,* 33**,** 108472.
WANG, Z., CUI, M., SHAH, A. M., YE, W., TAN, W., MIN, Y. L., BOTTEN, G. A., SHELTON, J. M., LIU, N., BASSEL-DUBY, R. & OLSON, E. N. 2019. Mechanistic basis of neonatal heart regeneration revealed by transcriptome and histone modification profiling. *Proc Natl Acad Sci U S A,* 116**,** 18455-18465.
WANG, Z., WEI, Q., HAN, L., CAO, K., LAN, T., XU, Z., WANG, Y., GAO, Y., XUE, J., SHAN, F., FENG, J. & XIE, X. 2018. Tenascin-c renders a proangiogenic phenotype in macrophage via annexin II. *J Cell Mol Med,* 22**,** 429-438.
WATSON, C. J., MONSTAD-RIOS, A. T., BHIMANI, R. M., GISTELINCK, C., WILLAERT, A., COUCKE, P., HSU, Y.-H. & KWON, R. Y. 2020. Phenomics-Based Quantification of CRISPR-Induced Mosaicism in Zebrafish. *Cell Systems,* 10**,** 275-286.e5.
WHITE, S. J. & CHONG, J. J. H. 2020. Growth factor therapy for cardiac repair: an overview of recent advances and future directions. *Biophysical Reviews,* 12**,** 805-815.
WHITE, Z. B., NAIR, S. & BREDEL, M. 2024. The role of annexins in central nervous system development and disease. *Journal of Molecular Medicine,* 102**,** 751-760.
WON, K. J., LEE, P., JUNG, S. H., JIANG, X., LEE, C. K., LIN, H. Y., KANG, H., LEE, H. M., KIM, J., TOYOKUNI, S. & KIM, B. 2011. 3-morpholinosydnonimine participates in the attenuation of neointima formation via inhibition of annexin A2-mediated vascular smooth muscle cell migration. *Proteomics,* 11**,** 193-201.
WU, C. C., KRUSE, F., VASUDEVARAO, M. D., JUNKER, J. P., ZEBROWSKI, D. C., FISCHER, K., NOËL, E. S., GRÜN, D., BEREZIKOV, E., ENGEL, F. B., VAN OUDENAARDEN, A., WEIDINGER, G. & BAKKERS, J. 2016. Spatially Resolved Genome-wide Transcriptional Profiling Identifies BMP Signaling as Essential Regulator of Zebrafish Cardiomyocyte Regeneration. *Dev Cell,* 36**,** 36-49.
WU, T., JIANG, D., ZOU, M., SUN, W., WU, D., CUI, J., HUNTRESS, I., PENG, X. & LI, G. 2021. Coupling high-throughput mapping with proteomics analysis delineates cis-regulatory elements at high resolution. *Nucleic Acids Research,* 50**,** e5-e5.
XIANG, K. & BARTEL, D. P. 2021. The molecular basis of coupling between poly(A)-tail length and translational efficiency. *Elife,* 10.

XU, H., YE, L., DU, C., TANG, H., ZHENG, Q., ZHU, C., LIANG, B., WANG, Y., MAO, X., LIANG, Q., ZHANG, J., SHAO, H., SUN, X., YUAN, R., YUN, W., LUO, C., XIU, J., SU, W., FAN, F., DAI, Z., CHEN, L., GUAN, Y. & ZHANG, X. 2025. EP4/ANXA2 axis in pulmonary arterial hypertension: therapeutic implications. *European Heart Journal*.

YANG, W., MEI, F. C. & CHENG, X. 2018. EPAC1 regulates endothelial annexin A2 cell surface translocation and plasminogen activation. *The FASEB Journal,* 32**,** 2212-2222.

YAO, C., CAO, X. & YU, B. 2021. Revascularization After Traumatic Spinal Cord Injury. *Front Physiol,* 12**,** 631500.

YARON, J. R., ZHANG, L., GUO, Q., HAYDEL, S. E. & LUCAS, A. R. 2021. Fibrinolytic Serine Proteases, Therapeutic Serpins and Inflammation: Fire Dancers and Firestorms. *Frontiers in Cardiovascular Medicine,* 8.

YASHASWINI, C., KIRAN, N. S. & CHATTERJEE, A. 2025. Zebrafish navigating the metabolic maze: insights into human disease - assets, challenges and future implications. *J Diabetes Metab Disord,* 24**,** 3.

YE, L., D'AGOSTINO, G., LOO, S. J., WANG, C. X., SU, L. P., TAN, S. H., TEE, G. Z., PUA, C. J., PENA, E. M., CHENG, R. B., CHEN, W. C., ABDURRACHIM, D., LALIC, J., TAN, R. S., LEE, T. H., ZHANG, J. & COOK, S. A. 2018. Early Regenerative Capacity in the Porcine Heart. *Circulation,* 138**,** 2798-2808.

YU, D., WANG, X. & YE, L. 2021. Cardiac Tissue Engineering for the Treatment of Myocardial Infarction. *J Cardiovasc Dev Dis,* 8.

ZANGI, L., LUI, K. O., VON GISE, A., MA, Q., EBINA, W., PTASZEK, L. M., SPÄTER, D., XU, H., TABEBORDBAR, M., GORBATOV, R., SENA, B., NAHRENDORF, M., BRISCOE, D. M., LI, R. A., WAGERS, A. J., ROSSI, D. J., PU, W. T. & CHIEN, K. R. 2013. Modified mRNA directs the fate of heart progenitor cells and induces vascular regeneration after myocardial infarction. *Nature biotechnology,* 31**,** 898-907.

ZGHEIB, C., ALLUKIAN, M. W., XU, J., MORRIS, M. W., CASKEY, R. C., HERDRICH, B. J., HU, J., GORMAN, J. H., GORMAN, R. C. & LIECHTY, K. W. 2014. Mammalian fetal cardiac regeneration after myocardial infarction is associated with differential gene expression compared with the adult. *The Annals of thoracic surgery,* 97**,** 1643-1650.

ZHANG, H., CHEN, X., XUE, P., MA, X., LI, J. & ZHANG, J. 2021. FN1 promotes chondrocyte differentiation and collagen production via TGF-β/PI3K/Akt pathway in mice with femoral fracture. *Gene,* 769**,** 145253.

ZHANG, L., JAMBUSARIA, A., HONG, Z., MARSBOOM, G., TOTH, P. T., HERBERT, B. S., MALIK, A. B. & REHMAN, J. 2017. SOX17 Regulates Conversion of Human Fibroblasts Into Endothelial Cells and Erythroblasts by Dedifferentiation Into CD34(+) Progenitor Cells. *Circulation,* 135**,** 2505-2523.

ZHANG, X., ALMASIAN, M., HASSAN, S. S., JOTHEESH, R., KADAM, V. A., POLK, A. R., SABERIGARAKANI, A., RAHAT, A., YUAN, J., LEE, J., CARROLL, K. & DING, Y. 2023a. 4D Light-sheet imaging and interactive analysis of cardiac contractility in zebrafish larvae. *APL Bioeng,* 7**,** 026112.

ZHANG, X., CHEN, Z., XIONG, Y., ZHOU, Q., ZHU, L. Q. & LIU, D. 2025. The emerging role of nitric oxide in the synaptic dysfunction of vascular dementia. *Neural Regen Res,* 20**,** 402-415.

ZHANG, Y., CHEN, C., LIU, Z., GUO, H., LU, W., HU, W. & LIN, Z. 2022. PABPC1-induced stabilization of IFI27 mRNA promotes angiogenesis and malignant

progression in esophageal squamous cell carcinoma through exosomal miRNA-21-5p. *J Exp Clin Cancer Res,* 41**,** 111.
ZHANG, Y., WANG, Y., LI, J., LI, C., LIU, W., LONG, X., WANG, Z., ZHAO, R., GE, J. & SHI, B. 2023b. ANNEXIN A2 FACILITATES NEOVASCULARIZATION TO PROTECT AGAINST MYOCARDIAL INFARCTION INJURY VIA INTERACTING WITH MACROPHAGE YAP AND ENDOTHELIAL INTEGRIN B3. *Shock,* 60.
ZHAO, L., BORIKOVA, A. L., BEN-YAIR, R., GUNER-ATAMAN, B., MACRAE, C. A., LEE, R. T., BURNS, C. G. & BURNS, C. E. 2014. Notch signaling regulates cardiomyocyte proliferation during zebrafish heart regeneration. *Proc Natl Acad Sci U S A,* 111**,** 1403-8.
ZHAO, S., HUANG, L., WU, J., ZHANG, Y., PAN, D. & LIU, X. 2009. Vascular endothelial growth factor upregulates expression of annexin A2 in vitro and in a mouse model of ischemic retinopathy. *Mol Vis,* 15**,** 1231-42.
ZHOU, B., HONOR, L. B., HE, H., MA, Q., OH, J. H., BUTTERFIELD, C., LIN, R. Z., MELERO-MARTIN, J. M., DOLMATOVA, E., DUFFY, H. S., GISE, A., ZHOU, P., HU, Y. W., WANG, G., ZHANG, B., WANG, L., HALL, J. L., MOSES, M. A., MCGOWAN, F. X. & PU, W. T. 2011. Adult mouse epicardium modulates myocardial injury by secreting paracrine factors. *J Clin Invest,* 121**,** 1894-904.
ZHOU, Z., ZHONG, Y., ZHANG, Z. & REN, X. 2023. Spatial transcriptomics deconvolution at single-cell resolution using Redeconve. *Nature Communications,* 14**,** 7930.
ZHU, L., LAMA, S., TU, L., DUSTING, G. J., WANG, J. H. & LIU, G. S. 2021. TAK1 signaling is a potential therapeutic target for pathological angiogenesis. *Angiogenesis,* 24**,** 453-470.
ZHU, S., KUBOTA, N., WANG, S., WANG, T., XIAO, G. & HOSHIDA, Y. 2024. STIE: Single-cell level deconvolution, convolution, and clustering in in situ capturing-based spatial transcriptomics. *Nature Communications,* 15**,** 7559.
ZHU, W., ZHANG, E., ZHAO, M., CHONG, Z., FAN, C., TANG, Y., HUNTER, J. D., BOROVJAGIN, A. V., WALCOTT, G. P., CHEN, J. Y., QIN, G. & ZHANG, J. 2018. Regenerative Potential of Neonatal Porcine Hearts. *Circulation,* 138**,** 2809-2816.
ZONG, L. & WANG, W. 2020. CircANXA2 Promotes Myocardial Apoptosis in Myocardial Ischemia-Reperfusion Injury via Inhibiting miRNA-133 Expression. *BioMed Research International,* 2020**,** 8590861.